Identification of mechanisms of gemcitabine resistance using a whole genome shRNA screen in a novel *in vitro* coculture model of pancreatic cancer.

Graham David Mills

Wolfson College

Cancer Research UK Cambridge Institute

University of Cambridge

This dissertation is submitted for the degree of

Doctor of Philosophy

August 2018

Declaration

This dissertation is the result of my own work and includes nothing which is the outcome of work done in collaboration except as declared in the Preface and specified in the text.

It is not substantially the same as any that I have submitted, or, is being concurrently submitted for a degree or diploma or other qualification at the University of Cambridge or any other University or similar institution except as declared in the Preface and specified in the text. I further state that no substantial part of my dissertation has already been submitted, or, is being concurrently submitted for any such degree, diploma or other qualification at the University of Cambridge or any other University or similar institution except as declared in the Preface and specified in the text. It does not exceed the prescribed word limit for the relevant Degree Committee.

Abstract

Identification of mechanisms of gemcitabine resistance using a whole genome shRNA screen in a novel in vitro coculture model of pancreatic cancer.

Graham David Mills

Pancreatic ductal adenocarcinoma (PDAC) remains one of the most difficult to treat major cancers, with a 5-year survival of less than 5%, and little to no improvement in prognosis over the previous fifty years. The complexity and heterogeneity of the pancreatic tumour and its highly desmoplastic stromal microenvironment present major physical and biochemical barriers to the delivery and efficacy of therapeutics. Improving the success rate of therapeutic interventions for this cancer requires both a detailed understanding of stromal dynamics and drug resistance within the tumour, as well validated *in vitro* and *in vivo* models through which novel therapeutic targets can be identified and investigated.

Within this project I focused initially on further developing, validating, and evaluating mechanistically a coculture model of gemcitabine resistance, established previously. I demonstrated that the gemcitabine resistance observed in coculture was a product of cell-cell contact, transient in nature, and related to cell density-mediated signalling processes. I discovered that the mesenchymal-like cell lines thought to drive the resistance effect within the model were epithelial cancer cells in origin, rather than a cancer associated fibroblast (CAF) line, verified through genotype and protein signature experiments.

This finding was expanded through demonstration that true pancreatic CAFs did not induce gemcitabine resistance in the coculture model and hence demonstrated the real challenge in isolating true pancreatic CAFs from genetically engineered mouse PDAC tumour tissue using canonical techniques. Nevertheless, the *in vitro* coculture model data was congruent with *in vivo* and clinical gemcitabine efficacy data, suggesting it may have utility as a lower cost model for evaluating efficacy of novel drug combinations with the aim of subsequent translation into the clinic.

The coculture model was used as the foundation of a genome-wide shRNA depletion screen to identify sensitizers of gemcitabine resistance in PDAC *in vitro* culture. The primary screen and subsequent validation screen identified 19 high confidence genes with potential

translational value, of which knockdown sensitised to gemcitabine within this model. This is alongside an expanded list of 444 genes significantly contributing to the resistance phenotype, representing pathways such as MTORC signalling and DNA damage response. This dataset serves as the first shRNA-mediated coculture screen for gemcitabine resistance in PDAC.

My findings lay credence to the value of this model of gemcitabine resistance for preclinical use and provides a robust and voluminous shRNA dataset supporting target identification for the ablation of gemcitabine chemoresistance in PDAC.

Acknowledgements

I would like to express sincere gratitude towards my supervisor Professor Duncan Jodrell for his support, guidance, and encouragement throughout my doctoral studies. Further, I would like to extend this gratitude to Dr Frances Richards, who has provided unwavering and truly invaluable scientific and pastoral support during my time in the laboratory. I would further like to thank Professor Greg Hannon, my secondary supervisor, for scientific guidance throughout my project as well as Dr Nicolas Erard, a fellow doctoral candidate of the Hannon laboratory, with whom I collaborated with extensively through my degree. I also would like to express thanks to the numerous members of the Jodrell laboratory who provided collaboration and support throughout my time, including Ms Jo Bramhall, Dr Séverine Mollard, Dr Siang Boon Koh, Dr Aarthi Gopinathan, and Dr Sandra Bernaldo de Quirós Fernández. The value of pastoral support and guidance provided by Dr Ann Kaminski will forever be appreciated, as will the funding by Cancer Research UK, and the scientific support of the CRUK CI core facilities, most notably from Chandra Sekhar Reddy Chilamakuri in Bioinformatics. Finally, I would like to acknowledge the unconditional support and encouragement from my parents, John and Felicity Mills, my sister Laura Mills, as well as from friendships old and new. A sympathetic friend can be quite as dear as a brother.

List of Abbreviations

CAF	Cancer-associated fibroblast
CDA	Cytidine deaminase
CRISPR	Clustered regularly interspaced short palindromic repeats
ECM	Extracellular matrix
EMT	Epithelial-mesenchymal transition
FLC	Fibroblast-like cell
GEDA	Genetically engineered mouse-derived allograft
GEMM	Genetically engineered mouse model
GSEA	Gene set enrichment analysis
IF	Immunofluorescence
LSL	Lox-stop-lox
PDAC	Pancreatic ductal adenocarcinoma
PK/PD	Pharmacokinetic/pharmacodynamic
PSC	Pancreatic stellate cell
shRNA	short hairpin RNA
TCGA	The cancer genome atlas

Table of Contents

1. Introduction

1.1 Introduction to PDAC

1.1.1 Biology of the pancreas

The pancreas is the primary glandular organ in the human body, forming a key component of both the endocrine and digestive systems. The endocrine system is responsible for production of key hormones such as insulin and glucagon, required to modulate circulating glucose levels, while the digestive system produces enzymes such as lipase and amylase, required for breakdown of food and absorption of nutrients in the stomach and small intestine.

Corresponding to the two functions, the cellular composition of the pancreas is divided between cells driving endocrine functions and those driving digestive functions.

Pancreatic islets are the primary hormone-producing cells, constituting 1-2% of the pancreas volume. The primary component by volume of the pancreas are acini – clusters of acinar cells producing digestive enzymes, or zymogens, required for intestinal absorption. These enzymes are secreted from acini into the interlobular and then main pancreatic duct, leading directly to the duodenum. Abrogated function, characterised by decreased to zero production of the key digestive enzymes, drives diseases such as Exocrine Pancreatic Insufficiency (EPI) (Wilschanski and Novak, 2013).

Investigation into human pancreas form and function as a step within the drug development process relies often on the use of murine models, and therefore corresponding cell types and functions. This similarity is of importance as candidate therapeutics are de-risked (efficacy and toxicity) with pre-clinical murine data on pharmacodynamic and pharmacokinetic effects before human testing. This therefore requires a degree of anatomical and functional parallels between both species. Similarities and differences in both have been reviewed previously, with functional roles of endocrine and exocrine cellular compartments maintained, despite moderately divergent anatomical structures of secretory ducts (Dolenšek, Rupnik, and Stožer, 2015). Coupling biological correlations with a long history of use in research into the pancreas, the mouse is an invaluable tool in pancreatic cancer research.

1.1.2 Pathology of disease

Abrogated endocrine or exocrine functions within the pancreas can lead to onset and development of diseases such as diabetes and EPI, respectively. Pancreatic neoplasia encompass several different diseases. Each is classified based primarily on the cell type of neoplastic origin.

The principal endocrine form of neoplastic disease is pancreatic neuroendocrine tumours (PNETs), making up 1-2% of the total number of clinically significant pancreatic cancers (Zhang et al., 2016). Developing from islet cells, PNETs are largely benign, further sub-divided based on the type of islet cell affected, and whether normal hormone function is abrogated.

Most pancreatic cancers though are carcinomas, arising from the exocrine compartment of the pancreas. Whilst several rare forms of exocrine cancers exist, such as acinar cell carcinoma and pancreatoblastoma, over 95% of exocrine cancers are pancreatic ductal adenocarcinoma (PDAC) (Warshaw and Castillo, 1992). PDAC neoplasms typically but not exclusively arise from epithelial cells lining the secretory exocrine ducts, most typically initiating in the head of the pancreas (Hezel, Kimmelman, Stanger, Bardeesy, and Depinho, 2006).There also exists a rare subset of mucin-related PDAC tumours called mucinous cystic neoplasm (MCNs) which arise in the tail and body of the pancreas separate to the ductal branch (Fernández-del Castillo, 2008).

PDAC evolves initially through progressive growth of non-invasive precursor lesions, most commonly pancreatic intraepithelial neoplasms (PanINs). Through clonally selected proteomic and genetic modifications PanINs progress rapidly, later stages characterised by increasing levels of nuclear atypia and dysregulated growth (Hruban, Goggins, Parsons, and Kern, 2000) (Fig 1.1).

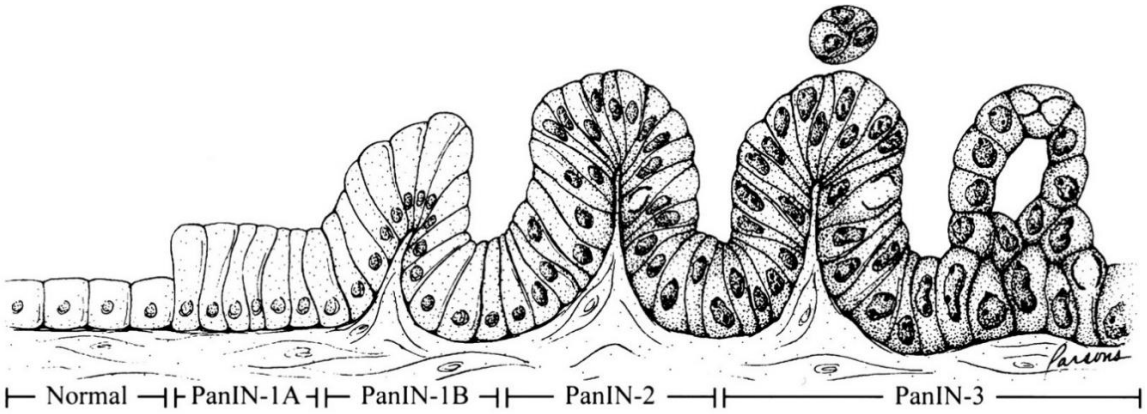

Figure 1.1 Growth stages of pancreatic intraepithelial neoplasms. *Adapted from* (Hruban et al., 2000).

Both PDAC and PanINs are further characterised histologically by a dense desmoplastic reaction within the developing tumour. This is a product of both a high density of non-tumour microenvironment cells such as fibroblasts, endothelial cells, and immune cells, as well as a highly elevated production rate of extracellular matrix (ECM) proteins such as fibronectin and collagen I and III (Erkan et al., 2008; Maitra and Hruban, 2008). This activity will be addressed in further detail later as a causative factor related to disease prognosis and treatment strategy.

A primary prognostic challenge of PDAC is the asymptomatic nature of early disease. Surgery is the only curative option for patients, but less than 20% of PDAC patients present early enough for surgical resection to be a consideration (Sohn et al., 2000). In the other 80% the disease may have invaded locally or spread to distal sites within the body, rendering local resection ineffective for total removal of tumour tissue.

Typical symptoms include malaise, nausea, back pain, weight loss, and often anorexia. All are highly nonspecific, and often attributable to other less morbid maladies. Diagnostic tests rely on endoscopic ultrasound, MRI, CT and PET scans, and can also include serum markers such as CA19-9. These may also provide information on prognosis (Pancreatic Cancer UK, 2016; Vincent, Herman, Schulick, Hruban, and Goggins, 2011).

As of 2011, only 4% of patients presenting with PDAC will be alive within 5 years post-presentation – the highest mortality rate amongst the major cancers (Cancer Research UK, 2014b) . Whilst pancreatic cancer is only the 11th highest cancer in terms of UK incidence

(Cancer Research UK, 2015), it is the 5th leading cause of cancer-related death (Cancer Research UK, 2016; Siegel, Ma, Zou, and Jemal, 2014), reflecting the clinical challenge the disease presents . Of all major cancers, PDAC has had both the lowest gross and relative improvements in survival in the last 50 years (Cancer Research UK, 2011). Reasons for such poor survival include late diagnosis and resistance to most available therapy, at least in part due to the highly desmoplastic nature of the tumours, as will be described later.

Age is one of the predominant risk factors for PDAC development, with the majority of patients in the UK >75 years of age upon presentation (Cancer Research UK, 2014b). Aside from this, there has been minimal conclusive evidence for lifestyle habits as risk factors for PDAC, although a meta-analysis of studies linking alcohol consumption and smoking suggest both have a mild correlation with development of the disease (Becker, Hernandez, Frucht, and Lucas, 2014). Non-lifestyle biochemical and genetic risk factors will be discussed later. Type 2 Diabetes has been demonstrated as a primary association with development of PDAC, although typically driven by genetic components coupled with poorly balanced diets and low levels of exercise (Huxley, Ansary-Moghaddam, Berrington de González, Barzi, and Woodward, 2005). Pancreatitis, or inflammation within the pancreas, is also a significant driver of carcinogenesis within the organ, itself typically driven by alcohol consumption or presence of gallstones (Bansal and Sonnenberg, 1995; Lowenfels et al., 1993).

1.1.3 Molecular and genetic characterisation

The pathophysiological profile of PDAC is well documented and provides mechanistic insights on disease establishment and growth - an invaluable tool for the development of novel treatment strategies.

From a molecular perspective, onset and growth of PDAC is driven by a combination of aberrant paracrine and autocrine signalling cascades, both within PDAC epithelial nests and between the tumour and the adjacent microenvironment. High expression of growth factors and their cognate receptors, such as IGF/R, HGF/R, and FGF/R are all drivers of PDAC cell growth and invasion (Coleman et al., 2014; Denduluri et al., 2015; Matsuda et al., 2014; Matsushita, Gotze, and Korc, 2007; Rucki et al., 2017), alongside broad-acting signalling molecules such as TGFβ, β-integrin, and focal adhesion kinase (FAK) (Begum et al., 2017; Jiang et al., 2016; Principe et al., 2016). Through activation of pro-tumourigenic signalling

pathways such as the MAPK and WNT cascades (Pasca di Magliano et al., 2007), as well as repression of pro-apoptotic pathways through JAK/STAT activation (Corcoran et al., 2011), these molecules form an integral component driving the rapid progression seen in PDAC.

PDAC is characterised genetically by somatic mutation of key cell growth and protection genes such as *KRAS*, *TP53* and *SMAD4*. Over 90% of all PDAC cancers contain mutant *KRAS*, and at least 50% have mutant *TP53* (Bailey et al., 2016; Biankin et al., 2012). The combination of both mutations accelerates growth through KRAS-mediated MAPK signalling whilst removing standard DNA repair and growth arrest systems mediated via TP53. Despite the known incidence of mutations, neither gene nor associated product is directly targetable, and due to wide-ranging cascade activations, form challenging barriers to repression of tumour growth in patients. Mutations in genes such as *CDKN2A*, *SMAD4*, and *ARID1A*, further account for driver mutations in >5% of PDAC tumours (Aguirre et al., 2017). As well as single genes, mutations in major pathways such as those of chromosome modification and DNA damage response are all associated with and causative of PDAC development (Bailey et al., 2016; Biankin et al., 2012; Collisson et al., 2011).

The last decade has seen development of multiple genome-wide gene expression prognostic signatures, in an effort to standardise disease classification and more importantly derive valuable and significant predictive insights from quantitative genetic meta-analysis. Four models in particular have been established and built traction: the Collisson's, Bailey's, and Moffitt's (tumour and stroma) classifications (Bailey et al., 2016; Collisson et al., 2011; Moffitt et al., 2015). Each model uses gene expression data directly from pancreatic cancer tissue to classify tumours into sub-types, with Moffitt's model further classifying the stromal subtype and associated prognosis. The true prognostic value of each and overlap in gene signatures was investigated by Birnbaum et al. using clinical and gene expression data from a further 846 primary PDAC samples, classifying the data using each of the above reported signatures. Of the four, only Collisson's signatures ("classical", "quasi-mesenchymal", and "exocrine-like") did not demonstrate significant prognostic value (Birnbaum, Finetti, Birnbaum, Mamessier, and Bertucci, 2017). Notably Moffitt's stroma classifier indicated a possible contribution of the activated stroma in PDAC progression, with 2-year median OS of 49% with "normal" stroma signature but only 34% with the "activated" stromal signature. Such classification schemes are still to be implemented into routine clinical practice for

helping define treatment strategy but may hold particular value in the future through investigation of signature correlation with therapeutic responses.

1.2 Clinical management of PDAC

1.2.1 Current clinical paradigms

Relative to other major cancers, PDAC treatment has experienced relatively minimal changes in treatment strategy through the last decade.

PDAC patients present at one of four primary clinical stages, i) local resectable, ii) borderline resectable, iii) locally advanced, and iv) metastatic. When patients present with local resectable or borderline resectable disease, Whipple resection (pancreaticoduodenectomy) surgery remains the only curative approach, with a 5 year survival of over 25% (Vincent et al., 2011). Operative mortality from tumour resection is low globally. Despite this, as 80-90% of patients present with non-resectable cancer (Varadhachary et al., 2006), this approach is rarely suitable for treatment. Instead, therapeutic options capable of targeting both primary and secondary sites of tumour growth are required.

Gemcitabine, a nucleoside analogue therapeutic, has formed a central part of this paradigm since approval in 1997, when a comparison to fluorouracil administration demonstrated an improvement in median overall survival from 4.4 months to 5.6 months (Burris et al., 1997), with a subsequent single agent phase 3 trials demonstrating a median OS range from 5.0 to 7.2 months (Di Marco et al., 2010). As per the mechanism of other nucleoside analogues such as cytarabine, gemcitabine exerts a cytotoxic effect through incorporation into replicating DNA strands and inducing replication fork stalling and DNA strand breaks. Acting selectively on rapidly growing cells, it exhibits preferential effect on cancer tissue over less replicative healthy tissue (Plunkett et al., 1995).

Recent years have seen the development and introduction of more advanced chemotherapy cocktails for treating PDAC, focused on marginal efficacy improvements through complex dosing regimens, to best maximise the effect of each agent alone. Few have demonstrated significant improvements when compared to gemcitabine alone. Despite this, the past decade has led to one primary chemotherapy regimen widely incorporated into clinical practice in place of gemcitabine - FOLFIRINOX (FOLinic acid, Fluorouracil, IRINotecan, and OXaliplatin). FOLFIRINOX can increase PDAC median OS to 11.2 months but introduces an

increased adverse event profile, which can be too harsh for weaker patients, common amongst the older population inflicted with this disease (Conroy et al., 2011).

The combination of albumin-bound paclitaxel (nab-paclitaxel; Abraxane^{TM}) and gemcitabine has also been shown to be advantageous over gemcitabine alone (median OS from 6.7 to 8.5 months), but similarly to FOLFIRINOX, has an increased side effect profile including myelosuppression to be wary of in clinical practice (Von Hoff et al., 2013).

1.2.2 Novel targeted strategies

Alongside the development and improvement of broad-acting chemotherapy combination strategies, there has been significant evaluation of the value of targeted treatment strategies for PDAC, as has demonstrated value in many other cancers.

Noting the majority of PDAC tumours express high levels of EGFR, there have been multiple trials combining approved EGFR inhibitors with gemcitabine. The EGFR inhibitor erlotinib was approved by the FDA for advanced PDAC in combination with gemcitabine after a minor increase in median overall survival (OS) of 5.91 to 6.24 months, but the EGFR extracellular domain-binding antibody cetuximab, did not show significant benefit (Moore et al., 2007), perhaps indicating an activity of EGFR that acts independent of activation of the extracellular domain

The highly fibrotic nature of the pancreatic tumour leads to a strict need for pervasive vasculature within tumours to provide growth nutrients and support metastatic spread. Despite preclinical studies indicating value in combining inhibitors of vascular endothelial growth factor (VEGF) receptor, typically required for tumour vasculature, a phase III 535 patient trial with VEGFR inhibitor bevacizumab with gemcitabine showed no significant OS benefit (Kindler et al., 2010).

With such minimal incremental improvements in PDAC survival from even the most successful of trials and regimens, a major challenge remains in addressing perhaps the major driver of PDAC, KRAS. Targeting and inhibiting mutant KRAS activity has been a primary goal of translational pancreatic cancer research over the past couple of decades, but due to the protein's fully internal and non-kinase, non-directly targetable activity this has been a challenge (Downward, 2003; Sun et al., 2012) and various approaches have not

been effective. After translation the KRAS protein needs to localise to the plasma membrane for activation of downstream proteins. This localisation requires farnesyltransferases to farnesylate the nascent protein. A farnesyltransferase inhibitor only increased median OS from 5.98 months to only 6.34 months, when compared to gemcitabine alone in Phase III (Van Cutsem et al., 2004). Whilst the targeting of KRAS remains elusive in patients, the development of advanced drug delivery and targeting technologies over recent years has led to new attempts at targeting mutant KRAS in mice. Exosomes loaded with siRNA targeting the primary *Kras* G12D mutation were trialled in orthotopic tumours as well as in a genetically engineered mouse model (GEMM) of PDAC with significant survival increases in each (Kamerkar et al., 2017). Targeting of downstream effectors of KRAS have also been investigated, with the MEK inhibitor selumetinib combined with the AKT inhibitor MK-2206 compared to FOLFOX in gemcitabine-resistance PDAC patients. With a median OS of 3.9 months in the experimental arm compared to 6.7 months on FOLFOX, this regimen was not progressed (Chung et al., 2017). Despite these challenges, recent years have seen the beginnings of development for small molecular inhibitors of KRAS (Ostrem and Shokat, 2016), which if feasible may hold exciting promise in PDAC treatment.

Other approaches currently progressing through preclinical development and clinical trials include those with approved utility in other major cancers, such as targeting of DNA damage response (DDR) pathways. Targeting of DDR pathways, and therefore the cells ability to recover from damage, alongside gemcitabine, has shown promise in pancreatic GEMMs, laying the foundation for an in-human combination trial (Fokas et al., 2012; S-B Koh et al., 2018; Siang-Boon Koh et al., 2015; Wallez et al., 2018). Another approach is immunotherapy - redirecting the immune system to target tumour tissue. Despite initial low response rates for anti-CTLA-4 and anti-PD-1 therapy in PDAC (Aglietta et al., 2014; Royal et al., 2010; Weiss et al., 2018), recent investigations into priming the PDAC tumour for immune targeting may yield value (Le et al., 2015). The PDAC desmoplastic stroma plays an important role in maintaining tumour immune privilege (Feig et al., 2013; Kraman et al., 2010) and so therapeutic approaches to targeting the PDAC stroma to overcome drug resistance (as described below) may have the added benefit of enabling immunotherapy.

1.2.3 Challenges in treatment resistance

Independent of the efficacy and value of a therapeutic, if a tumour either is inherently resistant or rapidly acquires resistance to it then value can be immediately negated. Drug resistance is a major obstacle in PDAC clinical strategy, and a major explanation for the low survival rates observed. A range of genetic and molecular markers of resistance have been documented (Hagmann, Jesnowski, and Löhr, 2010; K. P. Olive et al., 2009; Voutsadakis, 2011), as well as entire cellular transformation processes such as epithelial to mesenchymal transition (EMT) (X. Zheng et al., 2015). Each marker and panel can inform specific factors influencing drug effect and predict clinical efficacy.

Pancreatic cancer exhibits high levels of inherent resistance to most therapies above and beyond that typically seen in other major cancers (Brahmer et al., 2012; Chong and Jänne, 2013; Rahib et al., 2014; Royal et al., 2010). This is partly due to both intrinsic resistance mechanisms, such as altered gemcitabine metabolism via upregulation of cytidine deaminase (CDA) (Weizman et al., 2014), and extrinsic mechanisms, such as stroma-conferred immune evasion signalling and structural barriers to drug efficacy (Feig et al., 2013; K. P. Olive et al., 2009).

An ability to target and ablate these resistance mechanisms holds value not only for direct effects on tumour growth, but also for the larger potential survival increases for combination with already approved strategies such as gemcitabine and FOLFIRINOX. As such the past decade has included significant efforts towards identifying, understanding, and targeting these mechanisms, yielding some positive results, although alongside many associated challenges.

1.2.4 Molecular basis of resistance

Understanding the roles and functions of various proteins and genes driving this resistance forms an essential foundation to support development of resistance-targeting therapeutics. As an initial step to understand these mechanisms, research efforts have focused on identifying and validating informative biomarkers for gemcitabine efficacy, both pharmacokinetic (PK) and pharmacodynamic (PD).

Gemcitabine PK and resistance biomarkers in PDAC relate primarily to indicators of enhanced drug metabolism or reduced drug uptake. Overexpression of nucleoside efflux transporter molecules such as MRP5 correlates immunohistochemically to resistance to gemcitabine (Hagmann et al., 2010), indicating in some patients an increased level of gemcitabine efflux may explain reduced levels of efficacy. Similarly, low expression of nucleoside uptake molecules such as ENT1 have been correlated with increased gemcitabine resistance in PDAC (Spratlin et al., 2004). This may be a major factor driving drug resistance, as a cell's ability to rapidly expunge active molecules via membrane transporters will reduce the bioavailability. High expression of gemcitabine metabolising protein CDA correlates with gemcitabine resistance levels in patients, suggesting that increased metabolism of the active form of gemcitabine, dFdC, to the inactive metabolite dFdU may reduce cytotoxic effects (Ohhashi et al., 2008; Weizman et al., 2014). Downregulation of dCK is associated with gemcitabine resistance also (Ohhashi et al., 2008).

Coupled with this, recent years have highlighted interrogation of EMT as a mechanism through which PDAC cells evolve and become resistant to gemcitabine and other therapeutics (Rhim et al., 2012; X. Zheng et al., 2015), noting also poor prognosis significantly correlated with high expression of EMT-related genes (Aguirre et al., 2017). Pancreatic tumours expressing high levels of EMT factors and mesenchymal markers, such as ZEB1 and SDF1, are correlated significantly with therapeutic resistance (Arumugam et al., 2009; Weekes et al., 2012), indicating that perhaps either the more motile properties of mesenchymal cells, or signalling cascades induced via EMT may have direct causative implications in modulating resistance to gemcitabine. The specific mechanism through which EMT modulates resistance to gemcitabine has been explored further, with indications that mesenchymal transition can increase expression of nucleoside efflux transporters as detailed above.

While each of above presents opportunity for developing biomarkers with clinical utility in informing likelihood of resistance in the clinic, the challenge remains that independent of our awareness of resistance, alternate treatment options remain minimal.

1.2.5 Approaches to combat resistance

Leveraging this expanding understanding of mechanisms of treatment resistance, therapeutic targeting of resistance has begun to be explored, in particular around stroma-conferred resistance mechanisms.

For example, targeted depletion of sonic hedgehog (SHH) in the PDAC stroma with IPI-926 led to a commensurate depletion in PDAC stromal content itself, which within the KRas ^{G12D}; P53 ^{R172H}; PDX1-cre (KPC) model of pancreatic cancer enhanced delivery and therefore efficacy of gemcitabine on murine survival (K. P. Olive et al., 2009). Unfortunately, in a clinical trial (NCT01130142), the gemcitabine plus IPI-926 combination paradoxically reduced survival in patients when compared to gemcitabine alone (Kenneth P Olive, 2018). Following further preclinical investigation, it was revealed that SHH-targeted stromal ablation unveiled not only pro-tumourigenic effects of the stroma, but also anti-tumourigenic restraining effect (Özdemir et al., 2014; Rhim et al., 2014). Therefore, indicating the need to target therapeutically more specific elements in the stroma and associated resistance mechanism, without compromising any positive anti-tumourigenic functions.

1.3 Role of stroma and tumour micro-environment in PDAC

1.3.1 Cell type composition and introduction

Pancreatic tumours have amongst the highest stromal component and density when compared to other major cancers (A. Neesse et al., 2011). This dense and fibrotic component forms a major unit in the cancer's arsenal for growth and immune evasion, supporting both tumour seeding as well as later stage metastatic transformation. With such an active stromal component, pancreatic tumours present as one of the more heterogenous major cancers from both inter- and intra-tumour perspectives.

Intertumourally, heterogeneity is exemplified by the variety of WHO PDAC histological characterisations (Bosman, Carneiro, Hruban, & Theise, 2010), as well as the widely documented genetic heterogeneity observed across PDAC subtypes (Bailey et al., 2016; Donahue et al., 2012; Lili et al., 2014; Moffitt et al., 2015; Waddell et al., 2015). Such subtypes, whilst often not completely dissimilar in cellular composition (Adsay et al., 2000; Kosmahl et al., 2005; Lüttges et al., 1998), often contribute to a diverse range of clinical

outcome and treatment responses (Birnbaum et al., 2017), indicating the importance of accurate classifications as part of a physician's treatment evaluation.

Intratumourally, the wide range of cell types present in the stroma are a direct example of cellular heterogeneity within tumours. Cytogenetic heterogeneity has been observed even at in adjacent tumour glands, as has genetic heterogeneity been observed in distinct intratumour regions (Nakamura et al., 2007). While such diversity has inspired clinical trial design to personalise treatment approach (Chantrill et al., 2015), an underlying lack of understanding on the complex roles and interplay of tumour components remains a barrier to clinical success (Moffitt et al., 2015).

Elucidating specific roles of individual cell types within the tumour setting is difficult, although functions of the activated fibroblastic component, the extracellular matrix, as well immune cells in within the stromal nest have all been widely investigated.

Cancer-associated fibroblasts (CAFs) are a major mediator of both of pro- and anti-tumourigenic signalling in the PDAC microenvironment. CAFs are activated forms of pancreatic stellate cells (PSCs), themselves a canonical mesenchymal stellate cell with morphological and functional similarities to hepatic stellate cells (HSCs) (Erkan et al., 2011). In a quiescent non-activated state, PSCs support pancreatic functions and infrastructure through production of extracellular matrix (ECM) proteins such as collagen, MMPs, fibronectin, and laminin (Jaster, 2004), and through active matrix modelling and turnover, support homeostatic functions of pancreatic tissue. Tissue damage, carcinogenesis, and the associated release of stimulating factors such as reactive oxygen species and TNFα all serve to induce activation of PSCs into CAFs (Apte et al., 1999; Apte, Pirola, and Wilson, 2012; Mews et al., 2002), characterised by a morphological transition into myofibroblastic phenotypes, inducing rapid proliferation increases and increased production of ECM proteins, all of which contribute to the highly fibrotic nature of PDAC. CAFs themselves can further cluster into different functional populations, characterised by expression of molecular markers such as FAP, which can indicate further roles in modulating immune cell activity and growth of cancer cells (Feig et al., 2013; Öhlund et al., 2017).

Alongside mesenchymal cells, there exists a diverse population of immune and inflammatory cells, both resident and accumulated in response to pancreatitis and PDAC

development. Immunosuppressive cells such as tumour-associated macrophages (TAMs), myeloid-derived suppressor cells (MDSC), and regulatory T cells (T_{reg}s) all contribute towards immune evasion within PDAC through a combination of altered tumour metabolism, migration patterns, and protections from apoptotic signals (Campbell, Albo, Kimsey, White, and Wang, 2005; S. Hinz et al., 2007; Stromnes et al., 2014).

As part of the ECM, MMPs such as MMP-2 and MMP-9, produced by cancer cells as well as CAFs, regulate invasive properties of the epithelial cells within the tumour (Ellenrieder et al., 2000; Shan et al., 2017), while hyaluronic acid promotes angiogenesis, cell migration, and rapid proliferation within the PDAC compartment (Jacobetz et al., 2013). Further, the production of the structural protein collagen I in pancreatic cancer each have documented roles in supporting the carcinogenic process (Armstrong et al., 2004; Shields, Dangi-Garimella, Krantz, Bentrem, and Munshi, 2011), altogether exemplifying the major role the pancreatic stroma plays in tumour growth and metastatic expansion.

1.3.2 Pro- and anti-tumourigenic stromal components

Investigation into the effects of the stroma on pancreatic tumour form and function is challenging, given the diverse range of cells involved, alongside difficulty in disentangling the roles of each within the greater mass. Nevertheless, a complete understanding of cellular roles, and the effects of upregulation or depletion, are key to target identification, validation, and downstream drug development.

While the stroma has broadly pro-tumourigenic roles, there exist a range of essential tumour-suppressive processes conferred, alongside immunosuppressive activities of resident immune cells detailed above. These include anti-proliferation functions of adipose-derived stromal cells (Cousin et al., 2009), miRNA-controlled targeted apoptosis (Han et al., 2018), as well as general increases in EMT and PDAC proliferation and decreases in cell differentiation through genetically targeted stroma depletion (Rhim et al., 2014; X. Zheng et al., 2015).

Challenges such as with the IPI-926 trial highlighted above indicate the absolute imperative need for thorough understanding of stromal contributions to PDAC development and drug resistance, to support identifying techniques to target just those tumour-promoting

properties, whilst supporting the maintenance or enhancement of tumour-suppressive functions.

While tumour-suppressive functions of the stroma have been less documented, tumour-promoting functions have been numerous and diverse, perhaps due to the relatively recent realisation of the extent of tumour-suppressive stromal functions

From a structural perspective, enhanced collagen and hyaluronan in the ECM as produced by CAFs can compress the tumour vasculature and reduce perfusion throughout (Jacobetz et al., 2013; Özdemir et al., 2014; Provenzano et al., 2012). This creates a physical barrier for drug delivery as well as reducing oxygenation of tumour tissue, creating a hypoxic environment supporting tumour growth.

CAFs have well documented effects on driving tumour growth and development. Firstly, production of CXCL12 on FAP-expressing cells stimulates T cell exclusion, therefore protecting growing tumours from the deleterious eye of the immune system (Feig et al., 2013). Secondly, increased production of ECM components such as hyaluronan through CAF activation can enhance cell proliferation, migration, and subsequent invasion (Provenzano et al., 2012). Finally, production of the prostaglandin COX-2 can drive PDAC proliferation, as well as myofibroblastic activity enhancing oxidative phosphorylation through increased glucose absorption and lactate production, which in turn increases the invasive potential of PDAC cells (Omura et al., 2010; Shan et al., 2017).

Together there exist multiple mechanisms of tumour promotion within the stroma, although targeting them via cellular ablation may lead to deleterious effects given the wide range of functions that may be affected. Therefore, identification of subsets for targeting, or inhibition of singular pathways where possible, may lead to more predictable clinical outcomes.

1.3.3 Targeting stroma for clinical benefit

Historically targeted therapy development in pancreatic cancer has been challenging with minimal improvement on patient survival. This is true in particular when trialling targeted approaches that show clinical benefit in other major cancers, such as has been seen with anti-EGFR, AKT and VEGF approaches. The multi-factorial contributions of the stroma to

carcinogenesis means targeting of any one mechanism of tumour promotion may quickly be nullified through compensatory signalling and growth via one of the multiple other channels of growth, immune evasion, and proliferation support.

There are a range of approaches currently developing both towards and in the clinic, focused on disrupting the cancer-stroma relationship, and removing the stroma's ability to support and protect the tumour. Depletion of hyaluronic acid (HA) within the pancreatic stroma using a PEGylated human recombinant PH20 hyaluronidase (PEGPH20) increased gemcitabine delivery and efficacy through improving vascular perfusion (Jacobetz et al., 2013). This observation led to successful phase I and phase II trials in patients with advanced disease (S. Hingorani et al., 2018; S. R. Hingorani et al., 2016), culminating in a currently active phase III trial in stage IV disease (Doherty, Tempero, and Corrie, 2018). Further, focal adhesion kinase (FAK) plays a role in driving the highly fibrotic state of PDAC stroma, coupled with support of immunosuppressive exclusion of cytotoxic T cells (Furuyama et al., 2006; Jiang et al., 2016), with its specific inhibition through use of selective FAK inhibitor VS-4718 limiting tumour growth and progression with the KPC mouse model and improving response to a PD-1 antagonist. These data have led to an ongoing phase I trial of the FAK inhibitor in combination with gemcitabine and PD-1-targeting pembrolizumab (Wang-Gillam et al., 2017). Together these studies form a core of a body of developing clinical studies into the utility of stromal targeting in pancreatic cancer.

While PDAC is typically diagnosed late, stromal remodelling in the disease occurs throughout carcinogenesis, pre-seeding the pancreatic niche during inflammatory pancreatitis to support PDAC formation (Apte et al., 2004; Whatcott et al., 2015). If these stromal mechanisms are better understood and identified at an early stage, prophylactic targeting may yield benefit in reducing PDAC incidence. Nevertheless, focusing translational efforts on the stromal compartment in PDAC holds real opportunity in exploring novel treatment and therapy improving strategies for PDAC.

1.4 Use of models to identify and develop new treatment strategies

1.4.1 Overview

Breaking down translational drug development into its modular constituent parts, both target identification and preclinical lead optimisation lean heavily on the integrity and predictive power of *in silico*, *in vitro*, and *in vivo* research models. Each step has an inverse relationship between resource requirements and predictive power. For example, monoculture *in vitro* assays can be run high-throughput for screening, but *in vivo* low-throughput models of disease such as those in mouse and rat remain best for modelling predictive PK/PD in humans. There is a defined need to improve this ratio of cost to power for both *in silico* and *in vitro* models to better de-risk therapeutic development whilst maintaining relatively lower resource requirements.

1.4.2 *In silico* approaches for drug target identification

Improvements in *in silico* analysis have been driven by an increase in accrued -omics data, processing power, as well as machine learning and deep learning models for supporting target identification. Large datasets can be mined for correlative indicators of disease mechanisms, as well as for tracking response to therapeutics. Machine learning algorithms and toolsets have begun to be evaluated within PDAC alongside standard linear and logistic regression modelling of disease diagnosis and prognosis. Artificial neural networks (ANNs) can both decipher disease mechanisms as well as predict survival from varying clinical and histopathological data. When comparing performance to single risk attributes such as tumour size, logistic regression has remained superior (Hayward et al., 2010), although the real value of ANNs has been in combination of multivariate data and identification of novel correlative factors for PDAC progression, such as leukocyte counts (Ansari et al., 2013), or improved interpretation of complex output data such as that from elastography (Săftoiu et al., 2008). Development of *in silico* models to predict drug efficacy in PDAC has been minimal despite some indications of clinical utility (Kumar, Chaudhary, Singla, Gautam, and Raghava, 2014; Ma et al., 2016). As such, the field remains at an early stage with significant progress to be made before real applicability of output data in informing clinical selection.

1.4.3 *In vivo* model development

Murine *in vivo* models of PDAC remain the cornerstone data point preceding human testing for novel treatment strategies. Coupled with a broadly similar biological structure and functions between the murine and human pancreas, this system allows for an advanced insight into toxicity profiles of novel drugs, itself perhaps the single largest concern to be addressed prior to in-human studies.

The development of predictive murine models for cancer have recently focused on patient derived xenografts (PDXs), as well as cell line-derived xenografts. For PDXs, patient tumour tissue is isolated and is implanted subcutaneously or orthotopically into immune-compromised mice and used for subsequent preclinical testing. A major advantage is the ability to evaluate therapeutic efficacy in patient tissue within a murine model, and has led to validation of therapeutic regimens that subsequently led to clinical investigation (Kawaguchi et al., 2017; Lipner et al., 2016)

While this model allows assessment of individual patient tissue directly, it does not allow investigation of effects on human stromal or immune cells, due to the absence of these cells within PDX recipient immunodeficient mice. Further the biological differences between the human tumour tissue and the initial murine stromal compartments within most PDX models limits investigational utility in PDAC when compared to other less stroma-rich cancers, where evaluating the role of and effect on the stroma are of less importance.

This challenge can be compensated for through use of genetically engineered mouse models (GEMMs), such as the Kras ^{G12D}; p53 ^{R172H}; Pdx1-cre (KPC) model in pancreatic cancer, whereby both tumour and stroma are genetically matched to each other and the host mouse. In this model, through targeted genetic manipulation, the KPC mouse express mutant *Kras* and mutant *Tp53* restricted to pancreatic epithelial tissue (S. R. Hingorani et al., 2005). This leads to early onset development of focal PanIN and then PDAC, with abundant desmoplastic stroma, intact immune system, and metastatic PDAC growth associated with the same co-morbidities as in man. This model has been a major tool for PDAC translational development, in particular as a system to best understand stromal roles and structures *in vivo*, although additional GEMMs do exist for interrogation of further PDAC properties (Gopinathan, Morton, Jodrell, and Sansom, 2015).

Whilst murine studies certainly remain an essential component in translational development, they are extremely cost and time intensive tools, requiring many months per low-throughput study, and therefore not amenable to large scale genetic or chemical screening. As such their utility is reserved for higher confidence de-risked therapeutic programs.

There therefore exists a need for models supporting generation of novel biological data, unlike *in silico* modelling, and in a high-throughput and low-cost approach, unlike *in vivo* techniques. It is within this gap that the foundation of preclinical drug development sits, *in vitro*.

1.4.4 The role of *in vitro* models in the drug development process

In vitro models encompass cell-based experimentation performed outside of their normal biological context, by definition on glass, in practice plastic and media. Forming one of the primary steps within the cancer drug development process, there has been major focus over the preceding decades in improving both the models themselves as well as the techniques through which we can analyse and interpret their output data.

The primary advantages of these models traditionally lie within the simplicity of protocol, the low-cost of operation, and the capacity to be automated and scaled to interrogate large numbers of hypotheses simultaneously. One challenge though remains significant: the extrapolation of data back to the biology of human disease. This challenge is a particular barrier in pancreatic cancer, wherein the complex and dynamic interplay of many cell types in the tumour microenvironment, and their contribution to drug efficacy and resistance are less easily modelled and assayed.

These advantages noted above have been further solidified over the past decade, through the introduction of better cellular characterisation to normalise protocols and improve reproducibility, the creation of increasingly smaller scales of experimentation, such as in 1536-well plate drug screening (Minuesa et al., 2014), as well as the development and commercial production of large and powerful machinery with which these processes can be automated. Such developments have enabled large scale screens of cancer drugs that have identified genomic markers of drug sensitivity (Barretina et al., 2012; Garnett et al., 2012; Stransky et al., 2015).

Despite this, the challenge remains: improving our ability to accurately recapitulate the biological environment *in vivo* in an *in vitro* setting to improve translation and functional correlation between systems. By achieving this, the power of *in vitro* models within the drug development setting can be exponentially increased, with definitive benefits in strengthening the foundation of preclinical data in advance of *in vivo* experimentation.

1.4.5 Development of novel *in vitro* models

Despite their tenure and value, *in vitro* models have remained relatively basic, whereby monoculture cell line systems are a mainstay of preclinical therapeutic development. These can be particularly poor at predicting therapeutic efficacy in cancer, given the absence of tumour-specific geospatial architecture and the growth and survival variation introduced through growth on plastic. This paucity of prediction is exacerbated in PDAC specifically, due the significant contribution of different cell types within the stroma to drug efficacy. Nevertheless, *in vitro* monoculture models are a core of multiple successful preclinical investigations in PDAC, as has been seen for the foundation of targeting FAK in PDAC (Furuyama et al., 2006; Jiang et al., 2016).

The challenge of poor predictivity of *in vitro* data due to the poor representation of tumour dynamics has been tackled via one of two methods. Firstly, improvements in cell line handling technologies as well as improved characterisation of existing lines has allowed large high-throughput monoculture screening to become feasible. This supports generation of data on translational efficacy across wider heterogenous cell line panels and minimises cell line-specific artefacts of efficacy, with demonstrated value across multiple indications (Brammeld et al., 2017; Garnett et al., 2012).

Secondly, improving the complexity of *in vitro* models to better represent the tumour microenvironment within PDAC allows for a higher probability of identifying therapeutics that show efficacy in PDAC. This has been tackled to various degrees.

To better recapitulate the tumour architecture and geospatial cellular relationships there has been a movement towards development of three dimensional (3D) *in vitro* systems of experimentation, such as spheroids, organoids, and hydrogel-based culture, each of which has been studied in the context of PDAC.

Spheroids are rounded clusters of cells typically produced in a round bottomed low cell adhesion plastic well or via the hanging drop method, whereby cells cluster in a droplet hanging from the bottom of an inverted plastic cone. While they support investigation into clustering properties of tumour cells in monoculture and coculture with other cell types, the difficulty in producing uniformly sized and structured spheroids, as wells as being a relatively low-throughput system make large scale drug and genetic screening a challenge (Friedrich, Seidel, Ebner, and Kunz-Schughart, 2009).

Organoids represent a novel and rapidly evolving field focused on recapitulating organ-like cellular structures *in vitro* structurally similar to organs themselves (Clevers, 2016). For cancer research, tumour organoids have been grown using patient tumour tissue as well as tissue isolated from PDX mouse models, often embedded in Matrigel, modelling the ECM physical properties *in vivo*. While morphological variation and a high resource requirement remain challenges for the application of this model in high-throughput screening, histopathological correlation with donor tissue (Fujii et al., 2016; Sachs et al., 2018), including PDAC (Boj et al., 2015) presents an exciting avenue through which tumour dynamics can be modelled accurately in vitro. Further, recent studies have demonstrated both a correlation between host patient and organoid drug responses (Kawaguchi et al., 2017) as well as correlation between clinical efficacy and organoid efficacy for some smaller drug screens (Broutier et al., 2017; D. Gao et al., 2014; Verissimo et al., 2016; Vlachogiannis et al., 2018). The major burden of proof for organoids will be the ability for organoids to better predict therapeutic efficacy than predicted in other lower cost higher throughput *in vitro* assays, which is yet to be determined.

On a 2D scale, novel models have been developed that maintain the low-cost nature of *in vitro* experimentation while improving and diversifying the biological readouts. For example, development and incorporation of assays and plate technologies such as those used for transwell assays analysing paracrine signalling interactions, as well as scratch-wound assays for evaluating cell invasion properties (Cheng, Kohi, Koga, Hirata, and Sato, 2016; Joost et al., 2012). While each has value in understanding deep mechanistic relationships in cancer cell growth, applicability to high-throughput screening is less evident, as apoptosis and cell viability screens remain the cornerstone of drug efficacy evaluation.

1.4.6 Screening techniques for drug development *in vitro*

A major value of the low cost and high-throughput nature of 2D *in vitro* models is the amenability to interrogation using large scale genetic and drug screening. Genetic screening in particular, when performed on a whole-genome approach, allows assessment of cell phenotypes in response to manipulation of every single gene, independent of the existing body of literature surrounding it. This allows for novel target identification, which is not the case typically for drug screening, where there is a reliance on an existing synthesised drug showing unexpected efficacy.

Genetic manipulation screening techniques have seen rapid development over recent decades, with RNA interference techniques such as small interfering RNA (siRNA) and short hairpin RNA (shRNA) screening, as well as gene-editing screening techniques leveraging the activities of zinc finger nucleases (ZFNs), transcription activator-like effector nucleases (TALENs), and CRISPR/Cas9 screening. The current gold standards for mRNA manipulation, measured on specificity, stability, and ease of transduction are shRNA-based (Klinghoffer et al., 2010), and similar CRISPR-based for direct gene editing (Gaj, Gersbach, and Barbas Iii, 2013). While both of these techniques can lead to similar hit-calling in cell viability screens, both also identify true positive hits unique to that approach (Morgens, Deans, Li, and Bassik, 2016), exemplifying value in each alone as well as when performed together. Each of these techniques is a major tool in identifying novel drug targets through *in vitro* screening, and have been applied in PDAC monoculture already to this end (Kurahara et al., 2016; Muzumdar et al., 2017).

1.4.7 Incorporating stromal analysis into *in vitro* models in PDAC

As noted above, modelling the stromal dynamics pervasive in PDAC tumours is a defined need in *in vitro* models used for screening. Consideration of phenotype in the absence of these intratumoural dynamics may reduce the number of targets and drugs identified that also have efficacy in the presence of the stromal compartment. To this end, incorporation of coculture conditions, culturing cancer cells alongside stromal cells, in particular CAFs, has formed a major focus of recent *in vitro* model development in PDAC.

From the 3D landscape, and in particular with organoids, protocols have begun to be developed that incorporate multiple PDAC stromal cell types in culture (Öhlund et al., 2017;

Seino et al., 2018) to better build a model representative of the tumour microenvironment, including organotypic cultures (Froeling et al., 2009), themselves both cost and time-intensive techniques not amenable to high-throughput screening. Across additional cancers similar models have been further employed with defined correlation with *in vivo* screening results (Ivanov and Grabowska, 2017; Onion et al., 2016).

2D models of coculture on plastic have used the combination of breast tumour cells with stromal fibroblasts for the purpose of drug screening, generating a large dataset around ablating stroma-conferred RAF inhibitor resistance in breast cancer cells, with similar studies conducted in a multiple myeloma coculture model (McMillin et al., 2010; Straussman et al., 2012). Given the documented role of stromal cells and tumour geospatial dynamics in modulating drug resistance in PDAC (Chauhan et al., 2013; K. P. Olive et al., 2009; Phan et al., 2013; Provenzano et al., 2012), it follows there exists a value in incorporating such dynamics *in vitro* for screening, to improve the likelihood of clinical efficacy of therapeutics showing promise within the model. Given gemcitabine remains as one of the few single agent therapeutics to confer clinical benefit for PDAC patients, leveraging the stromal effect on gemcitabine efficacy through an *in vitro* model may hold value in preclinical drug development.

To this end, an *in vitro* coculture model of PDAC was previously developed within our lab, by culturing epithelial PDAC cells together with CAF-like cells (Xu, 2015). A major finding of this model was an ability to induce gemcitabine resistance in PDAC cells in coculture with the CAF-like cells, whilst the same PDAC cells were sensitive to gemcitabine in monoculture, mirroring coculture-driven resistance phenomena reported in similar coculture models across other cancers (Straussman et al., 2012). Noting the significant resistance to gemcitabine observed in patients, this model holds potential value as one of the first low-cost and novel systems of gemcitabine resistance in PDAC, laying the foundation for ongoing interrogation of the mechanistic nature of resistance and suitability for high-throughput screening within pancreatic cancer.

1.5 Project aims

The aim of this project was to perform mechanistic studies to further evaluate and validate a coculture model of gemcitabine resistance in PDAC whilst concurrently leveraging this model in a whole genome RNA interference screen to identify drivers of this resistance phenomenon, identifying the mechanistic drivers.

The specific project objectives were threefold:

1. To understand the nature of gemcitabine resistance conferred within the coculture model.
2. To undertake a whole-genome shRNA depletion screen within the model to identify drivers of gemcitabine resistance.
3. To analyse and validate the screen data to build a list of high confidence targetable genes causative of this effect.

2. Materials and methods

2.1 Materials

2.1.1 Reagents

Gemcitabine hydrochloride (Tocris Bioscience) was dissolved, aliquoted, and stored at -20°C in DMSO (Merck) at concentration ranges from 1mM to 0.001mM. Oxaliplatin (Merck) was dissolved, aliquoted, and stored at 4°C in water in concentration ranges from 100mM to 0.1mM. 5-Fluorouracil (Merck) was dissolved, aliquoted, and stored at 4°C in DMSO at concentration ranges of 100mM to 0.03mM. AZD2014 (Selleck Chemicals) was dissolved in DMSO and stored at -80°C in concentration ranges of 1mM to 0.003mM. AZD6738 (under MTA as part of a collaboration with AstraZeneca) was dissolved in DMSO and stored at -20°C in concentration ranges from 3mM to 0.01mM. Recombinant human HGF and IL-6 were obtained from Peprotech (London, UK). Tetrahydrouridine (THU) was sourced from Calbiochem (Merck), and DAPI (4',6-diamidino-2-phenylindole) from Life Technologies (California, USA).

2.1.2 Cell lines

K8484 cells were generated previously within the Tuveson Laboratory (CRUK CI) from $Kras^{G12D}$; $p53^{R172H}$;Pdx1--Cre (KPC) mice (S. R. Hingorani et al., 2005; K. P. Olive et al., 2009). K8484-GFP expressing cells were generated previously in the Jodrell Laboratory using retroviral transduction (using the same protocol as described in section 2.1.5). 3T3 cells were purchased from ATCC (NIH/3T3 CRL-1658). TB22150 CAF cells were kindly donated from the Neesse Laboratory (University of Goettingen) having been isolated from LSL-KrasG12D/+;Ptf1a-Cre (KC) mice originally (Hessmann et al., 2017). Human cancer associated fibroblasts were isolated originally within the Jodrell Laboratory by Ruiling Xu using the tumour outgrowth method of CAF isolation (M G Bachem et al., 1998) from human pancreatic tumour specimens removed from Whipple's operation, collected and provided by Addenbrooke's Hospital Tissue Bank with ethical approval under NRES/11/EE/0011. MH17031 cells were isolated previously by Ruiling Xu using an adapted serial trypsinisation and differential adhesion method (Albrecht Neesse et al., 2013; Walter, Omura, Hong, Griffith, and Goggins, 2008; Xu, 2015). NF18073 cells are pancreatic stellate cells isolated previously from normal pancreas of a $Kras^{WT}$; $p53^{R172H}$, Pdx1-cre (PC) mouse by Ruiling Xu using an adapted Histodenz gradient density centrifugation technique (Max G Bachem et al.,

2005; Froeling et al., 2011). Human pancreatic cancer cell line MIA PaCa2 was obtained from ECACC (Public Health England, Salisbury, UK) with a GFP-expressing clone created using retroviral transduction (protocol as per section 2.1.5) within the Narita Laboratory (CRUK CI). Fibroblast lines GDF14 and GDF17 were isolated from tumour using the differential adhesion method as described by Walter et. al from the GEDA (Genetically Engineered Mouse-Derived Allograft) model (Mollard, Frese, Gopinathan, Richards, and Jodrell, 2016; Walter et al., 2008), whereby KPC tumour fragments are grown subcutaneously in recipient $Kras^{WT}$; $p53^{R712H}$; Pdx1-Cre (PC) mice. All cells were tested and verified as mycoplasma-free by the CRUK-CI Biorepository Core Facility. MIA PaCa-2 cells were verified as authentic by STR genotyping by the Biorepository core facility. At the time of these studies, no STR genotyping panel was available to authenticate the mouse cell lines.

2.1.3 Cell culture reagents

Cells were maintained in DMEM with L-glutamine (Gibco, 11965092) supplemented with 10% (v/v) Fetal Bovine Serum (FBS) (Gibco, 10270) and 1% (v/v) of 100mM Sodium Pyruvate (Gibco, 11360). This media was used also for coculture with stromal cells. Cells within 3 passages of original isolation had medium further supplemented with 2% (v/v) of Penicillin-Streptomycin 5000U/ml (Gibco, 15070). Sterile Phosphate-Buffered Saline (PBS) was purchased from Gibco (20012), sterile 0.05% Trypsin-EDTA from Gibco (25300) also, and 30% bovine serum albumin solution in DPBS from Merck (A9576), used for IL-6 and HGF assays (Fig 3.4).

2.1.4 Buffers

Phosphate-Buffered Saline (PBS 1x): 11.9mM phosphate, 137mM Sodium Chloride, 2.7mM Potassium Chloride, pH7.4. Prepared by the CRUK CI media kitchen.

Tris-Buffered Saline (TBS 1x): 137mM Sodium Chloride, 2.7mM Potassium Chloride, 25mM Tris, pH7.4. Prepared by the CRUK CI media kitchen.

Low-salt RIPA buffer: 50mM Tris HCl pH 8.0, 150mM NaCl, 1% NP-40, 0.5% sodium deoxycholate, 0.1% Sodium Dodecyl Sulphate (SDS). Prepared by the CRUK CI media kitchen.

Tris-Buffered Saline with 0.1% Tween 20 (TBST): 1ml of Tween 20 (Fisher Scientific, BP337-100) was added to 1L of TBS and stirred for 10 minutes.

FACS sorting buffer: PBS + 2% foetal bovine serum (FBS) + 2mM ethylenediaminetetraacetic acid (EDTA, Invitrogen).

Cell lysis buffer: 10ml low-salt RIPA buffer (CRUK CI media kitchen, recipe above), 0.1% sodium dodecyl sulphate (Bio-Rad), 1 cOmplete ULTRA EDTA-free protease inhibitor tablet (Roche), 1 PhosSTOP phosphatase inhibitor tablet (Roche).

Running buffer: 50ml NuPAGE MOPS (3-(N-morpholino)propanesulfonic acid) SDS Running Buffer 20X (Thermo Fisher Scientific), 950ml de-ionized water.

4% Paraformaldehyde in PBS pH7.4 (4% PFA) was prepared by the CRUK CI Media Kitchen. All steps were performed in a fume cupboard. To make 1L, 500ml of PBS was added to a glass beaker. 40g of paraformaldehyde (Fisher Scientific, 30525) and 35 drops of 5M NaOH were added. The solution was heated on a stirrer until the solution reached 50°C. After the paraformaldehyde went into solution, the remaining 500ml of PBS was added and the solution was allowed to stir overnight at room temperature. The pH was adjusted to pH7.4 with HCl and sterile filtered. The solution was sub-aliquoted to 10ml per tube and stored at -20°C for 6 months. Any unused solution after thawing was discarded.

Immunofluorescence buffer: 333µl BSA (30% in DPBS), 10µl Triton X-100 (Merck Millipore), 500µl donkey serum (Merck) and 9.157ml PBS.

HEPES-buffered saline (HBS): 50mM HEPES (Gibco), 280mM NaCl (Merck), 1.5mM Na_2PO_4 (Merck), 12mM dextrose (Abcam), and 10mM KCl (Merck).

2.2 Cell line creation

2.2.1 Retrovirus-mediated generation of mVenus-expressing K8484 cells

K8484 cells were transduced to express the yellow fluorescent marker mVenus using a protocol adapted from the Narita Laboratory (CRUK CI), using a modified x-mVenus-pLPC described previously (Nagai et al., 2002). Retrovirus-producing Phoenix cells (ATCC, CRL-3213) were plated in DMEM cell culture media as described above at a density of $2x10^6$ cells in a 6cm dish at Day 0. On Day 1 a solution of 140µl H_2O, 21µl $CaCl_2$, and 7µg pLPC-mVenus DNA was created, and mixed dropwise with 166µl borate buffered saline (BBS, Merck). After 10 minutes of incubation at room temperature (RT), the mixture was added to the medium of the Phoenix cells in combination with chloroquine at a 25µM final concentration, which is

used to prevent lysosome-mediated degradation of DNA (Luthman and Magnusson, 1983). After overnight incubation, on Day 2 medium was gently replaced with 1.5ml of fresh medium. $6x10^5$ K8484 mouse PDAC cells were seeded in parallel in a 6cm dish with standard cell culture medium.

On Day 3, media from the Phoenix cells was removed, filtered through a 0.45µm filter to remove cell debris. To this filtrate the polycation polybrene was added to a concentration of 5µg/ml, increasing DNA uptake (Chaney, Howard, Pollard, Sallustio, and Stanley, 1988). Fresh media was added to the Phoenix cells and this process was repeated twice further, pooling the virus-containing filtrate. Media was then aspirated from the K8484 target cells and the Phoenix plate filtrate was added, leaving cells to incubate for 12 hours overnight. On Day 4, media was changed to prevent polybrene-induced toxicity.

On Day 5, K8484 cells were trypsinised and re-seeded under selection with 100µg/ml Hygromycin B (Thermo Fisher Scientific), and on Day 10 cells transduction was verified by mVenus fluorescence quantification compared to non-transduced K8484 controls using the CLARIOstar plate reader.

2.2.3 Isolation of mouse embryonic fibroblasts

All mouse experiments were carried out in the CRUK Cambridge Institute Biological Resources Unit, in accordance with the UK Animals (Scientific Procedures) Act 1986, with approval from the CRUK Cambridge Institute Animal Ethical Review and Welfare Body. To isolate mouse embryonic fibroblasts a pregnant $Kras^{WT}$; $p53^{R712H}$; Pdx1-Cre PC mouse (AN15CUK030247) were killed humanely and embryos extracted by Aarthi Gopinathan (CRUK CI), at embryonic stage E9.5 to E14.5. Approximately $1mm^3$ of the head section was removed for genotyping. Developing organs were identified, excised, and discarded. The remainder of the embryo was placed in 1ml 0.25% trypsin (Gibco) and diced finely. The resulting solution was incubated for 30 minutes at 37°C with 5% CO_2. Trypsin was then quenched with cell culture media (Section 2.1.3) supplemented with Pen/Strep (Gibco) and seeded overnight in a T75 flask (Corning). A flask was prepared for each isolated embryo, and propagating lines were expanded, and banked within 2 passages, prior to experimental use.

2.3 In vitro gemcitabine coculture assay

2.3.1 Cell culture and calculation of drug effect

At Day 0, 2,000 fluorescently-tagged pancreatic cancer cells (e.g, K8484-GFP or K84840mV) were seeded in 96 well clear flat bottom black polystyrene plates (Corning) in 50µl media, alongside 20,000 cells of the coculture line (e.g. MH17031), also in 50µl media, for a combined total volume of 100µl media. Cells were left to attach for 24 hours, following which, at Day 1, 100µl of media containing gemcitabine solution or 0.1% DMSO control was added to bring the total well volume to 200µl and the final gemcitabine concentration a range from 1µM to 1mM in the non-control wells. All conditions were run in triplicate wells, alongside a matched monoculture control of 2,000 pancreatic cancer cells only. Cells were left to incubate for 72 hours in a humidified atmosphere of 37°C and 5% CO_2. After this period media was aspirated and fluorescence per well was measured using either a CLARIOstar or PHERAstar plate reader with a filter setting of excitation at 485nm and emission at 520nm (BMG LABTECH). Fluorescence levels were used as a surrogate marker for degree of drug cytotoxicity, expressed as GI_{50} (concentration inhibiting cell growth by 50%):

$$GI_{50} = \frac{(T - T_0)}{(C - T_0)} \times \frac{100}{1}$$

T_0 refers to the fluorescence readout at the point of drug addition (measured using a replicate parallel plate seeded at same time as assay plate); T refers to the fluorescence measurement at 72 hours post drug addition; C refers to the fluorescence measurement of solvent control wells at the same time point. A dose response curve was created by plotting the concentration of drug used against the percentage of growth change observed relevant to solvent control, using Graphpad PRISM.

2.3.2 Cell handling and counting

After trypsinisation cells were resuspended in PBS with 1ml taken for counting using the Vi-CELL XR system (Beckman Coulter) as per manufacturer instructions.

2.3.4 Coculture conditioned medium

On sequential days duplicates of K8484-GFP (950,000 cells) and MH17031 ($9.5x10^6$) were seeded in 15cm dishes (Corning) with 20ml media. Following 72 hours of growth media was collected, filtered through a 0.45µm syringe filter, and mixed 1:1 with fresh media. This

solution was then used both for seeding and drug treatment of K8484-GFP cells in monoculture in a 96 well plate as per protocol in section 2.2.1.

2.3.5 Transience of gemcitabine resistance

K8484-GFP cells in monoculture were seeded at a density of $0.95x10^6$ cells per 15cm petri dish (Corning), and in coculture including $9.5x10^6$ cells of MH17031 cells, along with 10ml cell culture media. After 24 hours incubation, gemcitabine or DMSO control was added in a further 10ml cell culture media. After 72 hours, cells were trypsinised, washed in PBS, filtered through a 100µm filter (Thermo Fisher Scientific) to remove cell clumps, and then resuspended in 2ml FACS sorting buffer with DAPI (1/5000). Cells were provided to the CRUK CI Flow Cytometry core facility where $5x10^5$ live GFP+ cells were sorted from each condition on a FACSAria III cytometer (BD Biosciences). Cells were then immediately re-seeded in monoculture following the protocol in section 2.2.1, and sensitivity to gemcitabine treatment was assessed with a dose response curve as in 2.2.1.

2.3.6 Gemcitabine metabolism

Tetrahydrouridine (THU), an inhibitor of cytidine deaminase, was dissolved in methanol (Merck) and serially diluted in cell media and added to cell culture at the point of drug addition on Day 1 of the gemcitabine cytotoxicity assay in both monoculture and coculture conditions to the final desired concentration.

2.3.7 Combination and synergy screening

Plates were seeded in duplicate with K8484-mV cells either in monoculture or in coculture with MH17031 in 96 well plates at the ratios and volumes as per section 2.2.1. Following 24 hours of growth, cells were treated with a 6 x 6 grid combining two separate drugs each at six difference concentrations, alongside single agent control. Following 72 hours of incubation, cell fluorescence levels were read using CLARIOstar, then after calculation of growth inhibition relative to control, Combenefit software was used to visualise single agent data and synergy (Di Veroli et al., 2016), using both of the Bliss Independence and Loewe models (Bliss, 1939; Loewe, 1953).

2.3.8 Calculation of growth rate-adjusted drug efficacy

Growth-rate adjusted measurement of drug effect was calculated using the model developed by the Sorger Laboratory (Hafner, Niepel, Chung, and Sorger, 2016). Fluorescence values are

used as input data for the described model of determining relative cell counts between conditions, and therefore calculating GR_{50}, the concentration of drug at which the effect reaches a GR value of 0.5 based on interpolation of the fitted curve.

2.4 Cell line characterisation

2.4.1 Cell morphology imaging

Live cell culture was visualised using a Nikon Eclipse TS100 bright field microscope, with images captured using a Nikon Digital Sight.

2.4.2 Western blotting sample preparation

Cells were seeded at a density of $3x10^5$ cells per well in a 6 well plate and incubated for 48 hours at 37°C and 5% CO_2. Media was aspirated, and wells were washed twice in ice-cold PBS. 5ml of ice-cold TBS was twice added per well and cells were scraped and collected each time into a 15ml falcon tube (Merck), and cells pelleted through 5 minutes of centrifugation at 5,000g. Supernatant was aspirated, and cells were resuspended in 1ml ice-cold TBS, and transferred to a 1.5ml Eppendorf tube (Eppendorf). Samples were spun for 5 minutes at 10,000g at 4°C, supernatant was aspirated, and samples were stored at -80°C until further processing.

Samples were resuspended in 75µl Cell lysis buffer and placed at 4°C for 30 minutes. Samples were then sonicated in ice water for 2 minutes (Thomas Scientific), and centrifuged for 10 minutes at 12,000g at 4°C. Supernatant was then transferred to a fresh 1.5ml Eppendorf tube. Protein levels were quantified using a Direct Detect infrared spectrometer (Merck Millipore) as per manufacturer's instructions.

2.4.4 Western blotting

Samples to be analysed via western blotting were normalised for protein concentration through dilution with Cell lysis buffer. Each sample was combined with 4X Protein Sample Loading Buffer (LI-COR Biosciences) and 10X Novex NuPAGE Sample Reducing Agent (Fisher Scientific) to bring the total volume to 25µl with a protein concentration of 0.4µg/µl. Samples were heated for 10 minutes at 70°C to denature proteins. Samples were then loaded in NuPAGE 4-12% Bis-Tris Protein Gels, 1.5 mm, 10-wells (Thermo Fisher Scientific), alongside 5µl PageRuler Plus Prestained Protein Ladder (Thermo Fisher Scientific). Gels were run in a western blot box with 500ml running buffer, with the inner chamber filled with 200ml running

buffer mixed with 1ml NuPAGE Antioxidant. Gels were run for 30 minutes at 60V, followed by 90 minutes at 125V, or until the marker reached the end of the gel cassette. The gel was then removed from its case and subjected to a dry protein transfer using an iBlot dry blotting system (Thermo Fisher Scientific), as per manufacturer's instructions. The membrane was then blocked for 1 hour with 10ml of a 1:1 mix of TBST and Odyssey blocking buffer (LI-COR Biosciences). Membranes were then incubated with primary antibodies overnight at 4°C as per Table 2.1 below. Gels were then washed 4 times for 5 minutes each with TBST. Secondary antibody incubation was then carried out for 1 hour at room temperature using fluorescent antibodies as per Table 2.2 below. Membranes were again washed 4 times for 5 minutes each with TBST and left in TBS prior to imaging. Protein presence was imaged using an Odyssey CLx (LI-COR Biosciences), and protein bands quantified using the Image Studio software package (LI-COR Biosciences). As an addendum, significant experimentation was undertaken using an alternate antibody for N-Cadherin (Abcam, ab98952), which was subsequently identified to be non-specific based on discordant data when compared to control antibodies in control cell lines.

Antibody	Description	Manufacturer	Catalogue number
E-Cadherin	Rabbit monoclonal	Cell Signalling Technology	3195
N-Cadherin	Rabbit polyclonal	Abcam	ab76057
αSMA	Mouse monoclonal	Merck	A2547
Vimentin	Rabbit monoclonal	Abcam	SC-7557
Actin	Mouse monoclonal	Merck	118K4846
Actin	Rabbit polyclonal	Abcam	ab1801

Table 2.1 Primary antibodies used for western blotting.

Antibody	Description	Manufacturer	Catalogue number
Goat anti-mouse	IRDye 680 RD IgG (H+L)	LI-COR Biosciences	926-68070
Goat anti-rabbit	IRDye 800 CW IgG (H+L)	LI-COR Biosciences	926-32211

Table 2.2 Secondary antibodies used for western blotting

2.4.5 Immunofluorescence

Cells were seeding between 15,000 and 30,000 cells per well in a µ-Slide 8 well dish (Ibidi) and grown for 24 hours at 37°C and 5% CO_2. Cells approximating 70% confluency then had medium removed and replaced with 4% paraformaldehyde for fixing for 15 minutes. Wells were then washed 3 times for 5 minutes each with PBS. Wells were then blocked with 200µl immunofluorescence (IF) buffer and incubated overnight at 4°C with primary antibody solution (Table 2.3) with rocking.

Antibody	Description	Manufacturer	Catalogue number
DAPI	1µg/ml in IF buffer	Thermo Fisher Scientific	D3571
E-Cadherin	Rabbit monoclonal	Cell Signalling Technology	3195
N-Cadherin	Rabbit polyclonal	Abcam	ab76057
αSMA	Rabbit polyclonal	Abcam	ab5694
Vimentin	Rabbit monoclonal	Abcam	SC-7557
P53	Goat polyclonal	R&D Systems	AF1355

Table 2.3 Primary antibodies used for immunofluorescence

Wells were then washed 4 times for 5 minutes each in IF buffer with rocking, followed by 1 hour at room temperature in darkness with a secondary antibody solution (Table 2.4) whilst rocking.

Antibody	Description	Manufacturer	Catalogue number
Donkey anti-rabbit	AF546 IgG (H+L)	Thermo Fisher Scientific	A10040
Donkey anti-goat	AF647 IgG (H+L)	Jackson ImmunoResearch	705-605-147

Table 2.4 Secondary antibodies used for immunofluorescence

Wells were then washed 4 times for 5 minutes each with IF buffer with rocking, with inclusion of 250µl of DAPI solution (1µg/ml) for the first wash only. Wells were then filled with ice-cold PBS and stored at 4°C awaiting analysis. Wells were imaged using a Leica SP5 confocal

microscope with image analysis performed using the Fiji image processing package within ImageJ (NIH).

2.4.6 RNA Sequencing and data principal component analysis

RNA-Seq sample preparation was performed by Jo Bramhall in the Jodrell Laboratory (CRUK CI). In brief, $1x10^6$ cells were grown in monoculture in a 10cm petri dishes (Corning), with 4 replicates per cell line. After 24 hours incubation at 37°C with 5% CO_2 cells were harvested by scraping with PBS followed by centrifugal pelleting and stored at -80°C awaiting further batch processing. RNA was extracted using a RNeasy kit (Qiagen), quantified using a Quant-iT RNA kit (Thermo Fisher Scientific), with bioanalyser confirmation of sample RNA Integrity Numbers (RINs) >9.0. RNA was then diluted to 10ng/µl, adding 55µl to each well of 96 well plates, and transferred to the CRUK CI Genomics core facility for library preparation and sequencing on a HiSeq 2500 SE50 (Illumina). Raw sequencing reads were aligned to the mouse genome version GRCm38 (Kitts et al., 2016) using the TopHat alignment tool (Trapnell, Pachter, and Salzberg, 2009). Principal Component Analysis (PCA) was plotted for each sample group by Chandra Sekhar Reddy Chilamakuri of the CRUK CI Bioinformatics core facility.

2.4.7 Polymerase chain reaction for genotyping cell lines

Cells were grown in cell culture to a confluence of ~70% under passage 10 from isolation. Cells were then trypsinised, pelleted, resuspended in PBS and counted. $5x10^6$ cells per sample were taken and genomic DNA was extracted using the QIAamp DNA Mini Kit (Qiagen) as per manufacturer's instructions, eluting in 100µl nuclease-free water (Thermo Fisher Scientific). DNA concentration was then quantified using a Qubit 2.0 Fluorometer (Thermo Fisher Scientific) as per manufacturer's instructions using the Qubit dsDNA BR Assay Kit (Thermo Fisher Scientific). In preparation for PCR, DNA was diluted to a standardised 50ng/µl. 1µl of this solution was added to 25µl of Phusion® High-Fidelity PCR Master Mix with GC buffer (New England Biolabs) in 0.2ml PCR tubes (STARLAB), as per manufacturers instruction's, with the inclusion of 0.44µM of both forward and reverse primers (Table 2.5).

Gene target	Primer pair	Forward or reverse	Sequence (5' to 3')	Reference
Kras	P001	Forward	GTCTTTCCCCAGCACAGTGC	(Evans et al., 2016; Zou et al., 2015)
Kras	P001	Reverse	CTCTTGCCTACGCCACCAGCTC	(Evans et al., 2016; Zou et al., 2015)
p53	P002	Forward	AGCCTGCCTAGCTTCCTCAGG	(Evans et al., 2016)
p53	P002	Reverse	CTTGGAGACATAGCCACACTG	(Evans et al., 2016)
p53	P003	Forward	AGCTAGCCACCATGGCTTGAGTAAGTCTGCA	(Husain et al., 2013)
p53	P004	Forward	TTACACATCCAGCCTCTGTGG	(K. Olive et al., 2004)
p53	P003, P004	Reverse	CTTGGAGACATAGCCACACTG	(K. Olive et al., 2004)

Table 2.5 PCR primer sequences for* p53 *and* kras *genotyping

Samples were then placed on a thermocycler (CFX96, Bio-Rad) and subjected to thermocycling as per Table 2.6 and run out on an E-Gel iBase and E-Gel Safe Imager Combo Kit (Fisher Scientific), as per manufacturer's instructions. Gels were imaged on a Dyversity 2D Gel Imaging System (Syngene) using the manufacturer's GeneSys software package.

Step	Temperature (°C)	Time
1	95	3 minutes
2	95	30 seconds
3	65	30 seconds
4	72	1 minute
Repeat steps 2-4 34 times		
5	72	10 minutes
6	4	Forever

Table 2.6 Thermocycling conditions for PCR

2.5 shRNA screen design

2.5.1 Genome-wide shRNA libraries

A whole-genome shRNA library consisting of 63,677 shRNAs targeting a combined 18,402 genes was ordered from transOMIC technologies (Huntsville, US), leveraging the shERWOOD algorithm to optimise for potency whilst minimising potential off-target effects (Knott et al., 2014). Each of 7 pools was subcloned into MSCV-based LMH vectors, with shRNA expression under the control of a long terminal repeat (LTR) retroviral promoter. Vectors also drive expression of mCherry and the hygromycin resistance gene for selection. Nicolas Erard (Hannon Laboratory, CRUK CI) excised shRNAs from original LMN vectors using BGlII and MluI restriction enzymes (New England Biolabs). These cassettes were then ligated into LMH vectors cut with the same enzymes, purified on MinElute columns (Qiagen) and transformed into MegaX DH10B T1R electrocompetent cells (Thermo Fisher Scientific), with at least $5x10^6$ transformants per pool. DH10B cells were expanded and viral plasmid extracted (Qiagen Plasmid DNA Purification Kit) for use in virus production. The shRNA library used for the validation screen (Section 4.10) was prepared similarly.

2.5.2 Virus production

Phoenix-Eco viral packaging cells were plated in 15cm dishes at 50% confluency. After 24 hours of incubation at 37°C and 5% CO_2, cells were transfected via the calcium-phosphate method (Kingston, Chen, and Rose, 2003). A transfection mix was created (60µg viral vector for shRNA library, 7.5µg VSV-G, 200µl of 20nM pasha siRNA, 187.5µl 2M $CaCl_2$, water added to a total volume of 1.5ml) and added to equal volume 2X HBS buffer. The solution was

aliquoted and adjusted to pH of ~7.0. The mixture was bubbled using a Stripette (Corning), incubated for 15 minutes at room temperature and added to the packaging cells with 7.5µl chloroquine to a total media volume of 17ml. Cell cultures were incubated overnight at 37°C after which media was replaced and sodium butyrate (Merck) was added to a concentration of 1mM to increase transfection efficiency (Gorman, Howard, and Reeves, 1983). After 30 hours media was collected and filtered through a 0.45µm filter (Merck) collecting the virus, then stored at 4°C awaiting further use.

2.5.3 Cell lines

K8484 cells were used as the foundation infected cancer cell for the screen. For coculture conditions, MH17031 cells were transduced retrovirally to express both the diphtheria toxin receptor (DTR) as well as the fluorescent market ZsGreen and the neomycin resistance gene driven by the mouse phosphoglycerate kinase 1 (PGK1) promoter (LMN-PGK, Hannon Group, CRUK CI). Viral vector production was carried out using Phoenix-Eco cells (ATCC, CRL-3214), with MH17031 cells transduced at a low multiplicity of infection to ensure singly transduced cells and selected for 10 days with 300µg/ml of geneticin (Thermo Fisher Scientific).

2.5.4 Screen infection and selection

The shRNA library for the primary screen was split across 7 pools of ~9,000 shRNAs per pool. For each pool, the virus titre was calculated through test infections of K8484 cells, optimising for an approximate 30% infection rate, to minimise likelihood of two shRNA vectors infecting one cell. The infection efficiency was evaluated after 48 hours incubation by flow cytometry using a MACSQuant Analyzer 10 (Miltenyi Biotec), quantifying the proportion of cells expressing mCherry. With this titre larger scale infections were then performed in triplicate in 15cm petri dishes, through incubation of $10x10^6$ K8484-Mv cells along with the correct virus titre and 8µg/ml polybrene (Merck) along with 16ml of cell culture media. Successfully infected cells were then selected for 7 days with 500µg/ml Hygromycin B (Thermo Fisher Scientific).

2.5.5 Cell culture protocol

Each infected pool of K8484 cells (K8484-inf) was split into 5 samples. One timepoint zero sample (collected immediately for sequencing), two monoculture samples (plus gemcitabine and plus DMSO control), and two coculture samples (plus gemcitabine and plus DMSO

control). For the monoculture screen $5x10^6$ cells were seeded across 5 15cm dishes with 20ml media. After 24 hours of growth, 40µl of 5µM gemcitabine stock was added to experimental dishes (to 10 nM final concentration), with 40µl of DMSO added to control dishes. After 72 hours treatment, cells were split, counted on the Vi-CELL XR (Beckman Coulter), and reseeded again with $5x10^6$ cells per condition with fresh gemcitabine or DMSO. This cycle was repeated 6 times before trypsinisation and harvesting of gDNA from the final cell population. For coculture conditions, $5x10^6$ K8484-inf cells were seeded alongside $50x10^6$ MH17031-DTR cells, again across 5 15cm dishes. After 24 hours of incubation, 40µl of a 50µM gemcitabine stock was added to experimental dishes, bringing the gemcitabine concentration to 100nM. Similarly, 40µl DMSO was added to each control dish. After 72 hours of treatment, cells were trypsinised, counted, and relative counts of K8484-inf cells to MH17031-DTR cells were assessed using mCherry and ZsGreen fluorescence detected on the MACSQuant Analyzer 10. Through this calculation, $5x10^6$ of the K8484-inf cells were again seeded across 5 15cm dishes, with fresh MH17031-DTR cells added to bring the total of these cells to $50x10^6$ across the sample. After 6 cycles of this process, MH17031-DTR cells were selectively depleted using 100ng/ml diphtheria toxin (Merck) over 96 hours, following which remaining cells were trypsinised and harvested for subsequent processing with monoculture counterparts.

2.5.6 Screen sequencing

Genomic DNA from each of the samples, including the timepoint zero group, was extracted using the QIAamp DNA Blood Maxi Kit (Qiagen), as per manufacturer's instructions. shRNA cassettes were amplified from each population by PCR (forward primer: 5'-AGAATCGTTGCCTGCACATCTTGGAAAC-3', reverse primer: 5'-CTGCTAAAGCGCATGCTCCAGACTGC-3') using KOD Hot Start DNA Polymerase Kit (Merck) with 2µg gDNA, all in 96-well skirted white PCR plates (Thermo Fisher) (1: 5 minutes at 95°C; 2: 30 seconds at 95°C; 3: 30 seconds at 55°C; 4: 30 seconds at 72°C; 5: Cycle to step 2 24 times; 6: 5 minutes at 72°C; 7: Hold at 4°C). From this PCR 1ml of pooled reaction mix was purified using a QIAquick PCR Purification Kit (Qiagen) as per manufacturer's instructions, to remove non-amplicon reaction components. Secondary PCR was then performed to add barcoded Illumina adapters (forward primer P7-BCX-TS-Mir-Loop: 5'-CAAGCAGAAGACGGCATACGAGATNNNNNNGTGACTG GAGTTCAGACGTGTGCTCTTCCGATCTTAGTGAAGCCACAGATGTA-3', reverse primer P5-mir3:

5’-AATGATACGGCGACCACCGAGATCTACACCAGCAGTATGTTGAAGTCCGAGGCAGTAGGCA-3’ (Ns represent 6bp barcodes)). Two PCRs of 500ng amplicon were performed per sample in the same 96-well PCR plates (1: 5min at 95°C; 2: 30sec at 95°C; 3: 30sec at 52°C; 4: 30sec at 72°C; Cycle to Step 2 24 times; 5: 5min at 72°C; 6: Hold at 4°C). The resulting reaction solution was run on a 1.5% agarose gel with the ~150bp amplicon excised using a QIAquick Gel Extraction Kit (Qiagen) as per manufacturer’s instruction, with DNA again purified using a MinElute PCR Purification Kit. Each sample was then quantified using a Qubit 2.0 fluorometer, pooled, with precise quantification prior to sequencing then performed by Nicolas Erard by qPCR using a KAPA library quantification kit (Illumina). The pooled samples were then run on a HiSeq 4000 (Illumina) with a custom read 1 primer (5’-CAGCAGTATGTTGAAGTCCGAGGCAGTAGGCA-3’) to a depth of at least $10x10^6$ reads, by the CRUK CI Genomics core. Reads were mapped to a custom index made of the mouse shRNA sequences present in all pools using bowtie (Langmead, Trapnell, Pop, and Salzberg, 2009).

2.5.7 Validation screen

A custom library of 8,306 shRNAs targeting 1,973 genes was ordered from transOMIC technologies and used to infect K8484 cells as per sections 2.4.1, 2.4.2, and 2.4.4. Section 2.4.5 was replicated for this pool, again cycling 6 treatments of gemcitabine in both monoculture and coculture plus DMSO controls and sequencing the shRNA populations within surviving cells at the end of the experiment, as per section 2.4.6.

2.6 Analysis of shRNA screen data

2.6.1 Differential expression scoring

Differential expression of shRNAs between each culture condition compared to timepoint zero was performed, to identify the shRNA enrichment and depletion profiles within each sample, similar to as performed previously (Mendes-Pereira et al., 2012). Differential expression scoring was performed by Chandra Sekhar Reddy Chilamakuri in the CRUK CI Bioinformatics core facility, using both DESeq2 (Love, Huber, and Anders, 2014), an R Bioconductor package, as well as median Z scores (Cheadle, Vawter, Freed, and Becker, 2003). Genes were considered significantly differentially expressed for DESeq2 scoring indicated targeting shRNAs had an adjusted p-value of ≤ 0.05, log2 fold change ratio of normalized reads before and after treatment was less than 0, and ≥ 50% of shRNAs targeting that gene fit the first two criteria. Similarly, genes with 50% of targeting shRNAs with a median Z score value

of ≤ -2 were considered significantly depleted when compared to the timepoint zero sample. Comparison of gene lists between conditions and between scoring methods were compared using Venny (Oliveros, 2007).

2.6.2 Pathway and network analysis

Gene set enrichment analysis (GSEA) (Mootha et al., 2003; Subramanian et al., 2005) was performed also by Chandra Sekhar Reddy Chilamakuri using GSEA PreRanked with the ranked list as input , analysed across each of the Molecular Signature Database v6.1 gene sets (A. Liberzon et al., 2011; A Liberzon et al., 2015). MetaCore (v5.0, Thomson Reuters) was used for broad level pathway analysis of genes, as well as PANTHER v13.1 (Mi et al., 2017; Mi, Muruganujan, Casagrande, and Thomas, 2013) for identification of protein sequence-based clustering of screen data.

3. Development and validation of an in vitro coculture model of gemcitabine resistance in pancreatic cancer.

3.1 Introduction

The aim was to explore and interrogate further an *in vitro* coculture model of gemcitabine resistance in pancreatic cancer as developed previously by Ruiling Xu (Xu, 2015) in the Jodrell laboratory, to identify mechanisms driving gemcitabine resistance both within this model and within pancreatic cancer in general, identifying novel tumour ablation strategies that may have value in the clinic. Within this model it is shown that PDAC cells in monoculture are sensitive to the nucleoside analog gemcitabine, a mainstay of pancreatic cancer treatment. In contrast, when cultured in combination with cancer-associated fibroblast-like cells (FLCs), PDAC cells become resistant to gemcitabine. Within this chapter, both cancer and FLC cells are derived from separate KPC mice, as described in Chapter 2.1.2, both cell lines being immortal in cell culture. This model has potential as an *in vitro* system recapitulating the resistance to gemcitabine observed in the clinic, and therefore providing a medium through which the mechanisms of pancreatic cancer drug resistance can be understood.

The model developed comprises a 96-hour protocol (Fig 3.1). Upon seeding of cells and culturing for 24 hours, gemcitabine is added to culture medium for 72 hours, at which point cell growth in solvent control wells and gemcitabine-exposed wells are compared, as a surrogate for PDAC cell survival.

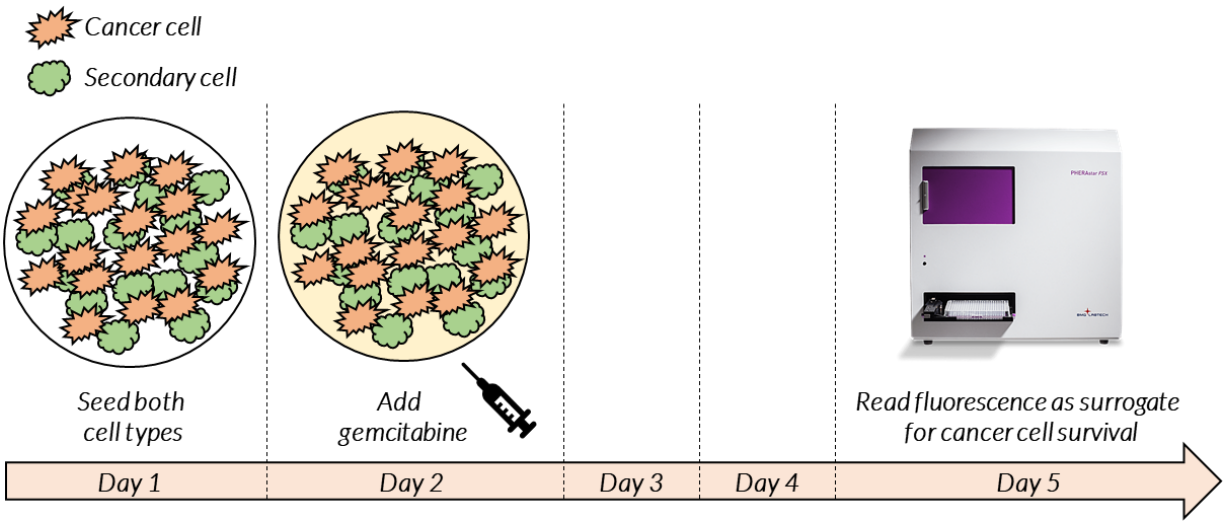

Figure 3.1 Schematic of PDAC cell co-culture assay used to investigate gemcitabine resistance within fluorescently-tagged cancer cells. *PDAC cell lines isolated from the KPC mouse and fluorescently tagged (GFP or mVenus) are grown in coculture with a secondary cell type for 24 hours. This coculture is then incubated with gemcitabine for 72 hours. PDAC cell growth over this period is assessed via measurement of fluorescence levels comparing treated samples and controls, using a spectrofluorometer (Section 2.3.1).*

3.2 Gemcitabine resistance induced in a coculture model of pancreatic cancer

To explore the pre-existing model and associated cellular resistance to gemcitabine, the model was reproduced by me and the conferred resistance effect confirmed (Fig 3.2). In monoculture the mouse PDAC cell line K8484-mV, which were isolated originally from the KPC mouse epithelial fraction and tagged with mVenus, the gemcitabine GI_{50} was 15nM ± 1.8nM. This contrasts to the sensitivity observed when K8484-mV cells were cocultured with MH17031 cells, a fibroblast-like line from the KPC mouse, with gemcitabine GI_{50} over 15-fold greater: 231nM ± 63nM. This therefore demonstrates a coculture-induced resistance effect. This result lays the foundation of the model for interrogation, to better understand the observed resistance mechanism.

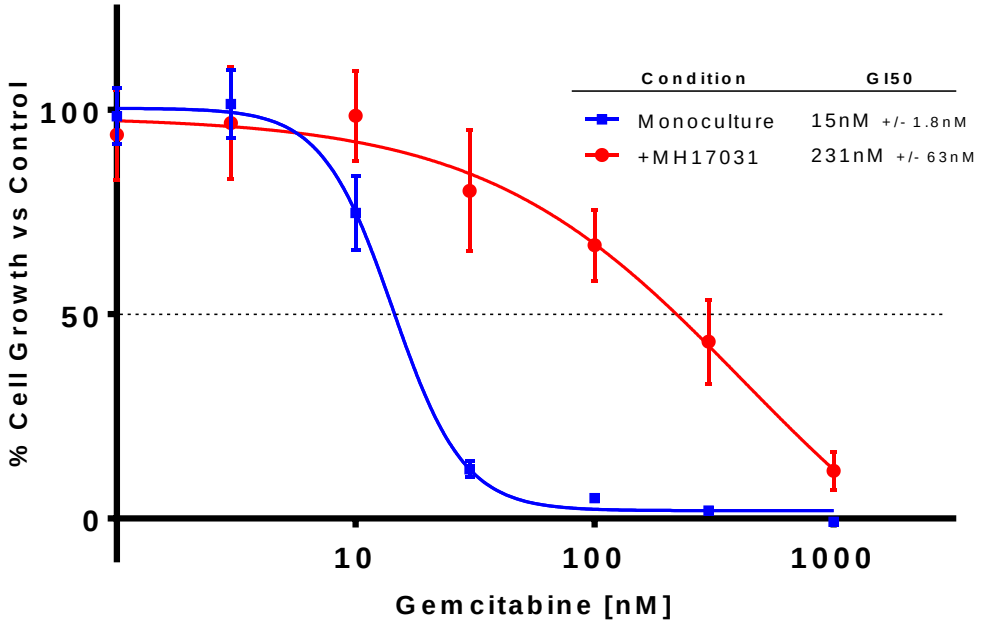

Figure 3.2 Sensitivity of K8484 cells to gemcitabine in monoculture and coculture. *K8484-mV PDAC cells grown in monoculture and coculture with MH17031 cells through a 72-hour growth assay with gemcitabine incubation. Cell growth in test wells was assessed in triplicate as a ratio to growth of cells with DMSO solvent control. Each point represents mean of triplicate biological and triplicate technical replicates, ±SE.*

With this demonstration of a complex *in vitro* model of gemcitabine resistance, the goals were to elucidate the mechanism and nature of the phenomenon, using both hypothesis-led experimentation (this chapter) coupled with broader unbiased explorative assessment (Chapter 4).

3.3 Extra-cellular signalling as a medium to confer gemcitabine resistance

Gemcitabine resistance in K8484-mV cells in coculture suggests that a form of inter-cellular communication between the cell types may drive this effect. Potential mechanisms include resistance conferred via secreted factors between cells, or via direct cell-cell interaction.

To assess the role of secreted factors, conditioned medium from K8484 and MH17031 coculture was collected and evaluated for its ability to induce gemcitabine resistance in K8484 cells in monoculture. Following 96 hours of coculture cell growth, medium was collected, filtered, and then added to a fresh monoculture of K8484 cells at v/v with fresh medium, minimising the dilution of conditioned medium, and therefore efficacy, of the

secretome of interest. Conditioned medium was neither frozen nor refrigerated, but collected fresh, to preserve the functionality of any unstable or sensitive signalling molecules that may be present. K8484 cells were then incubated with gemcitabine, and sensitivity assessed relative to K8484 cells in monoculture without conditioned medium (Fig 3.3).

No significant induction of gemcitabine resistance was observed through the addition of conditioned medium. This result corroborates data generated by Ruiling Xu within the lab using a transwell assay of both PDAC cells and fibroblast-like cells (FLCs) (Xu, 2015). In the transwell assay the two cell types are grown on opposite sides of a molecularly permeable membrane. This allows the transport of secreted molecules between cell types but maintains physical separation between the cells themselves. Taken together, these data suggest that a secreted factor is unlikely to be a primary driver of the coculture gemcitabine resistance effect, and that either some form of quorum sensing (gene regulation controlled by cell density) or direct cell-cell contact is more likely a driver.

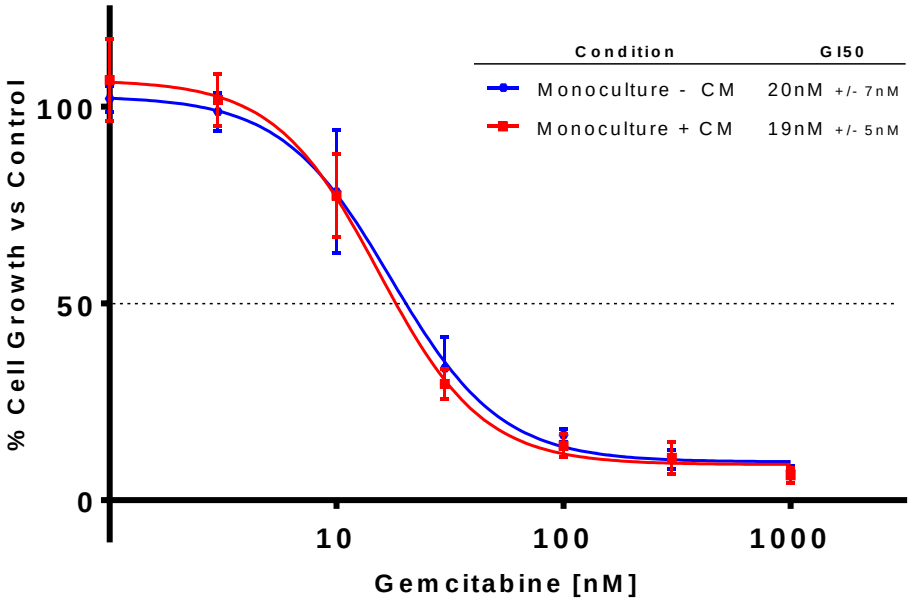

Figure 3.3 Effect of coculture-conditioned medium on K8484-GFP gemcitabine sensitivity. *K8484 cells were grown in parallel in both the absence and presence of coculture-conditioned medium with a dose range of gemcitabine. Sensitivity to gemcitabine was assessed using fluorescence as a surrogate marker for cell growth. For conditioning, medium was collected from dishes of K8484 and MH17031 coculture after 72 hours, mixed 1:1 with fresh media, and immediately incubated with K8484 cells. Each point represents mean of triplicate biological and triplicate technical replicates, ±SE.*

3.4 Evaluation of IL-6 and HGF as modulators of gemcitabine resistance

In parallel with the conditioned medium experiments, two candidate secreted factors were tested for their ability to modulate gemcitabine sensitivity in the model, based on existing literature: interleukin-6 (IL-6) and hepatocyte growth factor (HGF). Both molecules when secreted from fibroblast-like cells in tumour stroma have been documented as drivers of drug resistance (Duluc et al., 2015; Straussman et al., 2012). This provided two initial candidates for evaluation within this model.

Human recombinant forms of both factors (cross-reactive as according to manufacturer) were added exogenously to K8484 monocultures, recognising the effect of human HGF in activating mouse MET as previously documented (Francone et al., 2007). Both factors were tested across three concentrations of gemcitabine spanning the range used typically within

the coculture model. Neither was associated with significant resistance to gemcitabine, in fact both trending towards increasing sensitivity as opposed to resistance (Fig 3.4A).

In addition, neither IL-6 nor HGF induced gemcitabine resistance in monocultures of MIA PaCa-2 and Panc-1, two human PDAC lines, or an additional KPC mouse-derived PDAC line, DT8082-GFP (Fig 3.4B). This result does not explicitly discount these molecules as influencers of resistance in this model, as there remains a possibility that human recombinant forms did not cross-react efficiently with the mouse cognate receptors, therefore leading to insufficient concentration to induce change, although it serves as an initial indicator that an independent mechanism may be involved.

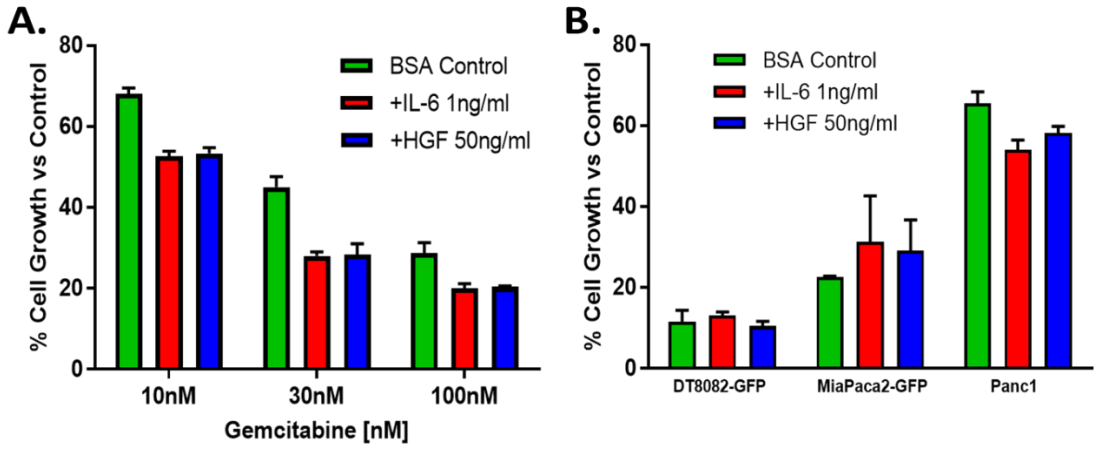

Figure 3.4 Effect of hypothesis-driven modulators of drug efficacy through exogenous addition in PDAC monoculture. (A) *K8484 cells grown in monoculture with three doses of gemcitabine alongside recombinant IL-6 (red), HGF (blue), or a BSA control (green). Effect of each protein in modulating gemcitabine effect at each dose was assessed.* ***(B)*** *Effect of IL-6 (red) and HGF (blue) in modulating gemcitabine efficacy (100nM) in an additional KPC PDAC line (DT8082-GFP), and two human PDAC lines (MIA PaCa-2-GFP and Panc1) was assessed using the sulforhodamine B assay using cellular protein levels as a surrogate for cell survival. Each point represents mean of triplicate biological and triplicate technical replicates, ±SE.*

3.5 Transience of resistance induced within the coculture assay

Under the premise that direct cell-cell contact appeared to be required to induce the observed resistance to gemcitabine, the next step was to develop a more holistic understanding of the nature of the change within the PDAC cells. One hypothesis was that

the coculture condition drives a more stable change in biological status of the PDAC cells, whether via RNA subtype, protein, epigenetic, or similar regulation.

To test this hypothesis the transience of the resistance effect within the PDAC cells was evaluated. K8484-GFP cells were grown for 96 hours in monoculture or coculture with MH17031 cells, plus gemcitabine. K8484-GFP cells were then isolated from the total population using flow cytometry sorting for GFP-fluorescent cells. This sorted population was then re-seeded immediately in monoculture and incubated with gemcitabine over 72 hours.

When comparing the gemcitabine GI_{50} of this population with standard K8484 monoculture, there was no significant change in sensitivity, independent of the original level of gemcitabine dosing and resistance level of the K8484-GFP cells (Fig 3.5). Therefore, this suggests that the conferred gemcitabine resistance in coculture is a transient effect, requiring constant cell-cell interaction between both cell types. This indicates that the driver of the effect may be more likely a proteomic or transcriptomic alteration as opposed to genetic, given these biological units are built and degraded constantly within cells.

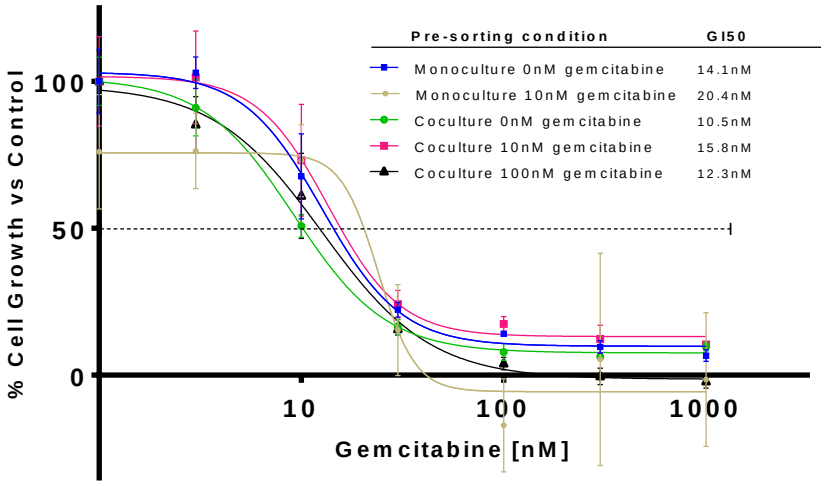

Figure 3.5 Transience of gemcitabine resistance when removed from coculture. *K8484-GFP cells were grown in monoculture and coculture with MH17031 and gemcitabine (0, 10 or 100 nM). Following 72 hours of drug exposure, surviving K8484-GFP cells were isolated using flow cytometry and fluorescence, and re-seeded in monoculture for 24 hours, then followed by 72 hours of gemcitabine exposure (6 concentrations), with sensitivities assessed by*

fluorescence. Each point represents mean of triplicate biological and triplicate technical replicates, ±SE.

3.6 Modulation of gemcitabine metabolism as a driver of resistance

Whilst the exact mechanism driving resistance to gemcitabine in this model is unknown, the mechanism through which gemcitabine in general induces a cytotoxic effect is, including the molecules driving activation and metabolism of the drug (Alvarellos et al., 2014; Plunkett et al., 1995). As a cell internalises gemcitabine (via nucleoside transporters) it is phosphorylated from dFdC to dFdCMP by deoxycytidine kinase (dCK) (Fig 3.6), and through two further phosphorylation steps the activated form of gemcitabine, dFdCTP, is created. dFdCTP exerts effect by being incorporated into replicating DNA inducing chain termination through inhibition of DNA polymerase activity (Plunkett et al., 1995). Gemcitabine effect can be abrogated through deamination of the initial dFdC form, induced by cytidine deaminase (CDA) to become dFdU, which is exported from cells and excreted. This deamination is a documented mechanism through which cells can become resistant to the drug (Funamizu et al., 2010; Weizman et al., 2014). Thus, another hypothesis through which K8484 cells are resistant to gemcitabine in coculture is that MH17031 cells may upregulate CDA in K8484 cells and therefore decrease intracellular concentration of the cytotoxic dFdCTP. Alternatively, CDA in MH17031 cells could deaminate dFdC making it unavailable for the K8484 cells.

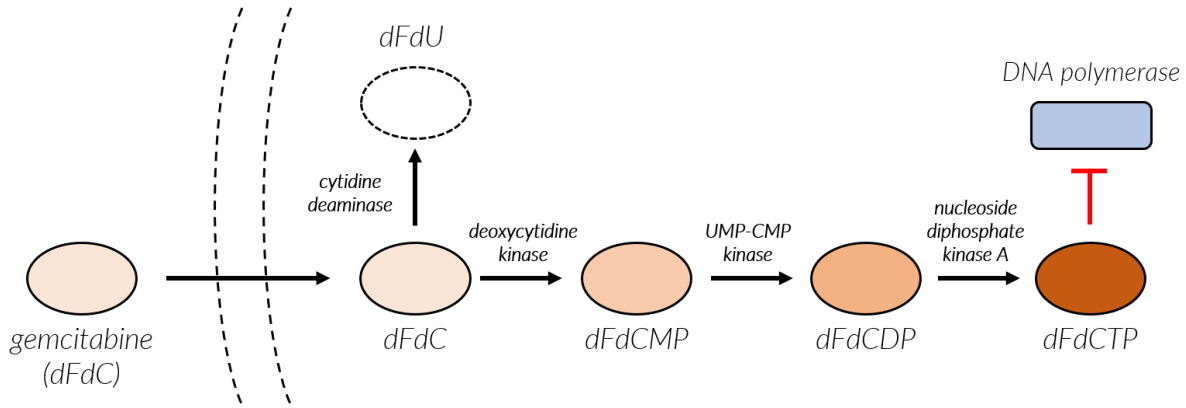

Figure 3.6 Schematic for intracellular gemcitabine metabolism and activation pathway.

To investigate this hypothesis, the coculture assay was performed with the addition of tetrahydrouridine (THU), a commercially available competitive CDA inhibitor. Through

addition of THU to the assay, any effect of CDA in metabolising gemcitabine would be minimised, therefore maximising dFdC levels available intracellularly. Further, as THU inhibits CDA in an allosteric manner (Stoller, Myers, and Chabner, 1978), its effect on minimising CDA metabolic activity on dFdC may be a product of stoichiometry with gemcitabine. As such two concentrations of THU were investigated in combination with gemcitabine.

Combination of THU and gemcitabine in the coculture model with MH17031 leads to no demonstrable change in K8484 sensitivity to gemcitabine, suggesting that within this model, elevated CDA activity is not a key driver of resistance to gemcitabine (Fig 3.7).

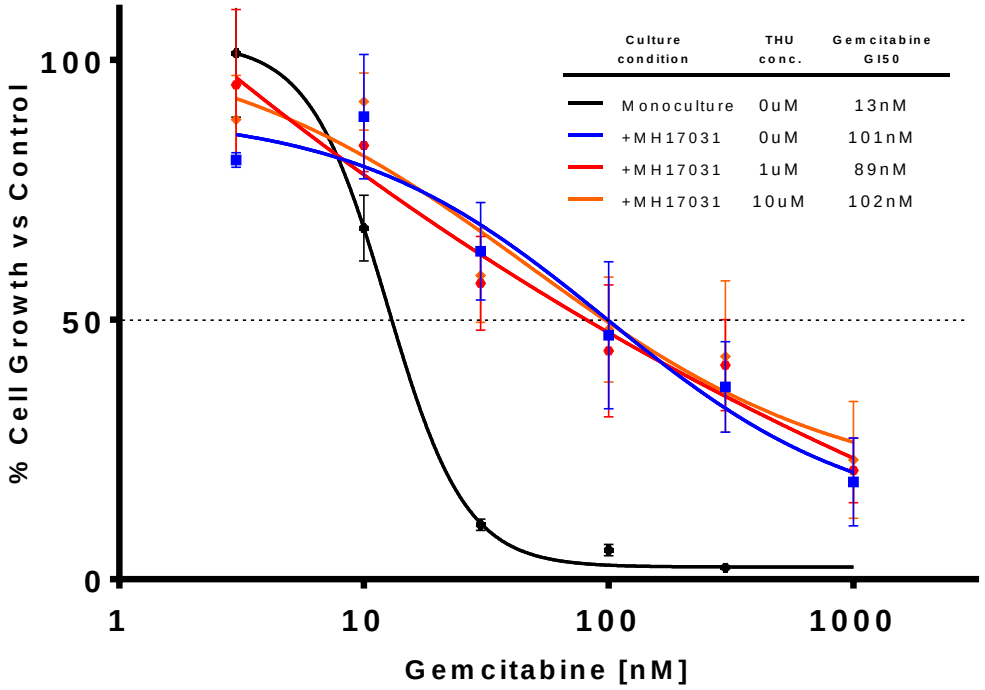

Figure 3.7 Effect of CDA inhibition on K8484-GFP gemcitabine sensitivity in coculture assay. *Two concentrations of tetrahydrouridine (THU), inhibitor of CDA, were assessed for effect on gemcitabine sensitivity in K8484-GFP coculture with MH17031 through a 72-hour assay. Each point represents mean of triplicate biological and triplicate technical replicates, ±SE.*

3.7 Comparison of coculture with mouse and human cells

These investigations indicate a transient gemcitabine resistance mechanism relying on cell-cell contact in mouse PDAC coculture, not driven by upregulated CDA activity, by IL-6 or by

HGF expression. Given the function of translational research in identifying treatment strategies for human patients, it was of value to further investigate whether the mechanism was a product of mouse cells or conserved in human counterpart cell lines.

The ability of mouse MH17031 cells to confer resistance to a human PDAC line in coculture was investigated, using the MIA PaCa-2 human cell line. Similar to the effect observed when in coculture with a mouse PDAC line, MH17031 drove a >50-fold increase in gemcitabine GI_{50} in MIA PaCa-2 cells, when compared to MIA PaCa-2 in monoculture (Fig 3.8A). This indicates the effect is conserved between the mouse K8484 line and a human PDAC line, and therefore holds potential value in human disease.

The next step was to assess whether a human counterpart of MH17031 could confer the same resistance effect to PDAC cells. Isolation and culture of human fibroblasts from the cancer stroma is a challenge given the non-transformed state of the cells, coupled with the rarity and value of human tissue. Despite this, a fibroblast line had previously been isolated from human PDAC tissue by Ruiling Xu using the tumour outgrowth method, HuCAF2650.

Culture of HuCAF2650 with K8484 cells induced no significant resistance to gemcitabine in the epithelial line, in contrast to the resistance conferred in coculture with MH17031. This indicates that this resistance-inducing effect may be restricted to mouse cell lines like MH17031. Of note, HuCAF2650 had a significantly slower growth rate when compared to MH17031 (doubling time of 14 days vs 1 day) appearing to reach replicative senescence significantly quicker. Both of these factors may influence the cell's ability to reach density levels required for quorum effects (density-based cell signalling) or provide sufficient cell surface area to induce cell-cell contact-driven resistance effects on the PDAC cell.

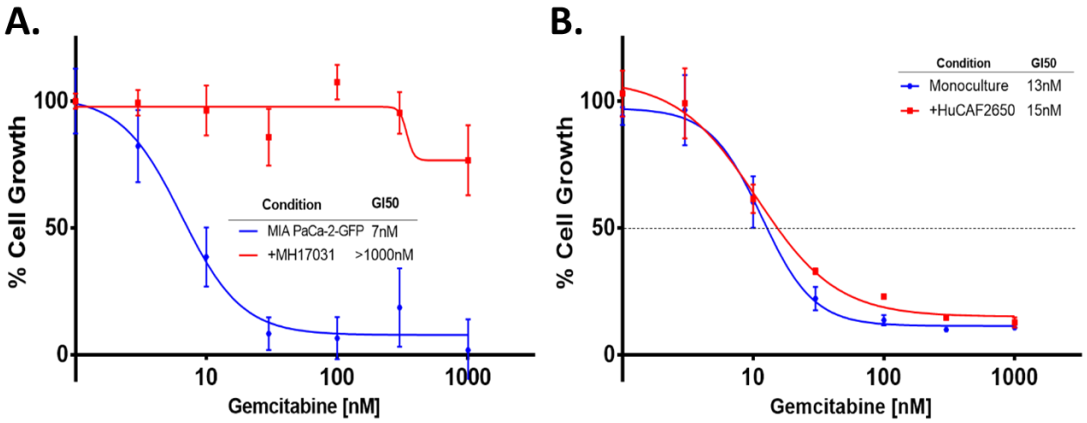

Figure 3.8 Occurrence of resistance phenomenon using human CAFs and PDAC cells with murine counterparts. (A) *Human GFP-tagged PDAC line MIA PaCa-2-GFP growth in monoculture and coculture with MH17031 with gemcitabine exposure over 72 hours;* ***(B)*** *K8484-GFP cell growth in monoculture and coculture with human CAF line HuCAF2650 with gemcitabine incubation over 72 hours. Each point represents mean of triplicate biological and triplicate technical replicates, ±SE.*

3.8 Characterisation of MH17031 morphology

Demonstrating a gemcitabine resistance effect derived from coculture of the MH17031 with K8484 cells, a similar result was observed by Ruiling Xu, Jo Bramhall (Jodrell laboratory) and I with additional fibroblastic lines isolated in a similar way. Subsequent investigations focused on profiling the specific subtype of mouse fibroblast-like cells capable of driving this effect, under the premise that it is a form of stroma-conferred effect exhibited specifically from cancer-isolated fibroblasts.

In addition to MH17031 cells, three mouse fibroblast lines were either isolated or purchased via commercial vendor. NF18073 cells are non-activated normal mesenchymal cells (pancreatic stellate cells) isolated from the normal pancreas of *KRAS* WT; P53 R172H; Pdx1-cre (PC) mice – non-tumour bearing siblings of KPC mice. MEF28412C cells are mouse embryonic fibroblasts isolated using differential adhesion from dissected embryos of PC mice. 3T3 cells are a canonical fibroblast line isolated originally from Swiss albino mouse embryo tissue. Together this panel allows comparison of MH17031 KPC derived fibroblast-like cells to a fibroblast line from a similar genotype (NF18073) and a similar mouse (MEF38412C), and to a canonical fibroblast line with regular use in academic investigations (3T3), and K8484 cells, to provide a more direct epithelial vs mesenchymal comparison.

A primary step in profiling these cells was to investigate whether morphologies differed in culture, and the extent to which MH17031 cells mirrored other defined mesenchymal cell lines. Typical mesenchymal cells exhibit elongated bodies, spindle-like appendages, and minimal clustering at dense growth. This is distinct from epithelial cells, which typically are more rounded/cobblestone in cell shape and grow in defined clusters.

Each cell line was grown at early passage to a confluency of 70-90%, with size and shape observed on a bright-field microscope. K8484 cells in culture exhibit each of these epithelial characteristics, growing in small rounded clusters with minimal visible appendages (Fig 3.9). This is in contrast to each of the fibroblastic lines, all exhibiting the above mesenchymal features such as spindle-like protrusions and less clustered growth. Within the fibroblast-like cell lines though, MH17031 exhibited fewer extreme levels of each of these properties, with a moderate degree of clustering and smaller appendages. Overall, they appeared distinct from each of the other fibroblasts and K8484 cells, with an overall profile approximating a general mesenchymal profile.

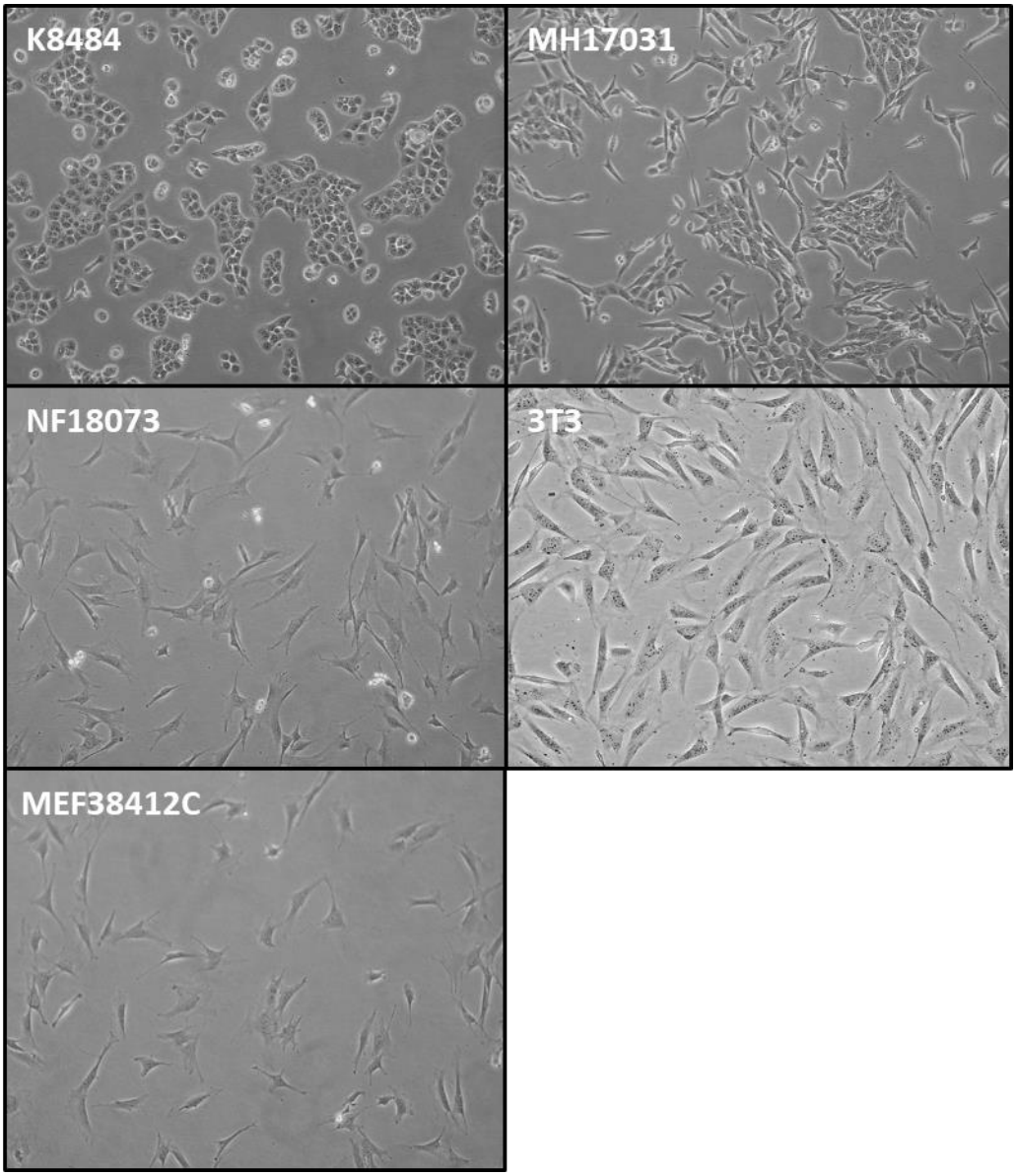

Figure 3.9 Cell culture morphologies for K8484 KPC tumour cell line and MH17031 KPC fibroblast-like cell line alongside canonical fibroblasts – commercial 3T3 fibroblasts, PC mouse-derived pancreatic stellate cells NF18073 and PC mouse-derived mouse embryo fibroblasts MEF38412C.

3.9 Ability of different mesenchymal cells to confer gemcitabine resistance in coculture

The rationale behind phenotypically characterising a mesenchymal cell line panel is to provide correlation data for deciphering the properties of MH17031 that allow induction of gemcitabine resistance in the coculture model. The primary data point required here is degree of resistance to gemcitabine conferred in coculture. To obtain this each of the cell

lines within the panel above was introduced into coculture with K8484 cells, with the degree of gemcitabine resistance conferred by each evaluated.

As shown previously, MH17031 increased gemcitabine GI_{50} of the K8484 cells over 15-fold to 269nM. Each of the other cell lines had either no effect on K8484 sensitivity, or even increased it, with coculture of 3T3 cells specifically reducing the GI_{50} by 31%, to 11nM (Fig 3.10). This result suggests that the resistance effect observed is a product of a specific cell-cell interaction requiring MH17031 cells and similarly derived cells.

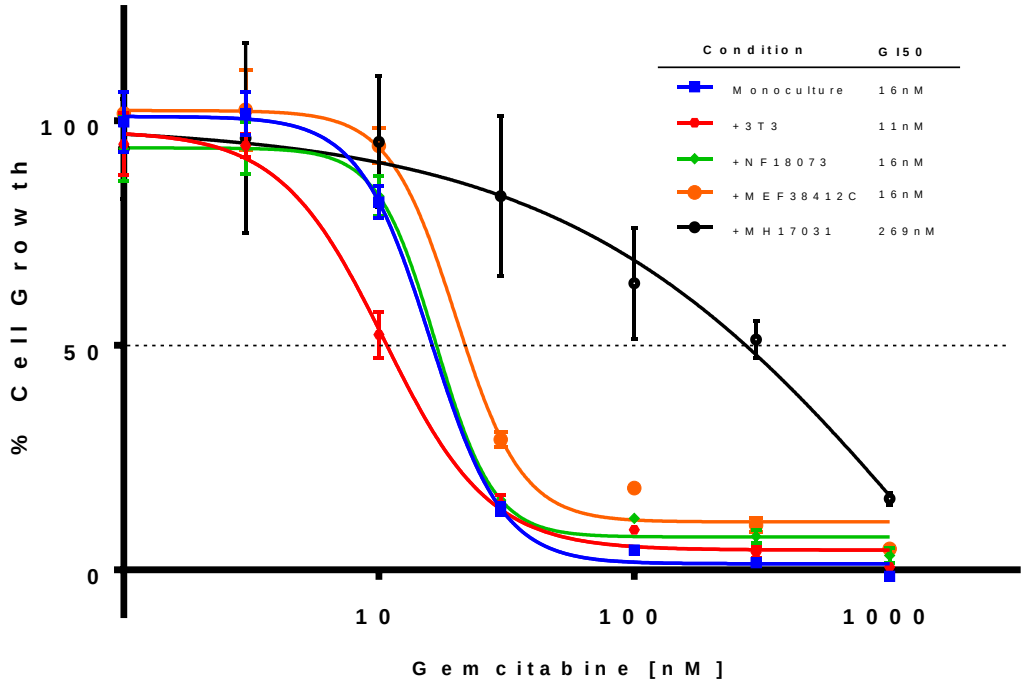

Figure 3.10 Effect of different fibroblasts in conferring gemcitabine resistance to K8484 cells in coculture. *Each fibroblast line was grown in coculture with K8484 cells at a 10:1 ratio for 24 hours, followed by 72-hour incubation with gemcitabine. Sensitivity of K8484 cells to gemcitabine within each condition was assessed via fluorescence reads on cell growth. Each point represents mean of triplicate biological and triplicate technical replicates, ±SE.*

3.10 Characterisation of protein marker expression MH17031 cells

With the further evidence that only a subtype of KPC-derived mouse fibroblast-like cell line could confer resistance, and morphological characteristics serving as only a minimally discriminating property, phenotypic protein markers were assessed to better elucidate the classification of resistance conferring cells. For this purpose, the presence and quantity of

four proteins were investigated, E-Cadherin, N-Cadherin, alpha smooth muscle actin (αSMA), and Vimentin. Of this panel, E-Cadherin is a canonical epithelial marker, with expression typically restricted to this cell type alone (Gumbiner, 1996). Both N-cadherin and Vimentin conversely are canonical mesenchymal markers (Sudo et al., 2013), with N-Cadherin postulated to be upregulated as E-Cadherin is downregulated during the process of epithelial to mesenchymal transition (Niessen, Leckband, and Yap, 2011). αSMA is documented as a highly expressed protein within activated CAFs in particular (Sappino, Skalli, Jackson, Schürch, and Gabbiani, 1988).

Protein levels were assessed using Western Blot in each of K8484, MH17031, and NF18073 cell lines. When assessing levels and presence of E-Cadherin, surprisingly (given its quasi-mesenchymal morphology by bright field microscopy) MH17031 had five-fold higher E-Cadherin expression when compared to K8484 (Fig 3.11A). NF18073 has non-detectable E-cadherin, as expected for normal pancreatic stellate cells. Given the epithelial profile of cells typically expressing this marker, mutually exclusive with canonical mesenchymal cells, this result indicated MH17031 cells to exhibit at minimum a partial epithelial profile, distinct from their predominantly mesenchymal morphology in culture.

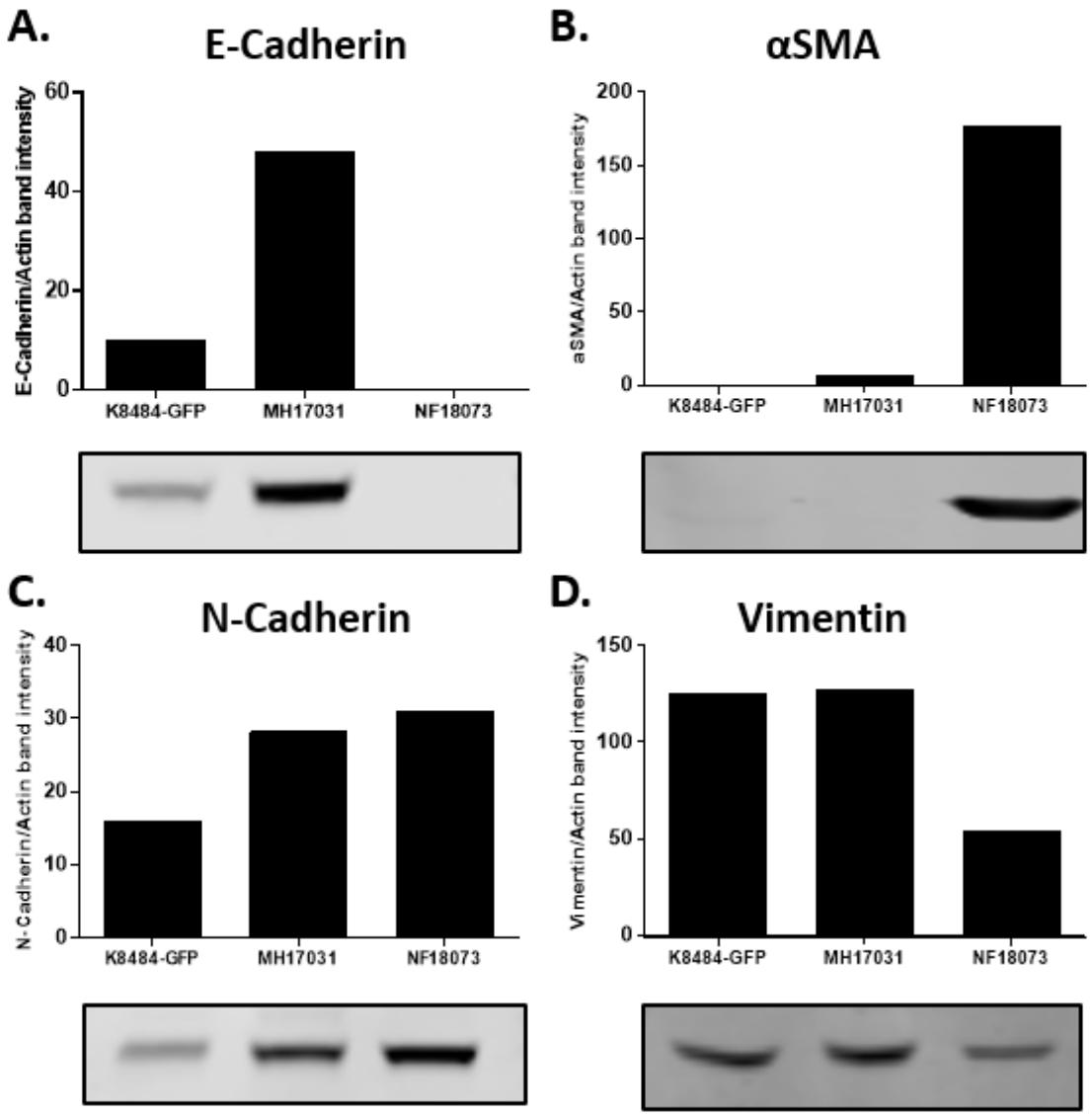

Figure 3.11 Protein expression levels for a panel of epithelial and mesenchymal markers. *Intracellular protein expression levels were assessed and quantified (comparing expression relative to Actin levels) using Western Blot in K8484, MH17031, and NF18073 cells, for each of* ***(A)*** *E-Cadherin,* ***(B)*** *αSMA,* ***(C)*** *N-Cadherin, and* ***(D)*** *Vimentin.*

αSMA was expressed in NF18073 normal pancreatic stellate cells, with minimal to no expression seen within K8484 and MH17031 cells (Fig 3.11B). Given αSMA is widely documented as a primary marker for the activation of stromal fibroblasts specifically, this result suggests that the NF18073 line may be the only true fibroblast line within this group.

While primary pancreatic stellate cells like NF18073, isolated by density gradient centrifugation due to their high lipid vesicle content, are expected not to express αSMA, it

has been reported that these cells do activate αSMA during culture in vitro (Erkan et al., 2011). This again suggests MH17031 cells to either be epithelial in subtype, or at a minimum containing a major epithelial subpopulation within it.

Of interest, N-Cadherin expression was detected within each of the three lines, with two to three-fold higher levels within NF18073 and MH17031 lines when compared to K8484 cells (Fig 3.11C). This result contradicts the dogma of E-Cadherin and N-Cadherin expression being mutually exclusive but supports a hypothesis that MH17031 cells exist either again as a mixed population, or perhaps within an intermediary state between epithelial and mesenchymal classifications.

Finally, with respect to expression of vimentin, another canonical mesenchymal marker, each cell line demonstrated comparable expression levels, with the epithelial K8484 cells having higher levels of this protein than NF18073 (Fig 3.11D). This result, coupled with the three above, solidifies the finding that while NF18073 do exhibit a classical mesenchymal signature as anticipated, both K8484 and MH17031 cells exhibit a more nuanced profile, with expression levels indicating a gradient between pure epithelial and pure mesenchymal classical signatures. As noted, this could arise either from mixed cell populations or through intermediate cell states, which can be further elucidated through investigation of protein localisation within cell populations, using a technique such as immunofluorescence.

3.11 Investigating protein localization using immunofluorescence

The above data suggest that the specific identity of MH17031, the single resistance-conferring cell examined herein, is not as purely mesenchymal as morphology as the initial extraction methodology would infer. It was therefore then imperative to determine whether cell populations were homogenous and therefore bulk protein levels, assayed using a western blot, an accurate reflection of the protein state of the cell populations.

To achieve this, immunofluorescence (IF) was used for each of E-Cadherin, N-Cadherin, αSMA, Vimentin, and P53. *Tp53* mutations such as that in KPC tumours (R172H) stabilise the protein enabling P53 to be detected by antibody binding methods, whereas wild type P53 has very short half-life and is typically undetectable. Thus, tumour cells are expected to be P53 positive on antibody staining, but other non-transformed cells are not. The added value of IF as a technique to complement western blotting here is an ability to visualise where

within a cell a protein is localizing too, which for a membrane-bound protein such as E-Cadherin, allows distinct confirmation of likelihood of antibody specificity.

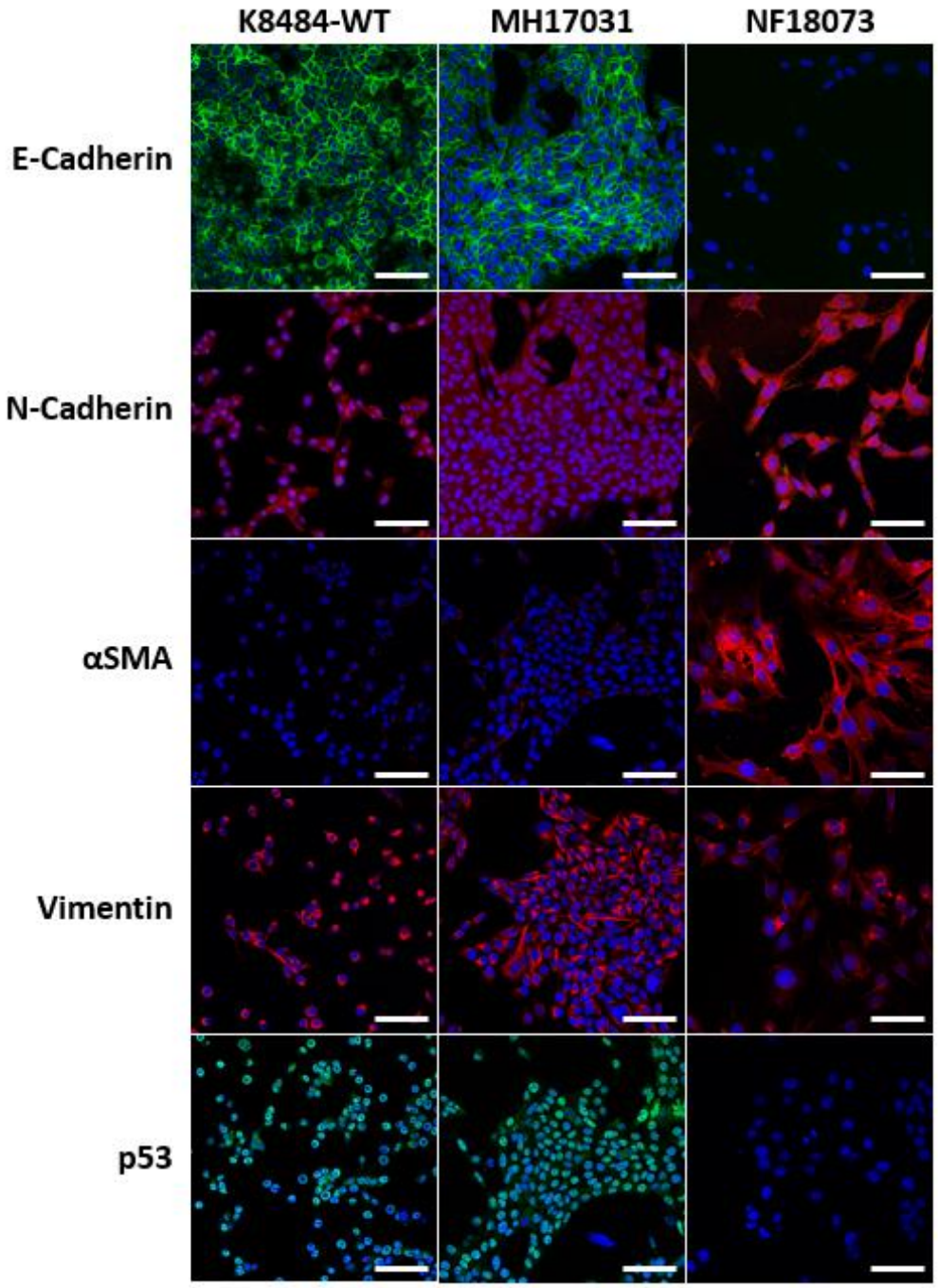

Figure 3.12 Protein localisation and expression analysis using immune-fluorescence. *Localisation and expression level of a panel of epithelial and mesenchymal proteins were assessed using immuno-fluorescent antibody tagging in K8484 KPC tumour cell line, MH17031 KPC fibroblast-like cell line and PC mouse-derived pancreatic stellate cells NF18073. Cells were incubated with specific primary antibodies, tagged with counterpart*

secondary fluorescent antibodies, and imaged using a Leica SP5 confocal microscope (scale bar = 100µm).

Using IF, E-Cadherin was detected in both K8484 and MH17031, with no detectable expression in NF18073 (Fig 3.12), consistent with Western blots. More specifically, E-Cadherin expression in the former two lines was localised to the cell membrane, and further, to cell-cell interaction points, or adhesions. This finding is consistent with known expression and localisation data for E-Cadherin, further confirming the significant presence of this marker within K8484, and the definite presence of this protein within MH17031. Also, it was clear that the overwhelming majority of the cells in the MH17031 culture were E-cadherin positive, suggesting that a mixed population is unlikely.

Similarly, for N-Cadherin, the total expression level within each cell line broadly correlated with that seen in western blotting. Vimentin was detected in almost all cells in all 3 cell lines, with multiple distinct punctas per cell within the cytoplasmic region.

αSMA expression also correlated with the Western blot data, with strong expression in NF18073, localised within apparent actin filaments as expected (B. Hinz, Dugina, Ballestrem, Wehrle-Haller, and Chaponnier, 2003). Expression in K8484 was minimal, as expected for a pure epithelial line, and was also barely detectable in MH17031.

These data altogether suggest with confidence that the MH17031 cell line may not be fibroblastic in origin, but perhaps epithelial, given the high level of homogenous E-Cadherin expression in addition, but with some mesenchymal features.

To explore this further, the expression level of P53 was interrogated, under the premise that were a cell to have the mutant form of the gene, an increased protein burden would be observed through accumulation (Yue et al., 2017; T. Zheng et al., 2013). Within the KPC mouse model, cells expressing *Pdx1* may recombine the transgenes and thus express both mutant *Tp53* and *Kras*, and therefore engage in carcinogenesis. *Pdx1* is typically only expressed in pancreatic cells; therefore, for a KPC-derived cell line to be mutant for P53, it would likely be a tumour cell line.

Using IF to assess the above point, as expected K8484 cells were strongly positive for (mutant) P53 protein, whereas in NF18073 P53 was undetectable, as expected from their

origin in normal pancreas in a PC mouse. MH17031 cells were strongly P53-positive, indicating these cells to be tumour in origin. This challenges an initial assumption in this project as to the subtype of these cells, which was that MH17031 were cancer-associated fibroblasts (CAF). As previously discussed, from a purely morphological perspective, coupled with the technique used for their initial isolation, this cell line exhibits defined mesenchymal characteristics, such as spindle-like appendages and minimal rounded clustering in culture growth. However, protein markers indicate MH17031 to be at least partly epithelial. The co-existence of both epithelial and mesenchymal characteristics is a widely documented and investigated phenomenon through the process of epithelial to mesenchymal transition (EMT). Investigation as to whether MH17031 had engaged in the EMT process was warranted, to support identification of the specific features of cell lines that drive the observed gemcitabine resistance-inducing phenomenon.

3.12 Applicability of EMT as mechanism for MH17031 marker expression

The value of techniques such as western blotting and immunofluorescence is an ability to assess the active protein state at a given point in time within the cell. This is not as feasible with purely transcriptomic analysis, due to the highly variable and often non-correlative relationship between the expression of mRNAs compared to the presence and activity of their associated proteins (Yansheng Liu, Beyer, & Aebersold, 2016). Nevertheless, an underlying value of transcriptome evaluation techniques such as RNA-Seq, when compared to protein techniques as mentioned above, is the lack of reliance on intermediary molecules such as antibodies to detect and quantify expression levels.

To better understand the origin and nature of the MH17031 cell line, and whether there is credibility in the hypothesis that this cell line may be a tumour cell line rather than a CAF that has undergone EMT and hence confers gemcitabine resistance in coculture, the expression level of transcripts for a range of epithelial, mesenchymal, and EMT-associated genes was investigated (Fig 3.13), leveraging an existing RNA-Seq dataset for each of K8484, MH17031, and NF18073. This was generated in the Jodrell lab by Frances Richards and Jo Bramhall. Genes related to epithelial, mesenchymal, and EMT-associated cells were quantified, interrogated, and contrasted between each of these cell lines.

In concordance with the above protein data, both K8484 and MH17031 expressed E-Cadherin transcript (and epithelial marker keratin 19), whereas NF18073 had no detectable expression, as before indicating MH17031 to be a phenotypically epithelial cell (Fig 3.13).

To assess the degree of mesenchymal identity within these cells, the expression levels of N-Cadherin, Vimentin, and αSMA were investigated. Expression data was tightly correlated to protein data, with similar expression levels of each N-Cadherin and Vimentin observed across each of the three cell lines. In concordance with above, NF18073 expressed the highest levels of αSMA, with expression in K8484-GFP also higher than in MH17031, further decreasing the likelihood that MH17031 is a true CAF cell line, using existing dogmas of origin and activation. The high level of αSMA expression in NF18073 though suggests this cell type to be an activated fibroblast. This is a transition documented to often occur following culturing of an isolated fibroblast line, so does not necessarily indicate that NF18073 was activated prior to isolation (Rhim et al., 2012). This profile though is consistent with a profile expected of a true CAF. Given this cell line does not confer resistance to gemcitabine within the coculture model of resistance, these results combined suggest that a true phenotypic CAF, or activated pancreatic fibroblast, as determined by protein and RNA transcript data, does not have an effect in inducing gemcitabine resistance within this model.

Leveraging the breadth of data available using RNA-Seq, the expression of additional stromal and EMT markers was evaluated within each of these three cell lines, to better understand whether EMT is truly a driver of the MH17031 cell type.

CXCL12 is a signalling molecule expressed within the stromal compartment of pancreatic tumours (Feig et al., 2013), subsequently secreted into the extracellular matrix within which it binds with its cognate receptor CXCR4 within the tumour microenvironment. This binding event induces the apparent exclusion of T cells from the pancreatic tumour nest, as a mechanism of immune evasion employed by pancreatic tumours. Given the widely documented expression of CXCL12 within the stromal cells specifically (Guo et al., 2016; Roy et al., 2014; Singh et al., 2012), the expression of this marker can be used to differentiate between stromal and epithelial cells within pancreatic cancer.

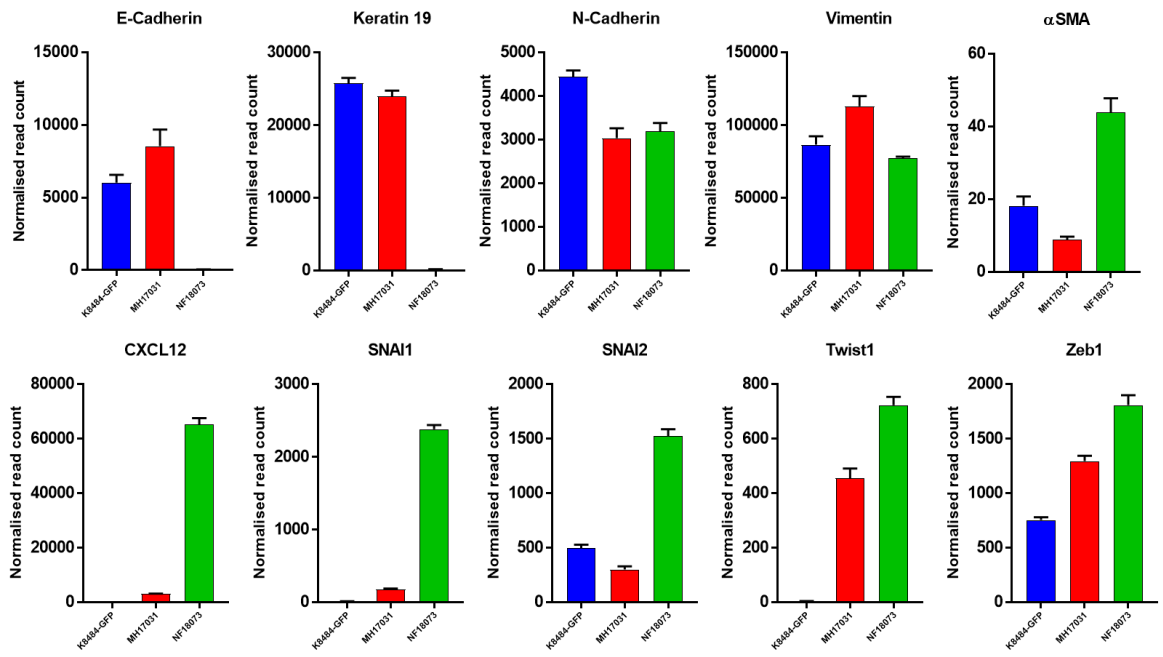

Figure 3.13 RNA expression levels for a panel of epithelial, mesenchymal, and EMT genes. *RNA Seq data for each of K8484-GFP (KPC tumour cell line), MH17031 (KPC fibroblast-like cell line), and NF18073 (PC mouse-derived pancreatic stellate cell line) was interrogated and contrasted for expression of a panel of genes to inform epithelial and mesenchymal status of cells, as well as likelihood of EMT activation. Each point represents mean of quadruplicate technical replicates, ±SD.*

Aligning with data above, only NF18073 expressed significant levels of CXCL12, whereas neither K8484 nor MH17031 expressed levels above the lower limit of quantification. This again indicates neither of these cell lines to be stromal in phenotype, but further indicating NF18073 to be an activated pancreatic fibroblast now exhibiting a CAF-like phenotype.

A primary goal of the transcriptomic analysis was to investigate whether there was any indication of MH17031 being a different cell type than purely epithelial, which perhaps drives the mechanism allowing this cell type to confer gemcitabine resistance in our coculture model. One hypothesis, matching a phenomenon documented within PDAC is EMT (X. Zheng et al., 2015). EMT is known to be driven primarily by a small panel of genetic master regulators, namely *Snai1*, *Snai2*, *Twist1*, and *Zeb1* (Lamouille, Xu, and Derynck, 2014). Interestingly when looking at transcript data for each of these genes in the three lines tested thus far, only NF18073 shows significant expression within each. For each of *Snai1* and *Snai2*, neither K8484 nor MH17031 had significant expression, and for *Zeb1* both

expressed at approximately 50% of the level of NF18073. As expression of *Zeb1* is found in defined non-epithelial cells also, it is not necessarily exclusively expressed in EMT cells (Sangrador et al., 2018).

Across the majority of the panel assessed above, there were no clear discrimination points between K8484 and MH17031, although meta-analysis of the global expression data using principal component analysis indicates that all three lines remain transcriptomically distinct from one another (Fig 3.14). The expression of one EMT-related factor though, *Twist1*, showed a significant difference between the lines. MH17031 expressed levels of *Twist1* at about 65% of the level of NF18073, whereas in K8484 there was no detectable level of transcript. Whether this factor is indeed a driver or strong causative factor for EMT, or perhaps merely correlative, it does serve to suggest that MH17031 cells may have a moderate mesenchymal phenotype driven by a position on the gradient of EMT progression.

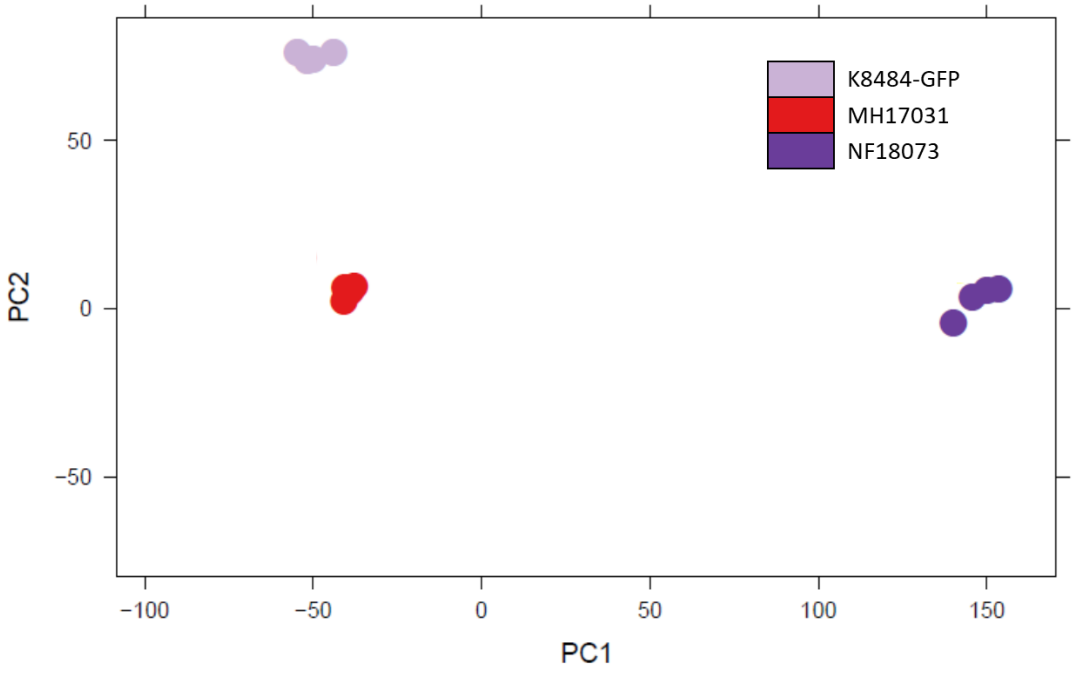

Figure 3.14 Principal component analysis for each RNA-Seq sample group. *Each circle represents one of 4 replicates per cell line.*

3.13 EMT expression data in human PDAC patients

Correlating transcriptomic expression in mouse cells with phenotypes of translational value in human patients is a difficult exercise and requires significant validation steps. One tool thought to de-risk the predictive power of murine translational studies is correlation of

identified targets and mechanisms with expression-linked survival data in patients, through some of the publicly available datasets, such as TCGA (Aguirre et al., 2017), a catalogue of key genomic changes and correlated survival analysis for 33 cancer types.

Factoring this in, TCGA data for pancreatic cancer patients, transcriptome data from a total of 172 tumour samples, can be investigated for markers of EMT to assess whether their expression level can serve as a prognostic factor for the disease, and therefore hold more validity as a target coming from murine studies.

For patients within the top quartile of expression versus those within the bottom quartile, neither *ZEB1* nor *SNAI1* show any significant difference in survival between the quartiles (Fig 3.15 B, C). This suggests that at least with regards to survival only, independent of treatment received and other predictive factors, there is no clear correlation of survival with expression of these genes alone.

Of interest though, both *TWIST1* and *SNAI2* show correlation between high levels of expression and decreased survival rates within patients (Fig 3.15 A, D), suggesting a potential functional role of these genes in either acceleration of disease progression or inhibition of therapeutic efficacy. In the mouse RNA-Seq data presented above, *Twist1* is highly expressed within the MH17031 cells, whereas not within the K8484 line. This alone might suggest a functional role of *Twist1* in inducing gemcitabine resistance, but, as with each of the EMT markers evaluated, NF18073 cells also highly express *Twist1*, despite an inability to confer resistance to gemcitabine within the coculture model documented. Together these data from patients hint at a driving role of EMT factors in worsening disease prognosis for PDAC patients, but when coupled with the RNA-Seq data also presented, indicates the activity of any one of these factors is unlikely to be a primary contributor to the gemcitabine resistance effect conferred by MH17031 cells within our coculture model specifically.

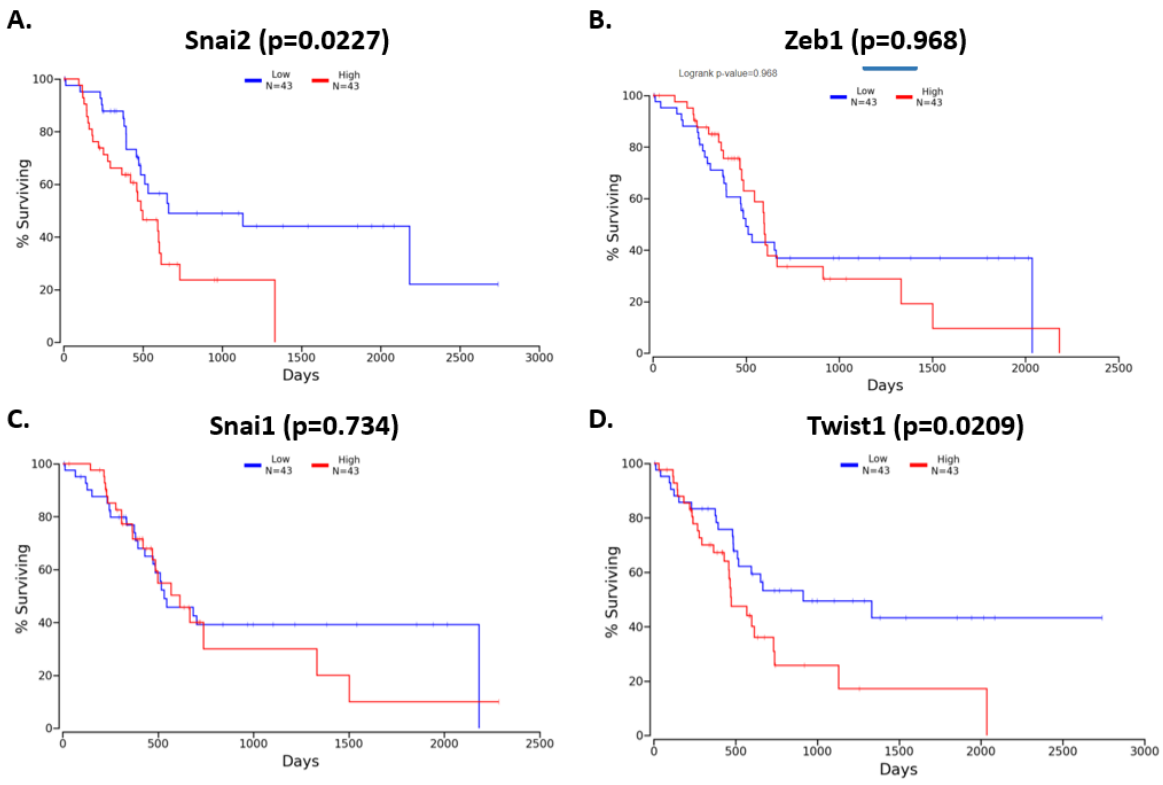

Figure 3.15 TCGA survival data for PDAC patients segregated into top and bottom quartiles of tumour EMT gene expression levels. *Top quartile of expression = red line; Bottom quartile of expression = blue line.*

3.14 Genomic characterisation of MH17031 cells

Recognising the plasticity of transcriptome and proteome profiles within cells, often changing significantly in response to changes in cellular environment, I attempted to identify the genetic origin of the MH17031 cells, by investigating the genotype encoded in the DNA.

As discussed previously, the KPC mouse model is genetically engineered to express mutant *Tp53* and mutant *Kras* in the epithelial/acinar cell compartment of the mouse pancreas. This is driven by expression of cre recombinase under the promoter for *Pdx1*, leveraging the lox-stop-lox model of recombination (S. R. Hingorani et al., 2005). Within this model, two lox sites are positioned either side of a genomic cassette containing a stop codon. Within KPC mice these cassettes are positioned within the code for both exogenous mutant *Kras* and within *Tp53*, disrupting its expression. Expression of cre recombinase catalyses the excision of this cassette, leaving behind just a small LSL scar of ~30 base pairs, inducing expression of the mutant gene (Fig 3.16, 3.17).

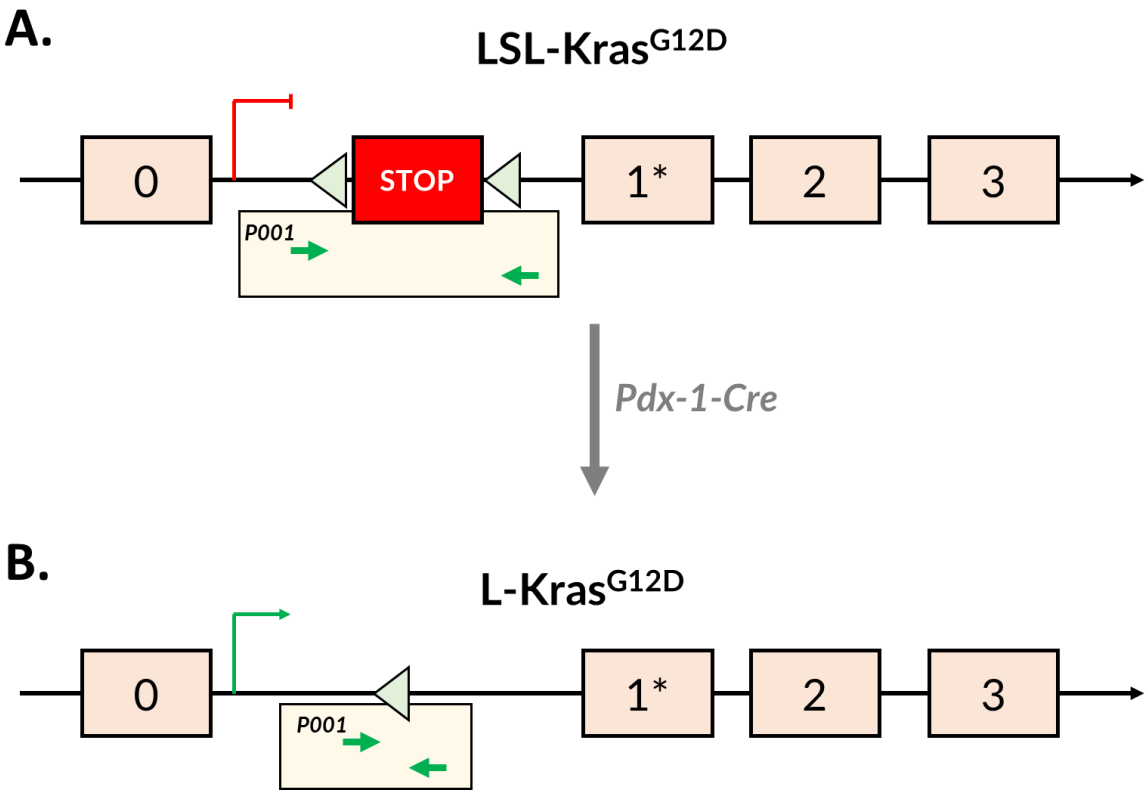

Figure 3.16 Cre recombinase-driven* Kras *mutation system in the KPC mouse model. *(**A**) KPC mice have a single copy of a G12D-mutated* Kras *gene in place of one wild-type allele. Expression is blocked due to insertion of an LSL cassette. (**B**) Upon* Pdx1*-driven cre recombinase expression the LSL cassette is excised, with cells then expressing* Kras *G12D. The P001 primer pair is designed to amplify from either side of the LSL cassette. When non-recombined, the amplification of this region is minimal due to the large distance between primers (>5kb). When recombined, an amplicon of ~325bp is produced, compared to a ~285bp long amplicon in the wild-type form of the gene without an inserted lox region.*

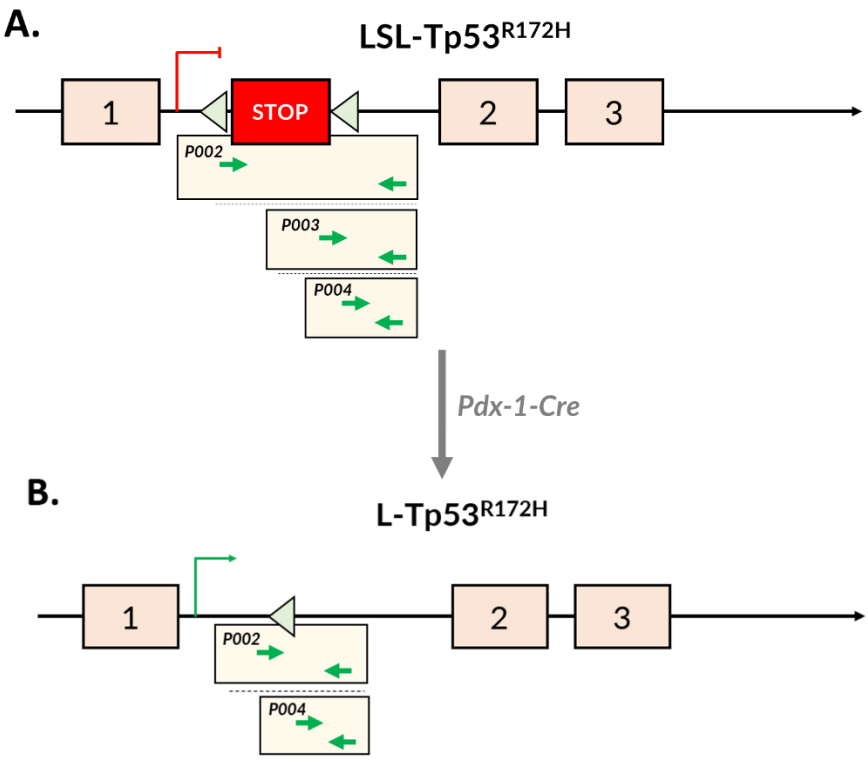

Figure 3.17 Cre recombinase-driven* Tp53 *mutation system in the KPC mouse model. *(**A**) KPC mice have two copies of a R172H-mutated* Tp53 *gene in place of both wild-type alleles. Expression is blocked due to insertion of an LSL cassette containing a stop codon. (**B**) Upon* Pdx1*-driven cre recombinase expression the LSL cassette is excised, with cells then expressing* Tp53 *R172H. The P002 primer pair is designed to amplify from either side of the LSL cassette. When non-recombined, the amplification of this region is minimal due to the distance between primers (>5kb). When recombined, an amplicon of ~325bp is produced, compared to a ~285bp long amplicon in the wild-type form of the gene without an inserted lox region. The P003 primer pair is designed to amplify from within the LSL cassette over one lox site. When the cassette is present and non-recombined an amplicon of ~300bp is produced, whereas in wild-type or recombined cells no amplicon is produced given the absence of the primer binding site within the gene. Finally, P004 is a positive PCR control primer pair set within the intronic region of* Tp53*, present in both mutant, wild-type, recombined, and non-recombined cells. Presence of an amplicon of ~170bp indicates sample integrity.*

Tumour cells isolated from this mouse model having arisen from a pancreatic epithelial cell will contain recombined transgenes and be mutant for each of *Kras* and *Tp53*, whereas cells from other origins within the mouse should be heterozygous for non-recombined and wild-type alleles for both genes.

To assess this, PCR was performed across each of the loci for these genes, with primers designed to produce amplicons accurately discriminating between cells that either have mutant (recombined LSL) and/or wild-type expression for each of these genes.

To investigate *Kras* status, a pair of primers designed to amplify from either side of the LSL cassette was used.

Primer ID	Target gene	Description	Approximate amplicon size (base pairs)		
			Wild-type	Transgene - recombined	Transgene - non-recombined
P001	Kras	Amplification across the LSL cassette	285	325	No amplicon
P002	Tp53	Amplification across the LSL cassette	285	325	No amplicon
P003	Tp53	Amplification within the LSL cassette across one lox site	No amplicon	No amplicon	300
P004	Tp53	Amplification within the intronic region (positive control)	170	170	170

Table 3.1 Primer design and amplification strategy for Kras and Tp53 genotyping.

For the three lines tested, only K8484 amplified mutant *Kras*, with both MH17031 and NF18073 only amplified the wild-type *Kras* amplicon (Fig 3.18A). This suggests that of the three only K8484 is truly a KPC tumour cell line. Because MH17031 is derived from a KPC mouse it would be expected to be heterozygous for the non-recombined LSL-*Kras* allele, but no amplification would occur at this site as distance between primers would be too great (>5.5kb). Retrospective analysis of RNA-Seq data generated by the lab indicated that MH17031, alongside K8484 cells, does express a level of mutant *Kras*. The apparent absence of the mutant form within MH17031 may be a product of PCR sensitivity, or heterogenous cell populations to different degrees between samples tested.

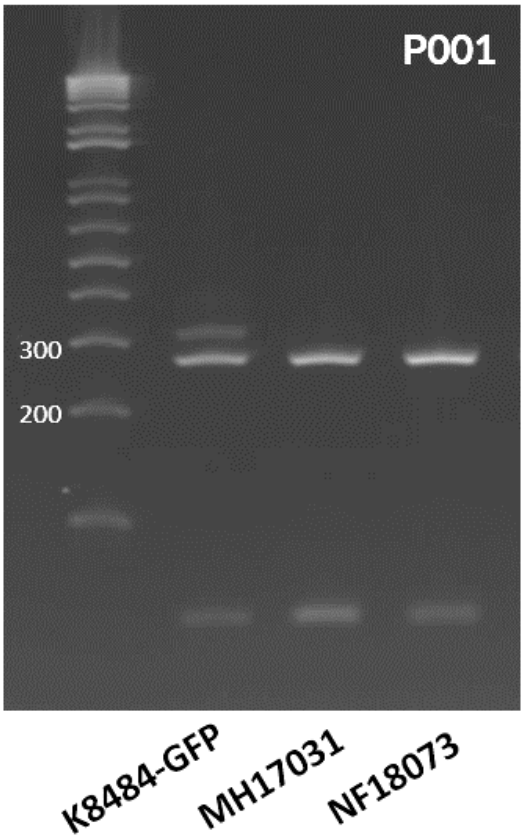

Figure 3.18* Kras *mutation status assessed via PCR. *Mutant* Kras *expression assessed via amplification over recombined LSL site, and wild-type* Kras *(~325bp = mutant, ~285bp = wt).*

Next, three pairs of primers around the *Tp53* locus were used. The first pair was designed similar in principle to the *Kras* pair above, wherein they amplified from either side of the LSL cassette. For this primer pair *Tp53* cells with the mutant form will express a single amplicon of ~320bp, the wild-type gene with a recombined LSL site, as opposed to a single amplicon of ~285bp if *Tp53* is wild-type.

Like the LSL *Kras* locus in KPC mice, which is a heterozygous ectopic insertion, LSL-*Tp53* it is also heterozygous in the mouse, but previous analysis of KPC tumours and tumour cell lines indicates that the wild type *Tp53* allele is typically lost in the tumours so that the only *Tp53* allele is the recombined R172H mutant transgene.

Within the cell panel both K8484 and MH17031 contained exclusively the mutated (recombined) form of the *Tp53* gene (Fig 3.19A), whereas NF18073 contained the non-recombined *Tp53* allele, noted as per confirmed sample integrity in Figure 3.19C.

This result was consistent through repeats and alternate primer pairings. This suggests one of two things: either MH17031 cells may be epithelial, with inefficient recombination of the *Kras* locus, or perhaps also that they are mesenchymal, but leaky expression of cre-recombinase induced recombination of the *Tp53* locus, which was then selected for given a competitive growth advantage.

Validating this finding further, when using primers to amplify from within the *Tp53* LSL cassette, only NF18073 results in an amplicon (Fig 3.19B), indicating that only this cell line of the three has a non-recombined LSL cassette at the *Tp53* locus, and therefore suggesting that both K8484 and MH17031 cassettes have undergone recombination removing the primer adhesion sites.

To ensure observed results (in particular absence of amplicons) were a true product of genetic characteristics, and not merely a product of degenerated template, a final pair of primers was used to amplify from within a non-mutated intron of *Tp53*, for which each cell line should produce an amplicon of ~170bp in length. All three lines showed this, therefore adding validity to the divergent data above (Fig 3.19C).

Taken together, these data suggest that MH17031 cells may not be a typical epithelial KPC tumour cell line, but perhaps an intermediary or mesenchymal line mutant for *Tp53* selected for due to a competitive growth advantage derived from this mutation. Coupling these data with protein and transcriptomic data exhibiting a strongly epithelial profile, it is possible that MH17031 is derived from an epithelial lineage, but without full recombination of the *Kras* LSL locus, perhaps through inefficient recombination in response to *Pdx1* expression. Cre-mediated recombination is a stochastic process, so it is not surprising that some cells may recombine only one of the two possible transgene loci.

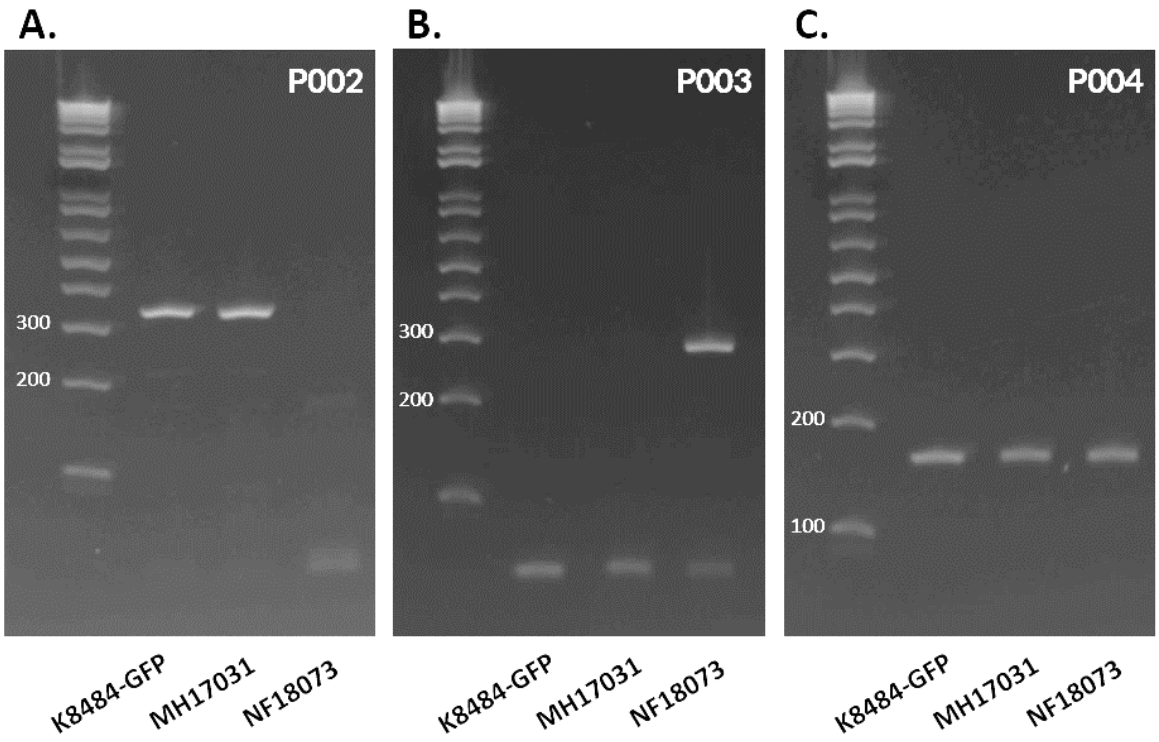

Figure 3.19 **Tp53** ***mutation and LSL recombination status assessed via PCR. (A)*** *Mutant* Tp53 *expression assessed via amplification over recombined LSL site, positioned within wild-type* Tp53 *(~325bp = mutant, no band = non-recombined LSL cassette or sample issue);* ***(B)*** *Non-recombined LSL cassette in* Tp53 *via amplification across cassette boundary (~300bp = non-recombined cassette, no band = recombined cassette, no cassette, or sample issue);* ***(C)*** *Assessing sample quality via PCR amplification within non-modified intron of* Tp53 *(170bp = sample present, no band = sample issue).*

3.15 Effect of density growth in monoculture in driving gemcitabine resistance

If MH17031 are derived from an epithelial or quasi-epithelial cell line originally, therefore the ability to confer resistance to gemcitabine within this coculture model may be a product of epithelial characteristics more so than a mesenchymal phenotype.

It was therefore necessary to investigate whether coculture of K8484 cells with another cancer line would drive the same resistance phenomenon observed when in coculture with MH17031. To do this, mirroring cell seeding ratios and conditions, the fluorescent K8484 line, K8484-mV, was grown in coculture with the non-fluorescent counterpart, K8484-WT, therefore maintaining the ratio of the fluorescent cells to be measured to the non-fluorescent cells as used within the standard assay.

When grown together, mirroring conditions outlined above, K8484-mV cells had a 10-20-fold increase in gemcitabine GI_{50} (Fig 3.20A). This increase is equivalent to that seen in MH17031 coculture. Thus, a dense layer of KPC cancer cells was able to confer resistance on the co-seeded cancer cells.

The next step was to identify whether a relationship exists between cell number seeded and degree of resistance. To test this, K8484-mV cells were seeded at varying ratios to K8484-WT cells, namely 1:10, 1:5, 1:2.5, and 1:1. Sensitivity to gemcitabine was assessed as before by using another standard cell survival assay, sulforhodamine B, which measures total protein levels as a surrogate for cell number.

There was an apparent direct relationship between seeding density and degree of conferred resistance to gemcitabine. At the lowest seeding ratio of 2,000 cells per well, or standard monoculture, gemcitabine GI_{50} was 22nM (Fig 3.20B). As this density increased to 5,000 and 10,000, cells per well, GI_{50} increased to 52nM and 1uM, and respectively, and 50% GI was not reached at 20,000 cells per well (E_{max} ~87% GI). This level of resistance was above that seen in coculture with MH17031 at a 20,000:2,000 cell seeding ratio, possibly indicating that cell density may be a true primary driver of the observed resistance phenomenon. This could be a product of one of two reasons: either cell density drove an artificial-assay dependent change in resistance levels, given the metrics used to assess survival, or that cell density drove a functional change within the K8484 cells that itself modified their sensitivity level to a nucleoside analog like gemcitabine, and may indeed represent a driver of resistance either in KPC mice *in vivo* and potentially in PDAC patients in the clinic. Discerning this effect is therefore an essential requirement to validating the translational value of this model, independent of the precise origin of cell lines used.

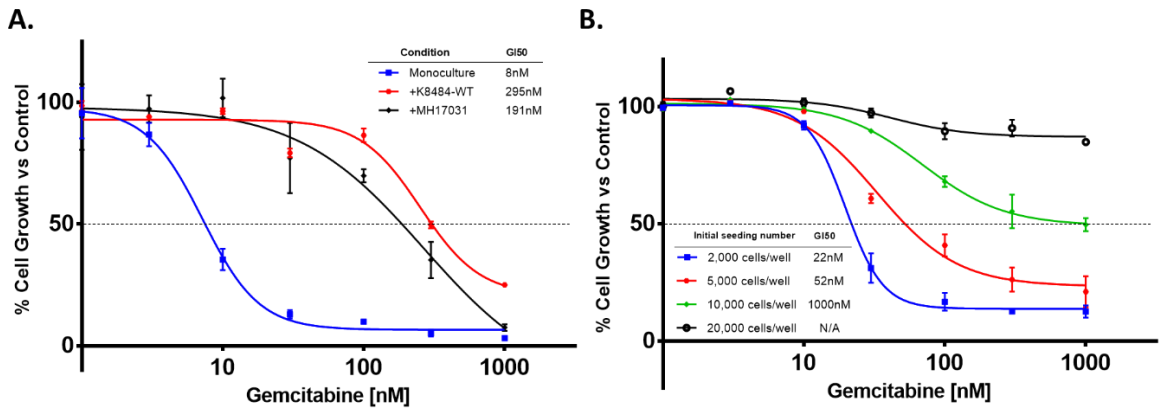

Figure 3.20 Effect of high-density K8484 monoculture in modulating gemcitabine sensitivity. (A) *Sensitivity to gemcitabine assessed for K8484-mV cells grown in monoculture (blue), coculture with MH17031 (black), and with K8484-WT (red);* ***(B)*** *Sensitivity to gemcitabine of K8484-mV cells grown for 24 hours at varying initial seeding densities followed by 72 hours incubation with drug. Each point represents mean of triplicate biological and triplicate technical replicates, ±SE.*

3.16 Contribution of proliferation rate to gemcitabine resistance phenomenon

The mechanism of action for gemcitabine is to integrate into replicating DNA strands, inducing stalled replication forks replication arrest, and DNA strand breaks. Sufficient DNA damage induces cell death. This mechanism induces an effect specifically on cells undergoing replication (i.e. in S phase), and as such a gradient of effect can exist dependant on cell proliferation rate, with more highly proliferative cells more sensitive the drug's effect (Yip-Schneider, Sweeney, Jung, Crowell, and Marshall, 2001).

Noting this, a potential factor discriminating the sensitivity of K8484 cells in coculture with different cell types may be a product of proliferation rate differences, whereby a condition in which K8484 grows at a lower rate may give an artificial indication of gemcitabine resistance. To investigate whether this is likely to be a contributing factor within the reported effect, growth rates of K8484-mV cells in each of sensitive and resistance conditions were compared, to identify a cell line-independent effect.

Growth rates of K8484-mV cells were assessed specifically between monoculture and coculture with each of NF18073, MEF38412C, and MH17031, the former two of the coculture conditions not inducing resistance to gemcitabine, as previously demonstrated in Figure 3.10.

Proliferation rate was significantly higher (p=0.0025) for K8484-mV cells in monoculture when compared to coculture with MH17031 (27-fold and 12-fold increases in cell number, respectively), with only a moderate decrease in rate when in coculture with each of NF18073 and MEF38412C (21-fold and 19-fold increases in cell number respectively) (Fig 3.21A). This result may partially be anticipated given the increase in total cell number per well in each of the coculture conditions, which itself might impede K8484 cell growth. The significantly decreased rate of K8484-MV in MH17031 coculture in particular may be a product of the high proliferation rate of the epithelial-like MH17031 cells themselves, which could compete with the K8484 cells through the entirety of the 72-hour assay. To determine whether the gemcitabine resistance in coculture was simply the result of inhibited proliferation, growth rate was correlated with gemcitabine GI_{50} for each coculture condition (Fig 3.21B)

A low growth rate was correlated with increasing gemcitabine GI_{50}, and therefore resistance (Fig 3.21C). With statistical analysis performed on the degree of correlation using Spearman's method, the relationship was calculated at a correlation coefficient of 0.67. This indicates a definite relationship between both, but concurrently suggests that growth rate is not the sole influencing factor in sensitivity to gemcitabine, with MH17031 inducing greater resistance than can be accounted for by inhibition of K8484-Mv proliferation alone. Therefore, cell type-specific mechanisms may still contribute to modulating gemcitabine sensitivity in K8484 cells, within this specific model.

The challenge of decoupling effects of cell proliferation on drug sensitivity from true sensitivity between cell lines and conditions is not a novel one and has been reported previously as a caveat and hurdle for *in vitro* translational drug development (Chauffert et al., 1998; Y. Fang, Sullivan, and Graham, 2007). Varying different methods have been developed to try discount this confounding effect (Fallahi-Sichani, Honarnejad, Heiser, Gray, and Sorger, 2013). One particular valuable tool for performing this analysis specifically is that developed by Hafner et al, GR_{50} (Hafner et al., 2016).

$$\mathrm{GR}(c) = 2^{\frac{log_2(\frac{x(c)}{x_0})}{log_2(\frac{x_{ctrl}}{x_0})}} - 1$$

Formula 3.1 Calculating GR values in endpoint drug-response data. *Growth rate-normalised drug efficacy can be calculated across conditions using a formula recently developed* (Hafner et al., 2016)*. For each condition, the relative cell count is defined as* $x(c)/x_{ctrl}$*, where* $x(c)$ *is the count in the presence of drug at concentration c and* x_{ctrl} *is the 50%-trimmed mean of the count for control cells.* x_0 *is the 50%-trimmed mean of the cell count from a timepoint zero sample, measured prior to drug exposure.*

GR_{50} is a metric for drug efficacy that factors in the proliferation rate of cells being assessed, to quantify and discount these discordant values from true comparisons of efficacy between conditions, calculated as per Formula 3.1. This tool supports addressing the question posed above, allowing for scaled and direct analysis of gemcitabine sensitivity effects between culture conditions.

Leveraging the same end-point data for the gemcitabine assay within each of the four cell type combinations detailed above, GR_{50} values were calculated within each condition, therefore producing growth rate-decoupled quantifications of sensitivity to gemcitabine. Through this model there remained a distinct and significant resistance effect driven specifically in the coculture with MH17031 cells, that was not the case for each of the other conditions (Fig 3.21D). Thus, reduced K8484-mV proliferation caused by dense culture did not account for all of the gemcitabine resistance in coculture with MH17031. Indeed, even in coculture with MH17031, the K8484-mV cells underwent more than 3 population doublings in the presence of gemcitabine, which would be expected to be sufficient for this S-phase-specific drug to be effective.

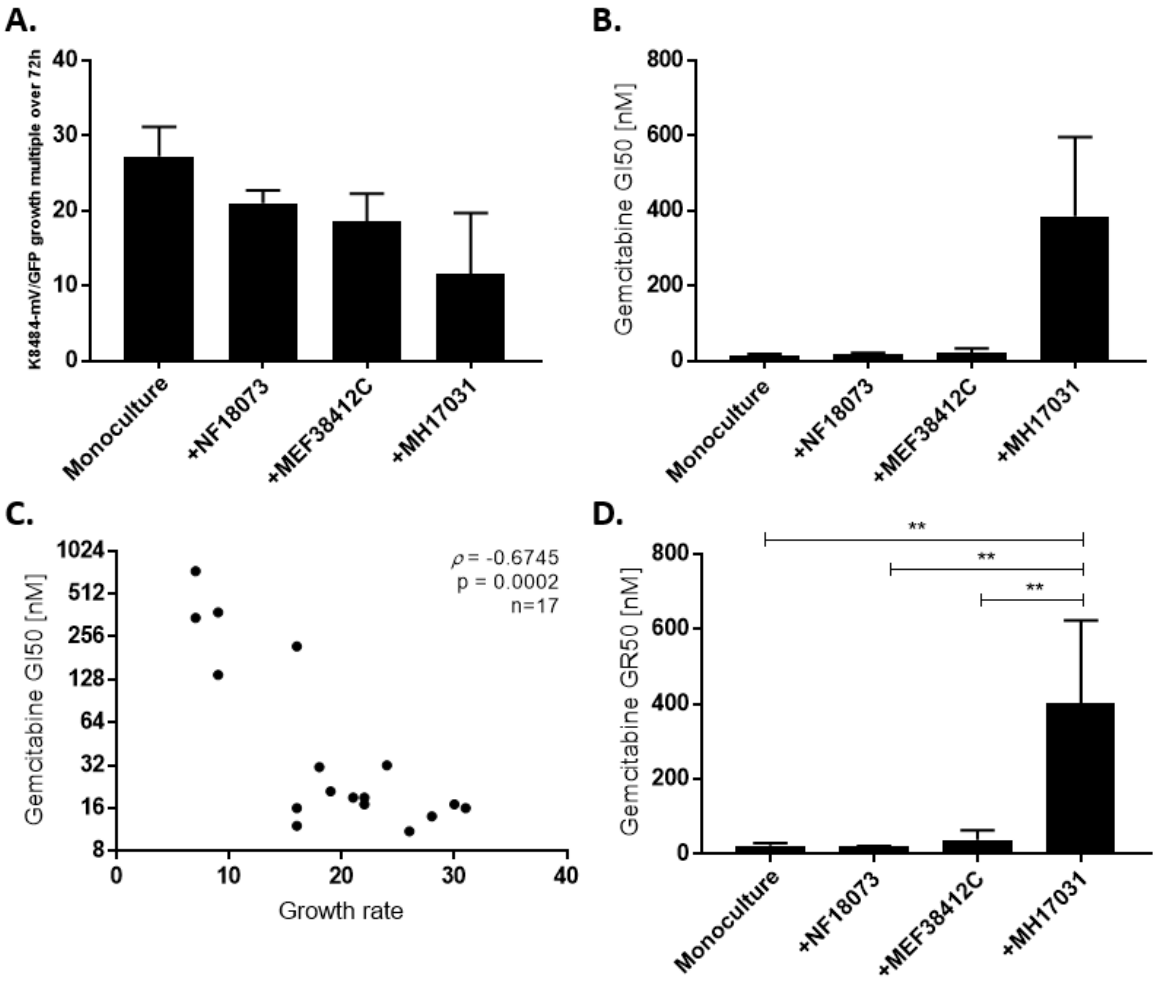

Figure 3.21 Evaluating the contribution of proliferation rate to coculture-driven gemcitabine resistance. (A) *Growth rate multiple of K8484-mV cells in monoculture as well as coculture with different lines. Each point represents mean of triplicate biological and triplicate technical replicates, ±SE.;* ***(B)*** *Mean (± SE) gemcitabine $_{GI50}$ of K8484-mV cells in monoculture and coculture with different cell types;* ***(C)*** *Correlation between gemcitabine growth rate and $_{GI50}$ plotted for all experiments from (A) using the Spearman method;* ***(D)*** *K8484 growth rate-adjusted gemcitabine sensitivity metric GR_{50} calculated and plotted for K8484 monoculture and coculture with each line from (A). Each point represents mean of triplicate biological and triplicate technical replicates, ±SE.*

3.17 Effect of cell density on conferring resistance to oxaliplatin and 5-fluorouracil in coculture

Uncoupling the confounding effect of proliferation rate on gemcitabine sensitivity is a challenge, although data above indicates proliferation is not the sole factor modulating resistance in this model. Another potential confounding factor in identifying true mechanistic resistance is cell seeding density, which has been reported to modulate drug sensitivity in certain models (Chauffert et al., 1998) . A simple and effective method through which this confounding factor can be decoupled from true drivers to a gemcitabine-specific resistance effect is through investigation of drug efficacy changes with cell density using additional different yet mechanistically similar agents to gemcitabine.

Oxaliplatin is a platinum-based cancer chemotherapy regularly tested in combination with gemcitabine for pancreatic cancer patients (Alberts et al., 2003; Demols et al., 2006). It exerts its effect through non-enzymatic conversion into reactive species such as monoaquo and diaquo DACH platinum (Raymond, Faivre, Woynarowski, and Chaney, 1998). Upon activation, these molecules covalently bind with guanine and cytosine moieties of DNA, leading to cross-linking, and therefore inhibition of DNA synthesis and cellular replication. Therefore, for oxaliplatin, proliferation rate would similarly modulate efficacy as seen with gemcitabine. Within this model, by investigating oxaliplatin $_{GI50}$ changes with seeding density of K8484 in monoculture, and through comparison with the significant effect of density on gemcitabine $_{GI50}$ (Fig 3.21B), the degree of influence of density as an assay artefact driving gemcitabine resistance can be investigated.

Through the same 72-hour assay, no comparably significant modulation of oxaliplatin sensitivity is observed with increasing cell density, with only a 3-fold increase between 2,000 cells per well and 20,000 cells per well, through 72 hours (Fig 3.22A). This stands in contrast to gemcitabine, where a 50-fold increase in gemcitabine was observed between only the 2,000 cells per well and 10,000 cells per well conditions. This result indicates both that cell density and proliferation rate are not likely primary drivers of the gemcitabine resistance effect observed, but instead that a cellular modulation in certain cocultures, be it perhaps proteomic or epigenetic, drives an effect within K8484 cells that drives resistance to gemcitabine specifically.

A further and similar comparison was investigated using 5-fluorouracil (5-FU) at varying cell densities. 5-FU is a nucleoside analogue, similar to gemcitabine, acting specifically on replicating cells. Its primary cytotoxic function is through its inhibition of thymidylate synthase (TS) (Longley, Harkin, and Johnston, 2003). TS is required for the synthesis of thymidine, one of the four core nucleotides required for DNA synthesis and replication. Between the highest and lowest seeding densities, a 9-fold increase in K8484 resistance to 5-FU was observed (Fig 3.22B), greater than the 3-fold increase observed using oxaliplatin. This suggests that a nucleoside analogue-specific resistance mechanism may be prevalent. However, when compared to the shift in gemcitabine sensitivity through scaled seeding densities, cell sensitivity to 5-FU is significantly less affected. This result indicates that independent of the specific modulation of K8484 cells at density or in coculture with MH17031, the change appears to be unique to gemcitabine. This suggests a true resistance effect less likely to be a direct product of assay characteristics, and perhaps a true reflection of gemcitabine resistance mechanisms observed in the dense tumour seen in mice and patients.

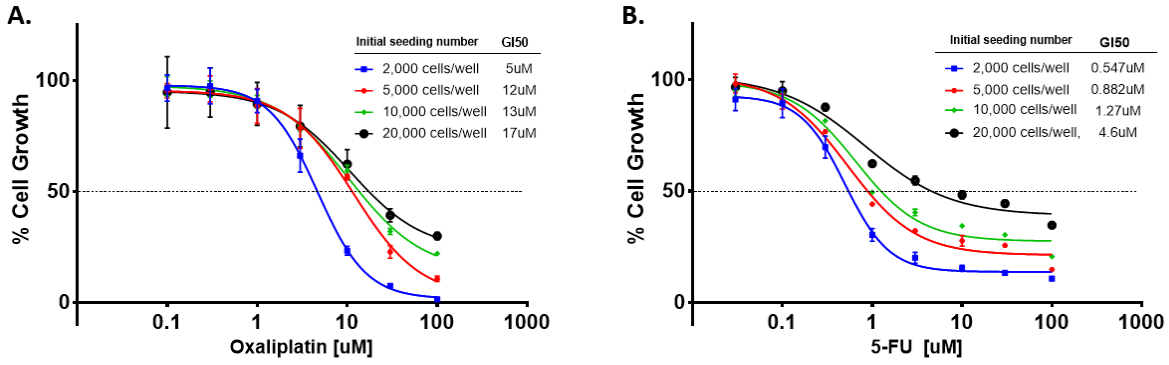

Figure 3.22 Effect of cell density in inducing resistance to alternative chemotherapeutic agents. *K8484-mV cells grown for 24 hours at different initial seeding densities followed by 72 hours incubation with either oxaliplatin* ***(A)*** *or 5-fluorouracil* ***(B)****. Each point represents mean of triplicate biological and triplicate technical replicates, ±SE.*

3.18 Assessment of effect of true CAFs on conferring resistance to gemcitabine.

An initial hypothesis within this project was that CAFs confer a specific functional change within KPC PDAC cells to induce resistance to gemcitabine in coculture. Through investigations detailed above, the original CAF-like cell line, MH17031, appears from genotypic, protein, and transcriptomic markers to more likely an epithelial cell in origin,

with expression of several mesenchymal markers. The original hypothesis of a CAF driving this resistance effect was partly supported by existing literature documenting their role in modulating drug efficacy in complex culture conditions (Hwang et al., 2008).

To assess whether within this model a true CAF is capable of inducing resistance to gemcitabine, a true and validated pancreatic CAF was required. As no cell line of this type is available commercially, alternate methods of CAF accrual were required. To leverage existing published and peer reviewed documentation of a true pancreatic cancer associated fibroblast, aliquots of TB22150 KC CAF were sourced from Albrecht Neesse's lab (Uni Goettingen) for validation within our model. This line was isolated from the KC mouse, a pancreatic cancer GEMM similar to the KPC mouse with mutant *Kras* expression in pancreatic epithelial cells driven here from *P48*, but without any *Tp53* mutation. This model, and associated CAFs, have been demonstrated to contribute to a resistance-conferring effect through "scavenging" of gemcitabine within the tumour, and therefore reducing the levels of drug available for uptake and effect in tumour cells (Hessmann et al., 2017).

Morphologically TB22150 cells exhibit classical mesenchymal phenotypes, notably elongated cellular protrusions, and minimally clustered growth at density (Fig 3.23A). To directly assess their contribution to gemcitabine sensitivity within our coculture model, the cells were grown with K8484 cells in the coculture protocol. Within this assay TB22150 cells quite significantly induce resistance to gemcitabine with a GI_{50} of 204nM for the K8484 cells within the coculture (Fig 3.23B). This result mirrors that seen for K8484 cells either in coculture with MH17031 or at high-density monoculture.

To further validate TB22150 cells and the observed results, the *Kras* and *Tp53* genotype was assessed using an identical protocol as used for validation of MH17031 genotype in Section 3.14. As expected (because it should not contain the corresponding transgene) TB22150 was wild type for *Tp53* (Fig 3.24B). Notably though, and in contrast to the reported genotype of this line, the cell line amplified mutant *Kras* (Fig 3.24A), mirroring a genotype expected from a KC pancreatic epithelial cell, and not a pure mesenchymal cell. This result contrasts with a conclusion on the genotype from validation within the initial publication, although a deeper interrogation of the original published Figure (CAF2 in Supp Fig 1C, Hessmann et al) suggests there may be a minor proportion of this cell line that was *Kras* mutant, and which may have since expanded in culture– mirroring the challenges faced in isolation of MH17031 as a pure

CAF population. Other groups working with KPC tumours have also found it virtually impossible to isolate wild type *Kras* and *Tp53* CAFs from these tumours, either because minor mutant contaminants have such a growth advantage, or perhaps because some recombination could occur *in vitro* (Kris Frese, Cancer Research UK Manchester Institute, unpublished data).

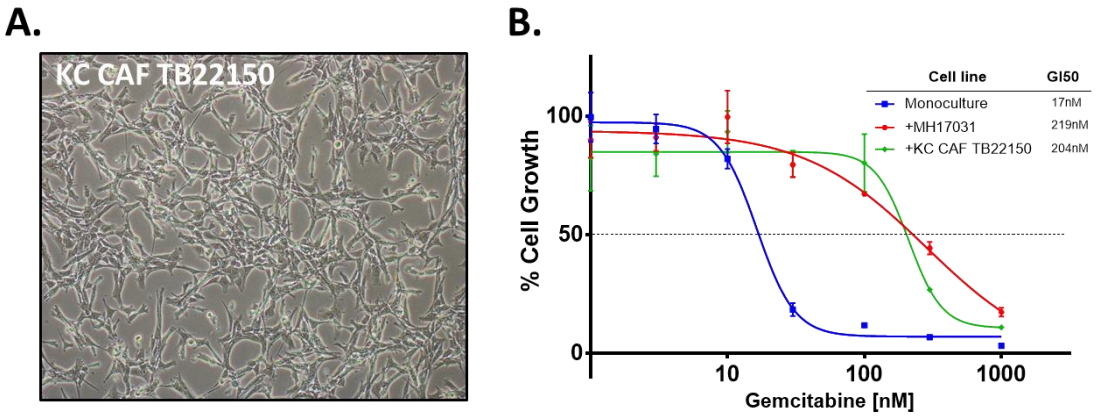

Figure 3.23 Characterising and evaluating TB22150 KC CAFs within the coculture model. ***(A)*** *Morphology of TB22150 cells grown* in vitro*;* ***(B)*** *TB22150 cells assessed in the coculture assay for ability to confer gemcitabine resistance to K8484 cells (green line). Each point represents mean of triplicate biological and triplicate technical replicates, ±SE.*

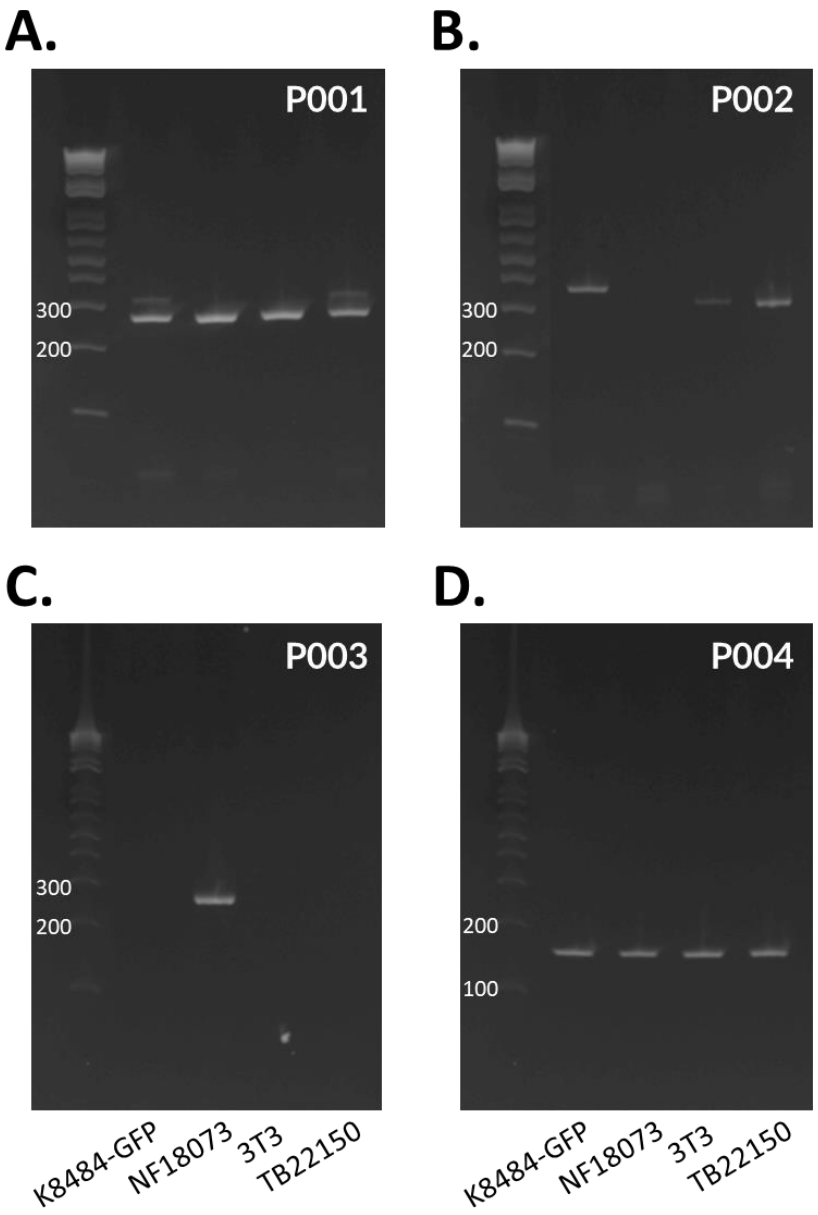

Figure 3.24 Assessing* Kras *and* Tp53 *genotype for TB22150 KC CAFs. (A) *Mutant* Kras *expression assessed via amplification over recombined LSL site, and wild-type* Kras *(~325bp = mut, ~285bp = wt); **(B)** Mutant* Tp53 *expression assessed via amplification over recombined LSL site, positioned within wild-type* Tp53 *(~325bp = mut, no band = non-recombined LSL cassette or sample issue); **(C)** Non-recombined LSL cassette in* Tp53 *via amplification across cassette boundary (~300bp = non-recombined cassette, no band = recombined cassette, no cassette, or sample issue); **(D)** Assessing sample quality via PCR amplification within non-modified intron of* Tp53 *(170bp = sample present, no band = sample issue). 3T3 cells serve as a wild-type control for both genes.*

3.19 In-house isolation and evaluation of a true CAF in the coculture model

A challenge with sourcing of a pure CAF line is the array of documented divergent techniques for their direct isolation from tumour tissue. Published reports include tumour outgrowth, differential adhesion, and differential trypsinisation protocols, each technique leveraging discerning growth properties of CAFs compared to non-CAF cells for their isolation (L. Fang et al., n.d.; Han et al., 2015; Albrecht Neesse et al., 2013). Given the difficulties we have had in isolating true CAFs from KPC tumours, we attempted to obtain CAFs from an alternative source. The Genetically Engineered Mouse-Derived Allograft (GEDA) model, developed in the Jodrell lab (Séverine Mollard, Frances Richards, unpublished), uses a subcutaneous implantation of KPC tumour fragments into recipient PC mice. Previous studies by Kris Frese (Tuveson lab, unpublished) demonstrated that the intratumoural αSMA+ CAFs in GEDA tumours are derived from the host not the donor tumour. To attempt to isolate CAFs, GEDA tumour tissue (AN16CUK004877, 16/4877) was segmented for isolation of CAF populations using each of differential adhesion and trypsinisation techniques, by Sandra Bernaldo de Quirós Fernández.

Multiple cell populations were grown out from this GEDA tumour tissue using each of the above techniques. Following seeding and growth, single cells were isolated from each population using flow cytometry and seeded in single wells of a 96 well plate. Upon clonal expansion cell lines exhibiting the most classical and homogenous mesenchymal morphologies were banked and expanded further. To ensure each population was homogenously non-epithelial, *Kras* and *Tp53* status was assessed within each. From an initial cohort of 19 cell lines isolated as above, only 2 lines, GDF14 and GDF17 both had mesenchymal morphologies (Fig 3.25A) and were verified wildtype status for *Kras* and presence of a non-recombined LSL cassette within *Tp53* (Fig 3.25B). Both were isolated using the differential adhesion method of fibroblast isolation. Each other line had presence of mutant *Kras* populations (indicating contamination with KPC tumour cells). This interestingly demonstrates the inadequacy of morphological characterisation serving the foundation of mesenchymal classification, and the ability for epithelial cells to exhibit mesenchymal properties. This plasticity perhaps indicates a potential source of confounding data and misaligned CAF classification in the wider literature.

To further confirm the identity of both GDF14 and GDF17, αSMA expression was investigated using western blotting. Similar to NF18073, both cell lines expressed high levels of αSMA, in contrast to both K8484 and MH17031 cells, both of which have minimal expression (Fig 3.25C). While αSMA expression in NF18073 indicates these cells may have been activated post culture, given GDF14 and GDF17 were isolated from tumour tissue, the expression of this marker suggests that both are canonical CAF cells. Independently, they appear to be true mesenchymal cells, without epithelial origins.

These GEDA-derived CAFs were investigated in the coculture model for their ability to confer gemcitabine resistance to K8484 cells. Neither cell line induced significant changes in K8484's sensitivity to gemcitabine (Fig 3.25D). Therefore, under the premise that each of these cell lines is indeed a true CAF, the hypothesis that this cell type can confer resistance to gemcitabine in our coculture model appears to be false, and in fact conferred resistance is a property of epithelial tumour cell growth at density. The underlying challenge of experimentation such as this is the opaque and varied classification techniques for identification of CAF cells within pancreatic cancer. To address this, larger panels of these fibroblast-like cells might be used in such experimentation to try identify whether the resistance effect is linked perhaps to specific subtypes of CAFs, which in turn can provide more insight into the functional heterogeneity of CAFs.

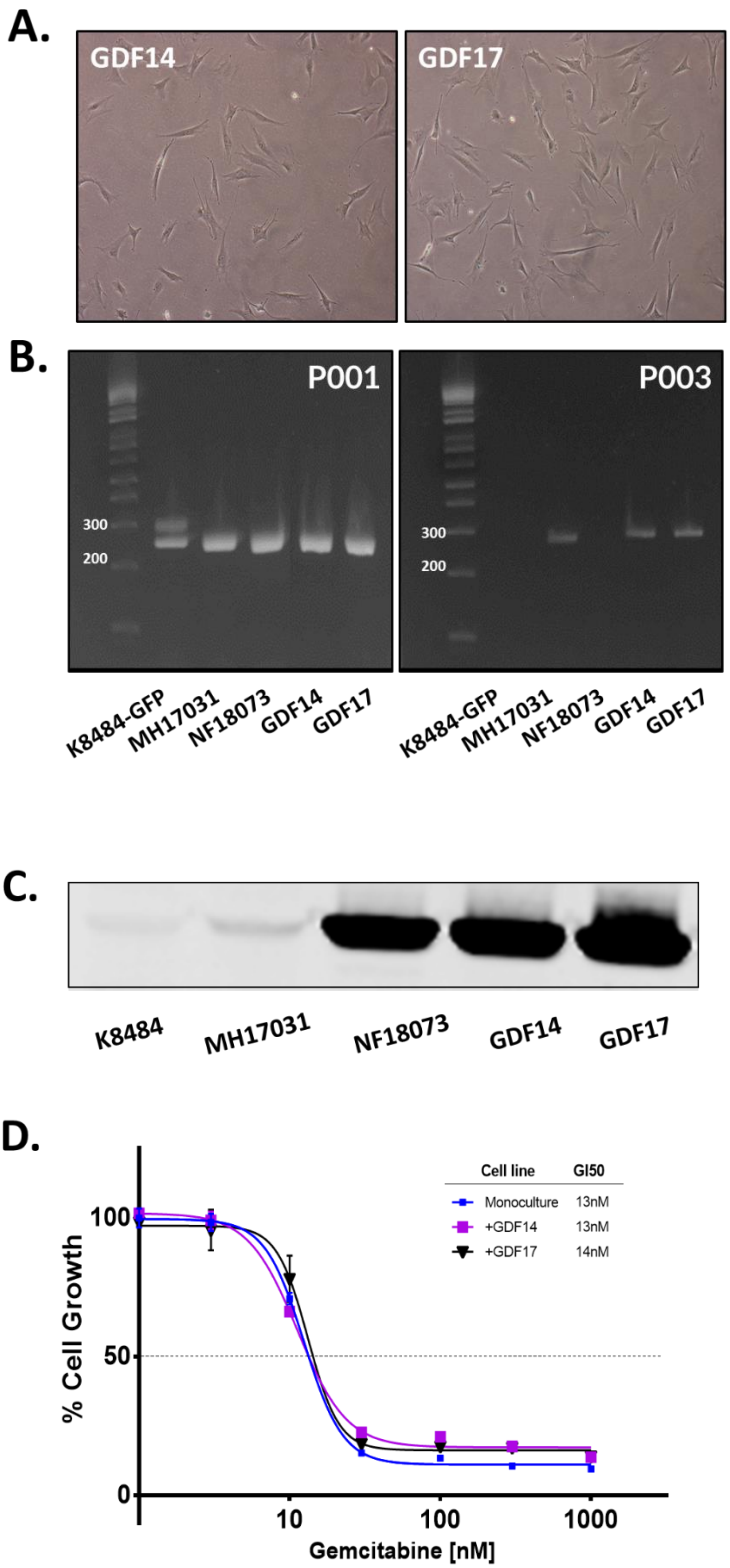

Figure 3.25 Isolating and characterising CAFs from GEDA mice within the coculture model. ***(A)*** *Cell morphology of GDF14 and GDF17 grown* in vitro*;* ***(B)*** Kras *and* Tp53 *genotype assessed via PCR (P001: Mutant* Kras *expression assessed via amplification over recombined LSL site, and wild-type* Kras *(~325bp = mut, ~285bp = wt)) (P003: Non-recombined LSL*

cassette in Tp53 *via amplification across cassette boundary (~300bp = non-recombined cassette, no band = recombined cassette, no cassette, or sample issue);* ***(C)*** *αSMA protein expression assessed using western blot in GDF14 and GDF17 cells alongside K8484, MH17031, and NF18073;* ***(D)*** *Effect of GDF14 (purple) and GDF17 (black) in conferring gemcitabine resistance to K8484 cells when compared to monoculture (blue). Each point represents mean of triplicate biological and triplicate technical replicates, ±SE.*

3.20 Value of model in predicting known gemcitabine synergies and exploring novel ones

The goal of this project was to develop a model of gemcitabine resistance that has value as a system for identifying agents that can sensitize cancer cells to gemcitabine, that may be predictive of therapeutic efficacy both *in vivo* and in patients.

Independent of the characterisation of the specific cell type driving this effect, the effect appears to be real and a product of cell type-specific interactions with pancreatic cancer murine epithelial cells. Factoring this in, the model was evaluated for its alignment with known therapeutic agents demonstrating synergy with gemcitabine either in mice or patients, to indicate an underlying predictive power of the model.

As a mainstay of pancreatic cancer treatment for the last fifty years, gemcitabine has formed a central focus in ongoing development of novel treatment strategies for patients. Combinatorial strategies of using multiple agents alongside nucleoside analogues such as gemcitabine have helped enhance overall efficacy for patients. FOLFIRINOX is an example of such a cocktail, treatment patients concurrently with folinic acid, fluorouracil, irinotecan, and oxaliplatin. A challenge though with such treatment regimens is increased side effects incurred through multiple non-targeted agents. As such, the past decade has seen a focus on leveraging combination strategies with more targeted agents, better addressing specific alterations within cancer cells through biomarker-driven therapeutic selection (Rahib et. al, 2016; Sheahan et. al, 2018).

One combination that has seen value *in vivo*, with prospects for a clinical trial within pancreatic cancer, is gemcitabine alongside AZD2014, a dual MTOR1/2 inhibitor. Pre-clinical studies have demonstrated a mild synergistic effect between both agents both *in vitro* and directly in KPC mice (Driscoll et al., 2016; Frese et al., 2012; Morran et al., 2014). The exact mechanism through which this synergy is derived is not clear, although as the MTORC

complex lies downstream of oncogenic KRAS activity, as an effector of PI3K, combination with gemcitabine may serve two functions in decreasing viability of *Kras*-mutant pancreatic cancer cells.

To assess the validity of our *in vitro* coculture model, a combination of gemcitabine and AZD2014 was trialled for efficacy on K8484 cells when in coculture with MH17031. As a single agent in coculture AZD2014 demonstrated mild effect on K8484 cells ($_{GI50}$ = 330nM) (Fig 3.26E), similar to single agent data seen in KPC mice referenced above. When combined with gemcitabine, a mild level of synergy is observed at ~30nM gemcitabine alongside 3-10nM AZD2014 (Fig 3.26B, C). This slight increase aligns with combination data from KPC mice, where the combination of agents had a median survival in KPC mice of 280 days compared to 195 days for AZD2014 alone, 147 days for gemcitabine and 132 days for untreated (Driscoll et al., 2016). This result indicates the coculture model herein developed may have power to predict combinations of value for *in vivo* studies in KPC mice. Uncertainty though remains due to the low number of cell lines for which this effect is observed, as well as the relatively low degree of synergy calculated. Additional experimentation here might include an expanded cell line panel for interrogation, as well as expanded dose ranges around the apparent synergistic concentration combinations to better evaluate the magnitude of the synergy.

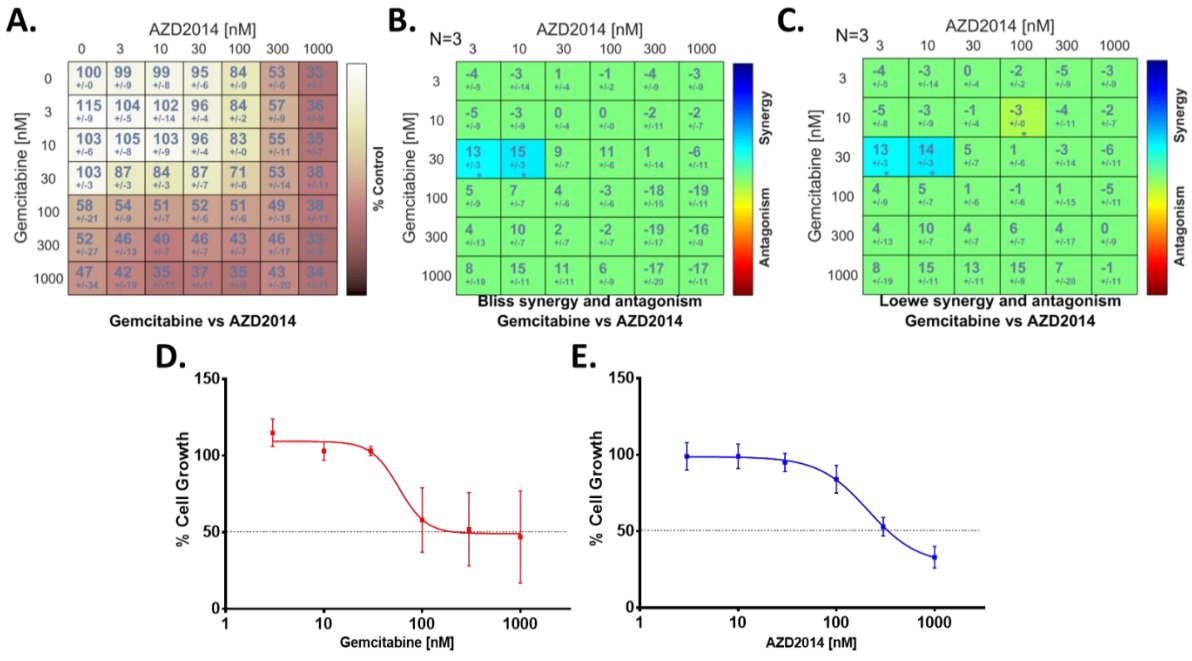

Figure 3.26 Combination of gemcitabine and AZD2014 in coculture model. (A) *Percentage growth relative to solvent for control for a 6x6 gemcitabine and AZD2014 combination range; Synergy quantification calculated in Combenefit using the Bliss Independence model* ***(B)*** *and the Loewe model* ***(C)*** *(blue = combinations demonstrating significant synergy); Single agent dose response curves for each of gemcitabine* ***(D)****, and AZD2014* ***(E)*** *for which each point represents mean of triplicate biological and triplicate technical replicates, ±SE.***.**

Gemcitabine's mechanism of action is to incorporate into replicating DNA, induce stalling of the replication fork, and therefore cause damage to DNA. Cells rely on a plethora of factors to repair such DNA, one of which is ATR (Ataxia telangiectasia and Rad3 related) (Blackford and Jackson, 2017). High levels of ATR expression is linked to decreased survival in PDAC patients, potentially a product of cancer cells' ability to mitigate DNA damage and therefore cell death induced by gemcitabine. Pre-clinical murine studies in our lab have further indicated the combination of ATR kinase inhibitor AZD6738 to potentiate gemcitabine effect (Wallez et al., 2018),laying the foundation for human clinical studies within pancreatic cancer specifically.

Recapitulating this combination in our coculture model was a final step to assess whether combinations with defined pre-clinical or clinical value could be accurately evaluated in this setting. AZD6738 as a single agent has minimal effect on K8484 cells in coculture, even at concentrations up to 3µM (Fig 3.27E). This is likely a product of inhibition of ATR alone, without the concurrent DNA damage induced by a nucleoside analog such as gemcitabine, unable to significantly effect growth potential of K8484 cells. Once in combination, quite significant levels of synergy are observed again at ~30nM of gemcitabine with a range of AZD6738 doses between 0.3 – 3uM (Fig 3.27B, C). This dose range has been demonstrated by our lab to be approximately equivalent to the EC50, and therefore likely resulting specifically from inhibition of ATR, as opposed to off-target effects that might be observed at high concentrations

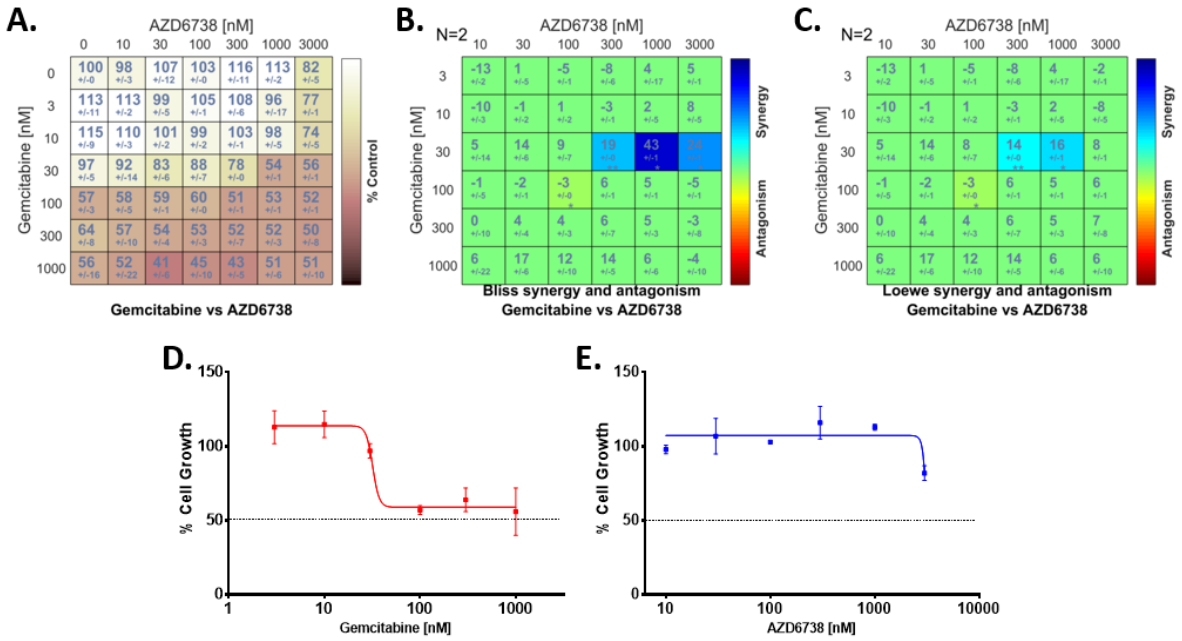

Figure 3.27 Combination of gemcitabine and AZD6738 in coculture model. (A) *Percentage growth relative to solvent for control for a 6x6 gemcitabine and AZD6738 combination range; Synergy quantification calculated using the Bliss Independence model* ***(B)*** *and the Loewe model* ***(C)*** *(blue = combinations demonstrating significant synergy); Single agent dose response curves for each of gemcitabine* ***(D)****, and AZD6738* ***(E)*** *for which each point represents mean of duplicate biological and triplicate technical replicates, ±SE.**.***

3.21 Conclusion

The goal and output of this chapter was to interrogate and document the characteristics of the *in vitro* model of gemcitabine resistance in PDAC developed originally within the Jodrell lab. Having described the nature of the resistance effect as transient in nature and reliant on cell-cell contact, I further demonstrated that the cell line driving the effect is not a CAF, as first proposed, but rather more likely an epithelial cell in origin having since developed more mesenchymal morphological features.

Demonstrating also that true pancreatic CAFs do not appear to drive resistance in this model, I hope to have exemplified the real challenges that exist in proper cell line isolation and characterisation within this space, and the potential pitfalls that may have hampered previous investigations. Future experimentation into CAF form and function, as well as intercellular interactions, would benefit greatly from more detailed characterisation of the different CAF and fibroblast-like intracellular subtypes in PDAC.

Despite the challenges around cellular identity though, I have demonstrated that the resistance effect observed is real, and perhaps a product of a quorum-sensing phenomenon within the model. Taken altogether, synergy with gemcitabine plus AZD6738, and gemcitabine plus AZD2014 indicates that independent of an understanding of the specific cell type inducing resistance to gemcitabine in this model, it remains predictive of therapeutic combinations with *in vivo* efficacy. Using this coculture model may enable reduction of the numbers of animal required for *in vivo* testing of drug combinations, with ethical and financial benefits.

Further, the development of a novel model of gemcitabine resistance in pancreatic cancer *in vitro*, with demonstrated efficacy data correlated to clinical studies, presents as a valuable system for high throughput therapeutic target identification requiring significantly lower resource investment when compared to *in vivo* studies or more complex multi-dimensional *in vitro* models.

4. An shRNA screen to investigate gemcitabine sensitivity in a coculture model of PDAC

This shRNA screen project was carried out in collaboration with Dr Nicolas Erard, a previous PhD student in Professor Greg Hannon's laboratory at the CRUK Cambridge Institute. For this thesis, I will outline my specific contributions to this project. The cloning of the shRNA libraries and retrovirus production were performed by Nicolas. The subsequent passaging of infected cells in mono and coculture was a collaborative effort between Nicolas and myself, as well as the gDNA extraction and PCR of shRNAs and sequencing library preparation. Sequencing was undertaken by the CRUK Cambridge Institute Genomics Core, with read normalisation and differential expression scoring performed by Chandra Sekhar Reddy Chilamakuri from the CRUK Cambridge Institute Bioinformatics core. All figures are a product of my own analysis.

4.1 Introduction

A primary challenge of translational research in pancreatic cancer, and associated target identification, is the difficulty in recapitulating the conditions found inside the tumour in a biologically correlative manner, amenable to high-throughput target validation. Our coculture model of PDAC gemcitabine resistance opens a novel and scalable modality for exploration into the genetic mechanisms driving resistance. Traditionally, such investigations are either hypothesis-driven targeted interrogations, or broader in scope -omic characterisations.

The former is valuable as a tool to drill into the intricacies of a phenotype's mechanism but relies on the presence and integrity of targets identified previously. This therefore limits experimental scope for identifying truly novel targets and mechanisms.

Broader -omic-based techniques can remove bias in target identification and validation, by interrogating entire genomes, proteomes, transcriptomes, among others, for phenotypic alterations of interest. Tools such as RNA-Seq and Cell Type specific labeling using Amino acid Precursors (CTAP) take an observational approach to investigation, identifying targets and phenotypes of interest through differential transcript and protein levels respectively (Gauthier et al., 2013; Wang, Gerstein, and Snyder, 2009).

To investigate the mechanism of gemcitabine resistance observed in the *in vitro* coculture model detailed in Chapter 3, I undertook a whole-genome shRNA screen (Fig 4.1). Despite considering both proteomic and RNA-Seq-based screening techniques for their observational value, the direct manipulation possible via shRNA screening was considered to be more effective in identifying single gene contributors to the observed gemcitabine resistance effect. Specifically, I used a short hairpin RNA library comprised of seven pools of around 10,000 shRNAs each, targeting approximately 19,000 genes within the mouse genome. This library, by infecting the pancreatic cancer cells, and exposing to gemcitabine, can support identification of genes driving resistance to gemcitabine within the model, using a dropout viability format (Diehl, Tedesco, and Chenchik, 2014; Sims et al., 2011). The screen involves assessing shRNA depletion through six gemcitabine or DMSO control cycles, in both monoculture and coculture, compared to timepoint zero (Figure 4.1). Different concentrations of gemcitabine were used for coculture and monoculture, 100nM and 10nM respectively, to approximate gemcitabine GI_{50} within each growth condition (Fig 3.2).

This approach has direct interrogative translational value to complement observational broad-based approaches. Whereas observational approaches rely on correlation to infer function, an shRNA depletion screen instead looks at phenotypic impact of gene knock-down to decipher function. Therefore, there is less reliance on correlative observations, and instead a focus on true functional effects conferred from genome manipulation.

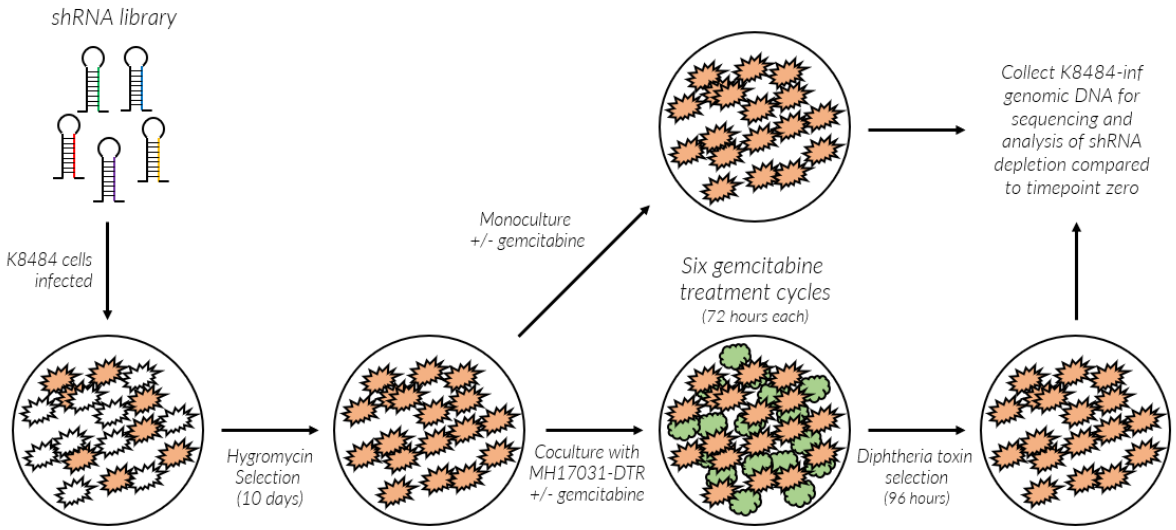

Figure 4.1 Schematic for whole-genome shRNA screen used to interrogate gemcitabine resistance mechanism in coculture. *K8484 pancreatic cancer cells, isolated from KPC tumours, were infected with a murine whole-genome shRNA library. Following selection with hygromycin for infected cells, and multi-passage depletion of cells targeting cell survival-essential genes, genomic DNA was extracted, and subsequent populations split into mono- and coculture arms, the latter to be grown alongside MH17031-DTR cells. Each arm was treated with six cycles of gemcitabine (72 hours) at a gemcitabine concentration between GI25 and GI50 values (10 nM gemcitabine for monoculture condition, and 100 nM for coculture condition, or DMSO control). Following the final cycle, the coculture condition was treated with 100ng/ml diphtheria toxin for 96 hours to deplete MH17031-DTR cells to less than 10% of the total population. Genomic DNA was extracted from the K8484 cells, and following DNA sequencing, shRNA representation was compared to the time timepoint zero sample to identify depleted shRNAs.*

4.2 Design and preparation of screening protocol

To undertake a whole-genome shRNA screen interrogating gemcitabine resistance mechanism in a coculture model of pancreatic cancer, two novel cell lines were created. Firstly, a mouse PDAC line infected with a whole genome shRNA library (K8484-inf), along with a modified MH17031 line engineered for selective ablation in coculture models, to allow leveraging their resistance-conferring effect whilst also supporting selective depletion

at the end of the assay to create a pure K8484-inf population. This is required to maximise shRNA levels within genomic DNA for normalising alongside the monoculture control protocol.

For the PDAC cell line, K8484 cells were used, due to extensive validation and characterisation in our lab both genetically and using protein markers (Chapter 3), as well as in relation to gemcitabine sensitivity in both mono- and co-culture with MH17031. The line was retrovirally infected with a mouse genome-wide shRNA library from Transomic Technologies, using shRNA designed using the SHERWOOD algorithm for maximising shRNA potency and minimising off-target effects (Knott et al., 2014), creating the K8484-inf line. The library contained 63,677 shRNAs covering 18,402 genes within the mouse genome, coupled with a panel of shRNAs targeting human olfactory receptor genes to serve as negative controls. Each gene had an average of 3.46 unique shRNAs targeting it (Fig 4.2), adding confidence in identifying true positives and minimising false positives resulting from off-target effects in the subsequent sequencing analysis.

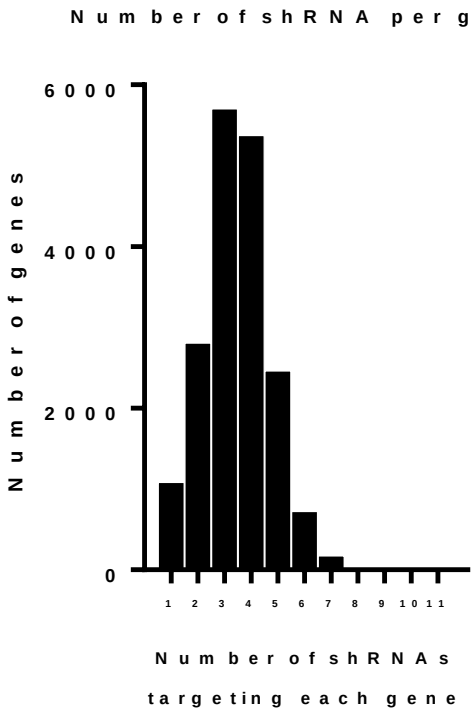

Figure 4.2 The number of shRNAs targeting each gene within the whole-genome library used.

Once created, the line was expanded in culture and selected with 500µg/ml hygromycin for 96 hours to approximate a pure fully transfected population, verified through homogenous expression of mCherry, a fluorescent marker expressed within each cell successfully infected with an shRNA. Cells were then grown for seven days to allow for dropout of shRNAs targeting genes required for cell survival. Genomic DNA was then extracted from an aliquot of this population and stored at -80C, to serve as a timepoint zero sample to be included in future analysis.

The second line to be created was a modified MH17031 line. As the data of interest at the end of this shRNA depletion screen is the shRNA qualitative and quantitative profile within the K8484-inf cell line, it is imperative that sequencing depth and coverage from the line is maximised, ensuring even slight, yet still statistically significant, changes are recorded. To support this, MH17031 needs to be selectively ablated from the coculture conditions prior to gDNA extraction at the end of the screen. To achieve this, MH17031 cells were transduced with a plasmid expressing human diphtheria toxin receptor (DTR), ZsGreen fluorescent protein, and a neomycin resistance cassette (MH17031-DTR).

4.3 Scaling of coculture resistance phenomenon to 15cm dishes

To assess drivers of gemcitabine resistance at the genome-wide level, it was necessary to scale up the coculture resistance assay, to enable ultra-high-throughput screening, by proportional scaling of the 96 well plate assay to 15cm plates, maintaining ratios of cell lines and media volume to surface area. A comparison was performed by investigating the percent growth inhibition of cells in monoculture and coculture at both 10nM and 100nM gemcitabine, between the standard 96 well assay format and the scaled assay in 15cm dishes. Growth of K8484 cells in coculture with 100nM gemcitabine in 96 well format and 15cm dish format were 64% and 62% when compared to DMSO control respectively (Fig 4.3). In monoculture with 100nM a gemcitabine growth rate of only 22% was observed when compared to non-treated control, therefore indicating that a coculture-driven

resistance effect is maintained in the scaled assay in 15cm dishes.

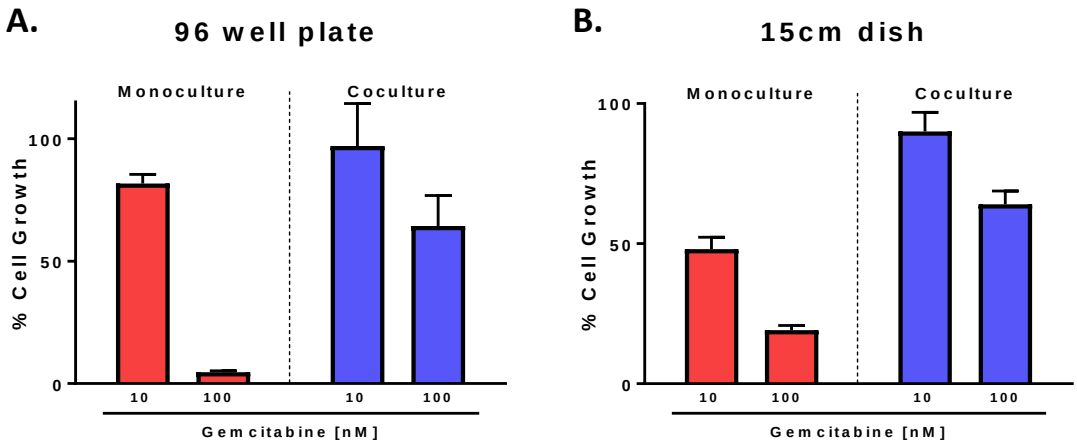

Figure 4.3 Maintenance of coculture-conferred resistance to gemcitabine in 15cm dish assay. *Degree of effect of two doses of gemcitabine on K8484 survival in both monoculture and coculture (with MH17031) in* ***(A)*** *96 well plates and* ***(B)*** *15cm dishes over 72 hours treatment, relative to growth in a DMSO untreated control.*

4.4 Primary genome-wide shRNA screen to investigate genetic drivers of gemcitabine resistance in coculture

The underlying principle of this shRNA depletion screen is that by comparison of population shRNA profiles at the start of the screen and after the drug cycles, shRNAs that are depleted throughout represent genes that normally serve to confer gemcitabine resistance in the cells. Further, by identifying those shRNAs depleted in the coculture model plus gemcitabine specifically, a list of genes involved in the specific coculture-driven resistance mechanism we have observed is elucidated.

For each condition, six cycles of 72 hours gemcitabine or DMSO control treatment were performed. After each cycle cells were split and reseeded to conserve the 10:1 MH17031-DTR:K8484-inf seeding ratio, typically requiring fresh MH17031-DTR cells, given the higher proliferation rate of K8484-inf.

To ensure cells maintained proliferative potential throughout the screen, and did not undergo replicative senescence, cell growth rates were monitored throughout. Mirroring proliferation rates seen in the original 96 well format (Fig 3.21), K8484-inf cells in monoculture in the 15 cm dishes proliferated 30-50X over 96 hours (24 hours of growth post-seeding prior to 72 hours gemcitabine treatment) (Fig 4.4). In coculture, both PDAC

and MH17031 cells proliferated at a reduced rate, of 1.2X – 3.5X over the 96 hours. Notably, this reduced rate has been discounted as the only driver of gemcitabine resistance in previous work detailed in Chapter 3.

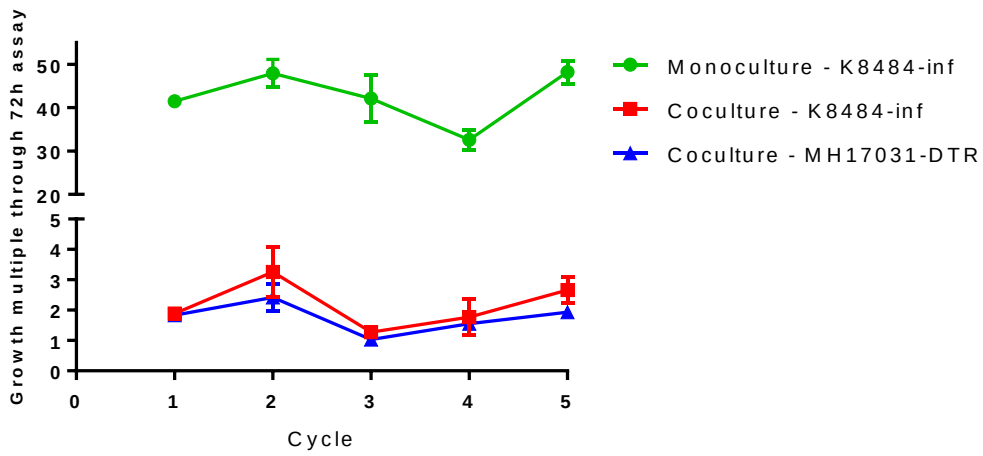

Figure 4.4 Cell growth rates through screen cycles. *The percentage of cells with mCherry expression at each cycle was used as a surrogate marker of K8484-inf cell numbers, with the remaining population ascribed as MH17031-DTR cells. Cell numbers were counted using Vi-CELL (Beckman Coulter), and percentage of populations fluorescent for mCherry measured with MACS Quant (Miltenyi Biotec).*

4.5 Sensitivity to gemcitabine through screen progression and cycling.

It was also important to ensure that the expected degree of gemcitabine sensitivity was maintained throughout each cycle. To assess this the growth rate of K8484-inf cells in both monoculture and coculture plus gemcitabine was compared to their counterpart in DMSO only. A reduction in survival of approximately 20-40% was anticipated, replicating that observed previously during screen validation (Fig 4.3). In monoculture there was a slight decrease in sensitivity between the first cycle and the fifth (Fig 4.3A), and conversely in coculture there was a minor increase in sensitivity (Fig 4.3B). Nevertheless, through all cycles and all conditions there were no major outliers when compared to the validation experiment sensitivities. Minor changes may be ascribed to factors such as increases in proportion of population resistance to gemcitabine over time, or changes in proliferation rate and viability as cells undergo continuous passaging. As such, there is further confidence that the output of the screen is a true reflection of genetic drivers of gemcitabine resistance, and not merely an artefact of intra-screen growth changes.

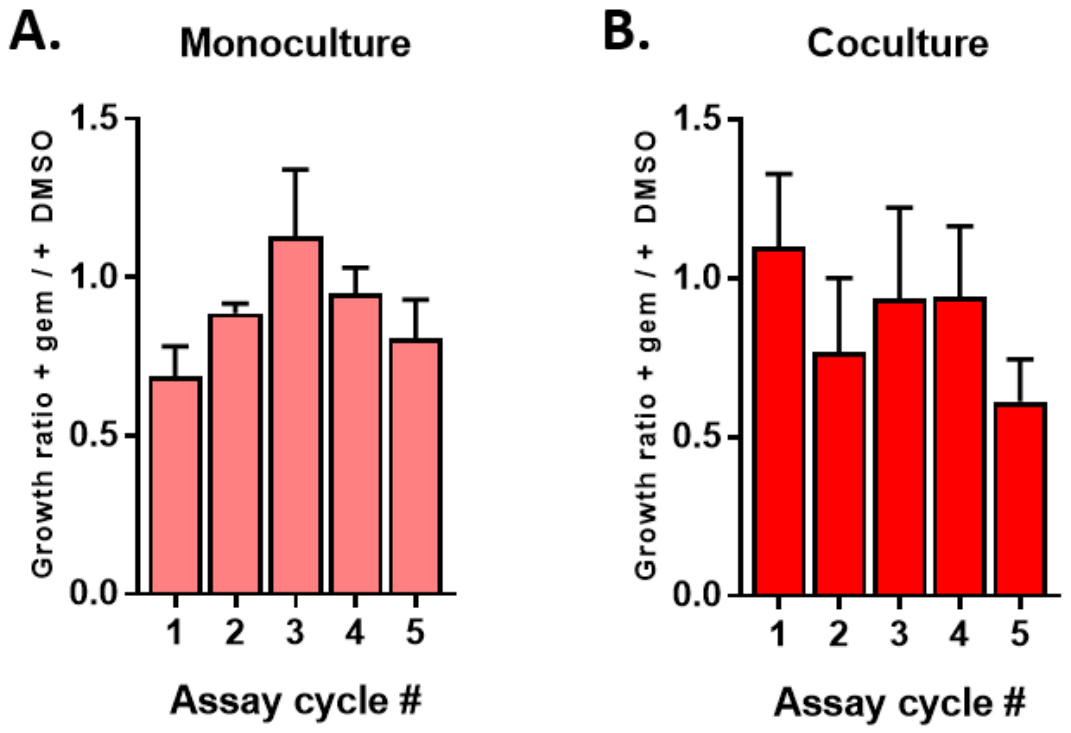

Figure 4.5 Gemcitabine sensitivity variation through screen cycles. *Sensitivity of K8484-inf cells to gemcitabine through each screen cycle in both* ***(A)*** *monoculture and* ***(B)*** *coculture conditions, inferred through growth rate relative to untreated DMSO controls.*

4.6 Post-screen sample preparation and sequencing

Upon completion of the screen, shRNA profiles for each assay condition and replicate were to be assessed, to identify enrichment and depletion changes incurred through the screen and allow for comparative analysis between conditions. As a first step, genomic DNA was extracted from surviving K8484-inf cells, to provide template for shRNA amplification, sequencing, and downstream analysis. For the coculture conditions this extraction was preceded by a 96-hour exposure to 100ng/ml diphtheria toxin for selective ablation of the MH17031-DTR cells, purifying a K8484-inf population. This genomic DNA was used to amplify out the shRNA cassette, following by a separate barcoding PCR to individually label each condition and each replicate within it for pooled sequencing. Samples were sequenced using Illumina HiSeq to a depth of at least 10 million reads.

Sequencing reads were analysed by first mapping to an index of each shRNA sequence and gene name, as provided by the shRNA library manufacturer, Transomic Technologies. Differential expression analysis was then performed by comparing shRNA representation in

each condition to the timepoint zero set. Differential expression was quantified using two separate tools, DESeq2 (Love et al., 2014), and median Z scores. DESeq2 is a purpose-built analytical tool for carrying out differential analysis of high-throughput sequencing data, using shrinkage estimators for expression variance and fold change to account for low sample number differential expression scoring calculations. Median Z scores are created using a function to calculate the mean and standard deviation of each shRNA, defining a Z-score where Z measures the number of standard deviations of the shRNA expression level is from the population median (DE scoring performed by Chandra Sekhar Reddy Chilamakuri, CRUK Cambridge Institute).

With genome-wide data, the threshold of what is termed a "hit" or not can be adjusted along a gradient, depending on the degree of confidence required and number of candidate shRNAs required for subsequent analytical steps, such as pathway analysis. Given the purpose of this primary screen in identifying a large list of genes of interest to inform later more targeted screening protocols and factoring in the confounding issue of off-target-driven false negatives and positives, hit scoring criteria were set to be minimally restrictive.

For DESeq2, shRNAs were considered as hits if they had a Log2(FoldChange) of ≤ 0 and an adjusted p value of ≤ 0.05. Similarly, for median Z scoring, shRNAs were termed a hit with a median Z score of ≤ -2, therefore an shRNA representation of a minimum of two standard deviations below the median shRNA representation value. Further, for a gene to be recorded as a hit, at least 50% of shRNAs targeting that gene needed to be hits, or if only one shRNA was targeting that gene, it had to be significantly depleted (Table 4.1).

Gene hit criteria	
DESeq2	**Median Z score**
≤ 0.05 p_{adj}	≤ -2 Z score
< 0 Log2(FoldChange)	≥ 50% targeting shRNAs hitting
≥ 50% targeting shRNAs hitting	

Table 4.1 Hit calling criteria using normalised primary shRNA screen data, for both DESeq2 and median Z score differential expression analysis methodologies.

The subset of most interest within this screen was the coculture condition plus gemcitabine. By identifying genes that are significantly depleted in this subset when compared to timepoint zero, and not depleted in any of the other three conditions, it is possible to identify genes which may have a functional role in driving the observed resistance in the original model of coculture-driven resistance. This coculture condition plus gemcitabine had the highest number of significantly depleted shRNAs using both scoring methodologies, with 2,357 shRNAs depleted using DESeq2 and 5,563 shRNA depletion hits using median Z scores (Table 4.2), with an associated 291 genes significantly depleted with DESeq2, and 959 genes with median Z score. The distributions of ShRNAs in DESeq2 analysis and median Z score analysis are shown in Figures 4.6 and 4.7 respectively. Notably, for DESeq2 analysis there were over eight times the number of shRNAs identified as depleted relative to timepoint zero in the coculture plus gemcitabine condition compared to the monoculture plus DMSO condition, and over three times the number relative to the monoculture plus gemcitabine condition. These differences are potentially a product of the presence and concentration of drug used, whereby higher doses of gemcitabine may induce changes in gene expression within cells through their enhanced dependence on resistance-driving genes for survival. Additionally, with a higher GI50 in the coculture plus gemcitabine condition, there exists a larger range of gemcitabine GI50s that cells can be sensitised to, and therefore an increased ability to exhibit statistically significant change versus the DMSO control.

Condition	**Median Z score**		**DESEq2**	
	shRNAs	**genes**	**shRNAs**	**genes**
Coculture + gemcitabine	5563	959	2763	291
Coculture + DMSO	2741	448	1043	159
Monoculture + gemcitabine	2064	298	738	78
Monoculture + DMSO	1545	212	345	38

Table 4.2 Number of shRNAs and genes significantly depleted within the coculture and monoculture conditions +/- gemcitabine. *Compared to timepoint zero, from primary ShRNA screen of* 63,677 shRNAs covering 18,402 genes within the mouse genome.

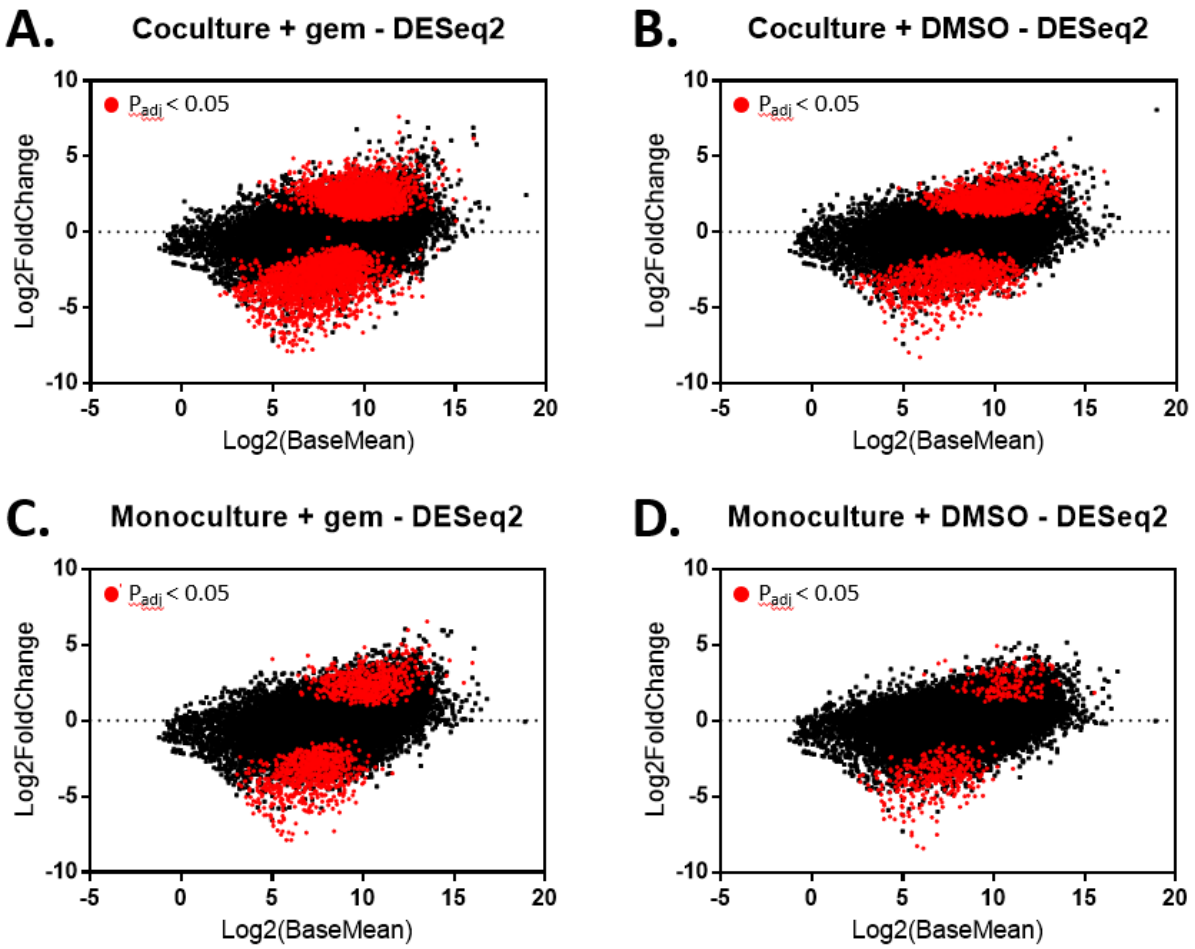

Figure 4.6 shRNA differential expression scoring between conditions using DESeq2. *Significantly differentially expressed shRNAs (red dots) called using R Bioconductor package DESeq2 for coculture plus* ***(A)*** *gemcitabine,* ***(B)*** *DMSO, and monoculture plus* ***(C)*** *gemcitabine and* ***(D)*** *DMSO. shRNAs with a Log2FoldChange value of less than 0 indicate depletion through the screen, whereas those greater than 0 indicate enrichment.*

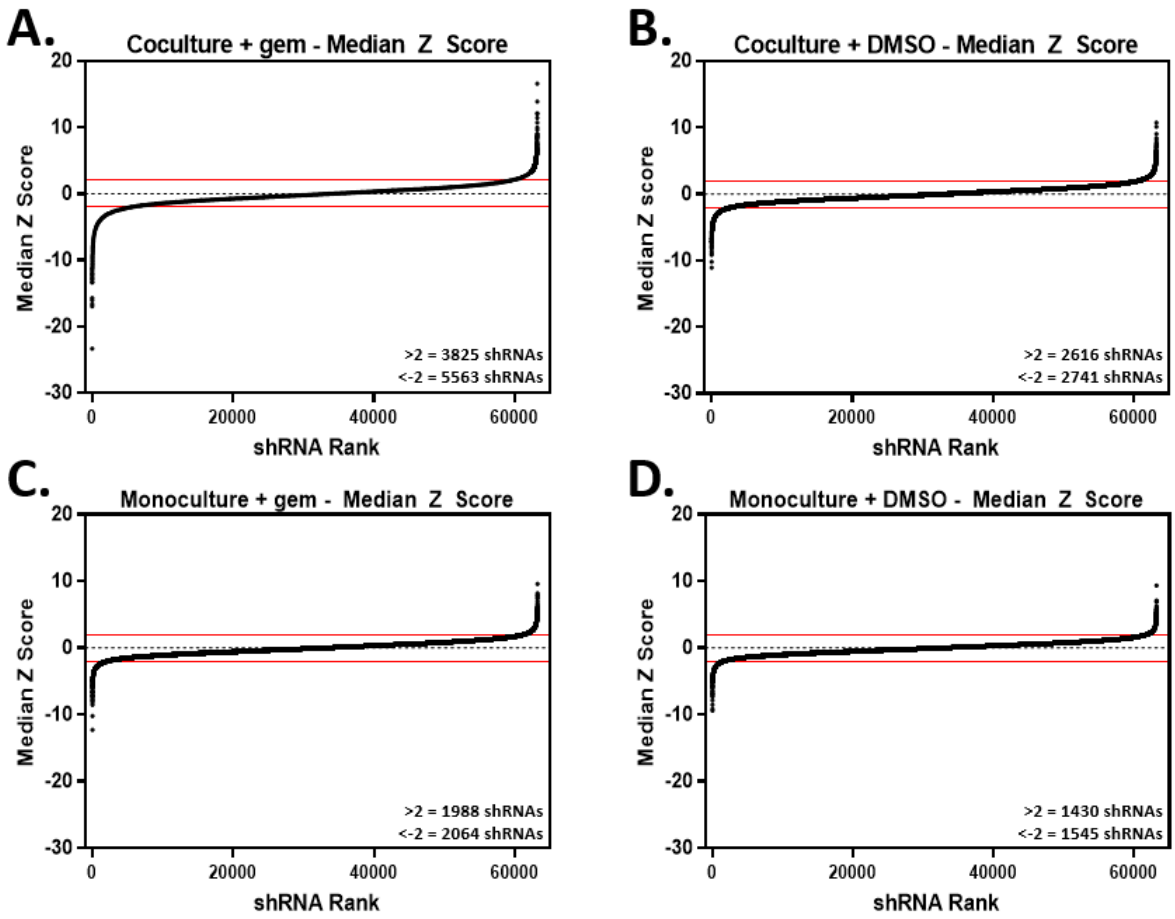

Figure 4.7 shRNA differential expression scoring between conditions using Median Z Scores. *Significantly differentially expressed shRNAs called using Median Z Scores for coculture plus* ***(A)*** *gemcitabine,* ***(B)*** *DMSO, and monoculture plus* ***(C)*** *gemcitabine and* ***(D)*** *DMSO. shRNAs were ranked based on Median Z Score value (standard deviations from population median expression), with shRNAs with a ≤-2 or ≥2 value (marked by red lines) considered significantly depleted or enriched, respectively.*

4.7 Evaluation of positive and negative screen controls

To build confidence in hits resulting from the screen, it was important to verify that both technical and biological controls within the screen hold true.

To assess this, four genes were assessed. As positive biological controls, *Chek1* and *Atr* were selected. Each has been documented that through inhibition *in vitro* and *in vivo* sensitivity to gemcitabine is increased (Siang-Boon Koh et al., 2015; S. Liu et al., 2017; Parsels et al., 2009; Prevo et al., 2012; Wallez et al., 2018),. Further, both have been targets of successful preclinical drug development programs, with molecules inhibiting their function currently or

previously being investigated in clinical trials (Banerji, Jones, and PLummer, 2017; Plummer et al., 2016). As a negative technical control, *Prss2* was selected, a serine protease expressed exclusively in hormone-producing glandular cells (J. Gao et al., 2010). Hence it is not expected to modulate gemcitabine resistance in this model, as it is unlikely to be expressed in the cell types used. Finally, *Dck* was used as a negative biological control. *Dck* codes for deoxycytidine kinase, a key enzyme required for the phosphorylation and activation of gemcitabine (dFdC) to dFdCMP (Ohhashi et al., 2008; Saiki et al., 2012). Therefore, through inhibition of its activity, cells are likely to become more resistant to gemcitabine, and shRNAs targeting this gene would enrich through the assay cycles as opposed to depleted like *Chek1* or *Atr*.

Using the DESeq2 calling methodology, two of the four shRNAs targeting both *Chek1* and *Atr* were significantly depleted, therefore as genes being called as hits (Fig 4.8). *Prss2* shRNAs showed minimal fold change variance when compared to the total mean, with no shRNA being significantly depleted or enriched. Finally, for *Dck* three of the seven targeting shRNAs were significantly enriched through the assay. So, while *Dck* as a gene did not match the criteria for being a hit, it did demonstrate a trend towards enrichment overall. Similarly, for median Z scores (Fig 4.9), both *Chek1* and *Atr* were depleted hits, with *Prss2* showing minimal change in either direction, and *Dck* again showing a trending but non-significant enrichment. Taken together the as-predicted results for the control genes add confidence that any novel hits coming out of the screen may have true mechanistic involvement in the gemcitabine resistance effect, and therefore hold potential translational value.

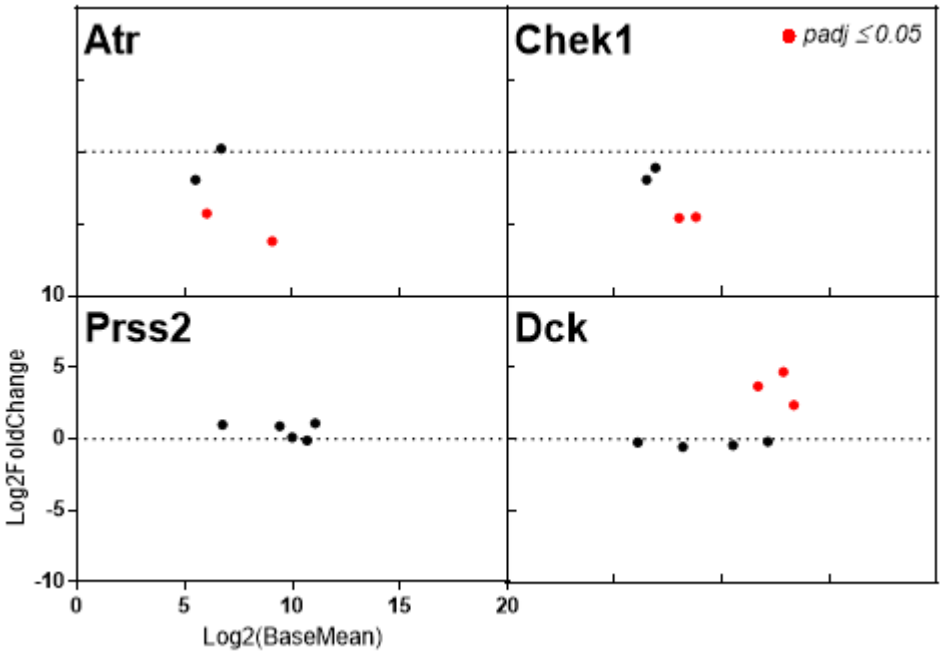

Figure 4.8 DESeq2 differential expression of select control shRNAs in coculture plus gemcitabine. *shRNA differential expression data for positive (*Atr, Chek1*), technical (*Prss2*), and negative (*Dck*) controls was analysed, each targeting shRNA plotted as a single dot (red = significantly enriched or depleted).*

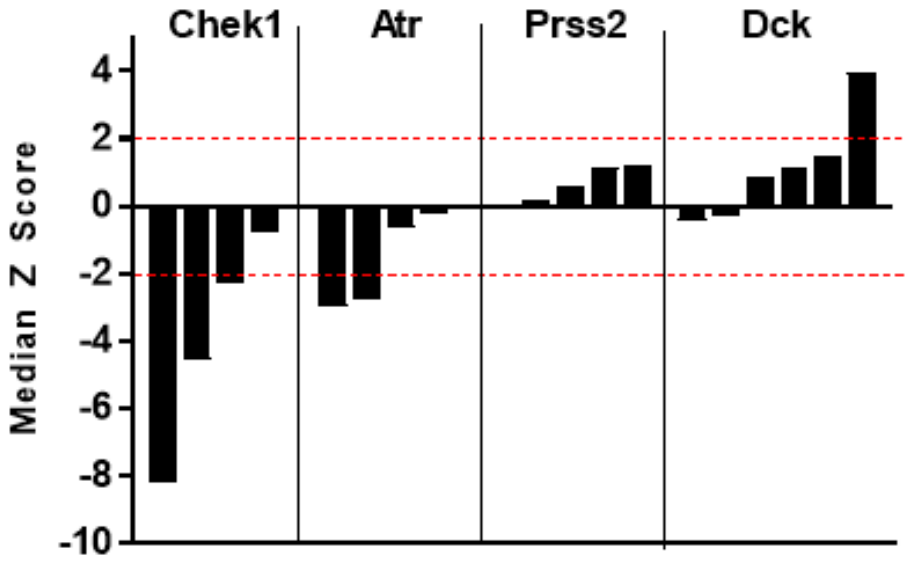

Figure 4.9 Median Z Score-called differential expression of select control shRNAs in coculture plus gemcitabine. *shRNA differential expression data for positive (*Atr, Chek1*), technical (*Prss2*), and negative (*Dck*) controls was analysed, each targeting shRNA plotted as*

a bar, y axis representing Median Z Score value. shRNAs above and below the red dotted line represent significantly enriched to depleted shRNAs respectively.

4.8 Meta-analysis of screen data

Verifying through controls that screen data holds validity, the real value of the project is investigation into novel genes being identified as influencers of the coculture resistance phenomenon. Specifically, those genes only depleted in the coculture indication plus gemcitabine.

Beginning with a library of 18,402 genes, with over 7,000 shRNAs significantly depleted in the coculture plus gemcitabine condition across both scoring methodologies, it is imperative to segment and filter the total data into more actionable and valuable sets delivering clear insights into the biology behind the phenotype. To do this, a list was created of each gene scored as a hit within each assay condition, for each of the two differential expression scoring methodologies. Upon collation, each gene set was contrasted against each other set across each of the other three conditions.

Initially, it was apparent that there were a higher number of hits being scored using median Z score when compared to DESeq2 to call differential expression across conditions (1513 to 496 genes across all conditions respectively). This is not unexpected, and a product of the selection of hit calling thresholds for each methodology, as observed previously (Mendes-Pereira et al., 2012). For the coculture plus gemcitabine condition for each tool, approximately 50% of the total hits across conditions were unique and absent from each of the other conditions, as per Figure 4.11 below. This provides a valuable confirmation that each scoring tool has no obvious skew towards certain conditions when compared against the other.

As each methodology used to score differential expression inevitably introduces its own set of technical biases (Conesa et al., 2016; Finotello and Di Camillo, 2015; Soneson and Robinson, 2017) the inclusion of a range of scoring tools on the same dataset can provide an even more robust insight into the genes of interest (Mendes-Pereira et al., 2012). This assumes that for a gene to be scored as a hit between tools, it is more likely a true positive, as despite factoring in technical variations in calling hits between tools, it remains a hit in each. Applying this principle, I investigated the common hits between scoring tools for each

culture condition (Fig 4.10).

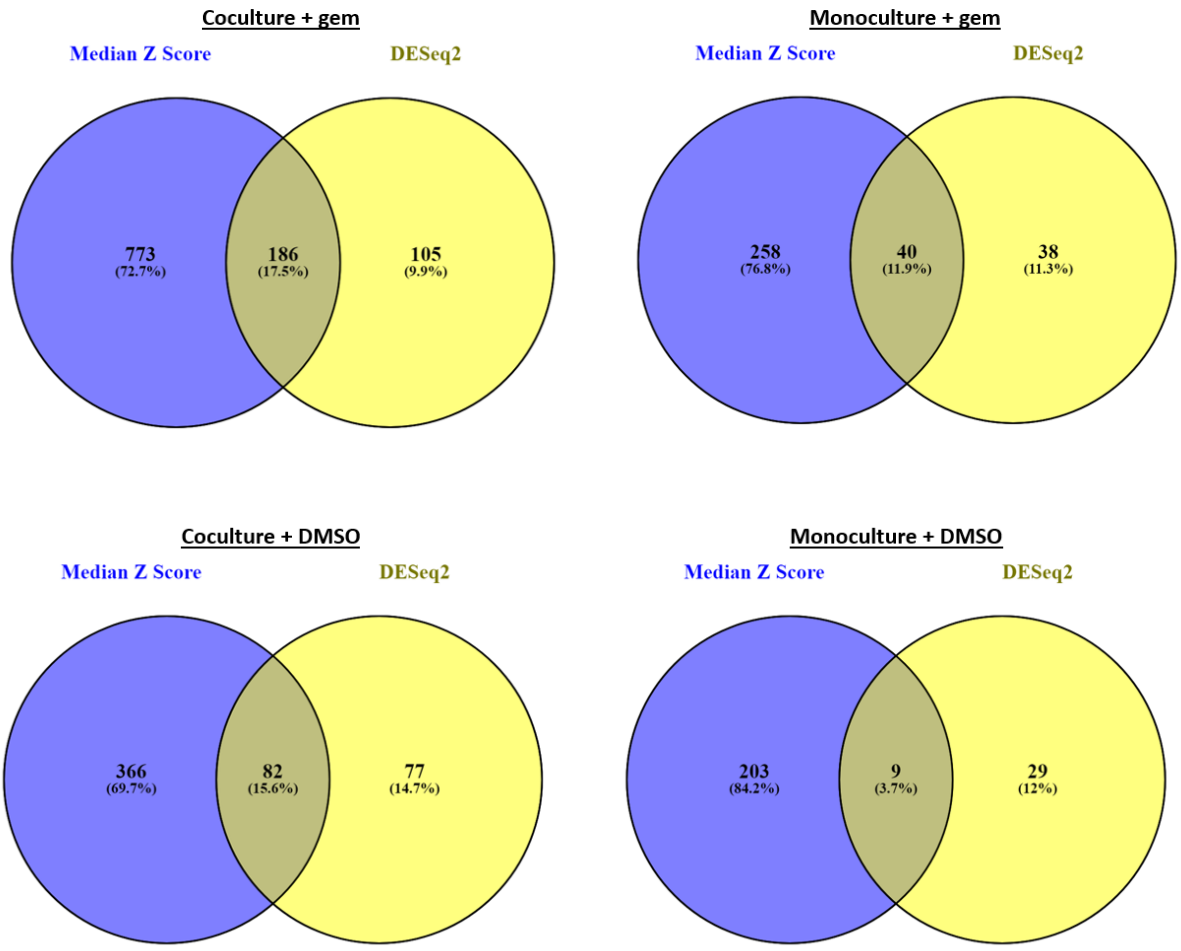

Figure 4.10 Overview of common hits called between differential expression scoring tools for each screen condition.

Within coculture plus gemcitabine 17.5% of hits were shared between DESEq2 calls and median Z score calling, or 186 genes. This represented only 19.4% of the median Z score hits, but 63.9% of the DESeq2 hits. This mirrors figures seen in other shRNA depletion screens using similar scoring methodologies (Mendes-Pereira et al., 2012). This subset of genes therefore warrants focus as potential true positives for gemcitabine sensitizers but does not warrant discounting of the non-common hits, given the propensity of the technical biases in scoring false negatives.

This dataset and segmentation can be interrogated in a wide variety of ways, depending on the underlying hypothesis being tested. For this project, the most interesting dataset remains those genes only depleted in coculture plus gemcitabine and not in the other

conditions. To identify the number and proportion of significantly depleted genes unique to this condition the gene sets for each were compared for and segmented on commonality (Fig 4.11). For each scoring methodology the hits unique to the coculture plus gemcitabine condition made up approximately 50% of the total depleted genes across conditions (763 genes for median Z score, 241 genes for DESEq2, with 137 genes common to both methods), providing a refined yet diverse subset for further analysis and interrogation. These lists of genes are in Appendix 6.1 and 6.5.

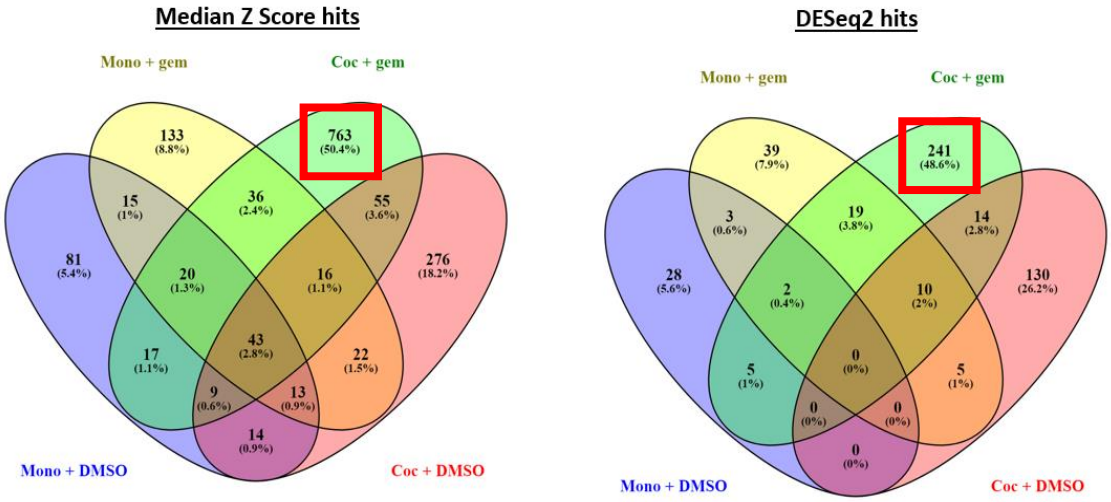

Figure 4.11 Venn diagram of genes scored as hits within each scoring methodology and each condition. *Gene hits unique to the coculture plus gemcitabine condition only lie within red squares. These genes were used for further downstream pathway and network analysis.*

4.9 Pathway and network analysis of hits from coculture + gemcitabine

Meta-analysis of screen data from a quantitative perspective aids the filtering of results from an un-biased perspective, building a list of genes likely to be involved in the observed phenotype. As genes are filtered down, introduction of more qualitative hypothesis-driven analysis can support further elucidation of genes with translational and actionable value. This can be performed using many techniques, such as pathway analysis, domain analysis, and survival analysis.

4.9.1 GSEA

To identify patterns of depletion in the coculture plus gemcitabine condition, gene set enrichment analysis (GSEA) was performed. GSEA is a computational tool to investigate

whether pre-assembled gene sets are significantly differentially expressed between two conditions (Subramanian et al., 2005), in this case coculture plus gemcitabine when compared to the timepoint zero control – specifically the list of 763 Z score hits and 241 DESq hits (total 867 genes, with overlap (listed in Appendix 6.1)) unique to the coculture plus gemcitabine condition (Fig 4.11). The "hallmark gene sets" were investigated in particular (Figure 4.12), which comprises a range of gene signatures representing canonical biological processes, annotated from the molecular signatures database version 3 (Arthur Liberzon et al., 2011).

From this panel, ShRNAs for multiple gene sets in both DNA repair and MYC signalling were significantly depleted (Appendix 6.2), both of which have documented evidence on their value as targets for combination therapy to sensitise to gemcitabine in cancer (Crul et al., 2003; Lewis, Voelkel-Johnson, and Smith, 2016; Seo et al., 2014). In addition, the MTORC1 signalling geneset was also one of the most significantly depleted sets, despite *Mtorc1* not being scored as a hit from the screen originally. Within this MTORC1 geneset, contributing depleted genes included *Aurka* (Aurora Kinase A) and *Asns* (Asparagine synthetase), the former of which have been the subject of pre-clinical and in-human drug development efforts as a sensitizer to gemcitabine (Azzariti et al., 2011; Hata et al., 2005; Raymond et al., 2014), and the latter of interest due to promising pancreatic cancer clinical data around the combination of gemcitabine with eryaspase, an L-asparaginase, which hydrolyses asparagine (Hammel et al., 2017). Other genesets of interest include TGF beta signalling, wherein both *Tgfb1* and its cognate receptor *Tgfbr1*, as well as *Smad3* and *Smad7*, downstream effectors of TGF-β1, were enriched in the coculture plus gemcitabine, correlating with reports of their contribution to cancer cell survival and growth (Culhaci et al., 2005; Melisi et al., 2008).

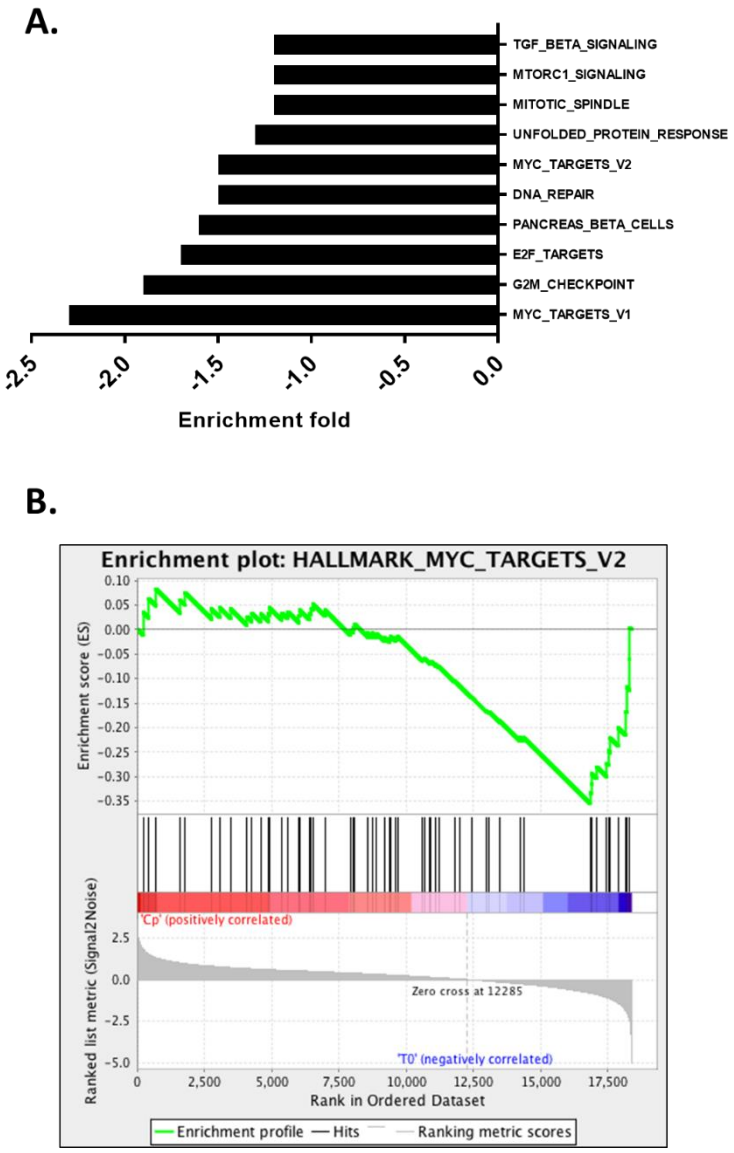

Figure 4.12 Gene Set Enrichment Analysis (GSEA) for the coculture plus gemcitabine condition (the 867 genes that were hits in z score and/or DESeq2) compared to timepoint zero shRNA representations. *To identify specific gene networks with significant depletion in coculture plus gemcitabine, patterns of differential expression was assessed using GSEA, across a combination of hypothesis-driven and unbiased computationally curated networks.* ***(A)*** *The ranked depletion of gene sets within the "Hallmark" networks based on degree of depletion within networks compared to timepoint zero, alongside* ***(B)*** *an illustrative GSEA plot summarising the degree and gradient of depletion of specific genes within the a specific "Hallmark" gene set.*

4.9.2 MetaCore

Similarly, MetaCore (Thomson Reuters), a software suite for functional analysis of genome-wide expression data, was used to further investigate biological processes of note depleted in the screen, comparing and contrasting with both the coculture and monoculture plus drug conditions, as well as within their total sets combined. Each gene network and pathway indexed within MetaCore collates data from on average of 50 genes. Due to a total of only 827 genes assessed for pathway convergence (the total number of genes depleted in the coculture plus gemcitabine condition only) the degree of depletion within specific gene processes or networks was limited, often only two or three genes within a pathway depleted to highlight the pathway as one of interest. Nevertheless, this tool provides a further guiding indicator of pathways worth further exploration. As with the GSEA findings, within each culture condition plus drug it is pathways around cell cycle and checkpoint control that through depletion sensitise to gemcitabine, further correlating the screen data with known successful combinatorial strategies in pancreatic cancer (Fig 4.13). For example, the "Cell cycle_G2-M" network leads depletion level within this geneset. Within this grouping, it is a depletion of genes such as *Chek1*, *Brca1*, *Erk1*, as well as *Aurka* and *Rps6ka1*, that lead to network depletion level, all of which are known chief mediators of cell cycle progression in cancer (Bartek and Lukas, 2003; Chambard, Lefloch, Pouysségur, and Lenormand, 2007; Deng, 2006; Fu, Bian, Jiang, and Zhang, 2007; Smith et al., 2005).

Similarly, two pathways relating to cellular response to DNA damage present as highly depleted ("DNA damage_checkpoint" and "DNA damage_DBS repair"), which as mediators of cell cycle progression when repairing DNA, corroborate the findings of the cell cycle-specific pathways mentioned above.

Conversely, the "Proteolysis Ubiquitin-proteasomal proteolysis", the 5th ranked depleted network does not have an obvious role in modulating gemcitabine efficacy. A network of 166 genes, it is only 21 genes within this network that through depletion contribute to the total network score. These genes often have minimal interaction and maintain diverse functions, with the depleted genes within this set including DDR-related genes such as *Bard1* and *Hsp90*, as well as *Siah2*, an E3 ubiquitin-protein ligase regulating cellular response to hypoxia, and *Usp7*, a direct antagonist of MDM2, the E3 ubiquitin ligase for P53. As such, whilst network analysis holds value in highlighting broad patterns of co-depletion and inter-

relatedness, a further step of interrogation into the specific drivers within these subsets is required. An expanded list of the specific depleted genes per MetaCore network can be found in Appendix 6.4.

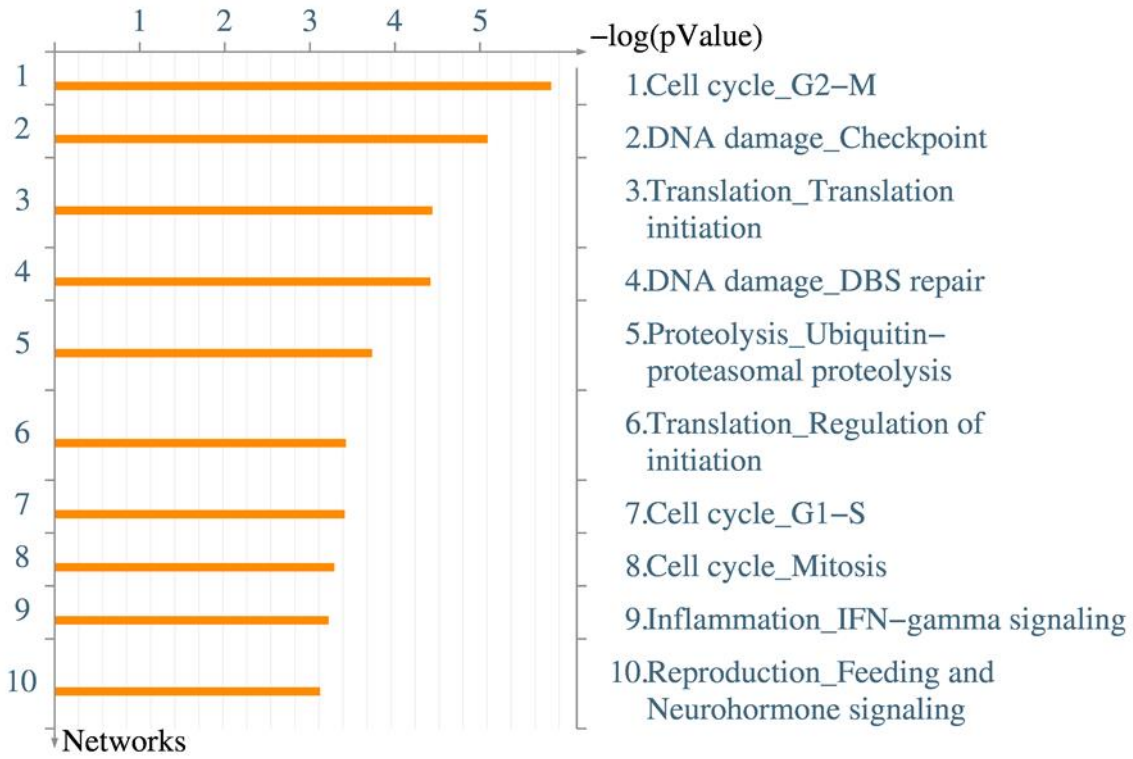

Figure 4.13 MetaCore pathway analysis for hits specific to the coculture plus gemcitabine condition (827 gene set that were hits in z score and/or DESeq2).

4.9.3 PANTHER

Pathway and network analysis tools such as GSEA and MetaCore derive value through aligning data with previously documented and annotated gene sets. This fundamentally introduces a degree of bias by informing network relationships from pre-existing biological documentation. To remove an element of this bias from the analysis, network clustering was undertaken using predicted evolutionary relationships between genes through analysis of sequence divergence, powered by the PANTHER classification system and bioinformatic algorithms (Mi et al., 2017, 2013). Looking at the coculture condition plus gemcitabine gene set, clustering and classifying by predicted molecular function (Figure 4.14), extracellular binding and signalling (Table 4.3), along with molecular transporters (Table 4.4) were each indicated as functional classes depleted within the set. Further within the binding subsets it was the receptor binding subset with the highest representation. Within the transporter

subset it was those genes coding for transmembrane transporters that were most highly represented (Fig 4.14). These results suggest cells may be leveraging some form of novel extracellular signalling and engagement from coculture and density growth to drive the observed resistance phenomenon. These cell surface proteins may potentially represent a set of actionable genes of interest. Further genesets analysed include those within the catalytic subgroup as defined by PANTHER, as have been collated in Appendix 6.3.

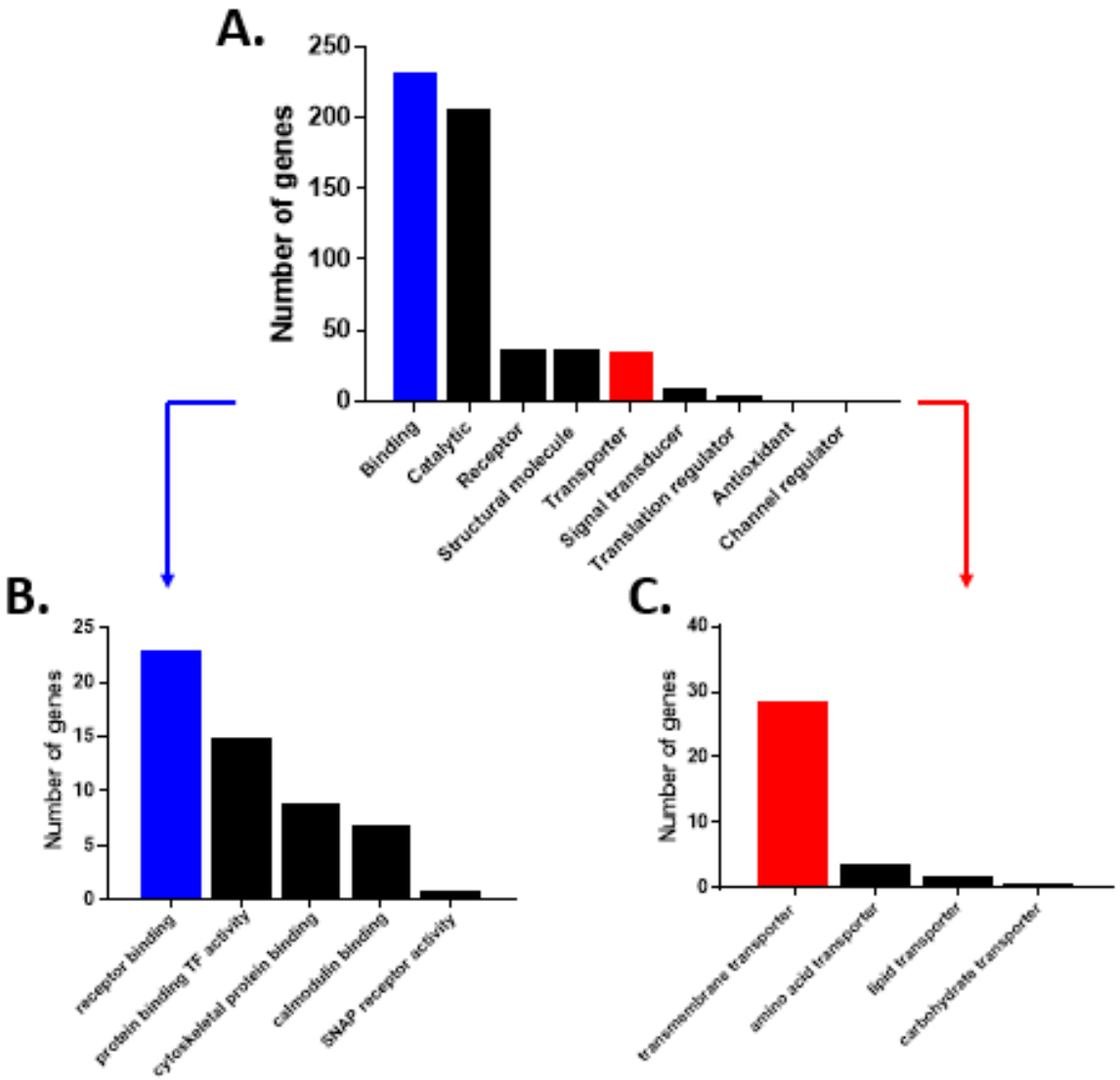

Figure 4.14 PANTHER pathway analysis highlighting actionable gene sets of interest within the coculture plus gemcitabine condition (the 867 genes that were hits in z score and/or DESeq2). (A) *PANTHER (Protein ANalysis Through Evolutionary Relationships)* (Mi et al., 2017)(Lewis et al., 2016) *was used to identify underlying protein classes correlating with depletion in the coculture plus gemcitabine screen condition. Each class was further*

*interrogated as per **(B)** and **(C)** to refine to a qualitative gene list amenable to identification of hypothesis-driven targets.*

PANTHER: Binding > Protein binding > Receptor binding	
Gene code	**Details**
Apof	Apolipoprotein F
Cck	Cholecystokinin
Cd28	T-cell-specific surface glycoprotein CD28
Crh	Corticoliberin
Efna4	Ephrin-A4
Elf1	Ephrin-A2
Elmod3	ELMO domain-containing protein 3
Fgf3	Fibroblast growth factor 3
Gcg	Glucagon
Ghr	Growth hormone receptor
Gm13271	MCG146419
Hamp2	Hepcidin-2
Klra3	Killer cell lectin-like receptor 3
Nrg2	Pro-neuregulin-2, membrane-bound isoform
Pdgfa	Platelet-derived growth factor subunit A
Pdgfd	Platelet-derived growth factor D
Plcg2	1-phosphatidylinositol 4,5-bisphosphate phosphodiesterase gamma-2
Prl8a6	Prolactin-8A6
Scg5	Neuroendocrine protein 7B2
Sema4b	Semaphorin-4B
Sirpa	Tyrosine-protein phosphatase non-receptor type substrate 1
Tnfsf11	Tumor necrosis factor ligand superfamily member 11
Traf3	TNF receptor-associated factor 3

Table 4.3 Genes encoding for receptor-binding proteins whose ShRNAs are depleted selectively in the coculture model plus gemcitabine, classified using PANTHER.

PANTHER: Transporter activity > Transmembrane transporter	
Gene code	**Details**
Abcc9	ATP-binding cassette sub-family C member 9
Apof	Apolipoprotein F
Aqp3	Aquaporin-3
Atp6v0b	V-type proton ATPase 21 kDa proteolipid subunit
Atp6v1b2	V-type proton ATPase subunit B, brain isoform
Cacna1f	Voltage-dependent L-type calcium channel subunit alpha-1F
Clic1	Chloride intracellular channel protein 1
Clns1a	Methylosome subunit pICln
Fkbp10	Peptidyl-prolyl cis-trans isomerase FKBP10
Gm14496	Protein Gm14496
Kcnj14	ATP-sensitive inward rectifier potassium channel 14
Orai1	Calcium release-activated calcium channel protein 1
Sec14l2	SEC14-like protein 2
Serinc3	Serine incorporator 3
Slc14a1	Urea transporter 1
Slc1a2	Excitatory amino acid transporter 2
Slc38a2	Sodium-coupled neutral amino acid transporter 2
Slc6a7	Sodium-dependent proline transporter
Slc7a15	Aromatic-preferring amino acid transporter
Tcirg1	V-type proton ATPase subunit a
Timm17b	Mitochondrial import inner membrane translocase subunit Tim17-B
Vmn2r11	Protein Vmn2r11
Vmn2r110	Protein Vmn2r110
Vmn2r26	Vomeronasal type-2 receptor 26
Vmn2r50	Protein Vmn2r50
Vmn2r57	Protein Vmn2r57
Vmn2r77	Protein Vmn2r77
Vmn2r94	Protein Vmn2r94
Vmn2r95	Protein Vmn2r95

Table 4.4 Genes encoding for transmembrane transporter proteins that are depleted selectively in the coculture model plus gemcitabine, classified using PANTHER.

4.10 Design and implementation of a validation screen to refine gene target list

There are major inherent challenges around biological and technical biases and reproducibility in large scale high-throughput screens, including for technologies such as CRISPR and RNA interference. This can drive a high false positive rate, often a product of off-target effects, the latter of which is widely documented as a confounding factor in data analysis (Jackson and Linsley, 2010). The primary risk of using shRNAs in a depletion screen is off-target effects, wherein an shRNA will appear to be depleted when an off-target non-specific effect decreases the viability of a cell type either in general or when exposed to gemcitabine. To counter this in the primary multiple unique shRNAs were included per gene, only scoring a gene as a hit when a majority of its shRNAs were significantly depleted. However, the large number of hits required further filtering to identify the most robust hits to follow up.

Taking a more refined panel of genes highlighted as potentially causative of gemcitabine resistance in the initial screen, a second more targeted validation screen was designed. For this screen, 1,973 genes were collated from a variety of sources, including all hits coming from the initial coculture and monoculture plus gemcitabine conditions, the gene sets from the most significantly depleted GSEA networks, as well as some hypothesis-driven panels, such as enzymes involved in the gemcitabine metabolic and transport processes. These were combined with a panel of 200 human olfactory receptors to serve as negative controls. Within this screen there was an average of 4.21 shRNAs targeting each gene (Fig 4.15), as opposed to 3.46 for the initial screen, thereby serving to minimise off-target related false positives.

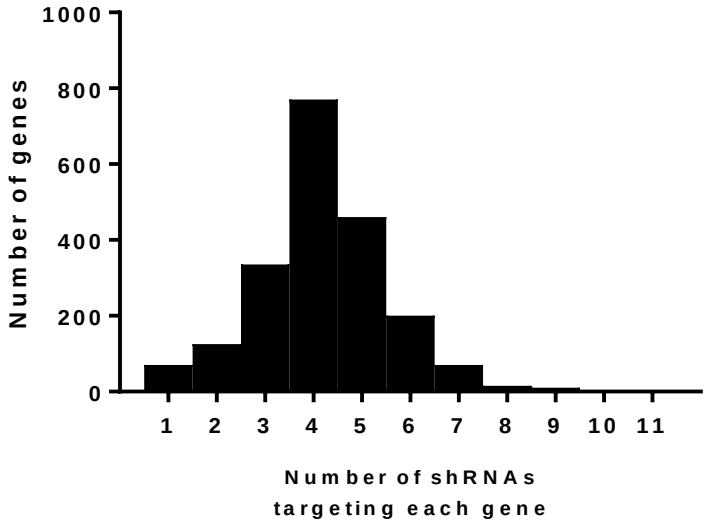

Figure 4.15 The number of shRNAs targeting each gene within the validation screen library used.

The screen protocol was replicated as per before, with six cycles of gemcitabine used for each condition of coculture and monoculture either plus gemcitabine or plus DMSO control. Data was analysed for differential expression within each condition using the same two scoring methodologies as above, DESeq2 and median Z scores.

Hit rates across each condition, except for coculture plus gemcitabine, were all significantly lower than in the initial screen, a product of validation screen library being built specifically to interrogate the hits arising from the coculture plus gemcitabine condition primarily.For the coculture plus drug condition, 17.2% of the library shRNAs were scored as significantly depleted when combining scoring methodologies, when compared to only 8.5% from the initial screen, indicating the targeted focus on this condition was evident in the output data (Table 4.5, Fig 4.16, 4.17).

Condition	Median Z score		DESEq2	
	shRNAs	genes	shRNAs	genes
Coculture + gemcitabine	1343	299	1317	281
Coculture + DMSO	221	40	164	11
Monoculture + gemcitabine	210	39	118	7
Monoculture + DMSO	157	35	66	5

Table 4.5 Number of shRNAs and genes in the validation screen (1973 genes targeted in total) significantly depleted within the coculture and monoculture conditions +/- gemcitabine, when compared to timepoint zero.

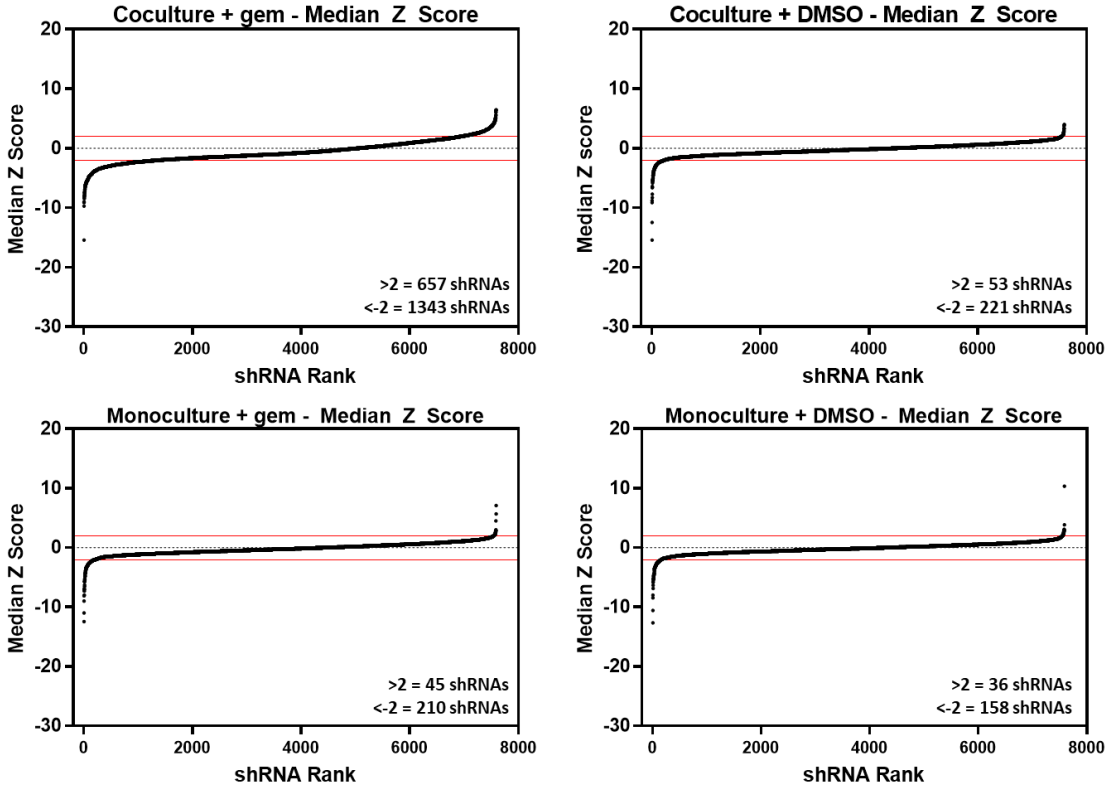

Figure 4.16 Differential depletion and enrichment of shRNAs in the validation screen calculated using Median Z Score.

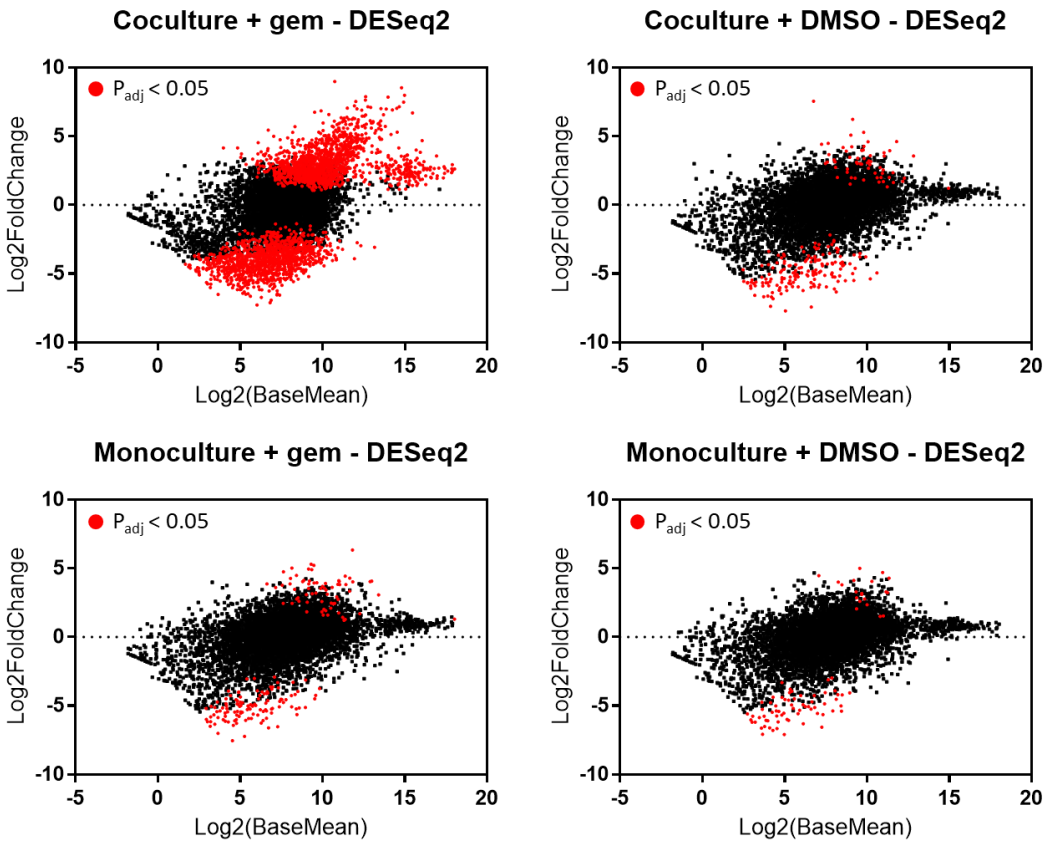

Figure 4.17 Differential depletion and enrichment of shRNAs in the validation screen calculated using DESeq2.

Reproducing the outcome from the initial screen, both *Chek1* and *Atr* both were scored as significantly depleted in the coculture plus gemcitabine condition, again adding confidence to the biological relevance and translational value of hits coming out (Fig 4.18). Similarly, *Dck* as a biological negative control, as its depletion increases gemcitabine resistance, was significantly enriched in the validation screen. Results held true through both for DESeq2 and median Z score scoring methodologies.

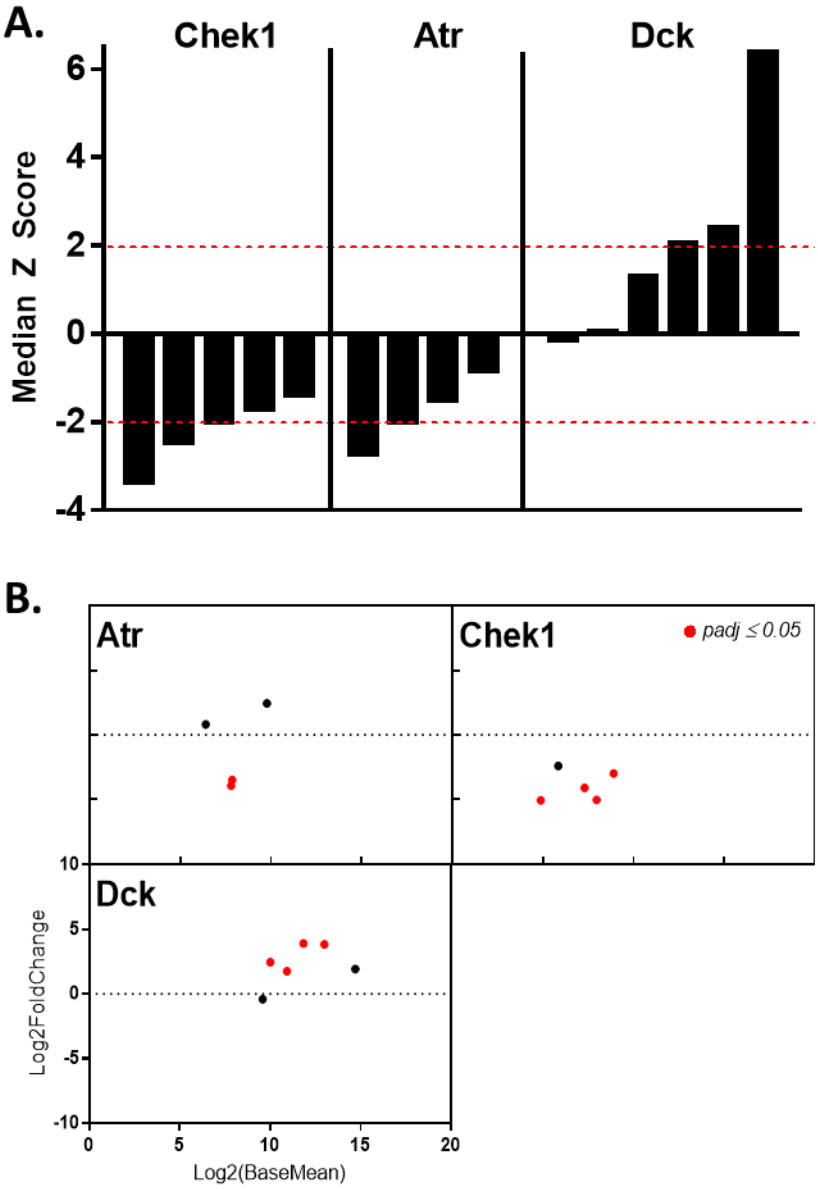

Figure 4.18 Differential expression of validation screen control shRNAs. *(**A**) Differential expression levels of positive controls* Atr *and* Chek1 *alongside negative control* Dck *from validation screen data, using both Median Z Scores. A value of ≤-2 is considered significant depletion of the corresponding shRNA. (**B**) Differential expression levels of the same shRNAs scores using DESeq2, with significant enrichment or depletion ($p_{adj} \leq 0.05$) represented using red dots.*

Interrogating the validation screen data there were 299 genes significantly depleted using median Z scores, which is 31% of the number called from the original screen. This contrasts with the DESeq2 output, wherein the 281 genes depleted in the validation screen was similar to the number called in the original screen (291). The median Z score total is reduced

to such an extent given the validation screen gene list had a strong skew towards genes with a role in the gemcitabine resistance effect, therefore the median expression level within the pool would be skewed similarly. As Z score is a relative score based on the median expression level in the entire population, a cut off of a < -2 Z score is significantly more restrictive. Whereas for DESeq2, with MA plots across conditions show similar distributions when compared to the timepoint zero population, indicating that calls of significance remain valid within the validation screen.

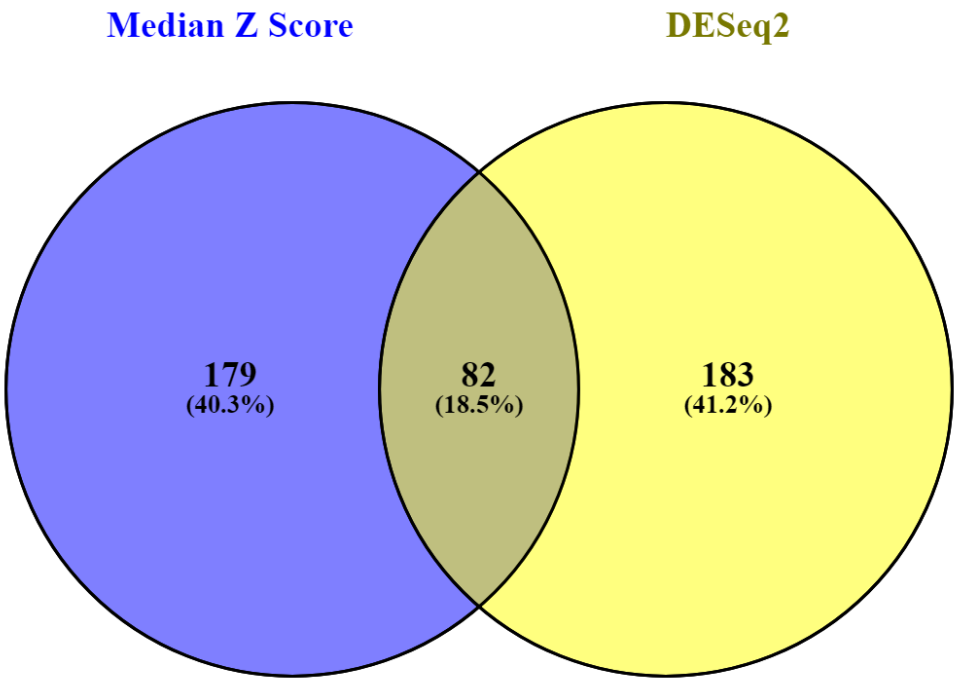

Figure 4.19 Validation screen common hits between differential expression scoring methodologies in coculture plus gemcitabine condition exclusively.

Of interest was the consistency of hit calling for each scoring methodology between the first screen and the validation screen. For median Z scores, approximately 43% of the hits exclusive to coculture plus gemcitabine in the validation screen were also hits in the original primary screen, whereas for DESeq2 this figure was lower at 17% (Fig 4.20). The additional hits called from the validation screen may be a product of the additional shRNAs added per gene in the validation screen involved in the networks and pathways of interest, which did not themselves significantly deplete in the primary screen but are associated with pathways that did exhibit depletion. Overall, the combined hit list from the validation screen supports

more thorough investigation into select biological process highlighted from the initial screen.

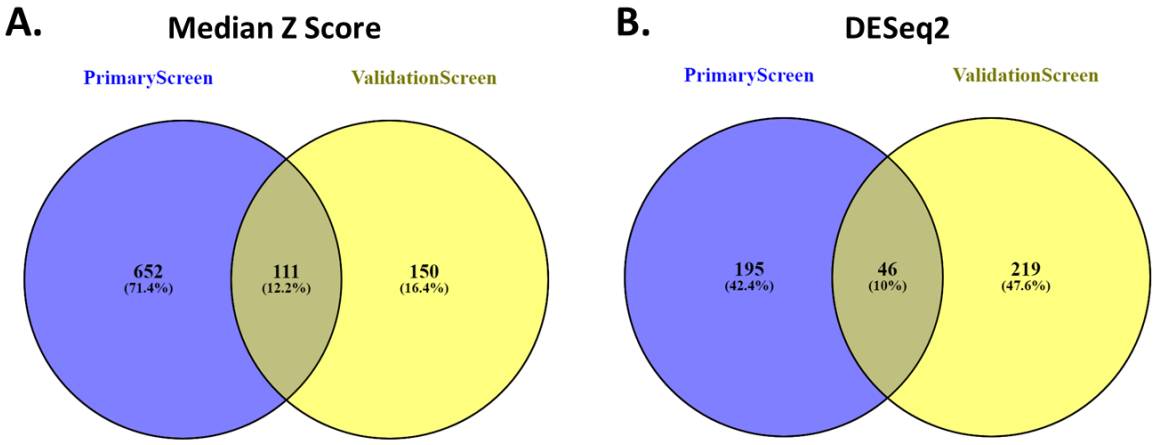

Figure 4.20 Common hits for DE methodologies between the initial whole-genome screen and the subsequent validation screen. *Shared hits between initial shRNA screen and validation screen in the coculture plus gemcitabine condition only for each of (**A**) Median Z Score and (**B**) DESeq2 differential expression scoring techniques.*

4.11 Qualitative identification of highest confidence genes driving gemcitabine resistance effect in coculture

The goal of the validation screen is to support filtering the screen data into as refined and high confidence a data set as possible. Analysis and integration thus far of validation screen data has focused on those hits called exclusively in the coculture plus gemcitabine condition, and common between differential expression scoring methodologies. While this approach holds value, the inclusion of a direct comparison to hits conserved in monoculture plus gemcitabine also supports control comparisons and identification of target genes with value in both culture settings.

To leverage these datasets to build final refined hitlist, all hits exclusively in the coculture plus gemcitabine condition were collated, as well as those present in this condition but not exclusive to it, using both scoring methodologies, across both screens. These sets were then compared to identify genes consistently called within all four sets, under the hypothesis that these genes, maintaining significant depletion, factoring in all technical and biological biases, would be the highest confidence hits.

The subset exclusive to coculture plus gemcitabine was comprised of 10 genes in total (Fig 4.21A, Table 4.5). Included within the set was *Chek1*, validating the group as a positive control. The wider set including all hits from coculture plus gemcitabine common between scoring tools was expanded to 19 genes, which included *Atr*, a further positive control for the screen. Of note amongst both sets were a variety of genes with published evidence supporting a synergy through inhibition with gemcitabine treatment, including *Desi1*, *Eif3e* and *Orai1*. Of the 19 genes, 8 have commercially available inhibitors, with genes such as *Arhgef5* with literature backing synergy with gemcitabine in pancreatic cancer (Takeda et al., 2016).

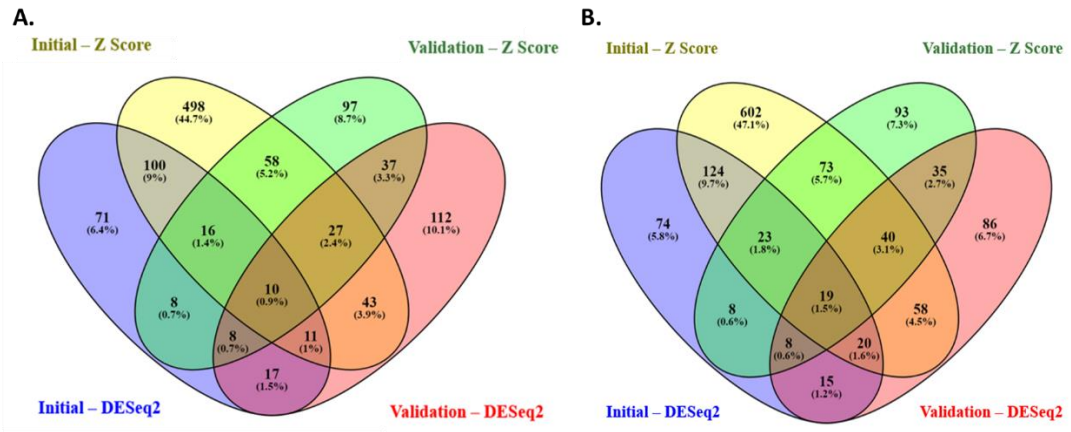

Figure 4.21 Common gene hits between the primary and validation screen using each scoring methodology for the coculture plus gemcitabine condition. (A) *Commonality of all hits exclusive to coculture plus gemcitabine, and* ***(B)*** *commonality of all hits for coculture plus gemcitabine, independent of presence in any other conditions.*

Gene	P value*	Coc + gem only	Role in PDAC	Reference	Effect on gem sensitivity	Reference	Commercial inhibitor	UniProt description
Chek1	0.00398	Yes	Yes	(Sahu, Batra, and Srivastava, 2009)	Yes	(Siang-Boon Koh et al., 2015; Liang, Zhao, Ma, and Guo, 2017)	AZD7762	Checkpoint Kinase 1. Serine/threonine-protein kinase which is required for checkpoint-mediated cell cycle arrest and activation of DNA repair in response to the presence of DNA damage or unreplicated DNA.
Eif3e	0.0111		Yes	(Doldan et al., 2008)			AZD2014	Eukaryotic Translation Initiation Factor 3 Subunit E. Component of the eukaryotic translation initiation factor 3 (eIF-3) complex, which is required for several steps in the initiation of protein synthesis. Bound to S6K1 in inactive state, activated through mTOR phosphorylation of S6K1 (Holz, Ballif, Gygi, and Blenis, 2005).
Atr	0.0234		Yes	(Fokas et al., 2012; S. Liu et al., 2017)	Yes	(S. Liu et al., 2017; Prevo et al., 2012; Wallez et al., 2018)	AZD6738, VE-821	Ataxia Telangiectasia And Rad3-Related Protein. Serine/threonine protein kinase which activates checkpoint signalling upon genotoxic stresses such as ionizing radiation (IR), ultraviolet light (UV), or DNA replication stalling, thereby acting as a DNA damage sensor.
Hsp60	0.0251		Yes	(Mahajan, Gupta, Wagh, Karpe, and Tikoo, 2011; Piselli et al., 2000)			Mizoribine (Itoh, Komatsuda, Wakui, Miura, and Tashima, 1999; Meng, Li, and Xiao, 2018)	Heat Shock Protein Family D (Hsp60) Member 1. Chaperonin implicated in mitochondrial protein import and macromolecular assembly. Together with Hsp10, facilitates the correct folding of imported proteins.
Desi1	0.0528	Yes	Yes	(Kang et al., 2014)	Yes	(Qiao et al., 2016; Zhu et al., 2012)	Triptolide	DeSUMOylating Isopeptidase 1. Protease which deconjugates SUMO1, SUMO2 and SUMO3 from some substrate proteins.
Arhgef5	0.0751	Yes	Yes	(Komiya et al., 2016)	Yes	(Takeda et al., 2016)		Rho Guanine Nucleotide Exchange Factor 5. Guanine nucleotide exchange factor which activates Rho GTPases. Strongly activates RHOA and RHOB.
Acer3	0.0921	Yes						Alkaline Ceramidase 3. Hydrolyses only phytoceramide into phytosphingosine and free fatty acid. Does not have reverse activity.
Polr1b	0.183							Subunit of the RNA polymerase I. DNA-dependent RNA polymerase catalyses the transcription of DNA into RNA using the four ribonucleoside triphosphates as substrates.
Rmdn1	0.211	Yes						Regulator of microtubule dynamics protein 1.
Lrp2	0.234	Yes	Yes	(Jones et al., 2008)				Low density lipoprotein-related protein 2. Multiligand endocytic receptor. Acts together with CUBN to mediate endocytosis of high-density lipoproteins. Mediates receptor-mediated uptake of polybasic drugs such as aprotinin, aminoglycosides and polymyxin B.
Supt5h	0.29	Yes						SPT5 Homolog, DSIF Elongation Factor Subunit. Component of the DRB sensitivity-inducing factor complex (DSIF complex), which regulates mRNA processing and transcription elongation by RNA polymerase II.
Rnf182	0.453	Yes						Ring Finger Protein 182. E3 ubiquitin-protein ligase that mediates the ubiquitination of ATP6V0C and targets it to degradation via the ubiquitin-proteasome pathway.
Cox1	0.462		Yes	(Omura et al., 2010)			Indomethacin	Cyclooxygenase-1. Converts arachidonate to prostaglandin H2 (PGH2), a committed step in prostanoid synthesis.
Srrm2	0.75							Serine/arginine repetitive matrix 2. Involved in pre-mRNA splicing. May function at or prior to the first catalytic step of splicing at the catalytic centre of the spliceosome.
Orai1	0.856	Yes	Yes	(Kondratska et al., 2014)	Yes	(Kondratska et al., 2014)	AnCoA4	ORAI Calcium Release-Activated Calcium Modulator 1. Ca2+ release-activated Ca2+ (CRAC) channel subunit which mediates Ca2+ influx following depletion of intracellular Ca2+ stores and channel activation by the Ca2+ sensor, STIM1.
Mvd	0.927						6-Fluoromevalonate	Mevalonate Diphosphate Decarboxylase. Performs the first committed step in the biosynthesis of isoprenes.
Tmem178b	N/A							Transmembrane Protein 178B.
Krtap16-8	N/A	Yes						Keratin Associated Protein 16-8.
Zfp213	N/A							Zinc finger protein 213.

Table 4.6 List of 19 gene hits conserved between screens and scoring methodologies in the coculture plus gemcitabine condition. **P value refers to significance of survival differences for top and bottom quartiles of TCGA PDAC gene expression.*

From this list of 19 genes, the majority have little or no published literature exploring their biological function (Table 4.6), making qualitative data-driven analysis of their translational value a challenge. To compensate for this, expression data for pancreatic ductal adenocarcinoma was investigated from The Cancer Genome Atlas, a catalogue of key genomic changes and correlated survival analysis for 33 cancer types (Cancer Genome Atlas Research Network et al., 2017)**,** to evaluate correlations between top and bottom quartiles of expression with survival of patients with PDAC. Only four genes showed significant differences between the quartiles: *Chek1*, *Atr*, *Eif3e*, and *Hsp60 (Hspd1),* with high expression correlating with worse survival in all 4. Given the known therapeutic value of targeting *Chek1* and *Atr* (Banerji et al., 2017; Prevo et al., 2012; Wallez et al., 2018), *Eif3e* and *Hspd1* were of interest, both with commercially available inhibitors targeting the pathway, and documented roles in PDAC pathophysiology (Table 4.6).

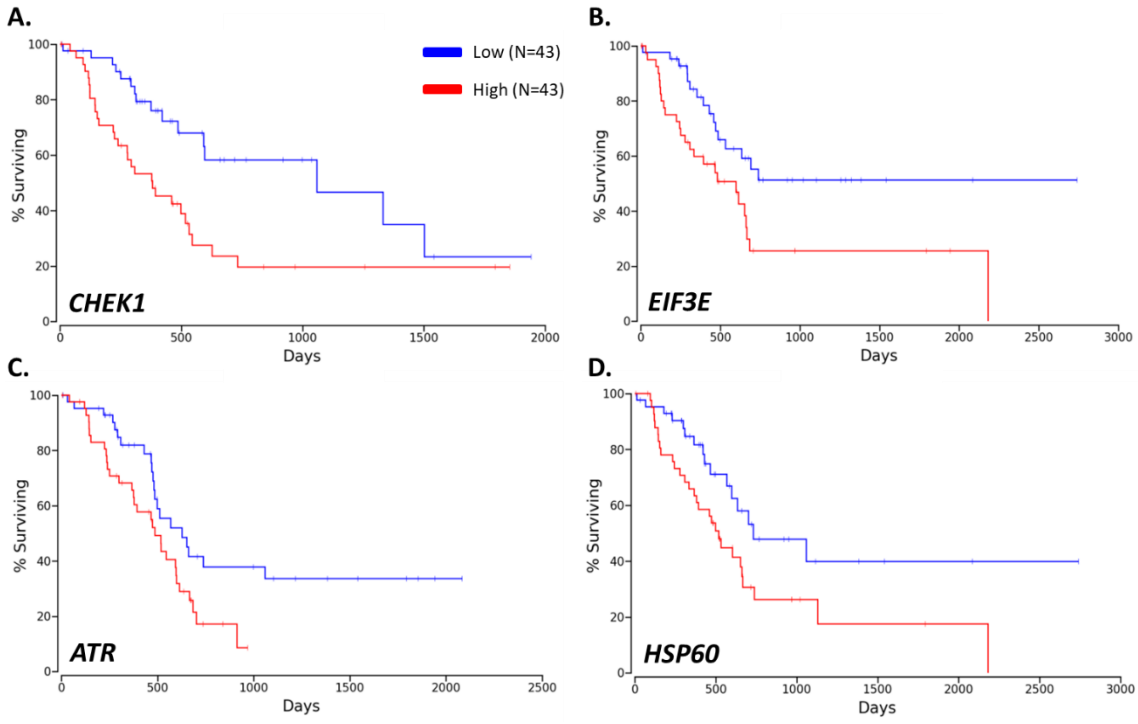

***Figure 4.22 Kaplan–Meier survival plots for TCDA PDAC data comparing top and bottom quartile gene expression for each of (A)* CHEK1, *(B)* EIF3E, *(C)* ATR, *and (D)* HSP60. These 4 genes showed significant difference (P values in Table 4.6)**

4.12 Conclusion

I have here leveraged the unbiased, explorative, and high-throughput properties of an shRNA depletion screen to identify drivers of gemcitabine resistance in high-density conditions in pancreatic cancer, leveraging the coculture model of resistance documented and characterised in Chapter 3. An initial primary genome-wide screen allowed for prioritisation and targeting of specific networks and pathways potentially implicated in the resistance effect. These included those involved in previously documented causative pathways such as DNA damage response, as well as novel yet hypothesis-driven functional groups such as those involved in cell-cell molecular transportation and extracellular signalling. Noting the challenge of the volume of resulting data for high-confidence analysis as well as potential for false positive results arising from screens of this size, a smaller more targeted validation screen was undertaken, here investigating further gene lists and networks selected from the primary screen as potentially causative of the resistance effect. Through analysis of this dataset, using two differential expression scoring methodologies and comparisons with equivalent conditions in the initial screen, a high-confidence subset of 19 genes, some of which are potentially actionable, was identified. Within this subset both *Chek1* and *Atr* remained, two of the strongest positive controls within this model with validated positive translational data *in vivo* as well with preparations for human clinical programs ongoing (Banerji et al., 2017; Wallez et al., 2018). Amongst the other 17 genes, 7 have previously documented roles in PDAC pathophysiology, and 6 with commercially available inhibitors, and 5 with previous studies demonstrating synthetic lethality with gemcitabine in PDAC *in vitro*. Subsequent pre-clinical validation of these subsets would include testing existing inhibitors where available, perhaps preceded by genetic knockdown and knockout techniques for more specific investigations into gene functions in the context of coculture gemcitabine resistance. The strength of the positive and negative controls through this project provide confidence that novel less understood genes and pathways highlighted here may indeed be drivers of gemcitabine resistance in pancreatic cancer yet undiscovered and warranting further pre-clinical focus and validation.

A valuable line of further investigation focused on the continuation of above, would be deeper interrogation of the specific sensitising effects of each of the 19 genes identified here within the coculture model of resistance. As well as testing with individually expanded

shRNA sets, one could also expand the cell lines within which these effects are tested, alongside use of other genetic manipulation techniques such as CRISPR or siRNA. Such investigations might further expand the nuances of each gene's effect on the resistance phenotype and serve as valuable data informing future *in vivo* experimentation.

5. Discussion

5.1 Introduction

Cancer drug development is both a time and cost intensive process, coupling robust efficacy studies with evaluations of toxicity tolerability profiles within patients. With less than 4% of all oncology-focused compounds entering Phase I clinical trials emerging the other end as approved compounds (Wong, Siah, and Lo, 2018), the failure rate is a significant challenge. This challenge is exemplified at its fullest within pancreatic cancer, wherein low approval rates compound the lack of improvement in patient survival over the last 40 years (Cancer Research UK, 2014a). This is further exacerbated by a lack of tools supporting pre-clinical development that can accurately predict efficacy outcomes by high-throughput approaches, whilst maintaining low cost. This project aimed to both improve the translational value and mechanistic understanding of pre-clinical models of drug development in PDAC, as well as leverage said models to build a novel list of high-confidence targets worth investigating further as mediators of gemcitabine resistance in patients with pancreatic cancer.

5.2 Conferred resistance to gemcitabine within our model is transient and requires direct cell-cell contact.

Mechanisms through which pancreatic tumours develop or maintain resistance to gemcitabine have been widely postulated and demonstrated in various models of the disease, such as a via depletion of intratumoural levels of the drug by non-cancer cells (Hessmann et al., 2017) as well as via enhanced abilities to restore the DNA damage induced by the drug (Siang-Boon Koh et al., 2015; S. Liu et al., 2017). Having developed a novel coculture model of gemcitabine resistance to PDAC within our lab, an initial step of this project prior to target identification and drug development was to better understand the specific conditions through which this effect was conferred, and the degree of influence each characteristic of the assay held in driving this effect.

Previous studies suggest that cancer cells can develop therapeutic resistance via secreted factors derived from non-tumour cells within the tumour microenvironment (Albrecht Neesse et al., 2013; Omura et al., 2010; Straussman et al., 2012; Weekes et al., 2012). This model has been further postulated to drive gemcitabine resistance within pancreatic cancer in particular, leveraging the pancreatic CAF secretome (Duluc et al., 2015). The relevance of

this mechanism within our model was investigated in multiple ways. Firstly, I demonstrated that neither MH17031-conditioned medium (CM) nor CM from the coculture of both K8484 and MH17031 cells was capable of inducing resistance in K8484 monoculture, nor secondly did exogenous addition of recombinant IL-6 or HGF induce any change, the former reported by Duluc et al as per above, the latter in a high throughput screen of CAF-driven resistance across cancers (Straussman et al., 2012). Further, previous work in our lab by Ruiling Xu assessed the effect of the MH17031 secretome via a transwell assay, to no effect (Xu, 2015). While these results are indicative of a secreted factor unlikely to be a key driver of the resistance effect, they also come with caveats. Were a causative secreted factor to either have a low half-life, and therefore not remain active in CM, or require paracrine signalling of a distance less than 1mm (transwell assay distance between cells), then neither of these assays would drive a resistance effect. Alternative tools that could have been used and not be affected by these properties include a micromachined silicon substrate created by Hui & Bhatia for the purpose of contact-independent close proximity coculture (Hui & Bhatia, 2007).

Together these data suggest that within our coculture model direct cell-cell contacts are required for driving the conferred gemcitabine resistance. The discordance with above data in PDAC may be derived from the observation in the Duluc paper that only CAFs expressing high levels of the somatostatin-1 receptor effected gemcitabine resistance via its secretome. Within both K8484 and MH17031, no detectable levels of this transcript were noted in RNA-Seq data (J. Bramhall, F. Richards, unpublished), suggesting perhaps a different subset of cells are investigated here. Similarly, my experiments show that the conferred resistance is transient, and requires constant cell-cell contact between K8484 cells and the resistance-conferring line. This effect may mirror that observed *in vivo*, given growing tumour cells are constantly exposed to concurrently proliferating mesenchymal cells within the micro-environment.

Through addition of tetrahydrouridine (THU) within the coculture model I was able to evaluate the role CDA activity has in driving resistance to gemcitabine. THU is a competitive inhibitor of CDA, and therefore can prevent metabolism of active gemcitabine metabolites upon cell entry. High expression of CDA has been noted previously as a correlative factor linked to gemcitabine resistance in PDAC (Funamizu et al., 2010; Weizman et al., 2014). I

found that THU had no effect in sensitising cells to gemcitabine in coculture, across a wide concentration range. This mechanism of gemcitabine resistance in PDAC has been reported previously as a macrophage-driven phenomenon (Weizman et al., 2014), but not within fibroblast-like cells, which may indicate a CDA-modulated effect is not relevant in this duo-culture. Further, recent work by Hessmann et al showing pancreatic CAFs sequester gemcitabine away from cancer cells suggests that independent of CDA activity within cancer cells (Hessmann et al., 2017), there may not be sufficient gemcitabine within these cells to induce an effect, which might also explain the result here. Despite the results documented above, further investigation into gemcitabine metabolism using mass spectrometry across CAF and cancer cell types in both monoculture and coculture conditions, matched alongside more in-depth classification of CAF subtypes used, would likely add valuable insights into the specifics of the CAF-driven effects of metabolism. These findings could independently form an important line research towards development of improved clinical practice and dosing guidelines.

These data together served to firstly demonstrate the requirement of direct cell-cell contact within this model, as well as further disqualify a number of documented gemcitabine resistance mechanisms in PDAC as drivers of the resistance phenomenon identified.

5.3 Gemcitabine resistance in this model is driven by cancer cells, not cancer-associated fibroblasts.

Next, I focused on identifying and understanding the specific subset of fibroblast-like cell capable of conferring resistance to gemcitabine within our model. As MH17031 cells exhibit a broadly mesenchymal morphology and were isolated originally using a traditional and documented tumour outgrowth method of CAF isolation, they were labelled as such within the lab. The initial hypothesis was therefore that CAFs within the PDAC tumour were the key factor driving the observed effect. This hypothesis was compounded with a wide body of pre-clinical and clinical investigations successfully targeting this stromal component to ablate gemcitabine resistance (Duluc et al., 2015; Hessmann et al., 2017; K. P. Olive et al., 2009; Shan et al., 2017).

The ability of MH17031 cells to confer resistance to gemcitabine was contrasted against non-CAF cells including the pancreatic stellate cells NF18073, a mouse embryonic fibroblast line, as well as the canonical 3T3 fibroblast line. The fact that only MH17031 conferred

resistance here aligned with the hypothesis of a cancer-related fibroblast line driving the effect. This effect was mirrored in the coculture of MH17031 cells with the human PDAC line MIA PaCa-2, supporting the likelihood of a conserved mechanism relevant in the human form of the disease.

To better understand the cellular profile of the resistance-conferring MH17031 cells, levels of both epithelial and mesenchymal protein markers were assessed and contrasted to the K8484 cancer line and the PSC line NF18073. Surprisingly, the MH17031 line expressed an almost exclusively epithelial signature through high expression of E-Cadherin and low or K8484-matched expression of mesenchymal markers such as αSMA, N-Cadherin, and Vimentin. Further, immune-fluorescence images indicated that MH17031 cells may also be mutant for P53. These findings were corroborated by RNA-Seq data across each of the three cell lines, further adding confidence to this unexpected observation. It was postulated that given the mesenchymal morphology of MH17031 cells, that they may have undergone EMT, as epithelial cells originally. This hypothesis was tested through investigation of EMT-related gene signatures in the line. While MH17031 did match K8484 cells in lacking expression of key EMT drivers such as SNAI1 and SNAI2, it expressed higher levels of both TWIST1 and ZEB1, all of which were highly expressed in NF18073. Thus, MH17031 clearly expressed both epithelial markers (e.g. E-Cadherin) and mesenchymal markers (Twist1, Zeb1), which suggested a cell type of epithelial origin that had undergone partial EMT.

Given the defined genetic manipulation within the KPC mouse model to induce tumour development, the specific origin of cell lines, in particular within the pancreatic epithelial lineage, could be assessed. To do this, PCR genotyping was used to assess *Kras* and *Tp53* status within the cell line, with K8484 and NF18073 cell lines as controls. Mutant *Kras* was not detected within MH17031, whereas it was within K8484 cells, which alone indicated the cells may not to be epithelial tumour-derived. This result was contradicted when MH17031 cells were shown to express mutant *Tp53* through a recombined LSL locus. Given cre recombinase expression is driven by expression of the pancreatic epithelial gene *Pdx1*, this result suggested that MH17031 may indeed be derived from an epithelial lineage. Given the contradictory nature of these results, additional primer pairs were used, providing the same paradoxical result, of genetic recombination in the *Tp53* transgene but not *Kras*. This result may be explained by a number of theories. Firstly, leaky expression of cre recombinase in

mesenchymal cells may lead to recombination of only one of the LSL sites, and therefore lead to expression of either mutant *Tp53* or mutant *Kras*. Divergence in recombination efficiency between LSL sites has been reported previously, which may explain this observation (Vooijs, Jonkers, and Berns, 2001). Also, stimuli-independent production of cre recombinase has been reported in another model of pancreas development, the RIP-CreER mouse, which while based upon basal reporter activity not relevant in the KPC mouse, serves to warn of potential non-specific LSL recombination is mouse models (Yanmei Liu et al., 2010).

Secondly, intercellular vesicular transport of cre recombinase may also lead to variable recombination levels in recipient cells. Extracellular vesicular transport of protein and genetic information has been documented (Costa-Silva et al., 2015), and its relevance specifically between cancer cells for cre recombinase mRNA transfer *in vivo* has been further demonstrated (Zomer et al., 2015).

Lastly, the sensitivity of the PCR genotyping assay may prevent accurate detection of mutant kras in MH17031, as the PCR product was not abundant even in K8484 cells, the defined epithelial line. This might be further compounded if MH17031 is a mixed population therefore with lower levels of mutant transcripts, although IF protein data revealed a relatively homogenous expression level of epithelial cell markers throughout the population.

This result not only challenges the initial assignment within our group of MH17031 being of CAF origin, but also serves to potentially challenge CAF cellular identity in existing literature, factoring in the documented prevalence of EMT in PDAC and therefore subsets of epithelial cells developing mesenchymal properties. This challenge is exemplified in a recent paper by Hessmann et al where it appears that isolation of CAFs, verified through similar PCR genotyping, may have led to misinterpretation of phenotypically mesenchymal cells as genotypically mesenchymal. These cells were used as validation of our CAF-driven resistance within our model, inducing significant resistance. This study exemplifies the challenge of isolating pure pancreatic CAFs. The absence of this validation technique in the majority of CAF-focused studies may lead to a larger number of misclassifications and therefore misinterpretations of phenotypic effects.

In order to test the original hypothesis that pancreatic CAFs do drive resistance within this model, a series of lines were isolated from tumours of KPC GEDA mice using the differential trypsinisation technique, validated for *Kras* and *Tp53* wildtype status, and checked for mesenchymal morphologies and high expression of αSMA. From an initial isolation of 384 single cell clones from this population, 2 validated CAF cell lines under the above definition were isolated, GDF14 and GDF17. This extremely low plating efficiency using two canonical techniques (differential adhesion and differential trypsinisation) further exemplifies the need for thorough validation of cell line origin prior to subsequent CAF analysis. Within the coculture model neither cell line conferred gemcitabine resistance to K8484 cells. These data indicate that at least within our model system, true CAFs do not confer resistance to gemcitabine.

Of particular interest both for our model here described, as well as any translational value subsequently derived, when K8484-mVenus cells were bedded on K8484 cells at the same 1:10 ratio used with MH17031 cells, resistance to gemcitabine was induced to an equal level as to that seen when in coculture with MH17031. This result, coupled with the genotyping above, suggested that the resistance effect observed within our coculture model is not necessarily a product of CAF coculture, but perhaps more a product of cancer-on-cancer culture, or perhaps high-density cancer growth.

5.4 Cancer cell-driven resistance is a product of cell density-related signalling and not an assay artefact.

Next, focusing on the cancer cell on cancer cell resistance result, I queried whether the resistance phenomenon may be simply an artefact of the coculture assay and not a reflection of a true and clinically relevant resistance mechanism. Noting the relatively high proliferation rate (doubling time of 20 to 24 hours) and therefore high cell density at assay completion of the K8484 and MH17031 cells, I assessed whether the initial seeding ratio/cell number used within the cancer cell-on-cancer cell assay modulated the degree of induced resistance. From a gemcitabine GI50 of 22nM when K8484 cells were seeded at 2,000 cells per well, this increased to 52nM, 1µM, and above the limit of quantification for each of the 5,000, 10,000, and 20,000 cells per well initial seeding count respectively. This suggested that the resistance effect observed, both with cancer cell monoculture as well as in coculture with MH17031, may be a direct product of cell density. The observation that the

other fibroblastic lines tested did not drive resistance despite similar seeding densities, may be a product of lower proliferation rates leading to lower cell density through the assay or contact inhibition preventing cellular accumulation, although the use of the protein-quantifying SRB assay indicated to an extent that cell numbers were similar between resistant and non-resistant coculture assays. In future experiments to better appraise the effect of density for non-resistance driving cells, I would employ more rigorous models of density assessment, to ensure it is controlled for between resistance-driving and non-resistance-driving cells, such as normalisation of nuclear counts at completion of the assay, not at the start.

Density-driven resistance phenomena have been reported previously, including in PDAC, adding credence that such a mechanism may contribute to the effect here observed (Chauffert et al., 1998; Y. Fang et al., 2007; Garrido et al., 1995). To assess whether this was an assay artefact or a true mechanism of gemcitabine resistance specifically, the experiment was replicated with the platinum-based antineoplastic oxaliplatin and the nucleoside analog 5-FU. While cell density had a minor effect in both in increasing resistance within K8484 cells, neither was shifted in the order of magnitude observed with gemcitabine, suggesting that the resistance mechanism was specific in some form to gemcitabine only.

As cell density is typically a product of cell proliferation rate as well as non-contact-inhibited growth, I re-designed my gemcitabine sensitivity analysis to control for the former. To do this, I used the GR metric, as developed by Hafner et al 2016, to evaluate gemcitabine sensitivities discounting for proliferation rate differences (Hafner et al., 2016). Within this analysis K8484 cells in coculture with MH17031 retained a significantly increased GR50 metric when compared to monoculture or coculture with either NF18073 or with a mouse embryonic fibroblast line. Cell line independent correlative analysis of gemcitabine GI50 to proliferation rate identified a notable and significant effect of growth rate of gemcitabine efficacy, but with a Spearman coefficient of < 0.7, is unlikely the sole contributor to the observed effect. Together these data indicated that while proliferation rate of cells is a known modulator of gemcitabine efficacy, it is likely not the sole contributor towards the effect within this model.

5.5 Development and validation of a high-throughput shRNA screen to interrogate gemcitabine resistance mechanisms.

Developing and validating a novel coculture model of gemcitabine resistance *in vitro*, I focused on leveraging this model in a high-throughput screening fashion to identify candidate targets and pathways causative in this phenomenon. To achieve this, and in collaboration with Nicolas Erard in the group of Professor Greg Hannon, I performed a whole-genome shRNA depletion screen within the K8484 cells both in monoculture in coculture with MH17031 cells with and without gemcitabine exposure. The primary goal was to identify the genes that when knocked down in the coculture plus gemcitabine condition specifically, when compared to a timepoint zero population, sensitised the cell to gemcitabine. Therefore, depletion in this condition of an shRNA suggested a causative role of its corresponding gene in driving the resistance effect.

Demonstrating that the resistance phenomenon was maintained when scaled into 15cm dishes, required to process the volume of cells cultured for the screen, an initial screen was undertaken using a whole-genome shRNA library, designed using the shERWOOD algorithm to optimise for potency and minimise off-target effects of the shRNA constructs (Knott et al., 2014). Differential expression was scored with two differed computational methodologies to increase true positives being missed and decrease false positive detection, due to methodology-specific artefacts or biases.

From this initial screen, a total of 827 genes were scored as hits within the coculture plus gemcitabine condition exclusively by at least one of the two scoring methodologies, DESeq2 and Median Z Scores, of which 137, or 15.8% of this total, were scored as hits by both. Preliminary pathway analysis using gene set enrichment analysis as well as MetaCore clustering and PANTHER sequence analysis revealed pathways such as MTORC1 signalling, DNA damage responses, and receptor-binding functional subgroups as key implicated pathways within this subset of genes. Positive controls for modulating gemcitabine sensitivity in this model as well as *in vivo* and in some cases in human, such as *Chek1* and *Atr* (Siang-Boon Koh et al., 2015; S. Liu et al., 2017; Prevo et al., 2012), held through following analysis of the primary screen data. This congruency with established literature provides a degree of confidence in the translational predictability that might be achieved through screening in this format.

5.6 Identification of 19 high-confidence genes with potential clinical value as mediators of gemcitabine resistance in patients.

siRNA-mediated RNA interference screens have been used previously to investigate different biological functions within pancreatic cancer (Azorsa et al., 2009; Bhattacharjee, Zhou, and Yen, 2014; Fredebohm, Wolf, Hoheisel, and Boettcher, 2013; Henderson et al., 2011; Sasaki et al., 2017). While this technique holds value, the more transient nature of siRNA vs shRNA knockdown, as well as the lower specificity (Klinghoffer et al., 2010) renders shRNA screening of additional value. Advent of CRISPR screening presents another novel approach to genome-wide targeting studies, although evidence thus far suggests that while both shRNA and CRISPR screening can have common hit-calling value, true positives unique to each approach can still be identified (Morgens et al., 2016).

As this was the first documented whole-genome *in vitro* shRNA depletion screen investigating gemcitabine resistance in pancreatic cancer, the output data has not been independently replicated. Despite this there is some crossover with existing similar datasets, for example *Rad17*, a previously reported hit in PDAC monoculture in a smaller screen was also a hit in the coculture plus gemcitabine condition here (Fredebohm et al., 2013). To remove possible false-positives due to the off-target effects often ascribed to shRNA targeting (Jackson and Linsley, 2010; Persengiev, Zhu, and Green, 2004), I performed a validation screen with an expanded average number of new shRNAs targeting each gene. This included a refined gene list composed of those genes scored as hits in monoculture and coculture conditions plus gemcitabine, additional genes within their pathways and networks, as well as a panel of hypothesis driven genesets, totalling 1973 genes.

Using the same scoring methodologies, within this validation pool both *Atr* and *Chek1* were again significantly depleted in the coculture plus gemcitabine condition, alongside the enrichment of *Dck* as a positive control. 444 of the 1,973 genes were depleted through the screen in the coculture plus gemcitabine condition only, with 82 of these called using both scoring tools. This provided an increasingly smaller and higher-confidence panel of genes for targeted interrogation as drivers of the resistance phenotype.

While pathway and network analysis can support refining of large datasets towards more actionable targets, it remains less effective when used to analyse smaller datasets, given the lower number of datapoints through which to identify true causative correlation. My goal

was to continue logical refinement of a gene list to the point at which gene by gene qualitative investigation was more feasible. To this end, the list of 82 genes was compared to the genes scored as hits in the coculture plus gemcitabine condition from the initial screen using both scoring tools. Amongst both datasets, 19 genes remained throughout, 10 of which were exclusive to the coculture plus gemcitabine condition in each screen. Amongst these 19 genes were again *Atr* and *Chek1*, as well as 7 genes with an already documented role in PDAC development, 3 with reported synergy with gemcitabine through targeting, and 6 with commercial inhibitors available for purchase, supporting further downstream target validation. Genes were further ranked by the significance of correlation of expression level to survival in pancreatic cancer patients within the PAAD TCGA dataset. Aside from *Atr* and *Chek1*, the only genes to significantly correlate high expression to worse survival were *Eif3e* and *Hsp60*. Both genes are reported in studies that through their inhibition the carcinogenic process of PDAC is delayed (Doldan et al., 2008; Mahajan et al., 2011; Piselli et al., 2000). Neither have been investigated in relation to their modulation of gemcitabine effect in PDAC. With inhibitors targeting the activity of each available, this may form a valuable line of future preclinical research within the model herein described.

A chief challenge in analysing and creating actionable readouts from screens of this size, addressing any phenotype, is the potential valuable data and insights that may be lost through high signal to noise ratios and biased ranking systems. In order or refine whole genome data this is typically a balance: creating as high confidence a list as possible of true positive datapoints, while minimising inclusion of any confounding false negatives. Within this project I erred on the side of optimising for detection of true positives by using stringent hit calling criteria, coupled with repeat rounds of independent assaying with expanded shRNA sets. Thresholds through which hits were called for DESeq2 and Median Z Scores, while benchmarked against those used and validated elsewhere, may also exclude true positives that for reasons independent of their functional role, were not scored as hits consistently throughout each the initial and validation screen.

5.7 Summary and future outlook.

This project serves to undertake two of the imperative and arduous first steps of the drug development process – development of a model through which we can identify and validate therapeutic targets for chemoresistance in pancreatic cancer and leveraging of this model to

identify a confidence-ranked list of targets with potential clinical value. This is the first shRNA-mediated whole genome depletion screen investigating gemcitabine resistance mechanisms in PDAC *in vitro* in the context of a coculture system.

The model itself was built with the observation that coculture of KPC cancer cells alongside KPC CAFs induced a 10 to 50-fold increase in gemcitabine resistance within the cancer cells. Further validation within this thesis verified the resistance effect to be a product of direct cell-cell contact, and unlikely to be mediated via secreted factors. Investigation in the identity of cell lines driving the effect led to the unexpected finding that the cell line driving the effect, MH17031, appeared to be a cancer cell in origin, confirmed via genotype and protein expression. Despite this observation, and the finding that true pancreatic CAFs herein defined did not modulate gemcitabine resistance in this model, the effect was deemed to be real, driven by cell density-related signalling, and not an artefact of the assay structure or protocol. Importantly, trialling of drugs known from *in vivo* and in human studies to be synergistic with gemcitabine within our model, yielded confirmatory and congruent data on the potential predictive utility of this assay. However, those predictions would require further validation in other cell line models and/or *in vivo* studies, prior to being translated into clinical studies.

Further development of this assay could focus on further interrogation of the cellular features causative of resistance in the model, as well as improving isolation and culture protocols for proliferative human CAFs, for evaluating in the same assay. The challenges faced in isolating pure CAFs from KPC murine tissue highlight the absolute importance in genotypic verification of mutation status prior to form and function investigation into murine CAFs for future studies. The heterogeneity of this cellular compartment is widely reported in the literature, and therefore isolation techniques should be suitably contrasted and understood when verifying the specific subtypes being studied.

With an assay demonstrating a targetable gemcitabine resistance mechanism generating data congruent with clinical studies in pancreatic cancer, the use of a whole genome shRNA screen for preclinical target identification was a valuable next step. The challenge faced within the confines of a single PhD project is deciding an analysis pipeline yielding the most actionable data possible for subsequent research. My approach here was to use the addition of a validation screen to find common high-confidence genes that when depleted

revert gemcitabine resistance in the coculture model specifically. This refined list consisted of a panel of 19 genes, for which literature on each was studied for its known roles within pancreatic cancer, interactions with gemcitabine, and targetability with commercially available inhibitors. If this project were to continue, resources would focus on further validation of the top-ranked hits, including individual ShRNA knockdown experiments, and also testing the available inhibitors *in vitro*, before progressing to test promising therapeutic approaches *in vivo*. In addition, further studies would include meta-analysis of total screen data, not only within the coculture plus gemcitabine condition, but also in the monoculture plus gemcitabine condition, as well as studying the signalling changes between monoculture and coculture DMSO control conditions. Whilst I have taken a very targeted approach to my refinement of genes here, the dataset remains a resource available for further genome-wide analyses, and a tool to investigate other hypotheses of gemcitabine effect in pancreatic cancer.

6. Appendix

6.1 Gene hits in initial shRNA screen in coculture plus gemcitabine condition only.

The list of 763 Z score hits and 241 DESq hits (total 867 genes, with overlap) unique to the coculture plus gemcitabine condition, related to Figure 4.11.

Gene	DESeq2 hit	Median Z Score hit
0610007L01Rik	Yes	
2310016M24Rik	Yes	
4732415M23Rik	Yes	
4922505E12Rik	Yes	
4933400C05Rik	Yes	
4933407C03Rik	Yes	
9530053A07Rik	Yes	
Aamp	Yes	
Actb	Yes	
Amn	Yes	
Arc	Yes	
Atp6v0b	Yes	
Aurka	Yes	
Bloc1s1	Yes	
Cacna1f	Yes	
Cap1	Yes	
Cd53	Yes	
Cdca8	Yes	
Chgb	Yes	
Chordc1	Yes	
Cldn13	Yes	
Clic1	Yes	
Cnot10	Yes	

Cog6	Yes	
Cops5	Yes	
Cul9	Yes	
Cwf19l2	Yes	
Cyb5rl	Yes	
Cyhr1	Yes	
Dhx38	Yes	
Dscc1	Yes	
Dync1i2	Yes	
E030010A14Rik	Yes	
E130203B14Rik	Yes	
E130309D02Rik	Yes	
Efna4	Yes	
Eif5a	Yes	
Elof1	Yes	
Ewsr1	Yes	
Fads6	Yes	
Ffar1	Yes	
Gbf1	Yes	
Gcet2	Yes	
Gm5567	Yes	
Gm6985	Yes	
Gosr1	Yes	
Gpr3	Yes	
H2-M10.5	Yes	
Hnrnpc	Yes	
Hsp90ab1	Yes	
Il17b	Yes	
Il5ra	Yes	
Kbtbd5	Yes	
Lin7b	Yes	

LOC547349	Yes	
Lrrc1	Yes	
March9	Yes	
Mat2a	Yes	
Mcm2	Yes	
Mettl21a	Yes	
Mrpl36	Yes	
Mtmr11	Yes	
Nasp	Yes	
Numa1	Yes	
Orc2	Yes	
Osgep	Yes	
Pdcd2l	Yes	
Pdha2	Yes	
Polr1b	Yes	
Ppp1cb	Yes	
Psma6	Yes	
Psma7	Yes	
Psmb3	Yes	
Psmc2	Yes	
Psrc1	Yes	
Rad23a	Yes	
Refbp2	Yes	
Rhox7	Yes	
Rps18	Yes	
Rps24	Yes	
Runx1t1	Yes	
Saa1	Yes	
Sbno1	Yes	
Sephs2	Yes	
Serbp1	Yes	

Sf3a3	Yes	
Sf3b5	Yes	
Slc25a48	Yes	
Socs1	Yes	
Spats1	Yes	
Srsf6	Yes	
Ssrp1	Yes	
Supt4h1	Yes	
Supt6h	Yes	
Svs3b	Yes	
Tesk1	Yes	
Tk1	Yes	
Tnfsf11	Yes	
Tsga10	Yes	
Usp7	Yes	
Vmn1r205	Yes	
Ywhag	Yes	
Zcrb1	Yes	
Zfp512	Yes	
0910001L09Rik	Yes	Yes
1700014N06Rik	Yes	Yes
1700061J05Rik	Yes	Yes
1700065D16Rik	Yes	Yes
2410001C21Rik	Yes	Yes
2610044O15Rik	Yes	Yes
2900092C05Rik	Yes	Yes
4930432K09Rik	Yes	Yes
4931423N10Rik	Yes	Yes
4932415M13Rik	Yes	Yes
6330408A02Rik	Yes	Yes
A530099J19Rik	Yes	Yes

Acer3	Yes	Yes
Adamts14	Yes	Yes
Agtrap	Yes	Yes
Amz2	Yes	Yes
Anp32b	Yes	Yes
Apcdd1	Yes	Yes
Apof	Yes	Yes
Arhgap25	Yes	Yes
Arhgef5	Yes	Yes
B3galt6	Yes	Yes
Bard1	Yes	Yes
BC031353	Yes	Yes
BC056474	Yes	Yes
Caml	Yes	Yes
Ccdc126	Yes	Yes
Ccdc129	Yes	Yes
Cd200r2	Yes	Yes
Cdc23	Yes	Yes
Chek1	Yes	Yes
Clec3a	Yes	Yes
Cops4	Yes	Yes
Csdc2	Yes	Yes
Cst3	Yes	Yes
Cux1	Yes	Yes
Cyp4a29-ps	Yes	Yes
Cytl1	Yes	Yes
Cyyr1	Yes	Yes
D17Wsu104e	Yes	Yes
D6Ertd527e	Yes	Yes
Ddrgk1	Yes	Yes
Dhcr24	Yes	Yes

Dnttip2	Yes	Yes
Dpcd	Yes	Yes
Dus2l	Yes	Yes
Dusp14	Yes	Yes
Eif2ak4	Yes	Yes
Eif2s2	Yes	Yes
Ell	Yes	Yes
Ercc2	Yes	Yes
Evx2	Yes	Yes
Fam190a	Yes	Yes
Fam82b	Yes	Yes
Fosl2	Yes	Yes
Gapvd1	Yes	Yes
Glt8d2	Yes	Yes
Gltp	Yes	Yes
Gm11937	Yes	Yes
Gm13103	Yes	Yes
Gm14496	Yes	Yes
Gm7257	Yes	Yes
Gm7534	Yes	Yes
Gmnn	Yes	Yes
Gpr114	Yes	Yes
Hoxb6	Yes	Yes
Hspd1	Yes	Yes
Ifi27l1	Yes	Yes
Igbp1	Yes	Yes
Igf2bp1	Yes	Yes
Il17d	Yes	Yes
Il20ra	Yes	Yes
Klhl21	Yes	Yes
Krtap16-8	Yes	Yes

Krtap5-3	Yes	Yes
Lce1e	Yes	Yes
Lman1	Yes	Yes
Lrp2	Yes	Yes
Mis18bp1	Yes	Yes
Mpi	Yes	Yes
Ms4a2	Yes	Yes
Mvd	Yes	Yes
Nbr1	Yes	Yes
Ndufa3	Yes	Yes
Nfix	Yes	Yes
Nfkbib	Yes	Yes
Nptn	Yes	Yes
Nr2c1	Yes	Yes
Orai1	Yes	Yes
Orc6	Yes	Yes
Pccb	Yes	Yes
Pcyt2	Yes	Yes
Pdcd10	Yes	Yes
Pdgfa	Yes	Yes
Pick1	Yes	Yes
Ppp1r11	Yes	Yes
Pppde2	Yes	Yes
Psmb4	Yes	Yes
Ptpro	Yes	Yes
Rbmxrt	Yes	Yes
Rif1	Yes	Yes
Rnf182	Yes	Yes
Rnf217	Yes	Yes
Scap	Yes	Yes
Scml2	Yes	Yes

Scml4	Yes	Yes
Sec14l2	Yes	Yes
Senp6	Yes	Yes
Serpina10	Yes	Yes
Sfmbt1	Yes	Yes
Sgsh	Yes	Yes
Slc25a25	Yes	Yes
Slc9a3r2	Yes	Yes
Sp5	Yes	Yes
Supt5h	Yes	Yes
Tbc1d20	Yes	Yes
Tcfap4	Yes	Yes
Tfpt	Yes	Yes
Tgm2	Yes	Yes
Top1	Yes	Yes
Tram1l1	Yes	Yes
Trappc1	Yes	Yes
Tubgcp2	Yes	Yes
Txndc8	Yes	Yes
Tymp	Yes	Yes
Tyw3	Yes	Yes
Ubc	Yes	Yes
Ubxn10	Yes	Yes
Usp15	Yes	Yes
Usp39	Yes	Yes
Vmn1r20	Yes	Yes
Vmn1r212	Yes	Yes
Vmn2r94	Yes	Yes
Wfdc10	Yes	Yes
Wnk1	Yes	Yes
Zbtb7a	Yes	Yes

Zfp142	Yes	Yes
1110012L19Rik		Yes
1600014C10Rik		Yes
1700013F07Rik		Yes
1700040I03Rik		Yes
2010015L04Rik		Yes
2310001A20Rik		Yes
2310010M20Rik		Yes
2310046A06Rik		Yes
2310061N02Rik		Yes
2610034B18Rik		Yes
2810002N01Rik		Yes
2810021J22Rik		Yes
2810030E01Rik		Yes
3110079O15Rik		Yes
3830417A13Rik		Yes
4921504E06Rik		Yes
4930571K23Rik		Yes
4930578N16Rik		Yes
4930579G24Rik		Yes
4931417G12Rik		Yes
4933407H18Rik		Yes
4933421E11Rik		Yes
8430406I07Rik		Yes
A730037C10Rik		Yes
Aarsd1		Yes
Aatk		Yes
Abcc9		Yes
Abi3bp		Yes
Abpa		Yes
Acsl1		Yes

Adal		Yes
Adam1b		Yes
Adam21		Yes
Adamts6		Yes
Aes		Yes
Afap1l1		Yes
Afp		Yes
Aftph		Yes
Ahrr		Yes
AI413582		Yes
AI428936		Yes
Akap17b		Yes
Akap6		Yes
Akap9		Yes
Akirin1		Yes
Aldh1l1		Yes
Aldh1l2		Yes
Alg5		Yes
Anapc5		Yes
Ankrd58		Yes
Anpep		Yes
Ap1s3		Yes
Ap2m1		Yes
Apbb1		Yes
Aplp1		Yes
Aqp3		Yes
Arap2		Yes
Arhgap9		Yes
Arid5b		Yes
Arl13b		Yes
Arrdc3		Yes

Atg4b		Yes
Atg9b		Yes
Atl1		Yes
Atp6v1b2		Yes
Atr		Yes
AU040320		Yes
B230208H17Rik		Yes
B630019K06Rik		Yes
Batf3		Yes
BC016495		Yes
BC048679		Yes
Bdp1		Yes
Birc3		Yes
Bmpr2		Yes
Brap		Yes
Brca1		Yes
Brf1		Yes
Brix1		Yes
Btg2		Yes
Bub1b		Yes
C1qtnf6		Yes
C1s		Yes
C77370		Yes
Cabp2		Yes
Calr		Yes
Camk1d		Yes
Capn1		Yes
Car5a		Yes
Cbl		Yes
Ccdc11		Yes
Ccdc88b		Yes

Ccdc89		Yes
Ccdc96		Yes
Cck		Yes
Cct2		Yes
Cd28		Yes
Cd300lg		Yes
Cdc37		Yes
Cdhr4		Yes
Cebpa		Yes
Cebpd		Yes
Cenpk		Yes
Cep192		Yes
Cep63		Yes
Chaf1a		Yes
Chaf1b		Yes
Chd4		Yes
Chd8		Yes
Chmp2a		Yes
Chn1		Yes
Chuk		Yes
Ciita		Yes
Ckap5		Yes
Cldn22		Yes
Clgn		Yes
Clip3		Yes
Clns1a		Yes
Cmpk2		Yes
Col11a2		Yes
Cops6		Yes
Cops7a		Yes
Corin		Yes

Coro1c		Yes
Cpa3		Yes
Cpeb3		Yes
Cpn2		Yes
Cpped1		Yes
Cpsf4		Yes
Cpsf7		Yes
Creb3l4		Yes
Crh		Yes
Csnk2a1		Yes
Csrnp1		Yes
Ctsb		Yes
Cul7		Yes
Cyp2d11		Yes
Cyp39a1		Yes
Cyp3a57		Yes
D4Ertd22e		Yes
Dach1		Yes
Dars		Yes
Dazl		Yes
Dcaf12l2		Yes
Dclk1		Yes
Ddb1		Yes
Ddx49		Yes
Ddx54		Yes
Defb8		Yes
Dennd4b		Yes
Depdc7		Yes
Dgkg		Yes
Dhrs9		Yes
Dhx9		Yes

Dlgap4		Yes
Dmrta1		Yes
Dmxl1		Yes
Dnahc5		Yes
Dnaja4		Yes
Dnajb6		Yes
Dnajc2		Yes
Dnm1		Yes
Dnm2		Yes
Dpp9		Yes
Dpy19l4		Yes
Dub1a		Yes
Duoxa1		Yes
Dusp15		Yes
Dut		Yes
Duxbl		Yes
Ear10		Yes
Ebf4		Yes
Ect2		Yes
Efcab1		Yes
Egln3		Yes
Eif3m		Yes
Eif4ebp1		Yes
Eif5b		Yes
Elf1		Yes
Elmod3		Yes
Endou		Yes
Entpd1		Yes
Eny2		Yes
Epb4.1l2		Yes
Epha4		Yes

Epx		Yes
Espl1		Yes
Ext2		Yes
F2r		Yes
F3		Yes
Fam131b		Yes
Fam163a		Yes
Fam184a		Yes
Fam46c		Yes
Fam98c		Yes
Fancc		Yes
Fancm		Yes
Fastk		Yes
Fastkd5		Yes
Fbn1		Yes
Fem1a		Yes
Fgf3		Yes
Fkbp10		Yes
Flywch2		Yes
Fmn1		Yes
Fos		Yes
Fosb		Yes
Foxa1		Yes
Foxf1a		Yes
Foxj1		Yes
Foxp2		Yes
Fpr1		Yes
Frmpd4		Yes
Fuz		Yes
Fxc1		Yes
G6pc3		Yes

Gabra6		Yes
Gal3st2		Yes
Gapt		Yes
Gata5		Yes
Gbp3		Yes
Gcg		Yes
Gcn1l1		Yes
Gfra3		Yes
Ghr		Yes
Gli2		Yes
Glis3		Yes
Glt6d1		Yes
Gm11062		Yes
Gm11565		Yes
Gm11568		Yes
Gm12171		Yes
Gm13040		Yes
Gm13212		Yes
Gm13271		Yes
Gm1661		Yes
Gm2897		Yes
Gm4934		Yes
Gm4987		Yes
Gm5595		Yes
Gm5800		Yes
Gm628		Yes
Gm6762		Yes
Gm8439		Yes
Gm9112		Yes
Gmeb1		Yes
Gmppa		Yes

Golgb1		Yes
Gpc6		Yes
Gpcpd1		Yes
Gpha2		Yes
Gpkow		Yes
Gpr149		Yes
Gpr172b		Yes
Gpr44		Yes
Gpx1		Yes
Gramd4		Yes
Grik2		Yes
Grp		Yes
Gsk3a		Yes
Gsn		Yes
Gtpbp10		Yes
Gucy2e		Yes
Gusb		Yes
H2afx		Yes
H3f3a		Yes
H47		Yes
Hamp2		Yes
Haus2		Yes
Hcfc1		Yes
Hcn4		Yes
Hdac1		Yes
Herc6		Yes
Hes5		Yes
Hfe		Yes
Hic2		Yes
Hist1h1c		Yes
Hist1h2bk		Yes

Hist1h4j		Yes
Hist2h2bb		Yes
Hist2h3c1		Yes
Hn1		Yes
Hormad2		Yes
Hoxa11		Yes
Hoxc5		Yes
Hpdl		Yes
Hrh4		Yes
Hsd3b2		Yes
Hsf5		Yes
Hus1		Yes
Huwe1		Yes
Iars		Yes
Id2		Yes
Id4		Yes
Ift20		Yes
Il10rb		Yes
Il1f10		Yes
Ildr1		Yes
Immp1l		Yes
Imp4		Yes
Impa2		Yes
Inca1		Yes
Ing4		Yes
Iqcf3		Yes
Irf1		Yes
Irf8		Yes
Isoc2a		Yes
Isoc2b		Yes
Kars		Yes

Kcnh3		Yes
Kcnh7		Yes
Kcnh8		Yes
Kcnj14		Yes
Kif2b		Yes
Kif4		Yes
Kifc2		Yes
Klf15		Yes
Klhdc7a		Yes
Klhl17		Yes
Klhl28		Yes
Klk15		Yes
Klra3		Yes
Kpna1		Yes
Kri1		Yes
Krtap13		Yes
Krtap27-1		Yes
L1td1		Yes
Lamb1		Yes
Lamc1		Yes
Lamp2		Yes
Lce3b		Yes
Lcmt1		Yes
Lcmt2		Yes
Leo1		Yes
Lgals3bp		Yes
Lipo1		Yes
Lmtk3		Yes
Lpcat2		Yes
Lrig1		Yes
Lrrc47		Yes

Lrrc50		Yes
Lrrn3		Yes
Ly6i		Yes
Lypd6		Yes
Lyrm4		Yes
Mab21l1		Yes
Mad1l1		Yes
Madcam1		Yes
Mapk14		Yes
Mapk3		Yes
March08		Yes
Mbd3l1		Yes
Mbnl3		Yes
Mc3r		Yes
Med1		Yes
Mei1		Yes
Mgp		Yes
Mib2		Yes
Mkl2		Yes
Mkrn3		Yes
Mlkl		Yes
Mll1		Yes
Mov10		Yes
Mrps16		Yes
Mxra8		Yes
Myo5b		Yes
Nars2		Yes
Ncbp2		Yes
Ncf4		Yes
Ncl		Yes
Ncoa6		Yes

Ndufv1		Yes
Nemf		Yes
Nfe2l1		Yes
Nfib		Yes
Nfkbie		Yes
Npcd		Yes
Nr3c2		Yes
Nras		Yes
Nrg2		Yes
Nudt9		Yes
Nup160		Yes
Ogt		Yes
Opn5		Yes
Osgin2		Yes
Otud5		Yes
Paf1		Yes
Parg		Yes
Parp4		Yes
Pbrm1		Yes
Pcca		Yes
Pcdh11x		Yes
Pcgf6		Yes
Pcid2		Yes
Pde4d		Yes
Pdgfd		Yes
Pds5b		Yes
Phc1		Yes
Phf15		Yes
Pid1		Yes
Pip4k2b		Yes
Pirt		Yes

Pkn1		Yes
Pkp4		Yes
Plcg2		Yes
Plekhm2		Yes
Plrg1		Yes
Pmaip1		Yes
Pnpla2		Yes
Pola2		Yes
Pot1b		Yes
Pou4f2		Yes
Ppdpf		Yes
Ppm1b		Yes
Ppm1e		Yes
Ppp1r12b		Yes
Ppp1r1c		Yes
Ppp2r1a		Yes
Ppp2r5e		Yes
Ppp6c		Yes
Prcc		Yes
Prima1		Yes
Prl8a6		Yes
Prom2		Yes
Prpf19		Yes
Prpf8		Yes
Prps1l3		Yes
Prrx2		Yes
Prss29		Yes
Prss57		Yes
Psg17		Yes
Pskh1		Yes
Psma1		Yes

Psma5		Yes
Psma8		Yes
Psmc4		Yes
Psmd8		Yes
Ptges3		Yes
Ptprc		Yes
Rabggta		Yes
Rad17		Yes
Rbfox1		Yes
Rbl1		Yes
Rbm25		Yes
Rbm3		Yes
Rcc2		Yes
Rce1		Yes
Rcn1		Yes
Rgs3		Yes
Rgs8		Yes
Rhox9		Yes
Riok1		Yes
Ripply2		Yes
Ripply3		Yes
Rnd3		Yes
Rnf19a		Yes
Rogdi		Yes
Rpgr		Yes
Rpl11		Yes
Rpl15		Yes
Rpl23		Yes
Rpl27a		Yes
Rpl3		Yes
Rpl37		Yes

Rpl7a		Yes
Rps13		Yes
Rps6ka2		Yes
Rps6kc1		Yes
Rps9		Yes
Rtn2		Yes
Rufy4		Yes
Sap130		Yes
Sap30l		Yes
Sardh		Yes
Scaf11		Yes
Scarb2		Yes
Scg5		Yes
Scrn2		Yes
Sdr39u1		Yes
Sel1l3		Yes
Sema4b		Yes
Serinc3		Yes
Serpina5		Yes
Serpinh1		Yes
Sfrs18		Yes
Siah2		Yes
Sirpa		Yes
Ska1		Yes
Slc14a1		Yes
Slc1a2		Yes
Slc25a13		Yes
Slc25a39		Yes
Slc27a2		Yes
Slc35d3		Yes
Slc38a2		Yes

Slc6a7		Yes
Slc7a15		Yes
Slit1		Yes
Slitrk3		Yes
Slmo2		Yes
Smok2b		Yes
Snrpd1		Yes
Snupn		Yes
Son		Yes
Sord		Yes
Sp110		Yes
Spata2L		Yes
Speer4a		Yes
Speer4b		Yes
Spink4		Yes
Srbd1		Yes
Srgap2		Yes
Srp72		Yes
Srrm2		Yes
Ssbp2		Yes
Ssxb9		Yes
St18		Yes
Stag2		Yes
Stau2		Yes
Stk30		Yes
Stk36		Yes
Stoml1		Yes
Sult3a1		Yes
Sumf2		Yes
Sympk		Yes
Tas2r102		Yes

Tbc1d15		Yes
Tbc1d2b		Yes
Tbca		Yes
Tceb2		Yes
Tcf20		Yes
Tcfcp2		Yes
Tcirg1		Yes
Tcof1		Yes
Tead1		Yes
Tead2		Yes
Thbs3		Yes
Thoc1		Yes
Thop1		Yes
Thumpd1		Yes
Tial1		Yes
Tigd3		Yes
Timm10		Yes
Timm17b		Yes
Tle6		Yes
Tmco2		Yes
Tmed1		Yes
Tmeff2		Yes
Tmem186		Yes
Tmem50b		Yes
Tnfrsf18		Yes
Tnks		Yes
Tox4		Yes
Traf3		Yes
Trat1		Yes
Trem3		Yes
Trim11		Yes

Trim28		Yes
Triobp		Yes
Trip6		Yes
Trp73		Yes
Tspan11		Yes
Tspan32		Yes
Ttc12		Yes
Tti1		Yes
Tuba3a		Yes
Twist1		Yes
Txn2		Yes
Txnrd1		Yes
Uba1		Yes
Ubac1		Yes
Ube2d3		Yes
Ube2o		Yes
Ube2q1		Yes
Ube4b		Yes
Ubxn1		Yes
Uck1		Yes
Ucp1		Yes
Uqcc		Yes
Usp19		Yes
Usp42		Yes
Utp23		Yes
Vdr		Yes
Vmn1r169		Yes
Vmn1r198		Yes
Vmn1r23		Yes
Vmn2r11		Yes
Vmn2r110		Yes

Vmn2r26		Yes
Vmn2r50		Yes
Vmn2r57		Yes
Vmn2r77		Yes
Vmn2r95		Yes
Vmp1		Yes
Wdhd1		Yes
Wdr1		Yes
Wdr12		Yes
Wdr33		Yes
Wdr75		Yes
Wfdc11		Yes
Wwtr1		Yes
Xlr3a		Yes
Xrcc6bp1		Yes
Ybey		Yes
Zbtb24		Yes
Zbtb40		Yes
Zbtb9		Yes
Zdhhc21		Yes
Zfp202		Yes
Zfp276		Yes
Zfp36l2		Yes
Zfp574		Yes
Zfp651		Yes
Zfp689		Yes
Zfp72		Yes
Zfp82		Yes
Zfp869		Yes
Zfp943		Yes
Zfr		Yes

Zfr2		Yes
Zkscan5		Yes
Zmat2		Yes
Zmpste24		Yes
Znrf3		Yes
Zp3r		Yes
Zscan21		Yes

6.2 Genes depleted in select MSigDB gene sets identified using GSEA.

Referred to in A list of 21 genes in total depleted within the gene sets referred to in Section 4.9.1.

Gene set	**Gene significantly depleted in Coculture plus gemcitabine**
HALLMARK_MYC_TARGETS_V2 (26 total in set)	*Mphosph10*
HALLMARK_MYC_TARGETS_V2	*Map3K6*
HALLMARK_MYC_TARGETS_V2	*Slc29A2*
HALLMARK_MYC_TARGETS_V2	*Utp20*
HALLMARK_MYC_TARGETS_V2	*Imp4*
HALLMARK_MYC_TARGETS_V2	*Las1L*
HALLMARK_MYC_TARGETS_V2	*Hspe1*
HALLMARK_MYC_TARGETS_V2	*Tcof1*
HALLMARK_DNA_REPAIR (48 total in set)	*Rpa3*
HALLMARK_DNA_REPAIR	*Pold1*
HALLMARK_DNA_REPAIR	*Sf3A3*
HALLMARK_DNA_REPAIR	*Supt5H*
HALLMARK_DNA_REPAIR	*Pold3*
HALLMARK_DNA_REPAIR	*Nudt21*
HALLMARK_DNA_REPAIR	*Supt4H1*

HALLMARK_DNA_REPAIR	*Thoc4*
HALLMARK_DNA_REPAIR	*Ncbp2*
HALLMARK_DNA_REPAIR	*Pola2*
HALLMARK_DNA_REPAIR	*Guk1*
HALLMARK_DNA_REPAIR	*Ddb1*
HALLMARK_DNA_REPAIR	*Ssrp1*

6.3 Genes depleted in coculture plus gemcitabine only with molecular functions around enzyme regulator activity.

Data analysed using PANTHER (Mi et al., 2017), taken from the subset of catalytically active genes.

Gene code	Details
Inca1	Protein INCA1
Pot1B	Protection of telomeres 1B
Tbc1D15	TBC1 domain family member 15
Gapvd1	GTPase-activating protein and VPS9 domain-containing protein 1
Triobp	TRIO and F-actin-binding protein
Myo5B	Unconventional myosin-Vb
Ppp1R12B	Protein phosphatase 1 regulatory subunit 12B
Ncf4	Neutrophil cytosol factor 4
Tbc1D2B	TBC1 domain family member 2B
Plcg2	1-phosphatidylinositol 4,5-bisphosphate phosphodiesterase gamma-2
Gmppa	Mannose-1-phosphate guanyltransferase alpha
Tbc1D20	TBC1 domain family member 20
Trappc1	Trafficking protein particle complex subunit 1
Ppm1B	Protein phosphatase 1B
Ppm1E	Protein phosphatase 1M
Rgs8	Regulator of G-protein signaling 8
Ppm1E	Protein phosphatase 1E

Ppp1R11	Protein phosphatase 1 regulatory subunit 11

6.4 Genes significantly depleted in coculture plus gemcitabine grouped using MetaCore network clustering.

A total of 205 genes referred to in Figure 4.13.

Gene network	**Name**
Cell cycle_G2-M	Ywhag
Cell cycle_G2-M	Anapc5
Cell cycle_G2-M	Aurka
Cell cycle_G2-M	Bub1b
Cell cycle_G2-M	Brca1
Cell cycle_G2-M	Cdc23
Cell cycle_G2-M	Cdc37
Cell cycle_G2-M	Herc6
Cell cycle_G2-M	*Chek1*
Cell cycle_G2-M	Dnm1
Cell cycle_G2-M	Dnm2
Cell cycle_G2-M	Mapk3
Cell cycle_G2-M	Hcfc1
Cell cycle_G2-M	Hus1
Cell cycle_G2-M	Hist1h1c
Cell cycle_G2-M	H3f3a
Cell cycle_G2-M	Rps6kc1
Cell cycle_G2-M	Ncl
Cell cycle_G2-M	Pdgfa
Cell cycle_G2-M	Cct2
Cell cycle_G2-M	Top1
Cell cycle_G2-M	Ubc
Cell cycle_G2-M	Uba1
Cell cycle_G2-M	Mapk14

Cell cycle_G2-M	Trp73
Cell cycle_G2-M	Rps6ka2
DNA damage_Checkpoint	14-3-3
DNA damage_Checkpoint	14-3-3 gamma
DNA damage_Checkpoint	ANAPC5
DNA damage_Checkpoint	Bard1
DNA damage_Checkpoint	Brca1
DNA damage_Checkpoint	BTG2
DNA damage_Checkpoint	CDC23
DNA damage_Checkpoint	Chk1
DNA damage_Checkpoint	ERK1 (MAPK3)
DNA damage_Checkpoint	ERK1/2
DNA damage_Checkpoint	Histone H2AX
DNA damage_Checkpoint	HUS1
DNA damage_Checkpoint	I-kB
DNA damage_Checkpoint	p38 MAPK
DNA damage_Checkpoint	p38alpha (MAPK14)
DNA damage_Checkpoint	RAD17
DNA damage_Checkpoint	RIF1
DNA damage_Checkpoint	Separase
DNA damage_Checkpoint	Stromalins 1/2
DNA damage_Checkpoint	Ubiquitin
Translation_Translation initiation	4E-BP1
Translation_Translation initiation	Casein kinase II
Translation_Translation initiation	Casein kinase II, alpha chain (CSNK2A1)
Translation_Translation initiation	Casein kinase II, alpha chains
Translation_Translation initiation	Casein kinase II, alpha' chain (CSNK2A2)
Translation_Translation initiation	DAZL
Translation_Translation initiation	eIF2S2
Translation_Translation initiation	eIF5A
Translation_Translation initiation	eIF5B (IF-2)

Translation_Translation initiation	GCN2
Translation_Translation initiation	RP40
Translation_Translation initiation	RPL11
Translation_Translation initiation	RPL15
Translation_Translation initiation	RPL17
Translation_Translation initiation	RPL23
Translation_Translation initiation	RPL27A
Translation_Translation initiation	RPL3
Translation_Translation initiation	RPL37
Translation_Translation initiation	RPL7
Translation_Translation initiation	RPL7A
Translation_Translation initiation	RPS13
Translation_Translation initiation	RPS18
Translation_Translation initiation	RPS27A
Translation_Translation initiation	RPS9
DNA damage_DBS repair	Brca1
DNA damage_DBS repair	Casein kinase II
DNA damage_DBS repair	Casein kinase II, alpha chain (CSNK2A1)
DNA damage_DBS repair	Casein kinase II, alpha chains
DNA damage_DBS repair	Casein kinase II, alpha' chain (CSNK2A2)
DNA damage_DBS repair	ChAF1 subunit A
DNA damage_DBS repair	ChAF1 subunit B
DNA damage_DBS repair	Chk1
DNA damage_DBS repair	FANCC
DNA damage_DBS repair	FANCM
DNA damage_DBS repair	Histone H2AX
DNA damage_DBS repair	Histone H3
DNA damage_DBS repair	Histone H4
DNA damage_DBS repair	NMP200
DNA damage_DBS repair	PP2A regulatory
DNA damage_DBS repair	PP2A structural

DNA damage_DBS repair	TOP1
DNA damage_DBS repair	Ubiquitin
Proteolysis_Ubiquitin-proteasomal proteolysis	Bard1
Proteolysis_Ubiquitin-proteasomal proteolysis	Brca1
Proteolysis_Ubiquitin-proteasomal proteolysis	Brca1/Bard1
Proteolysis_Ubiquitin-proteasomal proteolysis	c-Cbl
Proteolysis_Ubiquitin-proteasomal proteolysis	DORFIN
Proteolysis_Ubiquitin-proteasomal proteolysis	Elongin B
Proteolysis_Ubiquitin-proteasomal proteolysis	HSP90
Proteolysis_Ubiquitin-proteasomal proteolysis	PSMA1
Proteolysis_Ubiquitin-proteasomal proteolysis	PSMA5
Proteolysis_Ubiquitin-proteasomal proteolysis	PSMA6
Proteolysis_Ubiquitin-proteasomal proteolysis	PSMB3
Proteolysis_Ubiquitin-proteasomal proteolysis	PSMB4
Proteolysis_Ubiquitin-proteasomal proteolysis	PSMC2
Proteolysis_Ubiquitin-proteasomal proteolysis	PSMD8
Proteolysis_Ubiquitin-proteasomal proteolysis	SELS
Proteolysis_Ubiquitin-proteasomal proteolysis	SENP6
Proteolysis_Ubiquitin-proteasomal proteolysis	SIAH2
Proteolysis_Ubiquitin-proteasomal proteolysis	UBE1
Proteolysis_Ubiquitin-proteasomal proteolysis	UBE2D3
Proteolysis_Ubiquitin-proteasomal proteolysis	Ubiquitin
Proteolysis_Ubiquitin-proteasomal proteolysis	USP7
Translation_Regulation of initiation	4E-BP1
Translation_Regulation of initiation	c-Cbl
Translation_Regulation of initiation	Casein kinase II
Translation_Regulation of initiation	Casein kinase II, alpha chain (CSNK2A1)
Translation_Regulation of initiation	Casein kinase II, alpha chains
Translation_Regulation of initiation	Casein kinase II, alpha' chain (CSNK2A2)
Translation_Regulation of initiation	eIF2S2
Translation_Regulation of initiation	ERK1 (MAPK3)

Translation_Regulation of initiation	ERK1/2
Translation_Regulation of initiation	GSK3 alpha
Translation_Regulation of initiation	GSK3 alpha/beta
Translation_Regulation of initiation	IGBP1
Translation_Regulation of initiation	MLCP (cat)
Translation_Regulation of initiation	MSK1/2 (RPS6KA5/4)
Translation_Regulation of initiation	p38 MAPK
Translation_Regulation of initiation	p38alpha (MAPK14)
Translation_Regulation of initiation	PP1-cat
Cell cycle_G1-S	14-3-3
Cell cycle_G1-S	14-3-3 gamma
Cell cycle_G1-S	ANAPC5
Cell cycle_G1-S	Brca1
Cell cycle_G1-S	CDC23
Cell cycle_G1-S	CDC37
Cell cycle_G1-S	Ceb1
Cell cycle_G1-S	Chk1
Cell cycle_G1-S	Fe65
Cell cycle_G1-S	FosB
Cell cycle_G1-S	HUS1
Cell cycle_G1-S	I-kB
Cell cycle_G1-S	Importin (karyopherin)-alpha
Cell cycle_G1-S	JAB1
Cell cycle_G1-S	Karyopherin alpha 1
Cell cycle_G1-S	NFKBIB
Cell cycle_G1-S	NFKBIE
Cell cycle_G1-S	p107
Cell cycle_G1-S	UBE1
Cell cycle_G1-S	Ubiquitin
Cell cycle_Mitosis	14-3-3 gamma
Cell cycle_Mitosis	ANAPC5

Cell cycle_Mitosis	Aurora-A
Cell cycle_Mitosis	BUBR1
Cell cycle_Mitosis	CDC23
Cell cycle_Mitosis	DYI2
Cell cycle_Mitosis	Dynamin
Cell cycle_Mitosis	Dynamin-1
Cell cycle_Mitosis	Dynamin-2
Cell cycle_Mitosis	Dynein 1, cytoplasmic, intermediate chains
Cell cycle_Mitosis	Histone H1
Cell cycle_Mitosis	Histone H3
Cell cycle_Mitosis	Importin (karyopherin)-alpha
Cell cycle_Mitosis	Karyopherin alpha 1
Cell cycle_Mitosis	MAD1 (mitotic checkpoint)
Cell cycle_Mitosis	NUMA1
Cell cycle_Mitosis	Separase
Cell cycle_Mitosis	Stromalins 1/2
Cell cycle_Mitosis	TOP1
Cell cycle_Mitosis	Tubulin alpha
Cell cycle_Mitosis	Ubiquitin
Inflammation_IFN-gamma signalling	Brca1
Inflammation_IFN-gamma signalling	c-Cbl
Inflammation_IFN-gamma signalling	CIITA
Inflammation_IFN-gamma signalling	eIF2S2
Inflammation_IFN-gamma signalling	ERK1/2
Inflammation_IFN-gamma signalling	FANCC
Inflammation_IFN-gamma signalling	I-kB
Inflammation_IFN-gamma signalling	IKK-alpha
Inflammation_IFN-gamma signalling	IRF1
Inflammation_IFN-gamma signalling	NFKBIB
Inflammation_IFN-gamma signalling	NFKBIE
Inflammation_IFN-gamma signalling	p38 MAPK

Inflammation_IFN-gamma signalling	PLC-gamma
Inflammation_IFN-gamma signalling	PLC-gamma 2
Inflammation_IFN-gamma signalling	SOCS1
Reproduction_Feeding and Neurohormone signalling	14-3-3 gamma
Reproduction_Feeding and Neurohormone signalling	4E-BP1
Reproduction_Feeding and Neurohormone signalling	Antileukoproteinase 1
Reproduction_Feeding and Neurohormone signalling	Brca1
Reproduction_Feeding and Neurohormone signalling	c-Fos
Reproduction_Feeding and Neurohormone signalling	Casein kinase II
Reproduction_Feeding and Neurohormone signalling	Casein kinase II, alpha chains
Reproduction_Feeding and Neurohormone signalling	Corticoliberin
Reproduction_Feeding and Neurohormone signalling	ERK1 (MAPK3)
Reproduction_Feeding and Neurohormone signalling	Galpha(i)-specific peptide GPCRs
Reproduction_Feeding and Neurohormone signalling	Galpha(q)-specific Class A Orphan/other GPCRs
Reproduction_Feeding and Neurohormone signalling	Galpha(q)-specific peptide GPCRs
Reproduction_Feeding and Neurohormone signalling	GHR
Reproduction_Feeding and Neurohormone signalling	Histone H3

Reproduction_Feeding and Neurohormone signalling	IRF1
Reproduction_Feeding and Neurohormone signalling	LAMG1
Reproduction_Feeding and Neurohormone signalling	LRP2 (Megalin)
Reproduction_Feeding and Neurohormone signalling	PICK1
Reproduction_Feeding and Neurohormone signalling	PLC-gamma
Reproduction_Feeding and Neurohormone signalling	PLC-gamma 2
Reproduction_Feeding and Neurohormone signalling	PP2A regulatory
Reproduction_Feeding and Neurohormone signalling	PP2A structural
Reproduction_Feeding and Neurohormone signalling	SOCS1

6.5 List of all genes depleted in both coculture plus gemcitabine and monoculture plus gemcitabine condition in the initial shRNA screen.

A total of 138 genes in common.

Gene
Acpp
Accn3
Copa
Sympk
Cops3
Rpl23a
Gm5567

Ptgs1
E130203B14Rik
Supt4h1
Ugt2b5
6430704M03Rik
E030010A14Rik
Psma4
Psma7
Metap2
Eif3e
Syf2
Sf3b5
Tgm3
Fam89a
Rps27a
Csf2ra
Iars2
Rhox7
Zfp512
Actb
Eif3f
Higd2a
Cyhr1
Slc7a14
Cdc5l
Ltb4r2
1300001I01Rik
Tubb5
Smtnl2
Ssb
Mettl21a

Mtmr11
Rhox1
Svs3b
Saa1
Eml3
Megf10
Inpp5k
Akr1b8
Serpina1c
Supt6h
Rad23a
Dynlrb1
Il5ra
Ddx27
Slc16a1
Gm9513
Rpl26
Hist1h2bf
Smpd3
2310003L22Rik
Tktl2
Rpl36
Gm16387
AW146020
Mudeng
Fam100b
Nutf2
Nudt10
Kti12
Fbxo38
D10Wsu52e

1110014N23Rik
Ovca2
Rps17
Ctr9
Setd1a
Col18a1
Utp20
Tacc3
Wdr36
Ccdc59
Rpl31
Acp5
Rpl10a
B430306N03Rik
Myo16
Rps12
Cadm4
Mdc1
Gpr81
Eftud2
Sf3b3
Mtss1
Serpina3k
Rps11
Ubd
Pola1
Ptpdc1
Fam169b
Cdkn1c
Anapc1
Mepe

2700049A03Rik
Dedd2
Prl8a1
Ceacam20
Tmem167b
Rpf1
Slc36a2
Awat1
Ddx24
Rps4x
Gm14326
Ly6g6e
Pdzd2
Rhot2
Cse1l
Gm11567
2810408M09Rik
BC017158
Racgap1
Gabrb2
Alox12e
Fubp1
Tmem85
Ltb
Trappc9
Spink14
Mad2l2
Ppp1r7
Rps5
Eme1
Gm3285

Rpl5
Gm16404
Riiad1
Acad8
Alg6
D11Wsu99e
Tbrg4

7. Bibliography

Adsay, V., Logani, S., Sarkar, F., … J. C.-T. A. journal, & 2000, undefined. (n.d.). Foamy gland pattern of pancreatic ductal adenocarcinoma: a deceptively benign-appearing variant. *Journals.Lww.Com*. Retrieved from https://journals.lww.com/ajsp/Abstract/2000/04000/Foamy_Gland_Pattern_of_Pancreatic_Ductal.3.aspx

Aglietta, M., Barone, C., Sawyer, M. B., Moore, M. J., Miller, W. H., Bagalà, C., … Leone, F. (2014). A phase I dose escalation trial of tremelimumab (CP-675,206) in combination with gemcitabine in chemotherapy-naive patients with metastatic pancreatic cancer. *Annals of Oncology*, *25*(9), 1750–1755. https://doi.org/10.1093/annonc/mdu205

Aguirre, A. J., Moffitt, R. A., Yeh, J. J., Stewart, C., Robertson, A. G., Cherniack, A. D., … Zenklusen, J. C. (2017). Integrated Genomic Characterization of Pancreatic Ductal Adenocarcinoma. *Cancer Cell*, *32*(2), 185–203.e13. https://doi.org/10.1016/j.ccell.2017.07.007

Alberts, S. R., Townley, P. M., Goldberg, R. M., Cha, S. S., Sargent, D. J., Moore, D. F., … Mailliard, J. A. (2003). Gemcitabine and oxaliplatin for metastatic pancreatic adenocarcinoma: a North Central Cancer Treatment Group phase II study. *Annals of Oncology*, *14*(4), 580–585. https://doi.org/10.1093/annonc/mdg170

Alvarellos, M. L., Lamba, J., Sangkuhl, K., Thorn, C. F., Wang, L., Klein, D. J., … Klein, T. E. (2014). PharmGKB summary: gemcitabine pathway. *Pharmacogenetics and Genomics*, *24*(11), 564–574. https://doi.org/10.1097/FPC.0000000000000086

Ansari, D., Nilsson, J., Andersson, R., Regnér, S., Tingstedt, B., & Andersson, B. (2013). Artificial neural networks predict survival from pancreatic cancer after radical surgery. *American Journal of Surgery*, *205*(1), 1–7. https://doi.org/10.1016/j.amjsurg.2012.05.032

Apte, M. V, Haber, P. S., Darby, S. J., Rodgers, S. C., McCaughan, G. W., Korsten, M. A., … Wilson, J. S. (1999). Pancreatic stellate cells are activated by proinflammatory cytokines: implications for pancreatic fibrogenesis. *Gut*, *44*(4), 534–541. Retrieved from http://www.ncbi.nlm.nih.gov/pubmed/10075961

Apte, M. V, Park, S., Phillips, P. A., Santucci, N., Goldstein, D., Kumar, R. K., … Wilson, J. S. (2004). Desmoplastic reaction in pancreatic cancer: role of pancreatic stellate cells. *Pancreas*, *29*(3), 179–187. Retrieved from http://www.ncbi.nlm.nih.gov/pubmed/15367883

Apte, M. V, Pirola, R. C., & Wilson, J. S. (2012). Pancreatic stellate cells: a starring role in normal and diseased pancreas. *Frontiers in Physiology*, *3*, 344. https://doi.org/10.3389/fphys.2012.00344

Armstrong, T., Packham, G., Murphy, L. B., Bateman, A. C., Conti, J. A., Fine, D. R., … Iredale, J. P. (2004). Type I Collagen Promotes the Malignant Phenotype of Pancreatic Ductal Adenocarcinoma. *Clinical Cancer Research*, *10*(21), 7427–7437. https://doi.org/10.1158/1078-0432.CCR-03-0825

Arumugam, T., Ramachandran, V., Fournier, K. F., Wang, H., Marquis, L., Abbruzzese, J. L., … Choi, W. (2009). Epithelial to Mesenchymal Transition Contributes to Drug Resistance in Pancreatic Cancer. *Cancer Research*, *69*(14), 5820–5828. https://doi.org/10.1158/0008-5472.CAN-08-2819

Azorsa, D. O., Gonzales, I. M., Basu, G. D., Choudhary, A., Arora, S., Bisanz, K. M., … Mousses, S. (2009). Synthetic lethal RNAi screening identifies sensitizing targets for gemcitabine therapy in pancreatic cancer. *Journal of Translational Medicine*, *7*(1), 43. https://doi.org/10.1186/1479-5876-7-43

Azzariti, A., Bocci, G., Porcelli, L., Fioravanti, A., Sini, P., Simone, G. M., … Paradiso, A. (2011). Aurora B kinase inhibitor AZD1152: determinants of action and ability to enhance chemotherapeutics effectiveness in pancreatic and colon cancer. *British Journal of Cancer*, *104*(5), 769–780. https://doi.org/10.1038/bjc.2011.21

Bachem, M. G., Schneider, E., Gross, H., Weidenbach, H., Schmid, R. M., Menke, A., … Adler, G. (1998). Identification, culture, and characterization of pancreatic stellate cells in rats and humans. *Gastroenterology*, *115*(2), 421–432. Retrieved from http://www.ncbi.nlm.nih.gov/pubmed/9679048

Bachem, M. G., Schünemann, M., Ramadani, M., Siech, M., Beger, H., Buck, A., … Adler, G. (2005). Pancreatic carcinoma cells induce fibrosis by stimulating proliferation and matrix synthesis of stellate cells. *Gastroenterology*, *128*(4), 907–921. Retrieved from http://www.ncbi.nlm.nih.gov/pubmed/15825074

Bailey, P., Chang, D. K., Nones, K., Johns, A. L., Patch, A.-M., Gingras, M.-C., … Grimmond, S. M. (2016). Genomic analyses identify molecular subtypes of pancreatic cancer. *Nature*, *531*(7592), 47–52. https://doi.org/10.1038/nature16965

Banerji, U., Jones, R., & PLummer, E. (2017). A Phase 1 Trial of SRA737 in Combination With Gemcitabine Plus Cisplatin or Gemcitabine Alone in Subjects With Advanced Cancer - Full Text View - ClinicalTrials.gov. *ClinicalTrials.Gov*. Retrieved from https://clinicaltrials.gov/ct2/show/NCT02797977

Bansal, P., & Sonnenberg, A. (1995). Pancreatitis is a risk factor for pancreatic cancer. *Gastroenterology*, *109*(1), 247–251. Retrieved from http://www.ncbi.nlm.nih.gov/pubmed/7797022

Barretina, J., Caponigro, G., Stransky, N., Venkatesan, K., Margolin, A. A., Kim, S., … Garraway, L. A. (2012). The Cancer Cell Line Encyclopedia enables predictive modelling of anticancer drug sensitivity. *Nature*, *483*(7391), 603–607. https://doi.org/10.1038/nature11003

Bartek, J., & Lukas, J. (2003). Chk1 and Chk2 kinases in checkpoint control and cancer. *Cancer Cell*, *3*(5), 421–429. https://doi.org/10.1016/S1535-6108(03)00110-7

Becker, A. E., Hernandez, Y. G., Frucht, H., & Lucas, A. L. (2014). Pancreatic ductal adenocarcinoma: risk factors, screening, and early detection. *World Journal of Gastroenterology*, *20*(32), 11182–11198. https://doi.org/10.3748/wjg.v20.i32.11182

Begum, A., Ewachiw, T., Jung, C., Huang, A., Norberg, K. J., Marchionni, L., … Matsui, W. (2017). The extracellular matrix and focal adhesion kinase signaling regulate cancer

stem cell function in pancreatic ductal adenocarcinoma. *PloS One*, *12*(7), e0180181. https://doi.org/10.1371/journal.pone.0180181

Bhattacharjee, V., Zhou, Y., & Yen, T. (2014). A synthetic lethal screen identifies the Vitamin D receptor as a novel gemcitabine sensitizer in pancreatic cancer cells. *Cell Cycle*, *13*(24), 3839–3856. https://doi.org/10.4161/15384101.2014.967070

Biankin, A. V., Waddell, N., Kassahn, K. S., Gingras, M.-C., Muthuswamy, L. B., Johns, A. L., … Grimmond, S. M. (2012). Pancreatic cancer genomes reveal aberrations in axon guidance pathway genes. *Nature*, *491*(7424), 399–405. https://doi.org/10.1038/nature11547

Birnbaum, D. J., Finetti, P., Birnbaum, D., Mamessier, E., & Bertucci, F. (2017). Validation and comparison of the molecular classifications of pancreatic carcinomas. *Molecular Cancer*, *16*(1), 168. https://doi.org/10.1186/s12943-017-0739-z

Blackford, A. N., & Jackson, S. P. (2017). ATM, ATR, and DNA-PK: The Trinity at the Heart of the DNA Damage Response. *Molecular Cell*, *66*(6), 801–817. https://doi.org/10.1016/j.molcel.2017.05.015

Bliss, C. I. (1939). The Toxicity of Poisons Applied Jointly. *Annals of Applied Biology*, *26*(3), 585–615. https://doi.org/10.1111/j.1744-7348.1939.tb06990.x

Boj, S. F., Hwang, C.-I., Baker, L. A., Chio, I. I. C., Engle, D. D., Corbo, V., … Tuveson, D. A. (2015). Organoid Models of Human and Mouse Ductal Pancreatic Cancer. *Cell*, *160*(1–2), 324–338. https://doi.org/10.1016/j.cell.2014.12.021

Bosman, F. T., Carneiro, F., Hruban, R. H., & Theise, N. . (2010). *WHO Classification of Tumours of the Digestive System. Fourth Edition - WHO - OMS* -. WHO. Retrieved from http://apps.who.int/bookorders/anglais/detart1.jsp?codlan=1&codcol=70&codcch=4003&content=1

Brahmer, J. R., Tykodi, S. S., Chow, L. Q. M., Hwu, W.-J., Topalian, S. L., Hwu, P., … Wigginton, J. M. (2012). Safety and Activity of Anti–PD-L1 Antibody in Patients with Advanced Cancer. *New England Journal of Medicine*, *366*(26), 2455–2465. https://doi.org/10.1056/NEJMoa1200694

Brammeld, J. S., Petljak, M., Martincorena, I., Williams, S. P., Alonso, L. G., Dalmases, A., … McDermott, U. (2017). atr. *Genome Research*, *27*(4), 613–625. https://doi.org/10.1101/gr.213546.116

Broutier, L., Mastrogiovanni, G., Verstegen, M. M., Francies, H. E., Gavarró, L. M., Bradshaw, C. R., … Huch, M. (2017). Human primary liver cancer–derived organoid cultures for disease modeling and drug screening. *Nature Medicine*, *23*(12), 1424–1435. https://doi.org/10.1038/nm.4438

Burris, H. A., Moore, M. J., Andersen, J., Green, M. R., Rothenberg, M. L., Modiano, M. R., … Von Hoff, D. D. (1997). Improvements in survival and clinical benefit with gemcitabine as first-line therapy for patients with advanced pancreas cancer: a randomized trial. *Journal of Clinical Oncology*, *15*(6), 2403–2413. https://doi.org/10.1200/JCO.1997.15.6.2403

Campbell, A. S., Albo, D., Kimsey, T. F., White, S. L., & Wang, T. N. (2005). Macrophage

inflammatory protein-3α promotes pancreatic cancer cell invasion. *Journal of Surgical Research*, *123*(1), 96–101. https://doi.org/10.1016/j.jss.2004.07.013

Cancer Genome Atlas Research Network. Electronic address: andrew_aguirre@dfci.harvard.edu, B. J., Cancer Genome Atlas Research Network, R. H., Aguirre, A. J., Moffitt, R. A., Yeh, J. J., Stewart, C., … Zenklusen, J. C. (2017). Integrated Genomic Characterization of Pancreatic Ductal Adenocarcinoma. *Cancer Cell*, *32*(2), 185–203.e13. https://doi.org/10.1016/j.ccell.2017.07.007

Cancer Research UK. (2011). *Age-Standardised Ten-Year Net Survival Trends, Adults (Aged 15-99), Selected Cancers, England and Wales, 1971-2011*. Retrieved from http://www.cancerresearchuk.org/health-professional/cancer-statistics/survival/common-cancers-compared

Cancer Research UK. (2014a). Cancer survival for common cancers. Retrieved June 14, 2018, from http://www.cancerresearchuk.org/health-professional/cancer-statistics/survival/common-cancers-compared#heading-Three

Cancer Research UK. (2014b). *Pancreatic cancer survival statistics*. Retrieved from http://www.cancerresearchuk.org/health-professional/cancer-statistics/statistics-by-cancer-type/pancreatic-cancer

Cancer Research UK. (2015). *Cancer incidence for common cancers*. Retrieved from http://www.cancerresearchuk.org/health-professional/cancer-statistics/incidence/common-cancers-compared

Cancer Research UK. (2016). *Cancer mortality for common cancers*. Retrieved from http://www.cancerresearchuk.org/health-professional/cancer-statistics/mortality/common-cancers-compared

Chambard, J.-C., Lefloch, R., Pouysségur, J., & Lenormand, P. (2007). ERK implication in cell cycle regulation. *Biochimica et Biophysica Acta (BBA) - Molecular Cell Research*, *1773*(8), 1299–1310. https://doi.org/10.1016/J.BBAMCR.2006.11.010

Chaney, W. G., Howard, D. R., Pollard, J. W., Sallustio, S., & Stanley, P. (1988). DNA transfection of Mammalian cells using polybrene. *Methods in Molecular Biology (Clifton, N.J.)*, *4*, 363–370. https://doi.org/10.1385/0-89603-127-6:363

Chantrill, L. A., Nagrial, A. M., Watson, C., Johns, A. L., Martyn-Smith, M., Simpson, S., … Individualized Molecular Pancreatic Cancer Therapy (IMPaCT) Trial Management Committee of the Australasian Gastrointestinal Trials Group (AGITG). (2015). Precision Medicine for Advanced Pancreas Cancer: The Individualized Molecular Pancreatic Cancer Therapy (IMPaCT) Trial. *Clinical Cancer Research*, *21*(9), 2029–2037. https://doi.org/10.1158/1078-0432.CCR-15-0426

Chauffert, B., Dimanche-Boitrel, M.-T., Garrido, C., Ivarsson, M., Martin, M., Martin, F., & Solary, E. (1998). New insights into the kinetic resistance to anticancer agents. *Cytotechnology*, *27*(1/3), 225–235. https://doi.org/10.1023/A:1008025124242

Chauhan, V. P., Martin, J. D., Liu, H., Lacorre, D. A., Jain, S. R., Kozin, S. V., … Jain, R. K. (2013). Angiotensin inhibition enhances drug delivery and potentiates chemotherapy by decompressing tumour blood vessels. *Nature Communications*, *4*(1), 2516.

https://doi.org/10.1038/ncomms3516

Cheadle, C., Vawter, M. P., Freed, W. J., & Becker, K. G. (2003). Analysis of Microarray Data Using Z Score Transformation. *The Journal of Molecular Diagnostics*, *5*(2), 73–81. https://doi.org/10.1016/S1525-1578(10)60455-2

Cheng, X.-B., Kohi, S., Koga, A., Hirata, K., & Sato, N. (2016). Hyaluronan stimulates pancreatic cancer cell motility. *Oncotarget*, *7*(4), 4829–4840. https://doi.org/10.18632/oncotarget.6617

Chong, C. R., & Jänne, P. A. (2013). The quest to overcome resistance to EGFR-targeted therapies in cancer. *Nature Medicine*, *19*(11), 1389–1400. https://doi.org/10.1038/nm.3388

Chung, V., McDonough, S., Philip, P. A., Cardin, D., Wang-Gillam, A., Hui, L., … Hochster, H. S. (2017). Effect of Selumetinib and MK-2206 vs Oxaliplatin and Fluorouracil in Patients With Metastatic Pancreatic Cancer After Prior Therapy. *JAMA Oncology*, *3*(4), 516. https://doi.org/10.1001/jamaoncol.2016.5383

Clevers, H. (2016). Modeling Development and Disease with Organoids. *Cell*, *165*(7), 1586–1597. https://doi.org/10.1016/j.cell.2016.05.082

Coleman, S. J., Chioni, A.-M., Ghallab, M., Anderson, R. K., Lemoine, N. R., Kocher, H. M., & Grose, R. P. (2014). Nuclear translocation of FGFR1 and FGF2 in pancreatic stellate cells facilitates pancreatic cancer cell invasion. *EMBO Molecular Medicine*, *6*(4), 467–481. https://doi.org/10.1002/emmm.201302698

Collisson, E. A., Sadanandam, A., Olson, P., Gibb, W. J., Truitt, M., Gu, S., … Gray, J. W. (2011). Subtypes of pancreatic ductal adenocarcinoma and their differing responses to therapy. *Nature Medicine*, *17*(4), 500–503. https://doi.org/10.1038/nm.2344

Conesa, A., Madrigal, P., Tarazona, S., Gomez-Cabrero, D., Cervera, A., McPherson, A., … Mortazavi, A. (2016). A survey of best practices for RNA-seq data analysis. *Genome Biology*, *17*, 13. https://doi.org/10.1186/s13059-016-0881-8

Conroy, T., Desseigne, F., Ychou, M., Bouché, O., Guimbaud, R., Bécouarn, Y., … Ducreux, M. (2011). FOLFIRINOX versus Gemcitabine for Metastatic Pancreatic Cancer. *New England Journal of Medicine*, *364*(19), 1817–1825. https://doi.org/10.1056/NEJMoa1011923

Corcoran, R. B., Contino, G., Deshpande, V., Tzatsos, A., Conrad, C., Benes, C. H., … Bardeesy, N. (2011). STAT3 plays a critical role in KRAS-induced pancreatic tumorigenesis. *Cancer Research*, *71*(14), 5020–5029. https://doi.org/10.1158/0008-5472.CAN-11-0908

Costa-Silva, B., Aiello, N. M., Ocean, A. J., Singh, S., Zhang, H., Thakur, B. K., … Lyden, D. (2015). Pancreatic cancer exosomes initiate pre-metastatic niche formation in the liver. *Nature Cell Biology*, *17*(6), 816–826. https://doi.org/10.1038/ncb3169

Cousin, B., Ravet, E., Poglio, S., De Toni, F., Bertuzzi, M., Lulka, H., … Cordelier, P. (2009). Adult Stromal Cells Derived from Human Adipose Tissue Provoke Pancreatic Cancer Cell Death both In Vitro and In Vivo. *PLoS ONE*, *4*(7), e6278. https://doi.org/10.1371/journal.pone.0006278

Crul, M., van Waardenburg, R. C. A. M., Bocxe, S., van Eijndhoven, M. A. J., Pluim, D.,

Beijnen, J. H., & Schellens, J. H. M. (2003). DNA repair mechanisms involved in gemcitabine cytotoxicity and in the interaction between gemcitabine and cisplatin. *Biochemical Pharmacology*, *65*(2), 275–282. Retrieved from http://www.ncbi.nlm.nih.gov/pubmed/12504803

Culhaci, N., Sagol, O., Karademir, S., Astarcioglu, H., Astarcioglu, I., Soyturk, M., … Obuz, F. (2005). Expression of transforming growth factor-beta-1 and p27Kip1 in pancreatic adenocarcinomas: relation with cell-cycle-associated proteins and clinicopathologic characteristics. *BMC Cancer*, *5*(1), 98. https://doi.org/10.1186/1471-2407-5-98

Demols, A., Peeters, M., Polus, M., Marechal, R., Gay, F., Monsaert, E., … Van Laethem, J. L. (2006). Gemcitabine and oxaliplatin (GEMOX) in gemcitabine refractory advanced pancreatic adenocarcinoma: a phase II study. *British Journal of Cancer*, *94*(4), 481–485. https://doi.org/10.1038/sj.bjc.6602966

Denduluri, S. K., Idowu, O., Wang, Z., Liao, Z., Yan, Z., Mohammed, M. K., … Luu, H. H. (2015). Insulin-like growth factor (IGF) signaling in tumorigenesis and the development of cancer drug resistance. *Genes & Diseases*, *2*(1), 13–25. https://doi.org/10.1016/J.GENDIS.2014.10.004

Deng, C.-X. (2006). BRCA1: cell cycle checkpoint, genetic instability, DNA damage response and cancer evolution. *Nucleic Acids Research*, *34*(5), 1416–1426. https://doi.org/10.1093/nar/gkl010

Di Marco, M., Di Cicilia, R., Macchini, M., Nobili, E., Vecchiarelli, S., Brandi, G., & Biasco, G. (2010). Metastatic pancreatic cancer: is gemcitabine still the best standard treatment? (Review). *Oncology Reports*, *23*(5), 1183–1192. Retrieved from http://www.ncbi.nlm.nih.gov/pubmed/20372829

Di Veroli, G. Y., Fornari, C., Wang, D., Mollard, S., Bramhall, J. L., Richards, F. M., & Jodrell, D. I. (2016). Combenefit: an interactive platform for the analysis and visualization of drug combinations. *Bioinformatics*, *32*(18), 2866–2868. https://doi.org/10.1093/bioinformatics/btw230

Diehl, P., Tedesco, D., & Chenchik, A. (2014). Use of RNAi screens to uncover resistance mechanisms in cancer cells and identify synthetic lethal interactions. *Drug Discovery Today. Technologies*, *11*, 11–18. https://doi.org/10.1016/j.ddtec.2013.12.002

Doherty, G. J., Tempero, M., & Corrie, P. G. (2018). HALO-109–301: a Phase III trial of PEGPH20 (with gemcitabine and nab-paclitaxel) in hyaluronic acid-high stage IV pancreatic cancer. *Future Oncology*, *14*(1), 13–22. https://doi.org/10.2217/fon-2017-0338

Doldan, A., Chandramouli, A., Shanas, R., Bhattacharyya, A., Cunningham, J. T., Nelson, M. A., & Shi, J. (2008). Loss of the eukaryotic initiation factor 3f in pancreatic cancer. *Molecular Carcinogenesis*, *47*(3), 235–244. https://doi.org/10.1002/mc.20379

Dolenšek, J., Rupnik, M. S., & Stožer, A. (2015). Structural similarities and differences between the human and the mouse pancreas. *Islets*, *7*(1), e1024405. https://doi.org/10.1080/19382014.2015.1024405

Donahue, T. R., Tran, L. M., Hill, R., Li, Y., Kovochich, A., Calvopina, J. H., … Wu, H. (2012).

Integrative Survival-Based Molecular Profiling of Human Pancreatic Cancer. *Clinical Cancer Research*, *18*(5), 1352–1363. https://doi.org/10.1158/1078-0432.CCR-11-1539

Downward, J. (2003). Targeting RAS signalling pathways in cancer therapy. *Nature Reviews Cancer*, *3*(1), 11–22. https://doi.org/10.1038/nrc969

Driscoll, D. R., Karim, S. A., Sano, M., Gay, D. M., Jacob, W., Yu, J., … Morton, J. P. (2016). mTORC2 Signaling Drives the Development and Progression of Pancreatic Cancer. *Cancer Research*, *76*(23), 6911–6923. https://doi.org/10.1158/0008-5472.CAN-16-0810

Duluc, C., Moatassim-Billah, S., Chalabi-Dchar, M., Perraud, A., Samain, R., Breibach, F., … Bousquet, C. (2015). Pharmacological targeting of the protein synthesis mTOR/4E-BP1 pathway in cancer-associated fibroblasts abrogates pancreatic tumour chemoresistance. *EMBO Molecular Medicine*, *7*(6), 735–753. https://doi.org/10.15252/emmm.201404346

Ellenrieder, V., Alber, B., Lacher, U., Hendler, S. F., Menke, A., Boeck, W., … Gress, T. M. (2000). Role of MT-MMPs and MMP-2 in pancreatic cancer progression. *International Journal of Cancer*, *85*(1), 14–20. Retrieved from http://www.ncbi.nlm.nih.gov/pubmed/10585576

Erkan, M., Adler, G., Apte, M. V, Bachem, M. G., Buchholz, M., Detlefsen, S., … Wilson, J. (2011). StellaTUM: current consensus and discussion on pancreatic stellate cell research. https://doi.org/10.1136/gutjnl-2011-301220

Erkan, M., Michalski, C. W., Rieder, S., Reiser–Erkan, C., Abiatari, I., Kolb, A., … Kleeff, J. (2008). The Activated Stroma Index Is a Novel and Independent Prognostic Marker in Pancreatic Ductal Adenocarcinoma. *Clinical Gastroenterology and Hepatology*, *6*(10), 1155–1161. https://doi.org/10.1016/j.cgh.2008.05.006

Evans, R. A., Diamond, M. S., Rech, A. J., Chao, T., Richardson, M. W., Lin, J. H., … Vonderheide, R. H. (2016). Lack of immunoediting in murine pancreatic cancer reversed with neoantigen. *JCI Insight*, *1*(14). https://doi.org/10.1172/jci.insight.88328

Fallahi-Sichani, M., Honarnejad, S., Heiser, L. M., Gray, J. W., & Sorger, P. K. (2013). Metrics other than potency reveal systematic variation in responses to cancer drugs. *Nature Chemical Biology*, *9*(11), 708–714. https://doi.org/10.1038/nchembio.1337

Fang, L., Du, M., Li, Y., Lin, L., Zhang, C., & Zhao, Z. (n.d.). Using the differential adhesion method to isolate and culture mesenchymal stem cells and endothelial progenitor cells from rat bone marrow. Retrieved from https://www.alliedacademies.org/articles/using-the-differential-adhesion-method-to-isolate-and-culture-mesenchymal-stem-cells-and-endothelial-progenitor-cells-from-rat-bon.pdf

Fang, Y., Sullivan, R., & Graham, C. H. (2007). Confluence-dependent resistance to doxorubicin in human MDA-MB-231 breast carcinoma cells requires hypoxia-inducible factor-1 activity. *Experimental Cell Research*, *313*(5), 867–877. https://doi.org/10.1016/j.yexcr.2006.12.004

Feig, C., Jones, J. O., Kraman, M., Wells, R. J. B., Deonarine, A., Chan, D. S., … Fearon, D. T. (2013). Targeting CXCL12 from FAP-expressing carcinoma-associated fibroblasts

synergizes with anti-PD-L1 immunotherapy in pancreatic cancer. *Proceedings of the National Academy of Sciences of the United States of America*, *110*(50), 20212–20217. https://doi.org/10.1073/pnas.1320318110

Fernández-del Castillo, C. (2008). Mucinous Cystic Neoplasms. *Journal of Gastrointestinal Surgery*, *12*(3), 411–413. https://doi.org/10.1007/s11605-007-0347-0

Finotello, F., & Di Camillo, B. (2015). Measuring differential gene expression with RNA-seq: challenges and strategies for data analysis. *Briefings in Functional Genomics*, *14*(2), 130–142. https://doi.org/10.1093/bfgp/elu035

Fokas, E., Prevo, R., Pollard, J. R., Reaper, P. M., Charlton, P. A., Cornelissen, B., … Brunner, T. B. (2012). Targeting ATR in vivo using the novel inhibitor VE-822 results in selective sensitization of pancreatic tumors to radiation. *Cell Death & Disease*, *3*(12), e441–e441. https://doi.org/10.1038/cddis.2012.181

Francone, T. D., Landmann, R. G., Chen, C.-T., Sun, M. Y., Kuntz, E. J., Zeng, Z., … Weiser, M. R. (2007). Novel xenograft model expressing human hepatocyte growth factor shows ligand-dependent growth of c-Met-expressing tumors. *Molecular Cancer Therapeutics*, *6*(4), 1460–1466. https://doi.org/10.1158/1535-7163.MCT-06-0466

Fredebohm, J., Wolf, J., Hoheisel, J. D., & Boettcher, M. (2013). Depletion of RAD17 sensitizes pancreatic cancer cells to gemcitabine. *Journal of Cell Science*, *126*(15), 3380–3389. https://doi.org/10.1242/jcs.124768

Frese, K. K., Neesse, A., Cook, N., Bapiro, T. E., Lolkema, M. P., Jodrell, D. I., & Tuveson, D. A. (2012). nab-Paclitaxel Potentiates Gemcitabine Activity by Reducing Cytidine Deaminase Levels in a Mouse Model of Pancreatic Cancer. *Cancer Discovery*, *2*(3), 260–269. https://doi.org/10.1158/2159-8290.CD-11-0242

Friedrich, J., Seidel, C., Ebner, R., & Kunz-Schughart, L. A. (2009). Spheroid-based drug screen: considerations and practical approach. *Nature Protocols*, *4*(3), 309–324. https://doi.org/10.1038/nprot.2008.226

Froeling, F. E. M., Feig, C., Chelala, C., Dobson, R., Mein, C. E., Tuveson, D. A., … Kocher, H. M. (2011). Retinoic Acid–Induced Pancreatic Stellate Cell Quiescence Reduces Paracrine Wnt–β-Catenin Signaling to Slow Tumor Progression. *Gastroenterology*, *141*(4), 1486–1497.e14. https://doi.org/10.1053/J.GASTRO.2011.06.047

Froeling, F. E. M., Mirza, T. A., Feakins, R. M., Seedhar, A., Elia, G., Hart, I. R., & Kocher, H. M. (2009). Organotypic Culture Model of Pancreatic Cancer Demonstrates that Stromal Cells Modulate E-Cadherin, β-Catenin, and Ezrin Expression in Tumor Cells. *The American Journal of Pathology*, *175*(2), 636–648. https://doi.org/10.2353/ajpath.2009.090131

Fu, J., Bian, M., Jiang, Q., & Zhang, C. (2007). Roles of Aurora Kinases in Mitosis and Tumorigenesis. *Mol Cancer Res*, *5*(1), 1–10. https://doi.org/10.1158/1541-7786.MCR-06-0208

Fujii, M., Shimokawa, M., Date, S., Takano, A., Matano, M., Nanki, K., … Sato, T. (2016). A Colorectal Tumor Organoid Library Demonstrates Progressive Loss of Niche Factor Requirements during Tumorigenesis. *Cell Stem Cell*, *18*(6), 827–838.

https://doi.org/10.1016/j.stem.2016.04.003

Funamizu, N., Okamoto, A., Kamata, Y., Misawa, T., Uwagawa, T., Gocho, T., … Manome, Y. (2010). Is the resistance of gemcitabine for pancreatic cancer settled only by overexpression of deoxycytidine kinase? *Oncology Reports*, *23*(2), 471–475. Retrieved from http://www.ncbi.nlm.nih.gov/pubmed/20043109

Furuyama, K., Doi, R., Mori, T., Toyoda, E., Ito, D., Kami, K., … Fujimoto, K. (2006). Clinical Significance of Focal Adhesion Kinase in Resectable Pancreatic Cancer. *World Journal of Surgery*, *30*(2), 219–226. https://doi.org/10.1007/s00268-005-0165-z

Gaj, T., Gersbach, C. A., & Barbas Iii, C. F. (2013). ZFN, TALEN, and CRISPR/Cas-based methods for genome engineering. *Trends in Biotechnology*, *31*, 397–405. https://doi.org/10.1016/j.tibtech.2013.04.004

Gao, D., Vela, I., Sboner, A., Iaquinta, P. J., Karthaus, W. R., Gopalan, A., … Chen, Y. (2014). Organoid Cultures Derived from Patients with Advanced Prostate Cancer. *Cell*, *159*(1), 176–187. https://doi.org/10.1016/j.cell.2014.08.016

Gao, J., Zhu, F., Lv, S., Li, Z., Ling, Z., Gong, Y., … Ma, L. (2010). Identification of pancreatic juice proteins as biomarkers of pancreatic cancer. *Oncology Reports*, *23*(6), 1683–1692. Retrieved from http://www.ncbi.nlm.nih.gov/pubmed/20428826

Garnett, M. J., Edelman, E. J., Heidorn, S. J., Greenman, C. D., Dastur, A., Lau, K. W., … Benes, C. H. (2012). Systematic identification of genomic markers of drug sensitivity in cancer cells. *Nature*, *483*(7391), 570–575. https://doi.org/10.1038/nature11005

Garrido, C., Chauffert, B., Pinard, D., Tibaut, F., Genne, P., Assem, M., & Dimanche-Boitrel, M. T. (1995). Circumvention of confluence-dependent resistance in a human multi-drug-resistant colon-cancer cell line. *International Journal of Cancer*, *61*(6), 873–879. Retrieved from http://www.ncbi.nlm.nih.gov/pubmed/7790124

Gauthier, N. P., Soufi, B., Walkowicz, W. E., Pedicord, V. A., Mavrakis, K. J., Macek, B., … Miller, M. L. (2013). Cell-selective labeling using amino acid precursors for proteomic studies of multicellular environments. *Nature Methods*, *10*(8), 768–773. https://doi.org/10.1038/nmeth.2529

Gopinathan, A., Morton, J. P., Jodrell, D. I., & Sansom, O. J. (2015). GEMMs as preclinical models for testing pancreatic cancer therapies. *Disease Models & Mechanisms*, *8*(10), 1185–1200. https://doi.org/10.1242/dmm.021055

Gorman, C. M., Howard, B. H., & Reeves, R. (1983). Expression of recombinant plasmids in mammalian cells is enhanced by sodium butyrate. *Nucleic Acids Research*, *11*(21), 7631–7648. Retrieved from http://www.ncbi.nlm.nih.gov/pubmed/6316266

Gumbiner, B. M. (1996). Cell adhesion: the molecular basis of tissue architecture and morphogenesis. *Cell*, *84*(3), 345–357. Retrieved from http://www.ncbi.nlm.nih.gov/pubmed/8608588

Guo, F., Wang, Y., Liu, J., Mok, S. C., Xue, F., & Zhang, W. (2016). CXCL12/CXCR4: a symbiotic bridge linking cancer cells and their stromal neighbors in oncogenic communication networks. *Oncogene*, *35*(7), 816–826. https://doi.org/10.1038/onc.2015.139

Hafner, M., Niepel, M., Chung, M., & Sorger, P. K. (2016). Growth rate inhibition metrics correct for confounders in measuring sensitivity to cancer drugs. *Nature Methods*, *13*(6), 521–527. https://doi.org/10.1038/nmeth.3853

Hagmann, W., Jesnowski, R., & Löhr, J. M. (2010). Interdependence of gemcitabine treatment, transporter expression, and resistance in human pancreatic carcinoma cells. *Neoplasia (New York, N.Y.)*, *12*(9), 740–747. Retrieved from http://www.ncbi.nlm.nih.gov/pubmed/20824050

Hammel, P., Bachet, J.-B., Portales, F., Mineur, L., Metges, J.-P., de la Fouchardiere, C., … El-Hariry, I. (2017). A Phase 2b of eryaspase in combination with gemcitabine or FOLFOX as second-line therapy in patients with metastatic pancreatic adenocarcinoma (NCT02195180). *Annals of Oncology*, *28*(suppl_5). https://doi.org/10.1093/annonc/mdx369.005

Han, S., Delitto, D., Zhang, D., Sorenson, H. L., Sarosi, G. A., Thomas, R. M., … Hughes, S. J. (2015). Primary outgrowth cultures are a reliable source of human pancreatic stellate cells. *Laboratory Investigation*, *95*(11), 1331–1340. https://doi.org/10.1038/labinvest.2015.117

Han, S., Gonzalo, D. H., Feely, M., Rinaldi, C., Belsare, S., Zhai, H., … Hughes, S. J. (2018). Stroma-derived extracellular vesicles deliver tumor-suppressive miRNAs to pancreatic cancer cells. *Oncotarget*, *9*(5), 5764–5777. https://doi.org/10.18632/oncotarget.23532

Hata, T., Furukawa, T., Sunamura, M., Egawa, S., Motoi, F., Ohmura, N., … Horii, A. (2005). RNA Interference Targeting Aurora Kinase A Suppresses Tumor Growth and Enhances the Taxane Chemosensitivity in Human Pancreatic Cancer Cells. *Cancer Research*, *65*(7), 2899–2905. https://doi.org/10.1158/0008-5472.CAN-04-3981

Hayward, J., Alvarez, S. A., Ruiz, C., Sullivan, M., Tseng, J., & Whalen, G. (2010). Machine learning of clinical performance in a pancreatic cancer database. *Artificial Intelligence in Medicine*, *49*(3), 187–195. https://doi.org/10.1016/J.ARTMED.2010.04.009

Henderson, M. C., Gonzales, I. M., Arora, S., Choudhary, A., Trent, J. M., Hoff, D. D. Von, … Azorsa, D. O. (2011). High-throughput RNAi Screening Identifies a Role for TNK1 in Growth and Survival of Pancreatic Cancer Cells. https://doi.org/10.1158/1541-7786.MCR-10-0436

Hessmann, E., Patzak, M. S., Klein, L., Chen, N., Kari, V., Ramu, I., … Neesse, A. (2017). Fibroblast drug scavenging increases intratumoural gemcitabine accumulation in murine pancreas cancer. *Gut*, gutjnl-2016-311954. https://doi.org/10.1136/gutjnl-2016-311954

Hezel, A. F., Kimmelman, A. C., Stanger, B. Z., Bardeesy, N., & Depinho, R. A. (2006). Genetics and biology of pancreatic ductal adenocarcinoma. *Genes & Development*, *20*(10), 1218–1249. https://doi.org/10.1101/gad.1415606

Hingorani, S. R., Harris, W. P., Beck, J. T., Berdov, B. A., Wagner, S. A., Pshevlotsky, E. M., … Devoe, C. E. (2016). Phase Ib Study of PEGylated Recombinant Human Hyaluronidase and Gemcitabine in Patients with Advanced Pancreatic Cancer. *Clinical Cancer Research : An Official Journal of the American Association for Cancer Research*, *22*(12), 2848–2854. https://doi.org/10.1158/1078-0432.CCR-15-2010

Hingorani, S. R., Wang, L., Multani, A. S., Combs, C., Deramaudt, T. B., Hruban, R. H., … Tuveson, D. A. (2005). Trp53R172H and KrasG12D cooperate to promote chromosomal instability and widely metastatic pancreatic ductal adenocarcinoma in mice. *Cancer Cell*, *7*(5), 469–483. https://doi.org/10.1016/j.ccr.2005.04.023

Hingorani, S., Zheng, L., Bullock, A. J., Seery, T. E., Harris, W. P., Sigal, D. S., … Hendifar, A. E. (2018). HALO 202: Randomized Phase II Study of PEGPH20 Plus Nab-Paclitaxel/Gemcitabine Versus Nab-Paclitaxel/Gemcitabine in Patients With Untreated, Metastatic Pancreatic Ductal Adenocarcinoma. *Journal of Clinical Oncology*, *36*(4), 359–366. https://doi.org/10.1200/JCO.2017.74.9564

Hinz, B., Dugina, V., Ballestrem, C., Wehrle-Haller, B., & Chaponnier, C. (2003). Alpha-smooth muscle actin is crucial for focal adhesion maturation in myofibroblasts. *Molecular Biology of the Cell*, *14*(6), 2508–2519. https://doi.org/10.1091/mbc.E02-11-0729

Hinz, S., Pagerols-Raluy, L., Oberg, H.-H., Ammerpohl, O., Grussel, S., Sipos, B., … Kalthoff, H. (2007). Foxp3 Expression in Pancreatic Carcinoma Cells as a Novel Mechanism of Immune Evasion in Cancer. *Cancer Research*, *67*(17), 8344–8350. https://doi.org/10.1158/0008-5472.CAN-06-3304

Holz, M. K., Ballif, B. A., Gygi, S. P., & Blenis, J. (2005). mTOR and S6K1 mediate assembly of the translation preinitiation complex through dynamic protein interchange and ordered phosphorylation events. *Cell*, *123*(4), 569–580. https://doi.org/10.1016/j.cell.2005.10.024

Hruban, R. H., Goggins, M., Parsons, J., & Kern, S. E. (2000). Progression model for pancreatic cancer. *Clinical Cancer Research : An Official Journal of the American Association for Cancer Research*, *6*(8), 2969–2972. Retrieved from http://www.ncbi.nlm.nih.gov/pubmed/10955772

Hui, E. E., & Bhatia, S. N. (2007). Micromechanical control of cell-cell interactions. *Proceedings of the National Academy of Sciences*, *104*(14), 5722–5726. https://doi.org/10.1073/pnas.0608660104

Husain, K., Centeno, B. A., Chen, D.-T., Hingorani, S. R., Sebti, S. M., & Malafa, M. P. (2013). Vitamin E δ-tocotrienol prolongs survival in the LSL-KrasG12D/+;LSL-Trp53R172H/+;Pdx-1-Cre (KPC) transgenic mouse model of pancreatic cancer. *Cancer Prevention Research (Philadelphia, Pa.)*, *6*(10), 1074–1083. https://doi.org/10.1158/1940-6207.CAPR-13-0157

Huxley, R., Ansary-Moghaddam, A., Berrington de González, A., Barzi, F., & Woodward, M. (2005). Type-II diabetes and pancreatic cancer: a meta-analysis of 36 studies. *British Journal of Cancer*, *92*(11), 2076–2083. https://doi.org/10.1038/sj.bjc.6602619

Hwang, R. F., Moore, T., Arumugam, T., Ramachandran, V., Amos, K. D., Rivera, A., … Logsdon, C. D. (2008). Cancer-associated stromal fibroblasts promote pancreatic tumor progression. *Cancer Research*, *68*(3), 918–926. https://doi.org/10.1158/0008-5472.CAN-07-5714

Itoh, H., Komatsuda, A., Wakui, H., Miura, A. B., & Tashima, Y. (1999). Mammalian HSP60 is a major target for an immunosuppressant mizoribine. *The Journal of Biological*

Chemistry, *274*(49), 35147–35151. Retrieved from http://www.ncbi.nlm.nih.gov/pubmed/10574997

Ivanov, D. P., & Grabowska, A. M. (2017). Spheroid arrays for high-throughput single-cell analysis of spatial patterns and biomarker expression in 3D. *Scientific Reports*, *7*(1), 41160. https://doi.org/10.1038/srep41160

Jackson, A. L., & Linsley, P. S. (2010). Recognizing and avoiding siRNA off-target effects for target identification and therapeutic application. *Nature Reviews Drug Discovery*, *9*(1), 57–67. https://doi.org/10.1038/nrd3010

Jacobetz, M. A., Chan, D. S., Neesse, A., Bapiro, T. E., Cook, N., Frese, K. K., … Tuveson, D. A. (2013). Hyaluronan impairs vascular function and drug delivery in a mouse model of pancreatic cancer. *Gut*, *62*(1), 112–120. https://doi.org/10.1136/gutjnl-2012-302529

Jaster, R. (2004). Molecular regulation of pancreatic stellate cell function. *Molecular Cancer*, *3*, 26. https://doi.org/10.1186/1476-4598-3-26

Jiang, H., Hegde, S., Knolhoff, B. L., Zhu, Y., Herndon, J. M., Meyer, M. A., … DeNardo, D. G. (2016). Targeting focal adhesion kinase renders pancreatic cancers responsive to checkpoint immunotherapy. *Nature Medicine*, *22*(8), 851–860. https://doi.org/10.1038/nm.4123

Jones, S., Zhang, X., Parsons, D. W., Lin, J. C.-H., Leary, R. J., Angenendt, P., … Kinzler, K. W. (2008). Core Signaling Pathways in Human Pancreatic Cancers Revealed by Global Genomic Analyses. *Science*, *321*(5897), 1801–1806. https://doi.org/10.1126/science.1164368

Joost, S., Almada, L. L., Rohnalter, V., Holz, P. S., Vrabel, A. M., Fernandez-Barrena, M. G., … Lauth, M. (2012). GLI1 inhibition promotes epithelial-to-mesenchymal transition in pancreatic cancer cells. *Cancer Research*, *72*(1), 88–99. https://doi.org/10.1158/0008-5472.CAN-10-4621

Kamerkar, S., LeBleu, V. S., Sugimoto, H., Yang, S., Ruivo, C. F., Melo, S. A., … Kalluri, R. (2017). Exosomes facilitate therapeutic targeting of oncogenic KRAS in pancreatic cancer. *Nature*, *546*(7659), 498–503. https://doi.org/10.1038/nature22341

Kang, Y., Shen, C., Yao, Y.-Q., Yu, L., Cui, X., He, Y., … Gou, L. (2014). *Oncology letters. Oncology Letters* (Vol. 8). [Spandidos Publications]. Retrieved from https://www.spandidos-publications.com/ol/8/3/1229

Kawaguchi, K., Igarashi, K., Murakami, T., Kiyuna, T., Lwin, T. M., Hwang, H. K., … Hoffman, R. M. (2017). MEK inhibitors cobimetinib and trametinib, regressed a gemcitabine-resistant pancreatic-cancer patient-derived orthotopic xenograft (PDOX). *Oncotarget*, *8*(29). https://doi.org/10.18632/oncotarget.17667

Kindler, H. L., Niedzwiecki, D., Hollis, D., Sutherland, S., Schrag, D., Hurwitz, H., … Goldberg, R. M. (2010). Gemcitabine Plus Bevacizumab Compared With Gemcitabine Plus Placebo in Patients With Advanced Pancreatic Cancer: Phase III Trial of the Cancer and Leukemia Group B (CALGB 80303). *Journal of Clinical Oncology*, *28*(22), 3617–3622. https://doi.org/10.1200/JCO.2010.28.1386

Kingston, R. E., Chen, C. A., & Rose, J. K. (2003). Calcium Phosphate Transfection. *Current*

Protocols in Molecular Biology, *63*(1), 9.1.1-9.1.11. https://doi.org/10.1002/0471142727.mb0901s63

Kitts, P. A., Church, D. M., Thibaud-Nissen, F., Choi, J., Hem, V., Sapojnikov, V., … Kimchi, A. (2016). Assembly: a resource for assembled genomes at NCBI. *Nucleic Acids Research*, *44*(D1), D73-80. https://doi.org/10.1093/nar/gkv1226

Klinghoffer, R. A., Magnus, J., Schelter, J., Mehaffey, M., Coleman, C., & Cleary, M. A. (2010). Reduced seed region-based off-target activity with lentivirus-mediated RNAi. *RNA (New York, N.Y.)*, *16*(5), 879–884. https://doi.org/10.1261/rna.1977810

Knott, S. R. V, Maceli, A., Erard, N., Chang, K., Marran, K., Zhou, X., … Hannon, G. J. (2014). A computational algorithm to predict shRNA potency. *Molecular Cell*, *56*(6), 796–807. https://doi.org/10.1016/j.molcel.2014.10.025

Koh, S.-B., Courtin, A., Boyce, R. J., Boyle, R. G., Richards, F. M., & Jodrell, D. I. (2015). CHK1 Inhibition Synergizes with Gemcitabine Initially by Destabilizing the DNA Replication Apparatus. *Cancer Research*, *75*(17), 3583–3595. https://doi.org/10.1158/0008-5472.CAN-14-3347

Koh, S.-B., Wallez, Y., Dunlop, C. R., Bernaldo de Quirós Fernández, S., Bapiro, T. E., Richards, F. M., & Jodrell, D. I. (2018). Mechanistic distinctions between CHK1 and WEE1 inhibition guide the scheduling of triple therapy with gemcitabine. *Cancer Research*, canres.3932.2017. https://doi.org/10.1158/0008-5472.CAN-17-3932

Komiya, Y., Onodera, Y., Kuroiwa, M., Nomimura, S., Kubo, Y., Nam, J.-M., … Okada, M. (2016). The Rho guanine nucleotide exchange factor ARHGEF5 promotes tumor malignancy via epithelial–mesenchymal transition. *Oncogenesis*, *5*(9), e258–e258. https://doi.org/10.1038/oncsis.2016.59

Kondratska, K., Kondratskyi, A., Yassine, M., Lemonnier, L., Lepage, G., Morabito, A., … Prevarskaya, N. (2014). Orai1 and STIM1 mediate SOCE and contribute to apoptotic resistance of pancreatic adenocarcinoma. *Biochimica et Biophysica Acta (BBA) - Molecular Cell Research*, *1843*(10), 2263–2269. https://doi.org/10.1016/j.bbamcr.2014.02.012

Kosmahl, M., Pauser, U., Anlauf, M., pathology, G. K.-M., & 2005, undefined. (n.d.). Pancreatic ductal adenocarcinomas with cystic features: neither rare nor uniform. *Nature.Com*. Retrieved from https://www.nature.com/articles/3800446

Kraman, M., Bambrough, P. J., Arnold, J. N., Roberts, E. W., Magiera, L., Jones, J. O., … Fearon, D. T. (2010). Suppression of Antitumor Immunity by Stromal Cells Expressing Fibroblast Activation Protein-. *Science*, *330*(6005), 827–830. https://doi.org/10.1126/science.1195300

Kumar, R., Chaudhary, K., Singla, D., Gautam, A., & Raghava, G. P. S. (2014). Designing of promiscuous inhibitors against pancreatic cancer cell lines. *Scientific Reports*, *4*, 4668. https://doi.org/10.1038/srep04668

Kurahara, H., Bohl, C., Natsugoe, S., Nishizono, Y., Harihar, S., Sharma, R., … Welch, D. R. (2016). Suppression of pancreatic cancer growth and metastasis by HMP19 identified through genome-wide shRNA screen. *International Journal of Cancer*, *139*(3), 628–638.

https://doi.org/10.1002/ijc.30110

Lamouille, S., Xu, J., & Derynck, R. (2014). Molecular mechanisms of epithelial-mesenchymal transition. *Nature Reviews. Molecular Cell Biology*, *15*(3), 178–196. https://doi.org/10.1038/nrm3758

Langmead, B., Trapnell, C., Pop, M., & Salzberg, S. L. (2009). Ultrafast and memory-efficient alignment of short DNA sequences to the human genome. *Genome Biology*, *10*(3), R25. https://doi.org/10.1186/gb-2009-10-3-r25

Le, D. T., Crocenzi, T. S., Urum, J. N., Lutz, E. R., Laheru, D. A., Sugar, E. A., … Jaffee, E. M. (2015). Randomized Phase II study of the safety, efficacy and immune response of GVAX pancreas (with cyclophosphamide) and CRS-207 with or without nivolumab in patients with previously treated metastatic pancreatic adenocarcinoma (STELLAR). *Journal for ImmunoTherapy of Cancer*, *3*(Suppl 2), P155. https://doi.org/10.1186/2051-1426-3-S2-P155

Lewis, C. S., Voelkel-Johnson, C., & Smith, C. D. (2016). Suppression of c-Myc and RRM2 expression in pancreatic cancer cells by the sphingosine kinase-2 inhibitor ABC294640. *Oncotarget*, *7*(37), 60181–60192. https://doi.org/10.18632/oncotarget.11112

Liang, M., Zhao, T., Ma, L., & Guo, Y. (2017). CHK1 inhibition sensitizes pancreatic cancer cells to gemcitabine via promoting CDK-dependent DNA damage and ribonucleotide reductase downregulation. *Oncology Reports*, *39*(3), 1322–1330. https://doi.org/10.3892/or.2017.6168

Liberzon, A., Birger, C., Thorvaldsdóttir, H., Ghandi, M., Mesirov, J. P., & Tamayo, P. (2015). The Molecular Signatures Database Hallmark Gene Set Collection. *Cell Systems*, *1*(6), 417–425. https://doi.org/10.1016/J.CELS.2015.12.004

Liberzon, A., Subramanian, A., Pinchback, R., Thorvaldsdottir, H., Tamayo, P., & Mesirov, J. P. (2011). Molecular signatures database (MSigDB) 3.0. *Bioinformatics*, *27*(12), 1739–1740. https://doi.org/10.1093/bioinformatics/btr260

Liberzon, A., Subramanian, A., Pinchback, R., Thorvaldsdóttir, H., Tamayo, P., & Mesirov, J. P. (2011). Molecular signatures database (MSigDB) 3.0. *Bioinformatics (Oxford, England)*, *27*(12), 1739–1740. https://doi.org/10.1093/bioinformatics/btr260

Lili, L. N., Matyunina, L. V, Walker, L. D., Daneker, G. W., & McDonald, J. F. (2014). Evidence for the importance of personalized molecular profiling in pancreatic cancer. *Pancreas*, *43*(2), 198–211. https://doi.org/10.1097/MPA.0000000000000020

Lipner, M. B., Marayati, R., Deng, Y., Wang, X., Raftery, L., O'Neil, B. H., & Yeh, J. J. (2016). Metformin Treatment Does Not Inhibit Growth of Pancreatic Cancer Patient-Derived Xenografts. *PLOS ONE*, *11*(1), e0147113. https://doi.org/10.1371/journal.pone.0147113

Liu, S., Ge, Y., Wang, T., Edwards, H., Ren, Q., Jiang, Y., … Wang, G. (2017). Inhibition of ATR potentiates the cytotoxic effect of gemcitabine on pancreatic cancer cells through enhancement of DNA damage and abrogation of ribonucleotide reductase induction by gemcitabine. *Oncology Reports*, *37*(6), 3377–3386. https://doi.org/10.3892/or.2017.5580

Liu, Y., Beyer, A., & Aebersold, R. (2016). Leading Edge Review On the Dependency of Cellular Protein Levels on mRNA Abundance. https://doi.org/10.1016/j.cell.2016.03.014

Liu, Y., Suckale, J., Masjkur, J., Magro, M. G., Steffen, A., Anastassiadis, K., & Solimena, M. (2010). Tamoxifen-independent recombination in the RIP-CreER mouse. *PloS One*, *5*(10), e13533. https://doi.org/10.1371/journal.pone.0013533

Loewe, S. (1953). The problem of synergism and antagonism of combined drugs. *Arzneimittel-Forschung*, *3*(6), 285–290. Retrieved from http://www.ncbi.nlm.nih.gov/pubmed/13081480

Longley, D. B., Harkin, D. P., & Johnston, P. G. (2003). 5-Fluorouracil: mechanisms of action and clinical strategies. *Nature Reviews Cancer*, *3*(5), 330–338. https://doi.org/10.1038/nrc1074

Love, M. I., Huber, W., & Anders, S. (2014). Moderated estimation of fold change and dispersion for RNA-seq data with DESeq2. *Genome Biology*, *15*(12), 550. https://doi.org/10.1186/s13059-014-0550-8

Lowenfels, A. B., Maisonneuve, P., Cavallini, G., Ammann, R. W., Lankisch, P. G., Andersen, J. R., … Domellof, L. (1993). Pancreatitis and the Risk of Pancreatic Cancer. *New England Journal of Medicine*, *328*(20), 1433–1437. https://doi.org/10.1056/NEJM199305203282001

Luthman, H., & Magnusson, G. (1983). High efficiency polyoma DNA transfection of chloroquine treated cells. *Nucleic Acids Research*, *11*(5), 1295–1308. https://doi.org/10.1093/nar/11.5.1295

Lüttges, J., Vogel, I., Menke, M., … D. H.-B.-, & 1998, undefined. (n.d.). Clear cell carcinoma of the pancreas: an adenocarcinoma with ductal phenotype. *Europepmc.Org*. Retrieved from https://europepmc.org/abstract/med/9639120

Ma, Y., Hu, J., Zhang, N., Dong, X., Li, Y., Yang, B., … Wang, X. (2016). Prediction of Candidate Drugs for Treating Pancreatic Cancer by Using a Combined Approach. *PloS One*, *11*(2), e0149896. https://doi.org/10.1371/journal.pone.0149896

Mahajan, U. M., Gupta, C., Wagh, P. R., Karpe, P. A., & Tikoo, K. (2011). Alteration in inflammatory/apoptotic pathway and histone modifications by nordihydroguaiaretic acid prevents acute pancreatitis in swiss albino mice. *Apoptosis*, *16*(11), 1138–1149. https://doi.org/10.1007/s10495-011-0643-8

Maitra, A., & Hruban, R. H. (2008). Pancreatic Cancer. *Annual Review of Pathology: Mechanisms of Disease*, *3*(1), 157–188. https://doi.org/10.1146/annurev.pathmechdis.3.121806.154305

Matsuda, Y., Yoshimura, H., Suzuki, T., Uchida, E., Naito, Z., & Ishiwata, T. (2014). Inhibition of fibroblast growth factor receptor 2 attenuates proliferation and invasion of pancreatic cancer. *Cancer Science*, *105*(9), 1212–1219. https://doi.org/10.1111/cas.12470

Matsushita, A., Gotze, T., & Korc, M. (2007). Hepatocyte Growth Factor Mediated Cell Invasion in Pancreatic Cancer Cells Is Dependent on Neuropilin-1. *Cancer Research*,

67(21), 10309–10316. https://doi.org/10.1158/0008-5472.CAN-07-3256

McMillin, D. W., Delmore, J., Weisberg, E., Negri, J. M., Geer, D. C., Klippel, S., … Mitsiades, C. S. (2010). Tumor cell-specific bioluminescence platform to identify stroma-induced changes to anticancer drug activity. *Nature Medicine*, *16*(4), 483–489. https://doi.org/10.1038/nm.2112

Melisi, D., Ishiyama, S., Sclabas, G. M., Fleming, J. B., Xia, Q., Tortora, G., … Chiao, P. J. (2008). LY2109761, a novel transforming growth factor receptor type I and type II dual inhibitor, as a therapeutic approach to suppressing pancreatic cancer metastasis. *Molecular Cancer Therapeutics*, *7*(4), 829–840. https://doi.org/10.1158/1535-7163.MCT-07-0337

Mendes-Pereira, A. M., Sims, D., Dexter, T., Fenwick, K., Assiotis, I., Kozarewa, I., … Ashworth, A. (2012). Genome-wide functional screen identifies a compendium of genes affecting sensitivity to tamoxifen. *Proceedings of the National Academy of Sciences of the United States of America*, *109*(8), 2730–2735. https://doi.org/10.1073/pnas.1018872108

Meng, Q., Li, B. X., & Xiao, X. (2018). Toward Developing Chemical Modulators of Hsp60 as Potential Therapeutics. *Frontiers in Molecular Biosciences*, *5*, 35. https://doi.org/10.3389/fmolb.2018.00035

Mews, P., Phillips, P., Fahmy, R., Korsten, M., Pirola, R., Wilson, J., & Apte, M. (2002). Pancreatic stellate cells respond to inflammatory cytokines: potential role in chronic pancreatitis. *Gut*, *50*(4), 535–541. Retrieved from http://www.ncbi.nlm.nih.gov/pubmed/11889076

Mi, H., Huang, X., Muruganujan, A., Tang, H., Mills, C., Kang, D., & Thomas, P. D. (2017). PANTHER version 11: expanded annotation data from Gene Ontology and Reactome pathways, and data analysis tool enhancements. *Nucleic Acids Research*, *45*(D1), D183–D189. https://doi.org/10.1093/nar/gkw1138

Mi, H., Muruganujan, A., Casagrande, J. T., & Thomas, P. D. (2013). Large-scale gene function analysis with the PANTHER classification system. *Nature Protocols*, *8*(8), 1551–1566. https://doi.org/10.1038/nprot.2013.092

Minuesa, G., Antczak, C., Shum, D., Radu, C., Bhinder, B., Li, Y., … Kharas, M. G. (2014). A 1536-well fluorescence polarization assay to screen for modulators of the MUSASHI family of RNA-binding proteins. *Combinatorial Chemistry & High Throughput Screening*, *17*(7), 596–609. Retrieved from http://www.ncbi.nlm.nih.gov/pubmed/24912481

Moffitt, R. A., Marayati, R., Flate, E. L., Volmar, K. E., Loeza, S. G. H., Hoadley, K. A., … Yeh, J. J. (2015). Virtual microdissection identifies distinct tumor- and stroma-specific subtypes of pancreatic ductal adenocarcinoma. *Nature Genetics*, *47*(10), 1168–1178. https://doi.org/10.1038/ng.3398

Mollard, S., Frese, K. K., Gopinathan, A., Richards, F. M., & Jodrell, D. I. (2016). Abstract B54: Genetically engineered mouse-derived allografts (GEDAs): an immunocompetent mouse model of PDAC for the evaluation of novel therapeutic strategies. *Cancer Research*, *76*(24 Supplement), B54–B54. https://doi.org/10.1158/1538-7445.PANCA16-B54

Moore, M. J., Goldstein, D., Hamm, J., Figer, A., Hecht, J. R., Gallinger, S., … National Cancer Institute of Canada Clinical Trials Group. (2007). Erlotinib Plus Gemcitabine Compared With Gemcitabine Alone in Patients With Advanced Pancreatic Cancer: A Phase III Trial of the National Cancer Institute of Canada Clinical Trials Group. *Journal of Clinical Oncology*, *25*(15), 1960–1966. https://doi.org/10.1200/JCO.2006.07.9525

Mootha, V. K., Lindgren, C. M., Eriksson, K.-F., Subramanian, A., Sihag, S., Lehar, J., … Groop, L. C. (2003). PGC-1α-responsive genes involved in oxidative phosphorylation are coordinately downregulated in human diabetes. *Nature Genetics*, *34*(3), 267–273. https://doi.org/10.1038/ng1180

Morgens, D. W., Deans, R. M., Li, A., & Bassik, M. C. (2016). Systematic comparison of CRISPR/Cas9 and RNAi screens for essential genes. *Nature Biotechnology*, *34*(6), 634–636. https://doi.org/10.1038/nbt.3567

Morran, D. C., Wu, J., Jamieson, N. B., Mrowinska, A., Kalna, G., Karim, S. A., … Morton, J. P. (2014). Targeting mTOR dependency in pancreatic cancer. *Gut*, *63*(9), 1481–1489. https://doi.org/10.1136/gutjnl-2013-306202

Muzumdar, M. D., Chen, P.-Y., Dorans, K. J., Chung, K. M., Bhutkar, A., Hong, E., … Jacks, T. (2017). Survival of pancreatic cancer cells lacking KRAS function. *Nature Communications*, *8*(1), 1090. https://doi.org/10.1038/s41467-017-00942-5

Nagai, T., Ibata, K., Park, E. S., Kubota, M., Mikoshiba, K., & Miyawaki, A. (2002). A variant of yellow fluorescent protein with fast and efficient maturation for cell-biological applications. *Nature Biotechnology*, *20*(1), 87–90. https://doi.org/10.1038/nbt0102-87

Nakamura, T., Kuwai, T., Kitadai, Y., Sasaki, T., Fan, D., Coombes, K. R., … Fidler, I. J. (2007). Zonal Heterogeneity for Gene Expression in Human Pancreatic Carcinoma. *Cancer Research*, *67*(16), 7597–7604. https://doi.org/10.1158/0008-5472.CAN-07-0874

Neesse, A., Frese, K. K., Bapiro, T. E., Nakagawa, T., Sternlicht, M. D., Seeley, T. W., … Tuveson, D. A. (2013). CTGF antagonism with mAb FG-3019 enhances chemotherapy response without increasing drug delivery in murine ductal pancreas cancer. *Proceedings of the National Academy of Sciences of the United States of America*, *110*(30), 12325–12330. https://doi.org/10.1073/pnas.1300415110

Neesse, A., Michl, P., Frese, K. K., Feig, C., Cook, N., Jacobetz, M. A., … Tuveson, D. A. (2011). Stromal biology and therapy in pancreatic cancer. *Gut*, *60*(6), 861–868. https://doi.org/10.1136/gut.2010.226092

Niessen, C. M., Leckband, D., & Yap, A. S. (2011). Tissue organization by cadherin adhesion molecules: dynamic molecular and cellular mechanisms of morphogenetic regulation. *Physiological Reviews*, *91*(2), 691–731. https://doi.org/10.1152/physrev.00004.2010

Ohhashi, S., Ohuchida, K., Mizumoto, K., Fujita, H., Egami, T., Yu, J., … Tanaka, M. (2008). Down-regulation of deoxycytidine kinase enhances acquired resistance to gemcitabine in pancreatic cancer. *Anticancer Research*, *28*(4B), 2205–2212. Retrieved from http://www.ncbi.nlm.nih.gov/pubmed/18751396

Öhlund, D., Handly-Santana, A., Biffi, G., Elyada, E., Almeida, A. S., Ponz-Sarvise, M., … Tuveson, D. A. (2017). Distinct populations of inflammatory fibroblasts and

myofibroblasts in pancreatic cancer. *The Journal of Experimental Medicine*, *214*(3), 579–596. https://doi.org/10.1084/jem.20162024

Olive, K. P. (2018). *Update on IPI-926-03 trial*. Retrieved from https://www.olivelab.org/ipi-926-03.html

Olive, K. P., Jacobetz, M. A., Davidson, C. J., Gopinathan, A., McIntyre, D., Honess, D., … Tuveson, D. A. (2009). Inhibition of Hedgehog Signaling Enhances Delivery of Chemotherapy in a Mouse Model of Pancreatic Cancer. *Science*, *324*(5933), 1457–1461. https://doi.org/10.1126/science.1171362

Olive, K., Tuveson, D. A., Ruhe, Z. C., Yin, B., Willis, N. A., Bronson, R. T., … Jacks, T. (2004). Mutant p53 gain of function in two mouse models of Li-Fraumeni syndrome. *Cell*, *119*(6), 847–860. https://doi.org/10.1016/j.cell.2004.11.004

Oliveros, J. (2007). VENNY. An interactive tool for comparing lists with Venn diagrams. *BioinfoGP, CNB-CSIC*. http://bioinfogp.cnb.csic.es/tools/venny/index.html. Retrieved from citeulike-article-id:6994833

Omura, N., Griffith, M., Vincent, A., Li, A., Hong, S.-M., Walter, K., … Goggins, M. (2010). Cyclooxygenase-deficient pancreatic cancer cells use exogenous sources of prostaglandins. *Molecular Cancer Research : MCR*, *8*(6), 821–832. https://doi.org/10.1158/1541-7786.MCR-09-0336

Onion, D., Argent, R. H., Reece-Smith, A. M., Craze, M. L., Pineda, R. G., Clarke, P. A., … Grabowska, A. M. (2016). Models and Technologies 3-Dimensional Patient-Derived Lung Cancer Assays Reveal Resistance to Standards-of-Care Promoted by Stromal Cells but Sensitivity to Histone Deacetylase Inhibitors. https://doi.org/10.1158/1535-7163.MCT-15-0598

Ostrem, J. M. L., & Shokat, K. M. (2016). Direct small-molecule inhibitors of KRAS: from structural insights to mechanism-based design. *Nature Reviews Drug Discovery*, *15*(11), 771–785. https://doi.org/10.1038/nrd.2016.139

Özdemir, B. C., Pentcheva-Hoang, T., Carstens, J. L., Zheng, X., Wu, C.-C., Simpson, T. R., … Kalluri, R. (2014). Depletion of carcinoma-associated fibroblasts and fibrosis induces immunosuppression and accelerates pancreas cancer with reduced survival. *Cancer Cell*, *25*(6), 719–734. https://doi.org/10.1016/j.ccr.2014.04.005

Pancreatic Cancer UK. (2016). Tests and investigation for Pancreatic Cancer. Retrieved June 25, 2018, from https://www.pancreaticcancer.org.uk/information-and-support/facts-about-pancreatic-cancer/how-is-pancreatic-cancer-diagnosed/tests-for-pancreatic-cancer/

Parsels, L. A., Morgan, M. A., Tanska, D. M., Parsels, J. D., Palmer, B. D., Booth, R. J., … Maybaum, J. (2009). Gemcitabine sensitization by checkpoint kinase 1 inhibition correlates with inhibition of a Rad51 DNA damage response in pancreatic cancer cells. *Molecular Cancer Therapeutics*, *8*(1), 45–54. https://doi.org/10.1158/1535-7163.MCT-08-0662

Pasca di Magliano, M., Biankin, A. V., Heiser, P. W., Cano, D. A., Gutierrez, P. J. A., Deramaudt, T., … Hebrok, M. (2007). Common Activation of Canonical Wnt Signaling in

Pancreatic Adenocarcinoma. *PLoS ONE*, *2*(11), e1155. https://doi.org/10.1371/journal.pone.0001155

Persengiev, S. P., Zhu, X., & Green, M. R. (2004). Nonspecific, concentration-dependent stimulation and repression of mammalian gene expression by small interfering RNAs (siRNAs). *RNA (New York, N.Y.)*, *10*(1), 12–18. Retrieved from http://www.ncbi.nlm.nih.gov/pubmed/14681580

Phan, V. T., Wu, X., Cheng, J. H., Sheng, R. X., Chung, A. S., Zhuang, G., … Ferrara, N. (2013). Oncogenic RAS pathway activation promotes resistance to anti-VEGF therapy through G-CSF-induced neutrophil recruitment. *Proceedings of the National Academy of Sciences*, *110*(15), 6079–6084. https://doi.org/10.1073/pnas.1303302110

Piselli, P., Vendetti, S., Vismara, D., Cicconi, R., Poccia, F., Colizzi, V., & Delpino, A. (2000). Different expression of CD44, ICAM-1, and HSP60 on primary tumor and metastases of a human pancreatic carcinoma growing in scid mice. *Anticancer Research*, *20*(2A), 825–831. Retrieved from http://www.ncbi.nlm.nih.gov/pubmed/10810361

Plummer, E., Dean, E., Evans, J., Greystoke, A., Herbschleb, K., Ranson, M., … Middleton, M. (2016). Phase I trial of first-in-class ATR inhibitor VX-970 in combination with gemcitabine (Gem) in advanced solid tumors (NCT02157792). Retrieved from https://www.research.manchester.ac.uk/portal/en/publications/phase-i-trial-of-firstinclass-atr-inhibitor-vx970-in-combination-with-gemcitabine-gem-in-advanced-solid-tumors-nct02157792(ccb48dea-97d2-490a-91d3-4dfb5c485355)/export.html

Plunkett, W., Huang, P., Xu, Y. Z., Heinemann, V., Grunewald, R., & Gandhi, V. (1995). Gemcitabine: metabolism, mechanisms of action, and self-potentiation. *Seminars in Oncology*, *22*(4 Suppl 11), 3–10. Retrieved from http://www.ncbi.nlm.nih.gov/pubmed/7481842

Prevo, R., Fokas, E., Reaper, P. M., Charlton, P. A., Pollard, J. R., McKenna, W. G., … Brunner, T. B. (2012). The novel ATR inhibitor VE-821 increases sensitivity of pancreatic cancer cells to radiation and chemotherapy. *Cancer Biology & Therapy*, *13*(11), 1072–1081. https://doi.org/10.4161/cbt.21093

Principe, D. R., DeCant, B., Mascariñas, E., Wayne, E. A., Diaz, A. M., Akagi, N., … Grippo, P. J. (2016). TGFβ Signaling in the Pancreatic Tumor Microenvironment Promotes Fibrosis and Immune Evasion to Facilitate Tumorigenesis. *Cancer Research*, *76*(9), 2525–2539. https://doi.org/10.1158/0008-5472.CAN-15-1293

Provenzano, P. P., Cuevas, C., Chang, A. E., Goel, V. K., Von Hoff, D. D., & Hingorani, S. R. (2012). Enzymatic Targeting of the Stroma Ablates Physical Barriers to Treatment of Pancreatic Ductal Adenocarcinoma. *Cancer Cell*, *21*(3), 418–429. https://doi.org/10.1016/j.ccr.2012.01.007

Qiao, Z., He, M., He, M. U., Li, W., Wang, X., Wang, Y., … Yu, Q. (2016). Synergistic antitumor activity of gemcitabine combined with triptolide in pancreatic cancer cells. *Oncology Letters*, *11*(5), 3527–3533. https://doi.org/10.3892/ol.2016.4379

Rahib, L., Fleshman, J. M., Matrisian, L. M., & Berlin, J. D. (2016). Evaluation of Pancreatic Cancer Clinical Trials and Benchmarks for Clinically Meaningful Future Trials. *JAMA Oncology*, *2*(9), 1209. https://doi.org/10.1001/jamaoncol.2016.0585

Rahib, L., Smith, B. D., Aizenberg, R., Rosenzweig, A. B., Fleshman, J. M., & Matrisian, L. M. (2014). Projecting Cancer Incidence and Deaths to 2030: The Unexpected Burden of Thyroid, Liver, and Pancreas Cancers in the United States. *Cancer Research*, *74*(11), 2913–2921. https://doi.org/10.1158/0008-5472.CAN-14-0155

Raymond, E., Alexandre, J., Faivre, S., Goldwasser, F., Besse-Hammer, T., Gianella-Borradori, A., … Awada, A. (2014). A phase I schedule dependency study of the aurora kinase inhibitor MSC1992371A in combination with gemcitabine in patients with solid tumors. *Investigational New Drugs*, *32*(1), 94–103. https://doi.org/10.1007/s10637-013-9950-y

Raymond, E., Faivre, S., Woynarowski, J. M., & Chaney, S. G. (1998). Oxaliplatin: mechanism of action and antineoplastic activity. *Seminars in Oncology*, *25*(2 Suppl 5), 4–12. Retrieved from http://www.ncbi.nlm.nih.gov/pubmed/9609103

Rhim, A. D., Mirek, E. T., Aiello, N. M., Maitra, A., Bailey, J. M., McAllister, F., … Stanger, B. Z. (2012). EMT and Dissemination Precede Pancreatic Tumor Formation. *Cell*, *148*(1–2), 349–361. https://doi.org/10.1016/J.CELL.2011.11.025

Rhim, A. D., Oberstein, P. E., Thomas, D. H., Mirek, E. T., Palermo, C. F., Sastra, S. A., … Stanger, B. Z. (2014). Stromal elements act to restrain, rather than support, pancreatic ductal adenocarcinoma. *Cancer Cell*, *25*(6), 735–747. https://doi.org/10.1016/j.ccr.2014.04.021

Roy, I., Zimmerman, N. P., Mackinnon, A. C., Tsai, S., Evans, D. B., & Dwinell, M. B. (2014). CXCL12 chemokine expression suppresses human pancreatic cancer growth and metastasis. *PloS One*, *9*(3), e90400. https://doi.org/10.1371/journal.pone.0090400

Royal, R. E., Levy, C., Turner, K., Mathur, A., Hughes, M., Kammula, U. S., … Rosenberg, S. A. (2010). Phase 2 Trial of Single Agent Ipilimumab (Anti-CTLA-4) for Locally Advanced or Metastatic Pancreatic Adenocarcinoma. *Journal of Immunotherapy*, *33*(8), 828–833. https://doi.org/10.1097/CJI.0b013e3181eec14c

Rucki, A. A., Foley, K., Zhang, P., Xiao, Q., Kleponis, J., Wu, A. A., … Zheng, L. (2017). Heterogeneous Stromal Signaling within the Tumor Microenvironment Controls the Metastasis of Pancreatic Cancer. *Cancer Research*, *77*(1), 41–52. https://doi.org/10.1158/0008-5472.CAN-16-1383

Sachs, N., de Ligt, J., Kopper, O., Gogola, E., Bounova, G., Weeber, F., … Clevers, H. (2018). A Living Biobank of Breast Cancer Organoids Captures Disease Heterogeneity. *Cell*, *172*(1–2), 373–386.e10. https://doi.org/10.1016/j.cell.2017.11.010

Săftoiu, A., Vilmann, P., Gorunescu, F., Gheonea, D. I., Gorunescu, M., Ciurea, T., … Iordache, S. (2008). Neural network analysis of dynamic sequences of EUS elastography used for the differential diagnosis of chronic pancreatitis and pancreatic cancer. *Gastrointestinal Endoscopy*, *68*(6), 1086–1094. https://doi.org/10.1016/j.gie.2008.04.031

Sahu, R. P., Batra, S., & Srivastava, S. K. (2009). Activation of ATM/Chk1 by curcumin causes cell cycle arrest and apoptosis in human pancreatic cancer cells. *British Journal of Cancer*, *100*(9), 1425–1433. https://doi.org/10.1038/sj.bjc.6605039

Saiki, Y., Yoshino, Y., Fujimura, H., Manabe, T., Kudo, Y., Shimada, M., … Horii, A. (2012). DCK is frequently inactivated in acquired gemcitabine-resistant human cancer cells.

Biochemical and Biophysical Research Communications, *421*(1), 98–104. https://doi.org/10.1016/j.bbrc.2012.03.122

Sangrador, I., Molero, X., Campbell, F., Franch-Expósito, S., Rovira-Rigau, M., Samper, E., … Vaquero, E. C. (2018). Zeb1 in Stromal Myofibroblasts Promotes Kras-Driven Development of Pancreatic Cancer. *Cancer Research*, *78*(10), 2624–2637. https://doi.org/10.1158/0008-5472.CAN-17-1882

Sappino, A. P., Skalli, O., Jackson, B., Schürch, W., & Gabbiani, G. (1988). Smooth-muscle differentiation in stromal cells of malignant and non-malignant breast tissues. *International Journal of Cancer*, *41*(5), 707–712. Retrieved from http://www.ncbi.nlm.nih.gov/pubmed/2835323

Sasaki, K., Kurahara, H., Young, E. D., Natsugoe, S., Ijichi, A., Iwakuma, T., & Welch, D. R. (2017). Genome-wide in vivo RNAi screen identifies ITIH5 as a metastasis suppressor in pancreatic cancer. *Clinical & Experimental Metastasis*, *34*(3–4), 229–239. https://doi.org/10.1007/s10585-017-9840-3

Seino, T., Kawasaki, S., Shimokawa, M., Tamagawa, H., Toshimitsu, K., Fujii, M., … Sato, T. (2018). Human Pancreatic Tumor Organoids Reveal Loss of Stem Cell Niche Factor Dependence during Disease Progression. *Cell Stem Cell*, *22*(3), 454–467.e6. https://doi.org/10.1016/j.stem.2017.12.009

Seo, H. K., Ahn, K.-O., Jung, N.-R., Shin, J.-S., Park, W. S., Lee, K.-H., … Jeong, K.-C. (2014). Antitumor activity of the c-Myc inhibitor KSI-3716 in gemcitabine-resistant bladder cancer. *Oncotarget*, *5*(2), 326–337. https://doi.org/10.18632/oncotarget.1545

Shan, T., Chen, S., Chen, X., Lin, W. R., Li, W., Ma, J., … Kang, Y. (2017). Cancer-associated fibroblasts enhance pancreatic cancer cell invasion by remodeling the metabolic conversion mechanism. *Oncology Reports*, *37*(4), 1971–1979. https://doi.org/10.3892/or.2017.5479

Sheahan, A. V, Biankin, A. V, Parish, C. R., & Khachigian, L. M. (2018). Targeted therapies in the management of locally advanced and metastatic pancreatic cancer: a systematic review. *Oncotarget*, *9*(30), 21613–21627. https://doi.org/10.18632/oncotarget.25085

Shields, M. A., Dangi-Garimella, S., Krantz, S. B., Bentrem, D. J., & Munshi, H. G. (2011). Pancreatic Cancer Cells Respond to Type I Collagen by Inducing Snail Expression to Promote Membrane Type 1 Matrix Metalloproteinase-dependent Collagen Invasion. *Journal of Biological Chemistry*, *286*(12), 10495–10504. https://doi.org/10.1074/jbc.M110.195628

Siegel, R., Ma, J., Zou, Z., & Jemal, A. (2014). Cancer statistics, 2014. *CA: A Cancer Journal for Clinicians*, *64*(1), 9–29. https://doi.org/10.3322/caac.21208

Sims, D., Mendes-Pereira, A. M., Frankum, J., Burgess, D., Cerone, M.-A., Lombardelli, C., … Lord, C. J. (2011). High-throughput RNA interference screening using pooled shRNA libraries and next generation sequencing. *Genome Biology*, *12*(10), R104. https://doi.org/10.1186/gb-2011-12-10-r104

Singh, A. P., Arora, S., Bhardwaj, A., Srivastava, S. K., Kadakia, M. P., Wang, B., … Singh, S. (2012). CXCL12/CXCR4 protein signaling axis induces sonic hedgehog expression in

pancreatic cancer cells via extracellular regulated kinase- and Akt kinase-mediated activation of nuclear factor κB: implications for bidirectional tumor-stromal interactions. *The Journal of Biological Chemistry*, *287*(46), 39115–39124. https://doi.org/10.1074/jbc.M112.409581

Smith, J. A., Poteet-Smith, C. E., Xu, Y., Errington, T. M., Hecht, S. M., & Lannigan, D. A. (2005). Identification of the first specific inhibitor of p90 ribosomal S6 kinase (RSK) reveals an unexpected role for RSK in cancer cell proliferation. *Cancer Research*, *65*(3), 1027–1034. Retrieved from http://www.ncbi.nlm.nih.gov/pubmed/15705904

Sohn, T. A., Yeo, C. J., Cameron, J. L., Koniaris, L., Kaushal, S., Abrams, R. A., … Lillemoe, K. D. (2000). Resected adenocarcinoma of the pancreas-616 patients: results, outcomes, and prognostic indicators. *Journal of Gastrointestinal Surgery : Official Journal of the Society for Surgery of the Alimentary Tract*, *4*(6), 567–579. Retrieved from http://www.ncbi.nlm.nih.gov/pubmed/11307091

Soneson, C., & Robinson, M. D. (2017). Bias, Robustness And Scalability In Differential Expression Analysis Of Single-Cell RNA-Seq Data. *BioRxiv*, 143289. https://doi.org/10.1101/143289

Spratlin, J., Sangha, R., Glubrecht, D., Dabbagh, L., Young, J. D., Dumontet, C., … Mackey, J. R. (2004). The Absence of Human Equilibrative Nucleoside Transporter 1 Is Associated with Reduced Survival in Patients With Gemcitabine-Treated Pancreas Adenocarcinoma. *Clinical Cancer Research*, *10*(20), 6956–6961. https://doi.org/10.1158/1078-0432.CCR-04-0224

Stoller, R. G., Myers, C. E., & Chabner, B. A. (1978). Analysis of cytidine deaminase and tetrahydrouridine interaction by use of ligand techniques. *Biochemical Pharmacology*, *27*(1), 53–59. Retrieved from http://www.ncbi.nlm.nih.gov/pubmed/619907

Stransky, N., Ghandi, M., Kryukov, G. V., Garraway, L. A., Lehár, J., Liu, M., … Saez-Rodriguez, J. (2015). Pharmacogenomic agreement between two cancer cell line data sets. *Nature*, *528*(7580), 84–87. https://doi.org/10.1038/nature15736

Straussman, R., Morikawa, T., Shee, K., Barzily-Rokni, M., Qian, Z. R., Du, J., … Golub, T. R. (2012). Tumour micro-environment elicits innate resistance to RAF inhibitors through HGF secretion. *Nature*, *487*(7408), 500–504. https://doi.org/10.1038/nature11183

Stromnes, I. M., Brockenbrough, J. S., Izeradjene, K., Carlson, M. A., Cuevas, C., Simmons, R. M., … Hingorani, S. R. (2014). Targeted depletion of an MDSC subset unmasks pancreatic ductal adenocarcinoma to adaptive immunity. *Gut*, *63*(11), 1769–1781. https://doi.org/10.1136/gutjnl-2013-306271

Subramanian, A., Tamayo, P., Mootha, V. K., Mukherjee, S., Ebert, B. L., Gillette, M. A., … Mesirov, J. P. (2005). Gene set enrichment analysis: a knowledge-based approach for interpreting genome-wide expression profiles. *Proceedings of the National Academy of Sciences of the United States of America*, *102*(43), 15545–15550. https://doi.org/10.1073/pnas.0506580102

Sudo, T., Iwaya, T., Nishida, N., Sawada, G., Takahashi, Y., Ishibashi, M., … Mimori, K. (2013). Expression of Mesenchymal Markers Vimentin and Fibronectin: The Clinical Significance in Esophageal Squamous Cell Carcinoma. *Annals of Surgical Oncology*, *20*(S3), 324–335.

https://doi.org/10.1245/s10434-012-2418-z

Sun, Q., Burke, J. P., Phan, J., Burns, M. C., Olejniczak, E. T., Waterson, A. G., … Fesik, S. W. (2012). Discovery of Small Molecules that Bind to K-Ras and Inhibit Sos-Mediated Activation. *Angewandte Chemie International Edition*, *51*(25), 6140–6143. https://doi.org/10.1002/anie.201201358

Takeda, H., Okada, M., Suzuki, S., Kuramoto, K., Sakaki, H., Watarai, H., … Kitanaka, C. (2016). Rho-Associated Protein Kinase (ROCK) Inhibitors Inhibit Survivin Expression and Sensitize Pancreatic Cancer Stem Cells to Gemcitabine. *Anticancer Research*, *36*(12), 6311–6318. https://doi.org/10.21873/anticanres.11227

Trapnell, C., Pachter, L., & Salzberg, S. L. (2009). TopHat: discovering splice junctions with RNA-Seq. *Bioinformatics*, *25*(9), 1105–1111. https://doi.org/10.1093/bioinformatics/btp120

Van Cutsem, E., van de Velde, H., Karasek, P., Oettle, H., Vervenne, W. L., Szawlowski, A., … Von Hoff, D. (2004). Phase III Trial of Gemcitabine Plus Tipifarnib Compared With Gemcitabine Plus Placebo in Advanced Pancreatic Cancer. *Journal of Clinical Oncology*, *22*(8), 1430–1438. https://doi.org/10.1200/JCO.2004.10.112

Varadhachary, G. R., Tamm, E. P., Abbruzzese, J. L., Xiong, H. Q., Crane, C. H., Wang, H., … Wolff, R. A. (2006). Borderline Resectable Pancreatic Cancer: Definitions, Management, and Role of Preoperative Therapy. *Annals of Surgical Oncology*, *13*(8), 1035–1046. https://doi.org/10.1245/ASO.2006.08.011

Verissimo, C. S., Overmeer, R. M., Ponsioen, B., Drost, J., Mertens, S., Verlaan-Klink, I., … Snippert, H. J. (2016). Targeting mutant RAS in patient-derived colorectal cancer organoids by combinatorial drug screening. *ELife*, *5*, e18489. https://doi.org/10.7554/eLife.18489

Vincent, A., Herman, J., Schulick, R., Hruban, R. H., & Goggins, M. (2011). Pancreatic cancer. *Lancet (London, England)*, *378*(9791), 607–620. https://doi.org/10.1016/S0140-6736(10)62307-0

Vlachogiannis, G., Hedayat, S., Vatsiou, A., Jamin, Y., Fernández-Mateos, J., Khan, K., … Valeri, N. (2018). Patient-derived organoids model treatment response of metastatic gastrointestinal cancers. *Science (New York, N.Y.)*, *359*(6378), 920–926. https://doi.org/10.1126/science.aao2774

Von Hoff, D. D., Ervin, T., Arena, F. P., Chiorean, E. G., Infante, J., Moore, M., … Renschler, M. F. (2013). Increased Survival in Pancreatic Cancer with nab-Paclitaxel plus Gemcitabine. *New England Journal of Medicine*, *369*(18), 1691–1703. https://doi.org/10.1056/NEJMoa1304369

Vooijs, M., Jonkers, J., & Berns, A. (2001). A highly efficient ligand-regulated Cre recombinase mouse line shows that *LoxP* recombination is position dependent. *EMBO Reports*, *2*(4), 292–297. https://doi.org/10.1093/embo-reports/kve064

Voutsadakis, I. A. (2011). Molecular predictors of gemcitabine response in pancreatic cancer. *World Journal of Gastrointestinal Oncology*, *3*(11), 153–164. https://doi.org/10.4251/wjgo.v3.i11.153

Waddell, N., Pajic, M., Patch, A.-M., Chang, D. K., Kassahn, K. S., Bailey, P., … Grimmond, S. M. (2015). Whole genomes redefine the mutational landscape of pancreatic cancer. *Nature*, *518*(7540), 495–501. https://doi.org/10.1038/nature14169

Wallez, Y., Dunlop, C. R., Johnson, T. I., Koh, S.-B., Fornari, C., Yates, J. W., … Jodrell, D. I. (2018). The ATR inhibitor AZD6738 synergizes with gemcitabine in vitro and in vivo to induce pancreatic ductal adenocarcinoma regression. *Molecular Cancer Therapeutics*, molcanther.0010.2018. https://doi.org/10.1158/1535-7163.MCT-18-0010

Walter, K., Omura, N., Hong, S.-M., Griffith, M., & Goggins, M. (2008). Pancreatic cancer associated fibroblasts display normal allelotypes. *Cancer Biology & Therapy*, *7*(6), 882–888. Retrieved from http://www.ncbi.nlm.nih.gov/pubmed/18344687

Wang-Gillam, A., Lockhart, A. C., Tan, B. R., Suresh, R., Singh, P. P., Lim, K.-H., … DeNardo, D. G. (2017). Phase I study of defactinib combined with pembrolizumab and gemcitabine in advanced cancer. *Journal of Clinical Oncology*, *35*(4_suppl), TPS505-TPS505. https://doi.org/10.1200/JCO.2017.35.4_suppl.TPS505

Wang, Z., Gerstein, M., & Snyder, M. (2009). RNA-Seq: a revolutionary tool for transcriptomics. *Nature Reviews Genetics*, *10*(1), 57–63. https://doi.org/10.1038/nrg2484

Warshaw, A. L., & Castillo, C. F. (1992). Pancreatic Carcinoma. *New England Journal of Medicine*, *326*(7), 455–465. https://doi.org/10.1056/NEJM199202133260706

Weekes, C. D., Song, D., Arcaroli, J., Wilson, L. A., Rubio-Viqueira, B., Cusatis, G., … Hidalgo, M. (2012). Stromal cell-derived factor 1α mediates resistance to mTOR-directed therapy in pancreatic cancer. *Neoplasia (New York, N.Y.)*, *14*(8), 690–701. Retrieved from http://www.ncbi.nlm.nih.gov/pubmed/22952422

Weiss, G. J., Blaydorn, L., Beck, J., Bornemann-Kolatzki, K., Urnovitz, H., Schütz, E., & Khemka, V. (2018). Phase Ib/II study of gemcitabine, nab-paclitaxel, and pembrolizumab in metastatic pancreatic adenocarcinoma. *Investigational New Drugs*, *36*(1), 96–102. https://doi.org/10.1007/s10637-017-0525-1

Weizman, N., Krelin, Y., Shabtay-Orbach, A., Amit, M., Binenbaum, Y., Wong, R. J., & Gil, Z. (2014). Macrophages mediate gemcitabine resistance of pancreatic adenocarcinoma by upregulating cytidine deaminase. *Oncogene*, *33*(29), 3812–3819. https://doi.org/10.1038/onc.2013.357

Whatcott, C. J., Diep, C. H., Jiang, P., Watanabe, A., LoBello, J., Sima, C., … Han, H. (2015). Desmoplasia in Primary Tumors and Metastatic Lesions of Pancreatic Cancer. *Clinical Cancer Research : An Official Journal of the American Association for Cancer Research*, *21*(15), 3561–3568. https://doi.org/10.1158/1078-0432.CCR-14-1051

Wilschanski, M., & Novak, I. (2013). The cystic fibrosis of exocrine pancreas. *Cold Spring Harbor Perspectives in Medicine*, *3*(5), a009746. https://doi.org/10.1101/cshperspect.a009746

Wong, C. H., Siah, K. W., & Lo, A. W. (2018). Estimation of clinical trial success rates and related parameters. *Biostatistics*. https://doi.org/10.1093/biostatistics/kxx069

Xu, R. (2015). *Investigating stroma-mediated resistance to gemcitabine, using a novel*

fluorescencebased coculture model of pancreatic cancer. University of Cambridge.

Yip-Schneider, M. T., Sweeney, C. J., Jung, S. H., Crowell, P. L., & Marshall, M. S. (2001). Cell cycle effects of nonsteroidal anti-inflammatory drugs and enhanced growth inhibition in combination with gemcitabine in pancreatic carcinoma cells. *The Journal of Pharmacology and Experimental Therapeutics*, *298*(3), 976–985. Retrieved from http://www.ncbi.nlm.nih.gov/pubmed/11504793

Yue, X., Zhao, Y., Xu, Y., Zheng, M., Feng, Z., & Hu, W. (2017). Mutant p53 in Cancer: Accumulation, Gain-of-Function, and Therapy. *Journal of Molecular Biology*, *429*(11), 1595–1606. https://doi.org/10.1016/j.jmb.2017.03.030

Zhang, Q., Zeng, L., Chen, Y., Lian, G., Qian, C., Chen, S., … Huang, K. (2016). Pancreatic Cancer Epidemiology, Detection, and Management. *Gastroenterology Research and Practice*, *2016*, 1–10. https://doi.org/10.1155/2016/8962321

Zheng, T., Wang, J., Zhao, Y., Zhang, C., Lin, M., Wang, X., … Hu, W. (2013). Spliced MDM2 isoforms promote mutant p53 accumulation and gain-of-function in tumorigenesis. *Nature Communications*, *4*, 2996. https://doi.org/10.1038/ncomms3996

Zheng, X., Carstens, J. L., Kim, J., Scheible, M., Kaye, J., Sugimoto, H., … Kalluri, R. (2015). Epithelial-to-mesenchymal transition is dispensable for metastasis but induces chemoresistance in pancreatic cancer. *Nature*, *527*(7579), 525–530. https://doi.org/10.1038/nature16064

Zhu, W., Li, J., Wu, S., Li, S., Le, L., Su, X., … Yan, G. (2012). Triptolide Cooperates With Cisplatin to Induce Apoptosis in Gemcitabine-Resistant Pancreatic Cancer. *Pancreas*, *41*(7), 1029–1038. https://doi.org/10.1097/MPA.0b013e31824abdc0

Zomer, A., Maynard, C., Verweij, F. J., Kamermans, A., Schäfer, R., Beerling, E., … van Rheenen, J. (2015). In Vivo imaging reveals extracellular vesicle-mediated phenocopying of metastatic behavior. *Cell*, *161*(5), 1046–1057. https://doi.org/10.1016/j.cell.2015.04.042

Zou, M., Baitei, E. Y., Al-Rijjal, R. A., Parhar, R. S., Al-Mohanna, F. A., Kimura, S., … Shi, Y. (2015). KRAS G12D -mediated oncogenic transformation of thyroid follicular cells requires long-term TSH stimulation and is regulated by SPRY1. *Laboratory Investigation*, *95*(11), 1269–1277. https://doi.org/10.1038/labinvest.2015.90